USING CONTINUOUS COMPACTION CONTROL SYSTEMS WITHIN AN EARTHWORK COMPACTION SPECIFICATION FRAMEWORK

by

Daniel V. Cacciola

A thesis submitted to the Faculty of the University of Delaware in partial fulfillment of the requirements for the degree of Master of Civil Engineering

Summer 2013

© 2013 Daniel V. Cacciola
All Rights Reserved

USING CONTINUOUS COMPACTION CONTROL SYSTEMS WITHIN AN EARTHWORK COMPACTION SPECIFICATION FRAMEWORK

by

Daniel V. Cacciola

Approved: _____
Christopher L. Meehan, Ph.D.
Professor in charge of thesis on behalf of the Advisory Committee

Approved: _____
Harry W. Shenton III, Ph.D.
Chair of the Department of Civil and Environmental Engineering

Approved: _____
Babatunde A. Ogunnaike, Ph.D.
Dean of the College of Engineering

Approved: _____
James G. Richards, Ph.D.
Vice Provost for Graduate and Professional Education

ACKNOWLEDGMENTS

I would like to first express my deepest gratitude to my advisor Dr. Christopher L. Meehan, not only for his guidance and support throughout the development of this thesis document, but also for drawing my interest into the field of geotechnical engineering. Since Dr. Meehan was also my undergraduate studies advisor, I can truly say that he has been a positive influence from the beginning to the end of my journey at the University of Delaware, and for that I am extremely grateful.

I would also like to extend my sincerest appreciation to the Delaware Department of Transportation for funding the field study which made my research possible, and supporting me financially throughout my graduate studies.

I would also like to acknowledge Caterpillar, Inc.; Greggo & Ferrara, Inc.; Kessler Soils Engineering Products, Inc.; and Humboldt Inc., whose contributions of labor and equipment made the field study a success.

I would also like to thank geotechnical engineering professors Dr. Victor Kaliakin and Dr. Dov Leshchinsky, who provided me with guidance and the education which enabled me to complete my graduate studies.

I would also like to express my gratitude to the fellow students at the University of Delaware; Matthew Becker, Jason Hertz, Majid Khabbazian, Mohammad Khosravi, Meysam Mashayekhi, Andres Nieto Leal, Majid Talebi, and Farshid Vahedifard, whose support in studies, research, and friendship helped me throughout my graduate career.

I would also like to give a special thanks to Faraz Tehrani, whose previous research on the field study provided me with the necessary information to continue and expand the project which made development of my thesis possible.

I would like to thank my family for their unconditional love and support throughout my academic studies and entire life. I thank my brothers Brendan Cacciola and Cory Cacciola, who will always be my closest friends. I thank my mother, Marlene Cacciola, who has emotionally supported me through the good and the bad times. Without them I would never have been able to accomplish what I have today.

Finally, I would like to thank my father, Joseph Cacciola. Although he passed away before I began my graduate studies, the life lessons, love, and friendship that he provided outlined the framework for how I live my life. I know the completion of this thesis would make him proud, and for me there is no greater accomplishment.

TABLE OF CONTENTS

Appendix

LIST OF TABLES

LIST OF FIGURES

ABSTRACT

The objective of the study presented in this thesis is to investigate the use of continuous compaction control (CCC) systems within an earthwork compaction specification framework. For this purpose, the Delaware Department of Transportation (DelDOT) funded a field study to construct a small-scale soil embankment, utilizing CCC technology simultaneously with conventional in situ compaction verification test methods during the construction process. The material that was used to build the embankment classified as poorly-graded sand with silt. The CCC roller measured machine drive power (MDP) values, compaction meter values (CMV), and corresponding global positioning system (GPS) location values. For conventional in situ compaction verification, numerous density-based quality assurance test methods (e.g., Nuclear Density Gauge and Sand Cone) and modulus-based test methods (e.g., Lightweight Deflectometer and GeoGauge) were performed. A holistic analysis of the data collected from the field study was performed to assess the use of CCC systems in an earthwork compaction specification framework.

The first goal of this study was to examine the possibility of using data recorded by CCC systems to monitor and control the thickness of compacted soil lifts during earthwork operations. During the field study, the compaction roller utilized a real-time kinematic global positioning system (RTK-GPS) to determine the three dimensional location of the compactor in real-time. Data collected from the field study was then used to demonstrate how GPS measurements recorded by CCC equipment

could be used for field monitoring of lift thickness. The use of simple and sophisticated geospatial interpolation techniques were examined for interpolating measured field elevation data onto a uniform grid for lift thickness evaluation. The approach that is presented can be used to build spatial maps of compacted soil lift thickness, which are a useful decision-making tool for field inspectors.

The second goal of this study was to perform statistical regression analyses to compare the results of the in situ spot testing methods with the two CCC measurements (MDP and CMV) that were recorded during the compaction process. In order to accurately compare the in situ spot testing measurements and CCC measurements, Nearest Neighbor, Inverse Distance Weighting, and Ordinary Kriging interpolation techniques were utilized to predict CCC measurements at the corresponding in situ spot test locations. In general, regression analyses performed using the CCC predictions from the Ordinary Kriging method showed slightly higher correlations, however, the difference did not appear significant enough to outweigh the complex nature of this geospatial interpolation technique.

Univariate regression analysis was performed first for point-by-point comparisons of the data and then on a data set which comprised of average values for each lift and pass. The point-by-point comparisons yielded weak correlations, while the comparison of the average value data sets showed much stronger correlations; this finding agrees well with observations that have been reported by other researchers. As other researchers have also reported that moisture content can drastically affect the compaction process and resulting density of soil, additional analyses using a multivariate regression technique were performed, which introduced the use of in situ measured moisture content as an independent variable. The results from these

regression correlations showed generally much stronger correlation between the in situ test measurements and the CCC measurements for both the point-by-point and average data sets. This observation provided confirmation of the influence of moisture content on the in situ test measurements and the CCC measurements.

The final goal of the study was to evaluate the use of CCC technology within an earthwork compaction specification framework. To accomplish this goal, implementation of existing CCC compaction verification acceptance criteria using the data collected from the aforementioned field study was performed. The acceptance criteria that were assessed include: spot testing of roller measured weakest areas, limiting percentage change in roller measured values, and comparison of roller measured values to in situ measured values. Each of the three acceptance criteria show potential for implementation into an earthwork specification; however, since the spot testing of roller measured weakest areas method still utilizes conventional in situ methods, it shows the most promise for immediate adoption and transition into CCC technology.

Chapter 1

INTRODUCTION

Earthwork compaction specifications generally may be classified as either a method/procedure specification or an end-product/performance specification. Method specifications will usually specify the exact process for compaction and will not require verification of compaction. Method specifications are typically used when there is prior experience with the compaction material, or if there is not a reasonable means to verify compaction through in-situ testing. In contrast, end-product specifications verify that the desired soil properties have been achieved through in-situ testing or other assessment of the "final product" that results from the compaction process. Typically, in situ quality assurance/quality control (QA/QC) spot tests are performed after compaction to assess if the compaction process has been conducted near the optimum moisture content, and if it has yielded a soil density that is close to a standardized input value (i.e., yielding a soil density that is above 95% of the maximum density measured during a Standard Proctor test).

In both method-based and end-product based specifications, there is almost always a maximum lift thickness requirement. This is necessary to help ensure optimal compactor energy penetration, and more uniformly compacted soil. Additionally, many commonly QA/QC tests cannot be performed on thicker lifts of soil. Although QA/QC spot tests can provide relatively accurate compaction verification results when used in an end-product specification framework, there are many limitations to using any type of spot test for in situ compaction verification. The most apparent limitations

are the relatively low percentage of material being testing in comparison to the entire compaction zone and the inherent construction delays caused by performing the in situ spot tests. Additionally, the most commonly used spot test, the nuclear density gauge (NDG) test, has logistical and safety limitations due to the use of a radioactive source within the test device.

Advancements in technology have provided a new tool that shows significant promise for improving the efficiency of the compaction and compaction verification processes. Continuous Compaction Control (CCC) technology continuously and instantaneously measures machine parameters, global positioning system (GPS) location, and soil response, while offering nearly 100% coverage of the compaction zone. More recently, in recognition of this emerging technology, several state Departments of Transportation (DOT) have begun to adopt earthwork compaction specifications that utilize CCC systems for compaction verification. The Delaware Department of Transportation (DelDOT) set in motion a field study in 2007 at a borrow pit in Odessa, DE to better understand CCC technology. The field study involved the construction of a small-scale embankment, which was compacted using a compaction roller outfitted to record CCC measurements. In addition to the collection of all pertinent CCC data, an extensive in situ QA/QC spot testing plan was implemented. Amongst the in situ spot tests performed was the currently popular NDG test, which measured dry unit weight and moisture content of the compaction material. The DelDOT funded this study with the intent of developing earthwork compaction specifications that utilize CCC systems for compaction verification.

The purpose of this study is to analyze the results from the aforementioned field study and provide pertinent recommendations for the development of earthwork

compaction specifications using CCC systems for the DelDOT. Chapter 2 provides a summary of existing literature related to the current project. Included in the literature review is a comprehensive discussion on the considerations, methods, and limitations of implementing CCC technology into an earthwork compaction specification. In Chapter 3, the aforementioned field study, utilizing CCC technology, is discussed in a higher level of detail. In an attempt to improve upon the current options for regulating lift thickness control during compaction, an innovative method for monitoring field lift thickness using compaction equipment with GPS technology is provided in Chapter 4.

Before evaluating CCC technology in an earthwork compaction specification framework, it is important to investigate the relationship between in situ spot test measurements and the soil response measurements recorded by the compaction equipment. Since the locations of the in situ spot test measurements do not precisely match the locations of the CCC measurements, it was necessary to utilize interpolation techniques to predict CCC measurement values at the in situ spot test locations. Chapter 5 provides the results from examination of the relationships between in situ spot test measurements and kriged CCC measurements. Kriging interpolation has been widely used in research to predict CCC measurements because it is considered to produce the most accurate predictions; however, the kriging method is extremely complex and would be difficult to use in real time for compaction verification on active construction projects. Consequently, an evaluation of alternative techniques for interpolating CCC measurements for comparison with in situ spot test measurements is provided in Chapter 6. In Chapter 7, the earthwork compaction specification methodologies for CCC equipment that were provided in the literature review will be evaluated using real data which was collected during the previously mentioned field

study. Finally, in Chapter 8, the most significant conclusions from the research performed in this thesis will be presented, along with recommendations for development of earthwork compaction specifications for use with CCC systems.

Chapter 2

LITERATURE REVIEW

2.1 Soil Compaction

For many civil engineering applications including the construction of embankments, earthen dams, roadway subgrades, and slopes, compaction is necessary to increase the unit weight of loose soils (Das 2008). As defined by Holtz and Kovacs (1981), compaction is the densification of soils and rock by application of mechanical energy to minimize air voids. This densification process may be optimized by modification of the moisture content and/or the gradation of the soil. For soils, the degree of compaction is typically measured in terms of the dry unit weight. The various laboratory and field tests that are used to measure the dry unit weight of soil will be discussed in the following sections.

The overall purpose of soil compaction is to improve the engineering properties of the material. The following effects may result from compaction (Holtz and Kovacs 1981):

- Reduction and/or prevention of detrimental settlements
- Increase in soil strength (e.g., an increase in bearing capacity or an improvement in slope stability)
- Decrease in hydraulic conductivity
- Control of undesirable volume changes (e.g., frost action, swelling, and shrinkage of fine-grained soils)

The extent to which the improvements listed above may be seen is reliant on several factors. These control factors can loosely be classified into two groups, soil properties and densification process properties. In general, the specific control factors that affect the results of compaction are:

- Soil moisture content
- Soil type and gradation
- Compactive effort
- Process of compaction

In soils, the process of compaction is strongly affected by the soil's moisture content. The addition of water to soil will act as a softening agent and facilitate the rearrangement of individual particles within the soil mass. If there is zero percent moisture content, individual particles will have a difficult time rearranging, thus, not much compaction can be achieved. The addition of water facilitates particle rearrangement and allows for better compaction, up to a certain point. The soil mass will eventually reach a moisture content percentage (an "optimum" moisture content) beyond which the addition of more water will begin to reduce the achievable compaction. This phenomenon occurs because the water that was once acting as a facilitating agent for rearrangement of particles into a denser state will now cause the particles to flow within the soil mass, without achieving the desired increase in density. The soil moisture-density relationship described above is typically referred to as the compaction curve (Figure 2.1). It should be noted that, for soils, better compaction is defined as a process which achieves a higher dry unit weight for the soil.

The soil type will greatly influence the compaction curve. The specific properties that directly affect the moisture-density relationship are the: specific gravity of soil particles, shape of soil particles, grain-size distribution of particles, and clay mineralogy (Holtz and Kovacs 1981). Typically, different soil types (e.g., granular soils versus cohesive soils) require different types of compaction and levels of compactive effort to achieve the most effective and efficient compaction of the soil. Generally, as the compaction energy per unit volume increases, the maximum dry unit weight achievable by compaction will increase; in other words, an increase in compactive energy will increase the maximum dry unit weight (Figure 2.1). The method of compaction must be selected based on the soil type to ensure that the soil will be compacted efficiently.

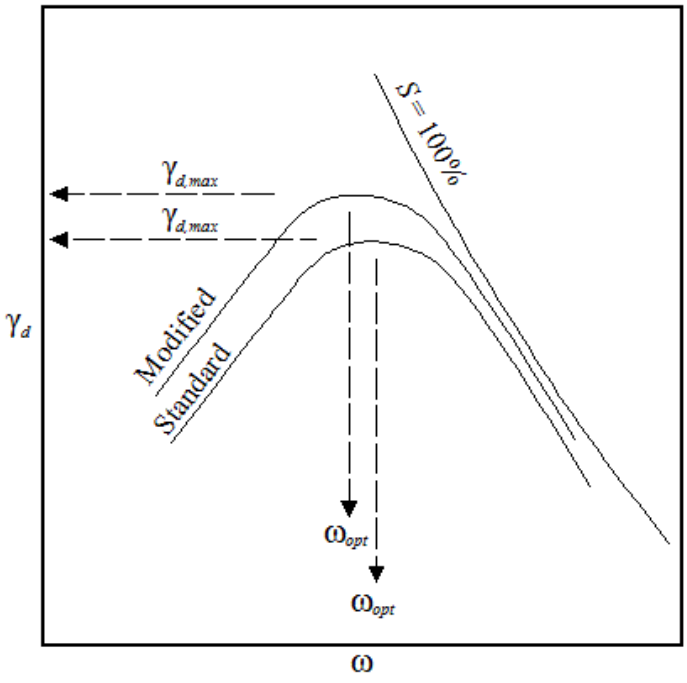

Figure 2.1 Effect of compaction energy on compaction curves (modified after Coduto 1999).

In Figure 2.1, typical compaction curves for identical soils compacted at different compactive efforts are shown. The compaction curves are labeled to correspond with the two most common standard laboratory procedures for determining the compaction curve: the standard proctor test (ASTM D 698) and the modified proctor test (ASTM D 1557). The standard test procedures will be discussed in more detail in Section 2.4.1.2. However, it should be noted that the modified proctor test utilizes higher compactive energy than the standard proctor test to develop the compaction curves. Typically, if the modified and standard proctor tests are performed on the same soil sample, the compaction curve will shift up and to the left, representing an increasing maximum dry unit weight ($\gamma_{d,max}$) and decreasing optimum moisture (ω_{opt}) as compactive energy increases.

2.2 Compaction Methods

There are three general compaction techniques into which all compaction processes can be classified: static compaction, kneading compaction, and dynamic compaction.

2.2.1 Static Compaction

Static compaction relies on the weight of a soil compactor and gravity to apply downward pressure onto the soil. The compactive effort of static compaction relies on the weight of the equipment and the contact area that the equipment has with the soil. For a given compactor, in order to increase the contact pressure/compactive effort, either weight must be added to the compactor or the contact area must be reduced, increasing the force that is applied per unit area. Higher contact pressures will generally result in increased compression of the soil mass, more effectively reducing

the volume of voids in the soil and increasing the soil's density (or unit weight). In general, the benefits of static compaction are limited to the upper layers of a compacted material, as the depth of influence of static compaction is typically low (Adam and Kopf 2004). Static compaction is most appropriate for fine-grained soils and bituminous materials like asphalt (Adam and Kopf 1998).

2.2.2 Kneading Compaction

For cohesive soils, the use of static compaction may not be the most efficient way to achieve densification. The application of instantaneous static pressure to certain cohesive soils will cause a rapid buildup of excess pore water pressure which will make it difficult to minimize the void space in the soil and achieve proper compaction. To reduce this "undrained" response of cohesive soils during compaction, a kneading process in which the compactor kneads and remolds compacted soil is employed. This process will facilitate the reduction of the void space to achieve the desired densification. The materials most suitable for kneading compaction are cohesive fine-grained soils such as clayey soils (Adam and Kopf 1998).

2.2.3 Vibratory Compaction

Vibratory compaction applies a periodic mechanical driven force, typically by rotating an eccentric mass along a shaft at the center of a cylindrical compactor drum axis (Figure 2.2). For a heavy compactor drum, the rotation of this eccentric mass leads to a downwards vibratory energy that acts simultaneously with the weight of the compactor to apply downward pressure and vibratory energy into the soil. This applied energy tends to change the nature of particle to particle contacts within the soil mass, facilitating the rearrangement of individual soil particles into a more compact state

(Adam and Kopf 2004). The materials most suitable for vibratory compaction are granular soils such as sands and gravels (Adam and Kopf 1998).

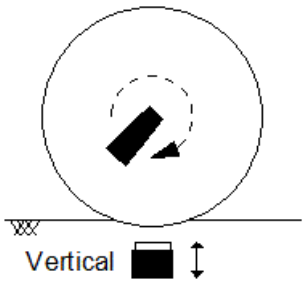

Figure 2.2 Excitation of vibratory roller drum and the resulting dynamic compaction effect (compression) (modified after Brandl and Adam 2004).

In some cases, vibratory rollers provide high vibrations to the soil that may be detrimental to the compaction process. Excessively high energy from a vibratory compactor may cause fracture of individual soil particles and damage to surrounding buildings and/or utilities. It is for this reason that two other types of "dynamic compaction" methods have been developed: oscillatory compaction and vario roller compaction.

2.2.3.1 Oscillatory Compaction

During oscillatory compaction, the roller drum oscillates parallel to the surface that is being compacted. The applied oscillation is caused by two opposite rotating eccentric masses, where the shafts are arranged on opposite sides of the axis of the drum (Figure 2.3).

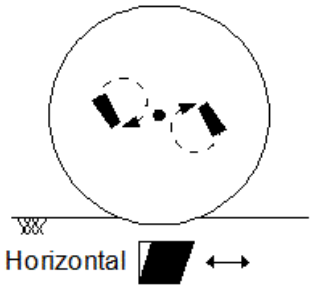

Figure 2.3 Excitation of oscillatory roller drum and the resulting dynamic compaction effect (shearing) (modified after Brandl and Adam 2004).

The motion of the roller causes the soil to be dynamically loaded in a horizontal direction, in addition to the vertical downward static pressure. The cyclic and dynamic horizontal forces result in additional soil shear deformation; dynamic compaction is achieved mainly by transmitted shear waves. Studies have shown that oscillatory rollers operate in two conditions depending on roller operation and soil parameters. If the applied force exceeds the friction force (including the adhesion) at the soil-drum interface, the drum starts slipping (Tehrani 2009). During slipping the compaction effect is reduced; however, the surface is "sealed" by this slip motion. Consequently, oscillatory rollers are mainly employed for asphalt compaction (Tehrani 2009). Oscillatory rollers are also often used near sensitive structures, because the resulting vibrations are typically significantly lower than those of traditional vibratory rollers (Thurner and Sandström 2000, Brandl and Adam 2004).

2.2.3.2 Vario Roller Compaction

In the late 1990's, Bomag Americas, Inc (Bomag) developed the vario roller (Tehrani 2009). The Vario roller system consists of two counter-rotating excitation

masses which are concentrically shafted on the axis of the drum to cause a directed vibration. The direction of excitation can be adjusted by turning the entire excitation unit, in order to optimize the compaction effect for the corresponding soil type (Figure 2.4). If the excitation direction is vertical or horizontal, the compaction effect of the Vario roller is similar to that of the vibratory or oscillatory rollers, respectively. Thus, Vario rollers can be used as a substitute for either vibratory and oscillatory compactors (Brandl and Adam 2004).

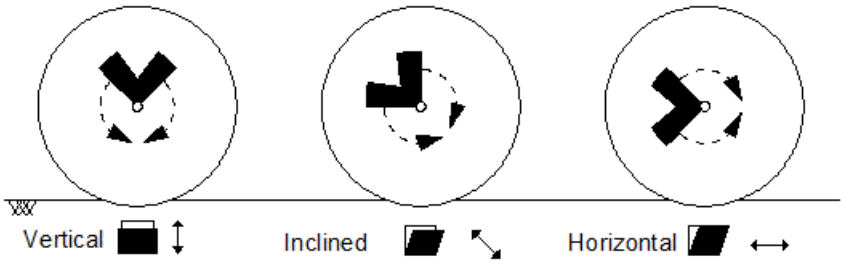

Figure 2.4 Ammann two-piece eccentric mass assembly and variable control of eccentric force amplitude and frequency (modified after Ammann brochure; Bomag brochure; Brandl and Adam 2004).

2.3 Compaction Equipment

Most field compaction equipment will use one of the previously mentioned compaction methods to achieve soil densification. The most commonly used compaction equipment on medium to large projects is compaction rollers. There are many different variations of compaction rollers that can perform static, kneading, and/or vibratory compaction (Table 2.1). For smaller projects, or detail areas on larger projects that require the use of low compactive effort, small compactors such as vibrating plates and tampers are also commonly utilized. Commonly utilized compaction equipment and the associated applications for which this equipment is

used are provided in Table 2.1 (Broms and Forssblad 1969; Holtz and Kovacs 1981; Holtz et al. 2011).

Table 2.1 Types and Applications of Soil Compactors (Modified after Holtz et al. 2011)

Compaction Equipment	Suitable soils	Typical Applications
Smooth-wheel rollers	Granular and cohesive soils	Running surface, base courses, subgrades.
Rubber tired rollers	Granular and cohesive soils	Pavement subgrade.
Sheepsfoot rollers	Cohesive soils	Dams, embankments, subgrades.
Mesh (grid) rollers	Rocky soils, gravels, and sands	Subgrade, subbase.
Vibrating tampers	Granular soils	Detail areas. Fills behind bridge abutments and retaining walls.
Vibrating plates	Granular soils	Detail areas. Fills behind bridge abutments and retaining walls.
Vibrating rollers	Granular soils	Base, subbase, and embankment compaction. Earth dam fills.

2.4 Current Specifications and Compaction Control

For earthwork projects, control of the contractor's compaction process is essential to ensure that the desired design parameters associated with optimal project performance are achieved. Typically, the design engineer will provide specifications for the compaction process. It is then the responsibility of the owner or design engineer to perform quality assurance (QA) testing to verify that the soil has reached the required densification specified by the engineer.

2.4.1 Specifications

There are two general types of specifications for earthwork compaction. They are: (1) method or procedure specifications, and (2) end-product or performance specifications. In addition to the compaction control portion of the specification, there is almost always an additional maximum lift thickness (compacted or loose) criterion.

2.4.1.1 Method Specifications

For a method specification, the type and weight of the compaction equipment, the number of passes, and the maximum lift thickness are specified by the design engineer. This method does not require any QA testing in the field, and therefore the engineer must be certain that the specified compaction process will be adequate to achieve proper compaction. This method requires the engineer have prior experience with the material being compacted. In the event that the engineer does not have experience with the fill material and the compaction equipment being utilized, test sections (test pad areas) must be constrcuted to determine the necessary number of compactor passes and adequate lift thickness. This process can be time consuming and costly, and thus, is usually only utilized for large scale fill projects such as earth dams (Holtz and Kovacs 1981).

2.4.1.2 End-Product Specifications

The end-product specification is much more popular for compaction of highways, building foundations, and embankments (Holtz et al. 2011). Most commonly, for this method, the design engineer will specify a relative compaction (*RC*) value that the contractor must achieve. Relative compaction is defined as the ratio between the measured field dry density and a laboratory measured maximum dry density determined using a standardized compaction test, displayed in percentage form

(Equation 2.1). It is important to note that there are other measurements or criteria in addition to *RC* that can be used in an end-product specification; however, for earthwork compaction specifications the *RC* measurement is the most common at this time.

$$RC = \frac{\rho_{d,\,field}}{\rho_{d,\max}} \times 100 \qquad (2.1)$$

where $\rho_{d,\,field}$ is an in situ measurement of dry density at a single location in the field and $\rho_{d,\max}$ is the maximum dry density of the material as determined from a standardized laboratory compaction test on the same soil.

The standardized laboratory compaction tests that are most commonly used to determine the maximum dry density are the standard proctor test (ASTM D 698) and the modified proctor test (ASTM D 1557). The resulting data from these tests allows for development of a compaction curve for the tested materials. From the compaction curve, the maximum dry density and the optimum soil moisture content can be determined (Figure 2.1). Typically, the engineer will specify that the contractor compact the soil to 90% or 95% relative compaction (Holtz et al. 2011). It should be noted that the soil unit weight may also be used to determine the *RC* value; in this case, the *RC* is the ratio between the field dry unit weight and the maximum dry unit weight.

In addition to the *RC* criteria, the engineer will also typically specify a moisture content range which the soil must be compacted within, and a maximum lift thickness. In the case of end-product specifications, the contractor is free to use the compaction equipment of his or her choice, as long as the specified end-product criteria are achieved. For this method, it is imperative that in situ QA compaction

verification tests be performed to ensure that the contractor has achieved the desired end-product criteria.

2.4.2 In Situ Test Methods

Soil compacted in the field must pass a QA test to verify that adequate compaction has been achieved, in order to ensure the performance of the project. There are various in situ test methods that may be used for this purpose and most of them fall into one of two categories: (1) Density-based tests, and (2) Strength-based tests. The density based tests, as the name implies, attempt to directly or indirectly measure the in situ soil density or unit weight. Strength-based tests, in contrast, attempt to directly or indirectly measure the soil modulus and/or soil stiffness. Some of these tests will measure the moisture content directly as part of the test; if not, then a sample must be taken at the test location and the moisture content must be later determined in the laboratory in accordance with ASTM D 2216-10.

Some of the most common in situ test methods, the respective ASTM references, and the associated units of measurement are provided in Table 2.2. An in depth literature review on the in situ test methods mentioned below, including calculations for all measurements, is provided in Tehrani (2009).

Table 2.2 Summary of In Situ Test Methods for Compaction Verification

Test Method	ASTM Reference	Measurement (units)
Nuclear Density Gauge (NDG)	ASTM D 6938 - 10	Dry Unit Weight, γ_d (kN/m^3), Moisture Content, ω (%)
Sand Cone Equivalent (SC)	ASTM D 1556-00	Dry Unit Weight, γ_d (kN/m^3)
Plate Load Test (PLT)	ASTM D 1196-93	Secant Modulus, E_{PLT} (MPa)
Light Weight Deflectometer (LWD)	ASTM E 2583–07	Elastic Modulus, E_{LWD} (MPa)
Falling Weight Deflectometer (FWD)	ASTM D 4694-96	Elastic Modulus, E (MPa)
Dynamic Cone Penetrometer (DCP)	ASTM D 6951-03	Penetration Index $DCPI_A$, $DCPI_M$
Soil Stiffness Gauge (SSG), also known as the GeoGauge	ASTM D 6758-02	Elastic Modulus, E_{SSG} (MPa)

2.4.2.1 Limitations of the In Situ Test Methods

Although the in situ test methods listed in Table 2.2 are largely used for QA of earthwork compaction, there are several problems associated with these test methods. A number of the limitations are listed below (Holtz and Kovacs 1981):

- Statistical quality control of compaction
- Presence of oversized particles
- Measurement depth limitations
- Lack of lift thickness control

The *statistical quality control of compaction* refers to the low percentage of the compaction area being tested. Since the in situ tests are spot tests, the volume of material involved in each test is an extremely small percentage of the total volume of compacted material, as low as one part in 100,000 (e.g., Holtz and Kovacs 1981).

The *presence of oversized particles* can be extremely problematic for several of the in situ test methods mentioned above. For example, the NDG test is not able to accurately measure the density soils with a high gravel content. This is more of an

issue in the density based test methods, but the strength based tests also have maximum particle size limitations which are noted in the respective ASTM references.

The *measurement depth limitations* corresponds to the measurement depth of the in situ test method not reaching the influence depth of typical compaction equipment. Typical in situ test methods have an influence depth of 20-60 cm and do not sufficiently represent the real influence depth of the compactor's applied energy (Adam 1997, Thurner and Sandström 2000).

The maximum lift thickness component of the compaction control specifications is often overlooked in the discussion of compaction verification. Typical inspection methods involve a field inspector performing visual inspection of the lifts and approving lifts without taking accurate thickness measurements. All of the aforementioned in situ testing devices have a *lack of thickness control*. The result can be non-uniform soils lifts that lead to differential settlements, among other issues (Adam 1997). In addition, the in situ methods discussed above are somewhat time consuming, and adequate field testing for a project can in some cases be relatively expensive (Thurner and Sandström 1980, Adam 1997).

2.5 Continuous Compaction Control and Intelligent Compaction Systems

In an attempt to account for the limitations associated with the current in situ QA test methods mentioned in Section 2.4.2.1, continuous compaction control (CCC) and intelligent compaction (IC) systems have been developed. CCC and IC systems seek to achieve more efficient compaction by reducing the overall compaction time, effectively avoiding: under-compaction (which increases the risk of settlement problems), over-compaction (which wastes time and may crush aggregates), and non-

uniform compaction (which increases the risk of differential settlements) (Thurner 1993).

As noted in Meehan and Tehrani (2011): "*Continuous Compaction Control systems are data acquisition systems installed on compaction equipment that continuously collects real-time information about the operation and performance of the compactor (Thurner and Sandström 1980, Adam 1997, Adam and Brandl 2003). Intelligent Compaction is a machine-driven process whereby CCC data is interpreted and used in real-time to adjust the operation of the compactor in an attempt to optimize the compaction process and to achieve more uniform soil compaction (Adam and Brandl 2003, Anderegg et al. 2006).*"

2.5.1 Components of CCC Systems

Traditional CCC systems consist of several components: the compaction roller, the material being compacted, a real-time global positioning system (GPS), and a data acquisition system. In addition, IC systems will have documentation and feedback control systems built into the compaction rollers. A brief discussion of the components is provided here; a more in-depth discussion can be found in Tehrani (2009).

The compaction roller is an integral component of CCC and IC systems, as it is the basis by which compaction will occur and the platform for the remaining components. Additionally, many of the roller operational parameters (e.g., the excitation frequency, the drum amplitude, the weight ratio between the effective weight of the frame and drum, and the speed of the roller) are used to determine the roller measured values (MV) which provide a basis for understanding the degree of compaction (Adam 1997).

To date, CCC and IC systems have proven applicable for both coarse-grained soils (granular soils) and fine-grained soils (cohesive soils) (Mooney et al. 2011). The only limitation is in regards to the types of roller MV that can be taken. As stated earlier, cohesive materials do not efficiently achieve densification through vibratory compaction (e.g., Holtz and Kovacs 1981; Adam and Kopf 1998). Many of the roller MV rely on soil response to vibratory compaction; consequently, these roller MV are not typically applicable during compaction of cohesive material.

The integration of GPS systems with the compaction rollers allows for the linkage of the roller MV to measurement point coordinates. As a result, the compaction process can be instantaneously recorded and displayed in graphical format (Anderegg et al. 2006). Conventional GPS systems consist of an external reference (base) station that includes a real-time kinematic global positioning system (RTK-GPS), an antenna, and a radio modem transmitter. In addition, these GPS systems use a mobile data acquisition and analysis station that is attached to the roller. The final component of the GPS system is a visual monitoring station, which consists of a computer with a radio modem receiver (Tehrani 2009).

2.5.2 History of CCC and IC Technology

Continuous Compaction Control (CCC) and Intelligent Compaction (IC) technologies can be traced back to 1930, when the first attempt to measure, record, and monitor vibration-integrated measurements during compaction were performed with vibratory plates (Mooney and Adam 2007). Initial development of modern roller integrated measurements dates back to 1974, when Dr. Heinz Thurner of the Swedish Highway Administration performed field studies with a 5-ton tractor-drawn Dynapac vibratory roller instrumented with an accelerometer (Thurner and Sandström 2000).

The tests indicated that, in the frequency domain, the ratio between the amplitude of the first harmonic of the recorded acceleration and the amplitude of the excitation could be correlated to the induced compaction effort and the soil stiffness measured by static plate load tests. Dr. Thurner founded the Geodynamik Company with partner Åke Sandström in 1975, to continue development of the roller-mounted compaction meter. Geodynamik teamed with Dr. Lars Forssblad of Dynapac to develop and introduce the compaction meter and the compaction meter value (CMV) in 1978. This development was introduced at the "First International Conference on Compaction" held in Paris, France in 1980 (Thurner and Sandström 1980, Forssblad 1980). Briefly after Dynapac made the CMV-based compactometer commercially available, many of the roller manufacturers (e.g., Caterpillar, Ingersoll Rand, and Sakai) adopted the Geodynamik CMV-based system for further research and installation on their own construction equipment (Mooney and Adam 2007).

Following the introduction of the CMV value by Dynapac, many other compactor manufacturers began to develop their own roller-integrated measurement values and systems. In 1982, Bomag developed the OMEGA value and corresponding Terrameter. The OMEGA value provided a continuous measurement of compaction energy. Bomag then introduced a new roller-integrated measurement, the vibration modulus (E_{vib}). The vibration modulus provides a measure of dynamic soil stiffness that was intended to serve as a replacement for the OMEGA value (e.g., Kröber et al. 2001). In 1999, Ammann introduced their own soil stiffness parameter (k_s), which similar to the E_{vib} value, offers an indicator measurement of the soil stiffness and/or modulus (Anderegg 1998, Anderegg & Kaufmann 2004). In 2004, Sakai introduced the compaction control value (CCV). The theory behind the CCV is similar in

principle to the CMV; it uses the content from the measured drum vibration to estimate the compacted state of the soil (Scherocman et al. 2007). Caterpillar realized that most of the existing roller-based measurement values (MV) were related to vibration theory. Vibratory compaction is not suitable for the densification of cohesive materials, as described in Section 2.2.3. Consequently, in the early 2000's, Caterpillar developed an alternative CCC system based around machine drive power (MDP) consumption. The MDP measurement offers the ability to quantify the effectiveness of compaction in cohesive materials which do not utilize vibratory compaction, instead using internal measurements of power consumption that are made by the roller during the process of soil compaction.

The aforementioned compaction systems and corresponding measurements fall under the general category of "Continuous Compaction Control" (CCC) technology. "Intelligent Compaction" (IC) systems have also been introduced to enhance the field application of CCC technology. IC systems were developed to help the roller operator optimize the compaction process, assist the contractor in a quality pre-test, and document compaction results (Thurner 1993). Geodynamik was the first to develop a system of this kind, in 1989, referred to as the compaction documentation system (CDS) (Thurner 1993). The introduction of the Vario roller in 1990 (e.g., Figure 2.3) allowed the operator to make real-time roller operation parameter changes during the compaction process. Similarly, Ammann introduced the Ammann Compaction Expert (ACE) roller with servo-hydraulic two-piece eccentric mass and frequency control. Several other compaction roller manufactures including Caterpillar and Dynapac have also pursued and adopted this technology (e.g., Mooney and Adam 2007).

Introduction of servo-controlled vibratory drum systems has led to the general advancement of IC technology. For IC systems, the vibratory force amplitude and/or frequency are automatically adjusted to improve roller performance and compaction (Tehrani 2009). The first prototype of a GEODYNAMIK "Intelligent Compaction Machine, ICM" was on display in 1992 (Sandström and Pettersson 2004). In the following years, development of this technology has continued, but a product has not been made broadly available to the construction community (Sandström and Pettersson 2004). Consequently, some researchers have noted that "Intelligent Compaction" technology is still in the early stages and there are several important issues with current CCC technology which need to be addressed before IC technology can become a reliable compaction approach on live projects (e.g., Mooney and Adam 2007).

2.5.3 Roller Measured Values

The section above offers a brief history of the development of CCC and IC systems and also the corresponding roller measurement values (MV) which have been developed to measure the soil response. The development of roller MV is extremely important, if CCC and IC technology is to be adopted as a QA method for compaction verification. The roller MV types that were discussed previously are summarized in Table 2.3 with a brief definition. For a more robust discussion of these roller MV, the author advises the reader to review Tehrani (2009). In this section, only the CMV and MDP parameters will be described in detail.

Table 2.3 Established CCC systems, CCC values, and the associated equipment manufacturers (Modified after Tehrani 2009)

CCC System	CCC Value	Definition of CCC Value	Manufacturer
Compactometer	CMV (unitless)	acceleration amplitude ratio (first harmonic divided by excitation frequency amplitude) – frequency domain	Geodynamik
Terrameter	OMEGA (N.m)	energy transferred to soil considering soil contact force displacement relationship of two excitation cycles – time domain	Bomag
Continuous Compaction Value	CCV (unitless)	acceleration amplitude ratio – frequency domain	Sakai
Terrameter	E_{vib} (MPa)	dynamic elasticity modulus of soil beneath drum (inclination of soil contact force displacement relationship during loading) – time domain	Bomag
Ammann Compaction Expert	k_s (MN/m)	spring stiffness of soil beneath drum (derived from soil contact force displacement relationship at maximum drum deflection) – time domain	Ammann
Machine Drive Power	MDP (kW)	net power to propel the roller	Caterpillar

2.5.3.1 Compaction Meter Value (CMV)

The Compaction Meter Value (CMV) is a dimensionless compaction parameter developed by Geodynamik that depends on roller dimensions, (i.e., drum diameter and weight) and roller operation parameters (e.g., frequency, amplitude, speed), and is determined using the dynamic roller response (Sandström 1994). CMV is calculated using the following equation (Thurner and Sandström 1980, 2000):

$$CMV = C \times \frac{\hat{a}(2\omega_0)}{\hat{a}(\omega_0)} \tag{2.2}$$

where C is a constant value chosen to empirically scale the CMV output values, $\hat{a}(2\omega_0)$ is the amplitude of the first harmonic of the acceleration response signal, and $\hat{a}(\omega_0)$ is the amplitude of the excitation frequency (Thurner and Sandström 1980, 2000). The typical C value used for calculating CMV values from measured vibratory roller data is 300 (Sandström and Pettersson 2004). The theory of development of different harmonic components of drum vibration with increasing ground stiffness is presented in Figure 2.5.

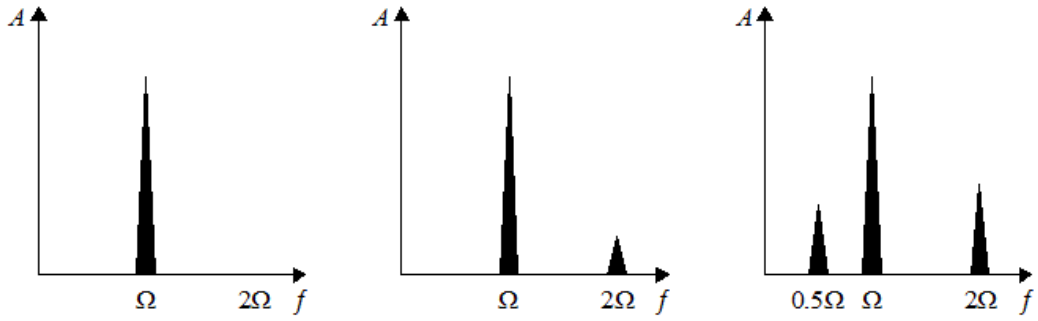

Figure 2.5 Illustration of changes in drum harmonics with increasing ground stiffness (modified after Thurner and Sandström 1980).

Many studies have been performed to develop the relationships between CMV and soil parameters (dry unit weight and stiffness). In general, the research has shown that CMV values tend to increase as the stiffness and dry unit weight of soil increases (e.g., Floss et al. 1983; Samaras et al. 1991; Tehrani 2009). Caterpillar, Dynapac, and Volvo/Ingersoll Rand CCC systems have made use of the Geodynamic CMV.

It is typical for Compactometer systems to simultaneously calculate resonant meter values (RMV) when recording CMV measurments (Vennapusa et al. 2010). The

RMV provides an indication of the drum behavior (e.g., continuous contact, partial uplift, double jump, rocking motion, and chaotic motion) and is calculated using the following equation:

$$RMV = C \times \frac{\hat{a}(0.5\omega_0)}{\hat{a}(\omega_0)} \tag{2.3}$$

where C is a constant value chosen to empirically scale the RMV output values, $\hat{a}(0.5\omega_0)$ is the amplitude of subharmonic acceleration caused by jumping (the drum skips every other cycle), and $\hat{a}(\omega_0)$ is the amplitude of the excitation frequency (Mooney et al. 2010). It is important to note that the drum behavior affects the CMV measurements, and thus RMV values must be interpreted simultaneously when evaluating CMV measurements (Brandl and Adam 1997; Vennapusa et al. 2010).

As noted in the previous paragraph, there are five modes of operation that are typically encountered during vibratory compaction of soils: (1) continuous contact; (2) partial uplift; (3) double jump; (4) rocking motion; and (5) chaotic motion (Anderegg and Kaufmann 2004). Continuous contact occurs during the beginning of the compaction process when the soil stiffness is extremely low (Adam 1997, Brandl and Adam 2004). As the soil stiffness increases the partial uplift and double jump modes set in. They are the most frequent during vibratory compaction with the only difference being that the double jump mode contains more excitation cycles (Adam 1997). The rocking motion phase can occur as the soil stiffness increases, as a result of the misalignment of the drum from the vertical axis (Adam 1997, Brandl and Adam 2004). The chaotic motion occurs when the soil stiffness becomes extremely high (Adam 1997). The chaotic behavior of the vibratory roller originates from the

nonlinearity and occurrence of subharmonics during compaction. The double jump, rocking motion, and chaotic motion modes are undesirable as they may have a loosening effect on the top layer of the soil and cause the roller to lose its maneuverability (Anderegg and Kaufmann 2004). This is why it is important to interpret the RMV simultaneously with CMV measurements. The five operation modes are summarized in Table 2.4.

Table 2.4 Operation Modes of a Vibratory Roller Drum (modified after Tehrani 2009)

Drum-Soil Interaction	Cycle*	Operation Mode	Application of CCC	Soil Stiffness	Roller Speed	Drum Amplitude
Contact	1	Continuous contact	Yes	Low	Slow	Small
Partial loss of contact	1	Partial uplift	Yes	↓	↓	↓
	2 (4)	Double jump	Not Recommend			
	2 (4)	Rocking motion	No			
	-	Chaotic motion	No	High	Fast	Large

*Cycles are specified as a multiple of the excitation cycle, $T = 2\pi/\omega_0$.

2.5.3.2 Machine Drive Power (MDP)

Machine drive power is a mathematically determined value of power that isolates the internal resistance to compactor drum rolling that is provided by the soil (White et al. 2006).The basic premise of determining soil densification from the changes in roller operational parameters is that the efficiency of mechanical motion

pertains to the physical properties of the material being compacted (White et al. 2011). The calculation process for MDP is shown in Equation 2.4 (White et al. 2006).

$$MDP = P_g - WV\left(\sin\alpha + \frac{a}{g}\right) - (mV + b) \quad (2.4)$$

where P_g is net power required to propel the compactor over the fill material, W is roller weight, V is roller velocity, a is acceleration of the machine, g is acceleration of gravity, α is the slope angle, and m and b are machine internal loss coefficients specific to a particular machine. The MDP value can be calculated during both static and vibratory compaction. Previous research has shown that when compacting with a drum roller, as the soil densification increases, the energy required to propel the roller decreases, and MDP decreases (White et al. 2006).

It is important to note that MDP calculations are specific to the compaction equipment being used. In order to compare the MDP values from different research projects, the MDP value must be standardized. It is for this reason that machine calibrated formulas have been developed to calculate the standardized machine drive power value (MDP*). The MDP* calculation is different for each specific compactor and, therefore, a general formula cannot be presented here. It should be noted that it is typical for MDP* to be referred to simply as MDP, thus, it is important to investigate the specific MDP calculation being used when comparing MDP measurements from different projects (e.g., Meehan and Tehrani 2011).

2.6 Field Evaluation of Roller MV

Modern CCC and IC systems make it possible to collect, transmit, and visualize a variety of roller MV (e.g. CMV and MDP) in real time (White et al. 2011). These roller MV were developed to produce a quantifiable measurement of the

compaction process. The purpose of the CCC and IC systems are to facilitate a more efficient compaction process by offering a real time QA tool with nearly 100 percent coverage of the compaction area. As described in Section 2.4.2, current compaction verification tools most commonly utilize “spot” measurements of material unit weight, modulus, stiffness, and/or moisture content. These soil properties are measured because they directly relate to the densification process. Therefore, it is only logical for the CCC and IC roller MV to be compared with these soil properties. Significant research has been performed comparing various common compaction verification in situ test method measurements to the recently developed roller MV. An extensive review of this research was performed by White et al. (2011), which will be discussed in more detail later in this chapter. It should be noted that in order for direct comparison of roller MV to be made versus in situ test measurements, geospatial interpolation techniques must be utilized to ensure that measurements are being compared at the same test locations. These geospatial interpolation techniques will be discussed in more detail in Section 2.8, and in later chapters in this thesis.

A comprehensive review of previous research comparing the results of in situ QA/QC test methods and roller CCC measurements was performed by White et al. (2011). In this literature review, the reference, project location, compaction roller type, roller MV, soil type, in situ test method, and the key findings from each study were summarized. A summary of the literature review results presented by White et al. (2011) is as follows:

2.6.1 Forssblad (1980)

In Sweden, a Dynapac smooth drum roller measuring CMV was utilized to compact fine and coarse rock fill. The in situ test methods performed included

water balloon, PLT, FWD, and surface settlement. Key findings and comments include:

- Linear correlations are observed between CMV and the in situ test method MV.
- Moisture content should be considered in correlations for fine-grained soils.
- Roller results in a composite value in a layered soil condition.
- CMV is affected by roller speed (higher roller speeds result in lower CMV).

2.6.2 Hansbo and Pramborg (1980)

In Sweden, a Dynapac smooth drum roller measuring CMV was utilized to compact gravelly sand, silty sand, and fine sand. The in situ test methods performed included sand cone, pressuremeter, PLT, cone penetrometer test (CPT), and DCP tests. Key findings and comments include:

- Compaction growth curves showed improvement in CMV and other mechanical properties (i.e., modulus and cone resistance) with increasing pass.
- Relative percent compaction (or density) was not sensitive to changes in CMV.

2.6.3 Floss et al. (1983)

In Munich, Germany, a Dynapac smooth drum roller measuring CMV was utilized to compact sandy to silty gravel fill. The in situ test methods performed

included water balloon and sand cone, PLT, and DCP. Key findings and comments include:

- Correlations with modulus and DCP measurements are generally better than density.
- CMV measurements are dependent on speed, vibration frequency and amplitude, soil type, gradation, moisture content, and the strength of the subsoil.

2.6.4 Brandl and Adam (1997)

A Bomag smooth drum roller measuring CMV was utilized and the in situ test method performed was the PLT. Key findings and comments include:

- Correlation between CMV and PLT modulus (initial) showed different regression trends for partial uplift and double jump operating conditions.
- Regressions in partial uplift and double jump conditions yielded R^2 = 0.9 and 0.6, respectively.

2.6.5 Nohse et al. (1999)

In Tomei, Japan, a Sakai smooth drum roller measuring CMV was utilized to compact clayey gravel, and the in situ test measurement recorded was the soil radio-isotope. Key findings and comments include:

- Dry density and CMV increased with increasing roller pass on a calibration test strip.
- Linear regression relationships with $R^2 > 0.9$ are observed for correlations between dry density and CMV.

2.6.6 White et al. (2004; 2005)

In Edwards, Illinois, a Caterpillar pad-foot drum roller measuring MDP was utilized to compact lean clay. The in situ test methods performed included NDG, drive core, DCP, and clegg hammer. Key findings and comments include:

- Correlations between MDP and in situ test measurements using simple and multiple regression analyses are presented.
- MDP correlated better with dry density ($R^2 = 0.86$) than with DCP ($R^2 = 0.38$) or Clegg impact value ($R^2 = 0.46$).
- Including moisture content via multiple regression analysis improved the R^2 values for DCP and Clegg impact value ($R^2 > 0.9$). Results are based on data averaged along a 20m long strip per pass.

2.6.7 Peterson and Peterson (2006)

In Duluth, Minnesota, a Caterpillar smooth drum roller measuring CMV and MDP was utilized to compact fine sand. The in situ test methods performed included LWD, DCP, and GeoGauge. Key findings and comments include:

- Weak correlations are obtained on an in situ test method by-point basis comparison between in situ test measurements and roller measurements, likely due to the depth and stress dependency of soil modulus and the heterogeneity of the soils.
- Good correlations are obtained between CMV values and DCP measurements for depths between 200 and 400 mm.

2.6.8 White et al. (2006a; 2006b)

In Edwards, Illinois, a Caterpillar smooth drum roller measuring MDP was utilized to compact well-graded silty sand. The in situ test methods performed included NDG and DCP. Key findings and comments include:

- Average MDP values showed a decreasing trend on a log scale, and dry unit weight and DCP index values showed an asymptotic decrease with increasing roller pass.
- Correlations between MDP and in situ test method MV showed good correlations (R^2 = 0.5 to 0.9). Incorporating moisture content into the analysis is critical to improve the correlations for dry unit weight.

2.6.9 Thompson and White (2008)

In Edwards, Illinois, a Caterpillar pad-foot drum roller measuring MDP was utilized to compact silt and lean clay. The in situ test methods performed included NDG, DCP, clegg hammer, and LWD. Key findings and comments include:

- Correlations between MDP and the in situ test method MV are presented using simple and multiple regression analysis.
- Averaging the data along the full length of the test strip (per pass) improved the regressions.
- Multiple regression analyses that incorporating moisture content as a regression parameter further improved the correlations.

2.6.10 White et al. (2008)

In Ackley, Minnesota, a Caterpillar smooth drum roller measuring CMV was utilized to compact poorly graded sand well-graded sand with silt. The in situ test

methods performed included NDG, DCP, and LWD. Key findings and comments include:

- Project scale correlations by averaging data from different areas on the project are presented, which showed R^2 values ranging from 0.52 for density and 0.79 for DCP index value. Correlations with LWD showed poor correlations due to the effect of loose material at the surface.
- The variability observed in the CMV data was similar to DCP and LWD measurements but not to density measurements.

2.6.11 Vennapusa et al. (2009)

In Edwards, Illinois, a Caterpillar pad-foot drum roller measuring MDP was utilized to compact crushed gravel base. The in situ test methods performed included DCP and LWD. Key findings and comments include:

- Correlations were obtained on a test bed with multiple lifts placed on a concrete base and a soft subgrade base.
- Correlations between MDP and in situ test method MV yielded R^2 = 0.66 to 0.85 for spatially nearest point data, and R^2 = 0.74 to 0.92 for averaged data (over the length of concrete or soft subgrade).

2.6.12 Mooney et al. (2010)

In 2010, the National Cooperative Highway Research Program (NCHRP) published a comprehensive report (Final Report NCHRP 21-09) titled “Intelligent Soil Compaction Systems”. In this report CCC and IC technologies are extensively discussed and, most relevant for this discussion, the results of research on the correlations between roller MV and in situ test methods are presented.

The report discusses projects which took place in Minnesota, Colorado, Maryland, North Carolina, and Florida. The compaction rollers utilized in these projects included a Caterpillar pad-foot drum roller measuring MDP, a Caterpillar smooth drum roller measuring CMV, and a Dynapac smooth drum roller measuring CMV. In addition, several in situ test methods were conducted including NDG, DCP, LWD, FWD, PLT, clegg hammer, and GeoGauge. Key findings and comments from these studies include:

- Simple and multiple regression analysis results are presented.
- Simple linear correlations between roller MV and in situ test method MV are possible for a compaction layer underlain by relatively homogenous and a stiff/stable supporting layer.
- Heterogeneous underlying conditions can adversely affect the correlations.
- A multiple regression analysis approach is described that includes parameter values to represent underlying layer conditions to improve correlations.
- Modulus measurements generally capture the variation in roller MV better than dry unit weight measurements.
- DCP tests are effective in detecting deeper “weak” areas that are commonly identified by roller MV and not by compaction layer in situ test method MV.
- High variability in soil properties across the drum width and soil moisture content contribute to scatter in relationships.

- Averaging measurements across the drum width, and incorporating moisture content into multiple regression analysis, can help mitigate the scatter to some extent.
- Relatively constant machine operation settings (i.e., amplitude, frequency, and speed) are critical for calibration strips and correlations are generally better for low amplitude settings (e.g., 0.7 to 1.1mm).

2.6.13 Summary of Findings

Based upon the findings from the aforementioned field studies examining the relationships between soil properties and CCC measurements, the common factors that affect correlations are as follows (White et al. 2011):

- Heterogeneity in underlying layer support conditions
- Moisture content variation
- Narrow range of measurements
- Machine operation setting variation (e.g., amplitude, frequency, speed, and roller "jumping")
- Nonuniform drum/soil contact conditions
- Uncertainty in spatial pairing of point measurements and roller MV
- Limited number of measurements
- Not enough information to interpret the results
- Inherent measurement errors associated with the roller MV and in situ point measurements

2.7 CCC Specifications

The use of CCC during earthwork compaction as a tool for quality assurance/quality control (QA/QC) has been employed in European specifications for nearly 30 years (e.g., Thurner and Sandström 1980; Forssblad 1980). CCC specifications have been developed in Austria (1990, 1993, 1999; see RVS 8S.02.6 1999), Germany (1994, 1997, 2009; see ZTVA-StB 1997), Sweden (1994, 2004; see VVR VÄG 2009), and Switzerland (2006); followed by The International Society for Soil Mechanics and Geotechnical Engineering which loosely based it's specifications on the Austrian CCC specifications (ISSMGE 2005, Adam 2007).

The United States has been comparatively slow to adopt CCC technology, but in recent years several draft specifications have been developed. The first specification was published by the Minnesota DOT (Mn/DOT 2007, Mn/DOT 2010), then the Texas DOT (TxDOT 2008) followed suit. In 2011, the FHWA established a general IC specification document to encourage more state DOT's to develop CCC and IC specifications (FHWA 2011a, 2011b). The Indiana DOT (InDOT 2012) was the last to develop a specification. An in-depth discussion of current CCC specifications can be found in Tehrani (2009) and Mooney et al. (2010).

In general, the specifications listed above fall under two compaction verification approaches. The first is field calibration of roller MV to stiffness or moisture content/dry unit weight test data using calibration areas. The other method is the identification of weak areas for assessment with conventional QA in situ test methods (e.g., NDG, LWD, etc.). In this section, the three most commonly recommended QA/QC acceptance options (QA/QC Options 1, 2a, 2b, and 3a in Mooney et al. 2010) for compaction control using CCC and IC technology will be presented. All of the acceptance methods utilized in the aforementioned specifications,

both in the United States and in Europe, can be categorized into one of these QA/QC options.

Prior to introducing specific details of the existing specifications and associated compaction verification approaches there are several issues which must be further clarified, following the recommendations outlined in Mooney et al. (2010).

2.7.1 Specification Terminology

For consistency with current CCC/IC practice in the United States, the following terminology that is presented uses the exact definitions that are presented by Mooney et al. (2010):

- "*Automatic Feedback Control*: automatic adjustment of roller *Operating Parameters* such as vibration frequency and amplitude based on real-time feedback from measurement system.
- *Calibration Area*: an area representative of an *Evaluation Section* but typically smaller and used to establish a *MV-TV*.
- *Compaction Pass*: a static or vibratory roller pass performed during earthwork compaction, not necessarily employing an *Instrumented Roller*.
- *Continuous Compaction Control (CCC)*: continuous monitoring and documentation of earthwork compaction using an Instrumented Roller.
- *Evaluation Section*: an area of earthwork with consistent properties where acceptance is evaluated.

- *Instrumented Roller*: a roller compactor outfitted with drum vibration instrumentation or other means to compute a *Roller Measurement Value*, onboard computer, and position monitoring equipment.
- *Intelligent Compaction*: the combined use of an *Instrumented Roller* and *Automatic Feedback Control* in an attempt to improve earthwork compaction.
- *Layer*: a component of the pavement earthwork with distinct soil properties (e.g., subgrade, subbase, or base course).
- *Lift*: a unit of material within a *Layer* that is deposited at one time for compaction. A *Layer* may be comprised of a single lift or multiple lifts.
- *Measurement Depth*: the soil depth to which *Roller Measurement Values* or *In Situ-Test Measurements* are representative.
- *Measurement Pass*: a pass performed by an Instrumented Roller during which all required information, including *Roller Measurement Values* and machine position, are recorded. Roller *Operating Parameters* must be held constant, and thus no *Automatic Feedback Control* is permitted during a Measurement Pass.
- *MV Reporting Rate*: the time-dependent rate at which new *Roller Measurement Values* are reported.
- *MV-TV*: a target *Roller Measurement Value* (e.g., the measurement value corresponding to a *QA-TV*).
- *Operating Parameters*: roller machine parameters used during operation, including forward speed, driving direction, vibration frequency, and eccentric force amplitude.

- *Pass Sequence*: a record of the roller pass history (pass number, *Operating Parameters*) over a specified area.
- *Quality Assurance (QA)*: evaluation methods and procedures administered by the owner or owner's representative to ensure that the constructed earthwork meets contract obligations.
- *QA-TV*: the *In Situ-Test measurement*–based QA target value specified in the project contract.
- *Quality Control (QC)*: testing performed by the contractor or contractor's representative to ensure that the constructed earthwork meets contract obligations.
- *Roller Measurement Value (MV)*: the roller-based parameter used for assessment of soil stiffness during compaction and based on roller vibration measurements.
- *Rolling Pattern*: the path traversed by the roller during a *Measurement Pass*.
- *In Situ Test Measurement*: a field test used during earthwork QC and QA that provides a measurement at a discrete location; common examples include the nuclear gauge for density and moisture and the lightweight deflectometer."

2.7.2 Important Considerations

2.7.2.1 Applicable Soil Types

Continuous compaction control specifications are applicable to cohesive soils, cohesionless soils, and aggregate base materials. However, particular attention must be

given to the soil moisture content during compaction, especially for cohesive soils (Mooney et al. 2010).

2.7.2.2 Personnel Requirements

The implementation of CCC technology for earthwork compaction verification requires QA personnel (e.g., Field Technicians/Inspectors) that are familiar with the aspects of CCC and IC equipment, compaction implementation, and specification implementation. The QA personnel must be able to facilitate and verify appropriate evaluation sections and calibration areas. In addition, the QA personnel must be able to direct the compaction process in regards to the roller operational parameters and measurement pass procedures. This requires that the QA personnel be able to analyze measurement pass data in a timely and efficient matter. It is recommended that all field personnel assigned to the QA process of CCC and IC compaction undergo a certification process (Mooney et al. 2010).

2.7.2.3 Roller Operating Parameters

As mentioned in Section 2.5.3, the roller MV are dependent on the roller operating parameters (e.g., the theoretical vertical drum vibration amplitude (*A)*, excitation frequency (*f*), forward velocity (*v*), and roller travel direction. Consequently, roller operating parameters, including *A*, *f*, *v*, and travel direction must remain constant during all measurement passes. Therefore, IC technology which utilizes automatic feedback control cannot be used during measurement passes.

Variations in roller *Operating Parameters* should remain within the following tolerances: ±0.2 mm (0.0008 in) for *A*, ±2 Hz for *f*, and ±0.5 km/h (0.3 mph) for *v* (Mooney et al. 2010). If provided, vibration amplitudes recommended by the

manufacturer should be used. If not, *A* values between 0.7 and 1.1 mm are recommended for *Measurement Passes*. Common vibration frequencies range from 28 to 32 Hz, and common roller speeds range from 3.0 to 5.5 km/h (1.9 to 3.4 mph) (Mooney et al. 2010). Roller MV acquired during startup, stopping, and turning should not be used for QA because they typically violate the aforementioned tolerances.

2.7.2.4 Evaluation Section

For compaction verification using CCC and IC technologies, acceptance testing must be performed on evaluation sections (Mooney et al. 2010). An evaluation section is a section of the compaction zone where the compacted material exhibits consistent properties. These consistent properties may be examined by viewing the spatial map of roller MV. A typical evaluation section will incorporate the full width of the compaction zone and a length that is dependent on the pace of construction and the longitudinal heterogeneity of the compacted material, among other factors. In the longitudinal direction, factors such as change in borrow material or a transition from a cut to a fill section could justify the separation of evaluation sections. In the transverse direction, the edge material will commonly show highly variable roller MV and, thus, should not be included within the evaluation section (Mooney et al. 2010).

2.7.2.5 Calibration Area

One of the possible acceptance criteria methods requires the development of correlations between in situ test measurements and roller MV. With these correlations, a MV-TV can be selected that corresponds to the acceptance criteria for the in situ test approach that is currently employed within a given QA/QC framework (e.g., for NDG testing, a MV-TV that corresponds with 95 % relative compaction may be selected).

Using this approach, it is necessary to define a calibration area for determination of the MV-TV. The calibration area must be representative of the evaluation section and, therefore, it is best that the calibration area be a portion of the evaluation section when possible. The typical calibration area should range in size from a single roller lane width by 30m (100ft) long to the full width of the earthwork section by 100 m (330 ft) long (Mooney et al. 2010). In addition, the calibration area material must be constructed in the same manner as the evaluation section. To this end, the roller operating parameters, material type, material placement procedures, lift thickness, underlying sub-lift conditions, and the material moisture content must be the same as the evaluation section. It is recommended that the calibration area should capture at least 50 % of the roller MV variation seen in the evaluation section. As mentioned previously, roller start up, stopping, and turning all dramatically affect the roller MV and MVs during these operations should not be included in the calibration of the MV-TV (Mooney et al. 2010). Additionally, the material stiffness of the edge lanes and areas near detail work (e.g., compaction above shallow utilities) can be vastly different than the rest of the compaction zone. Consequently, roller MV from these areas should not be included in the calibration readings. However, if a large portion of the compaction zone is to be influenced by these conditions, then separate MV-TV must be determined for the detail compaction areas (Mooney et al. 2010).

In the event that the evaluation section conditions are significantly changed from the calibration area, then recalibration of the MV-TV is required. Periodically, the validity of the MV-TV must be verified by comparing roller MV and in situ-test measurements from the current evaluation section to the relationship developed in the initial calibration area (Mooney et al. 2010).

2.7.3 Instrumented Roller Requirements

The selected instrumented roller for compaction must be approved to meet the minimum requirements with respect to roller MV reliability, documentation, and measurement position reporting. Additionally, it is extremely important that the selected roller be proven capable of achieving the required level of compaction in a timely manner (Mooney et al. 2010).

2.7.3.1 Roller MV and Position Reporting

Roller MV should be recorded in a constant spatial resolution within a range of 0.2 to 1.0 m (8 to 40 in) and each recorded roller MV should be a unique measurement. Each recorded roller MV should represent a spatial average over, at a minimum, the distance of the roller MV acquisition resolution (Mooney et al. 2010).

For all recorded roller MV, a corresponding three-dimensional position measurement, determined via roller-mounted GPS, must be recorded. A RTK-GPS is recommended for the positional measurements. Each recorded position should reflect the geometric mid-point of the compacted area over which the corresponding roller MV was determined (Mooney et al. 2010).

2.7.3.2 Documentation

The following parameters must be documented by the instrumented roller (Mooney et al. 2010):

- Roller MV
- Three-dimensional position and corresponding time stamp (via GPS)
- Vibration amplitude, A
- Vibration frequency, f
- Roller travel speed, v

- Driving direction
- Status of automatic feedback control (on/off)
- Indication of jumping (vibratory mode of operation)

The recorded parameters mentioned above should be easily accessible through the instrumented roller's on-board computer system. Proper units should be recorded for each of the parameters of interest noted above. Additionally, the recorded data should be easily exportable to simple text files for analysis and documentation. Proprietary formatted files that are only compatible with a specific manufacturer's software are unacceptable.

Basic statistical variables for the collected roller MV and operating parameters should be easily attainable. Of particular importance are the minimum, maximum, mean, standard deviation, and histogram of roller MV, vibration amplitude, frequency, and speed. This will provide the QA personnel with necessary information to efficiently determine if the measurement pass has reached the acceptance criteria (Mooney et al. 2010).

2.7.3.3 Verification of Roller MV Repeatability

The ability of the instrumented rollers to provide precise repeatable roller MV is extremely important. The procedure to verify the instrumented roller's ability to provide repeatable roller MV is as follows (Mooney et al. 2010):

1. Perform two measurement passes on a fully compacted test strip at least 100 m (330 ft) long. The measurement passes must be performed in the same direction, with static passes performed in the reverse direction between measurement passes.

2. Using the recorded roller MV from the two measurement passes, calculate the spatial percent difference array $\%\Delta MV_i$ using the following equation(Mooney et al. 2010):

$$\%\Delta MV_i = \frac{MV_i - MV_{i-1}}{MV_{i-1}} \times 100 \qquad (2.4)$$

where MV_i and MV_{i-1} represent the *MV* data arrays from pass *i* and pass *i–1*, respectively. When necessary, simple linear interpolation may be used to transform the data onto a grid for precise spatial comparison. If the mean of the spatial percent difference array ($\mu_{\%\Delta MV_i}$) is greater than 5%, the lift has likely not achieved the desire level of compaction and the procedure should be repeated.

3. Compute the standard deviation of the spatial percent difference array ($\sigma_{\%\Delta MV_i}$). The standard deviation offers a quantitative measure of the roller MV repeatability. The recommended acceptable values are $\sigma_{\%\Delta MV_i} \leq 10\%$, though visual inspection and engineering judgment should be employed by the QA personnel during investigation of repeatability and when deciding the necessary level of repeatability on a given project (Mooney et al. 2010).

2.7.3.4 Roller Position Reporting

The accuracy of the roller-mounted GPS position, the position offset between the receiver and the center of the drum (e.g., where MVs are computed), and/or errors due to data averaging must be properly accounted for and verified. This is particularly important for acceptance criteria which rely on direct comparisons between roller MV

and in situ test measurements and options that use spatial comparison of roller MV from consecutive measurement passes. Therefore, the accuracy of the roller MV position recording must be verified, both when the roller is stationary and moving.

For stationary verification, the roller-mounted GPS position can be compared with the position from a handheld RTK GPS unit (which is commonly referred to as a "rover") placed at the drum center. Another method is to establish a marker having a known position on the ground and drive over the marker with the roller from different directions. The GPS position measurements from each direction can then be compared and a correction should be implemented, if necessary.

To verify the roller MV position recording accuracy while the roller is moving, the following process is recommended (Mooney et al. 2010):

1. Place two obstructions in the compaction zone, minimally spaced 10 m apart, that will result in obvious outlier readings in the roller MV data. The obstructions should span the full width of the roller drum and may include a wooden beam and/or narrow trenches perpendicular to the direction of roller travel.
2. Perform two measurement passes, in opposite travel directions, over the obstructions.
3. Overlay the recorded roller MV and position data from the two measurement passes. The corresponding spike in the roller MV data should occur at the same location. Any difference in location is indication of GPS position error. If the position error is greater than one-half of the Roller MV reporting resolution or the accuracy of the GPS, the position error must be corrected.

2.7.4 Acceptance Option 1: Spot Testing of Roller Measured Weakest Areas

Option 1 uses CCC roller MV to identify the weakest areas of the evaluation section. The weakest areas are defined as the areas with roller MV representing lower compaction. If the roller MV has a positive correlation with the in situ test measurements, then this area is defined as the area with the lowest roller MV (i.e., CMV versus density/unit weight). On the contrary, if the roller MV has a negative correlation with the in situ test measurements, then this area is defined as the area with the highest roller MV (i.e., MDP versus density/unit weight). In order for Option 1 to be valid, it must be shown that a direct correlation exists between the roller MV and the in situ test measurements. The correlation can be shown through a direct comparison of roller MV and in situ spot test measurements at identical locations. The QA personnel must prove this correlation before Option 1 may be used for compaction verification.

For Option 1, acceptance of compaction will be determined by the QA personnel based upon in situ spot test measurements at the weakest areas of the evaluation section. If the in situ spot test results from the weakest areas meet the spot-test measurement requirement (QA-TV), then the lift meets the acceptance criteria. The QA spot testing procedure within the weakest areas should be performed in accordance with existing earthwork compaction specifications for spot test measurements. A more detailed explanation of Option 1 may be found in Mooney et al. (2010).

2.7.5 Acceptance Option 2: Limiting Percentage Change in Roller Measured Values

QA Option 2 utilizes the percent change in roller MV from successive passes to determine acceptance of the evaluation section. Acceptance is met when the percent

change in roller MV from pass to pass has met the specified target percent change in roller MV for successive passes (%Δ-*TV*). There are two alternative approaches to implement Option 2. The more simplistic approach is Option 2a, in which a comparison of the mean of the roller MV from pass to pass ($\%\Delta\mu_{MV_i}$) is performed. The more complex approach, Option 2b, utilizes a comparison of the spatial change in roller MV from pass to pass. This method requires that the roller MV from successive measurement passes be at the exact same locations to determine the spatial percent change in roller MV ($\%\Delta MV_i$). The nature of the data acquisition systems on the rollers does not allow for the roller MV to be recorded at identical locations from pass to pass, therefore, the data must be interpolated onto a consistent grid for comparison purposes. Due to the directional influence of the roller on the roller MV, it is important that the measurement passes be performed with an identical driving pattern, speed, and amplitude of vibration. Option 2 verifies that the material has reached the compaction limit for the roller in use and does not necessarily verify that maximum density has been met. Verification of the compaction capability of the roller to reach the specified compaction criteria is necessary before Option 2 may be implemented.

2.7.5.1 Acceptance Option 2a: Limiting Percentage Change in the Mean of the Roller-Measured Values

QA Option 2a requires that the $\%\Delta\mu_{MV_i}$ from two successive measurement passes be less than or equal to the specified target value for $\%\Delta\mu_{MV_i}$. If $\%\Delta\mu_{MV_i} \leq \%\Delta - TV$, then the acceptance criteria is met and compaction is complete. The computation for $\%\Delta\mu_{MVi}$ is as follows:

$$\%\Delta\mu_{MV_i} = \left(\frac{\mu_{MV_i} - \mu_{MV_{i-1}}}{\mu_{MV_{i-1}}} \right) \times 100 \qquad (2.5)$$

where μ_{MV_i} is the average roller MV for measurement pass *i*, and $\mu_{MV_{i-1}}$ is the average roller MV for the measurement pass immediately preceding measurement pass *i*. A typical recommended value for the %Δ-*TV* is 5 percent (Mooney et al. 2010). Due to the magnitude of range variability of roller MV and the influence of material on the variability of roller MV, a given recommended value of %Δ-*TV* may not be applicable for all projects. Several methods have been proposed to determine the %Δ-*TV* based on site specific data; for the sake of brevity these will not be discussed herein – interested readers are referred to Facas et al. (2011).

2.7.5.2 Acceptance Option 2b: Limiting Spatial Percentage Change in the Roller-Measured Values

QA Option 2b relies on a spatial comparison of roller MV from successive measurement passes. The roller MV for each measurement pass must be interpolated onto a consistent grid by the QA personnel, and then the spatial percent difference in roller MV for successive measurement passes, $\%\Delta MV_i$, may be computed according to the following equation:

$$\%\Delta MV_i = \left(\frac{MV_i - MV_{i-1}}{MV_{i-1}} \right) \times 100 \qquad (2.6)$$

where $\%\Delta MV_i$ is a vector of the spatial percent difference in roller MV for successive measurement passes, MV_i is a vector of the roller MV for measurement pass *i*, and MV_{i-1} is a vector of the roller MV of the pass immediately preceding measurement pass *i*.

Theoretically, acceptance would require that 100% of the grid points in the evaluation section meet the %Δ-*TV* requirement. Due to measurement error and soil variability, it is not practical that all of the data meet the requirement. Instead, acceptance of the evaluation section occurs when a specified percentage of

$\%\Delta MV_i \leq \%\Delta - TV$ (e.g., acceptance of the evaluation section occurs when 95% of the roller MV increase by %Δ-*TV*). The recommended range for percentage of the roller MV that meet the %Δ-TV requirement is 80% to 95%. The recommended value for %Δ-*TV* is double the standard deviation of the roller MV, $\sigma_{\%\Delta MV}$, determined through assessment of the measurement repeatability of the CCC roller. This process is site specific and further explanation can be found in Mooney et al. (2010). The maximum allowable $\sigma_{\%\Delta MV_i}$ is 10% and, therefore, the recommend maximum value for %Δ-*TV* is 20% for QA Option 2b.

2.7.6 Acceptance Option 3: Comparison of Roller-Measured Values to In Situ Measured Values

QA Option 3 relies on statistical regression analysis between roller MV and in situ spot test measurements. The target roller measured value (MV-TV) is determined based on the in situ test measurement acceptance value (QA-TV), which is typically established using a regression analysis approach (Figure 2.6a).

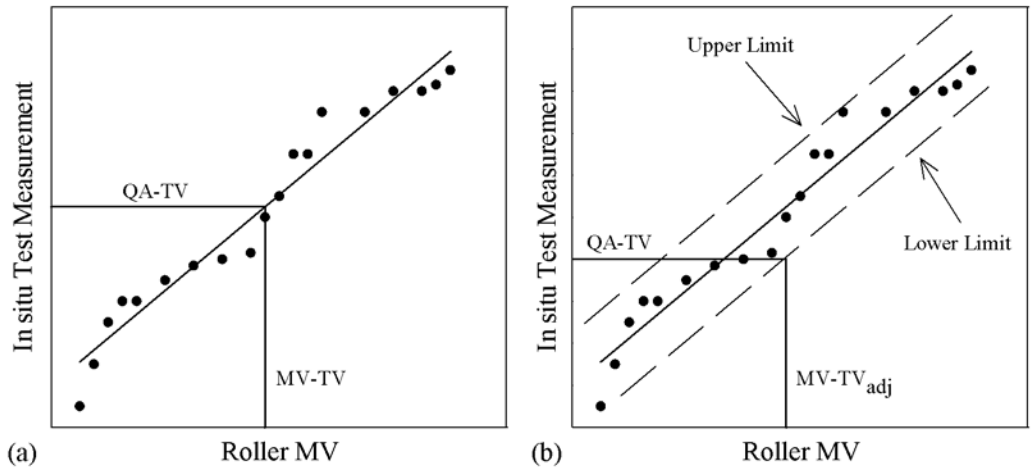

Figure 2.6 Option 3: (a) Determination of MV-TV; (b) Determination of MV-TV_{adj}.

A calibration area constructed with site specific soil will need to be tested with both an instrumented roller and an accepted QA/QC in situ test, in order to determine the appropriate MV-TV via regression analysis (Figure 2.6a). The calibration area should be compacted to represent areas of low, medium, and high compaction, with the highest level of compaction being greater than or equal to the QA-TV. This will ensure a statistically representative data set for the earthwork material. In situ test measurements and roller MV are then collected throughout the calibration area. The MV-TV is determined through correlation with the QA-TV (Figure 2.6a). For stiffness-based in situ test measurements (e.g., LWD, SSG, FWD), univariate regression analysis is typically suitable for correlation purposes(Mooney et al. 2010). For density-based in situ test measurements (e.g., NDG, Sand Cone), multivariate regression analysis may be necessary if the earthwork material is sensitive to moisture variability (e.g., Thompson and White 2008, Tehrani 2009).

The acceptability of the correlation is generally determined by the coefficient of determination (R^2). Typically, when correlating soil property measurements from alternative devices, $R^2 \geq 0.5$ is used to define acceptable correlations (e.g., Ping et al. 2002, Vennapusa and White 2009). Therefore, it is recommended that the same criteria be used for correlations between roller MV and in situ test measurements (Mooney et al. 2010). If the coefficient of determination criteria has been reached, the MV-TV is then calculated from the regression equation based on the QA-TV (e.g., 95% relative compaction).

Similar to Option 2a, acceptance of the evaluation area will require that a specified percentage of roller MV in the evaluation section exceed the MV-TV requirement. The recommended range for percentage of the roller MV that meet the

MV-TV requirement is 80% to 95% (Mooney et al. 2010). The evaluation section is accepted when this criteria has been reached.

Prediction limits may be used during regression analysis in order to increase confidence in compaction. This is implemented by introducing a confidence limit above and below the regression equation line and using an adjusted MV-TV that represents a higher level of compaction (e.g., an upper limit for CMV, or a lower limit for MDP); an example of this process is shown in Figure 2.6b (Mooney et al. 2010).

2.8 Geospatial Statistical Analysis

Geostatistics is an applied branch of mathematics developed in the 1950's mainly to solve ore reserve estimation problems in the mining industry. Since then, geostatistics has expanded for use in many other areas of the earth sciences (Wackernagel 1998). Over the past 30 years, an abundance of publications have applied geostatistics to geotechnical engineering problems.

Geostatistical analysis tools offer many advantages over conventional statistical analysis tools for application with CCC/IC technology. Unlike conventional statistical approaches, geostatistics can be used to measure the spatial variability of a dataset. This is of particular interest because it offers a way to assess the spatial uniformity of a dataset. The importance of soil uniformity for performance of pavement foundations has been shown in recent research (e.g., Dore et al. 2001, White et al. 2004). Additionally, spatial analysis tools allow for identification of "problematic areas" within a dataset. This is particularly useful for identification of "low compaction zones" when analyzing CCC measurements.

In addition to assessing the spatial variability of a dataset, geostatistical tools may also be used to perform spatial predictions in areas where measurements do not

exist. Throughout this study, it is necessary to “determine” or predict a value or property at unsampled locations. There are many interpolation techniques that exist, but all are based on the principle of spatial continuity; e.g., the fact that data points that are close to each other are more likely to have similar values than data points that are located farther apart from each other (Issaks and Srivastava 1989). A select few of these spatial prediction methods will be presented within this chapter and used in subsequent chapters for various purposes.

2.8.1 Interpolation in Geospatial Statistical Analysis

In Geospatial Statistical Analysis, sample points taken at discrete locations in an area are used to predict values at desired locations in that area and create (interpolate) a continuous surface. The sample points can be measurements of any phenomenon such as soil properties, or elevation heights. In addition to providing various interpolation techniques, Geostatistical Analysis also provides many supporting tools. These tools allow exploration and a better understanding of the data so that accurate surfaces may be created based on the available information.

Three of the most common interpolation methods that are used to predict a value at an unmeasured location from a known surrounding data set are Nearest Neighbor (NN), Inverse Distance Weighting (IDW), and Kriging techniques (Krige 1951). The simplest of the techniques, NN, only considers the measured value that is closest in spatial distance to the unsampled location when performing predictions. IDW is a deterministic technique that uses the existing configuration of the sample points to create a surface. Kriging is the most advanced method of the three, in that it uses geostatistical techniques to create surfaces that incorporate the statistical properties of the measured data. Although kriging has been widely accepted as the

best linear unbiased predictor (BLUP) from a mean squared error (MSE) standpoint (Facas et al. 2010), NN and IDW are simplistic predictor methods with easy repeatability. Thus, the appropriateness of kriging must be investigated to justify the additional computational effort. A more thorough explanation of the three spatial predictors is presented herein.

2.8.2 Nearest Neighbor Interpolation

Unlike other interpolation methods that tend to "smooth" the data by applying weighting functions to multiple known values to predict a value at an unknown location, the nearest neighbor (NN) method does not utilize weighting functions. Instead the NN will, simply, find the known value at the location that is closest in spatial distance to the prediction location, and use that value for the prediction. In the event that there are multiple known locations equidistant from the prediction location then there will be a tiebreak. The tiebreak is selected by the user and can either be an average of the known values or a random selection. For this study, the average tiebreak method was utilized.

2.8.3 Inverse Distance Weighting Method

Another geospatial statistical method used for interpolation of spatially oriented data sets is the inverse distance weighting (IDW) method (e.g., Isaaks and Srivastava 1989). For the IDW method, a neighborhood about the prediction location is identified and a weighted average is taken of the measured values within this neighborhood. The relative weights of known values are assigned based upon their spatial distance from the interpolation point. The most basic IDW method uses a

simple inverse power weighting function, with a neighborhood size that was equal to the domain of the entire data set (Isaaks and Srivastava 1989):

$$w_i(h) = \frac{\sum_{i=1}^{n} \frac{1}{h_i^p} z(x_i)}{\sum_{i=1}^{n} \frac{1}{h_i^p}} \qquad (2.7)$$

where, $h_i \ldots h_n$ are the distances from each of the n sample locations to the point being estimated, $z(x_1) \ldots z(x_n)$ are the sample values, and the exponent p is the power weighting function (Isaaks and Srivastava 1989). As shown in Equation 2.6, the weighting function that is used is dependent upon the selected exponent value, p. When $p = 1$, a linear decay function is applied to all measured values within the defined neighborhood. Similarly, if $p = 2$, a second order decay function is used to weight the measured values as a function of h, and so on. In general, the value of p is chosen by the user through assessment of the spatial data set, using their judgment and experience.

2.8.4 Ordinary Kriging Method

As noted previously, kriging is a geostatistical interpolation method that predicts values at unmeasured locations. Kriging estimates consider both the distance and the degree of variation while implementing a weighted linear combination of the sample measured values for prediction. Unlike other geostatistical tools, kriging does not apply the same weighting functions to all sample measured values. Instead weighting functions are applied based on the distance and orientation of the sample measured values with respect to the location of the estimated value and the way in which the sample measured values are grouped. The assignment of these functions

attempts to minimize the variance error and to obtain a value of zero for the mean of prediction errors to prevent over or under estimation (Krige 1951). The user-derived weighting functions allow the kriging method to result in unbiased estimates making it the BLUP gridding method. There are several different kriging techniques; in the current study, ordinary kriging is used, which assumes that a data set has a stationary variance and also a non-stationary mean value within the sample measured values.

2.8.4.1 Semivariograms and Models

The concept of empirical semivariance is used to quantitatively measure the degree of spatial dependence between measured values within a dataset (e.g., Isaaks and Srivastava 1989, Cressie 1993, Clark and Harper 2002). The semivariance is computed by taking half the variance of the differences between measured values for all possible points in a data set that are spaced at a constant distance apart (Equation 2.8). The empirical semivariogram $\gamma(h)$ is a plot of the semivariances as a function of different point spacing distances, h (Olea 2006).

$$\gamma(h) = \frac{1}{2N_h}\sum_{i=1}^{N_h}[z(x_i + h) - z(x_i)]^2 \qquad (2.8)$$

where x is the vector of spatial coordinates. $z(x)$ is the variable under consideration as a function of the spatial location (e.g., elevation measurements, density measurements, zinc concentration measurements, etc.). The vector h is the lag spacing representing the separation between two spatial locations, and N_h is the number of pairs separated by a lag spacing of h.

In order to better visualize this process, a semivariogram of zinc concentration values at measured locations from the topsoil in a flood plain area is shown in Figure 2.7. The data presented in this figure is from the Meuse data set, which includes concentration measurements of four metals that are measured at various locations in the topsoil of a flood plain beside the Meuse River. The Meuse data set is openly accessible, and can be found in demonstration problems as part of the R package *gstat* (Pebesma 2004, R Development Core Team 2012). R is a language and environment for statistical computing (R Development Core Team 2012). It is an open-source tool that contains many packages to aid in geostatistics. The *gstat* package provides basic functionality for univariable and multivariable geostatistical analysis, and will be used throughout this thesis to generate semivariogram plots (Pebesma, 2004).

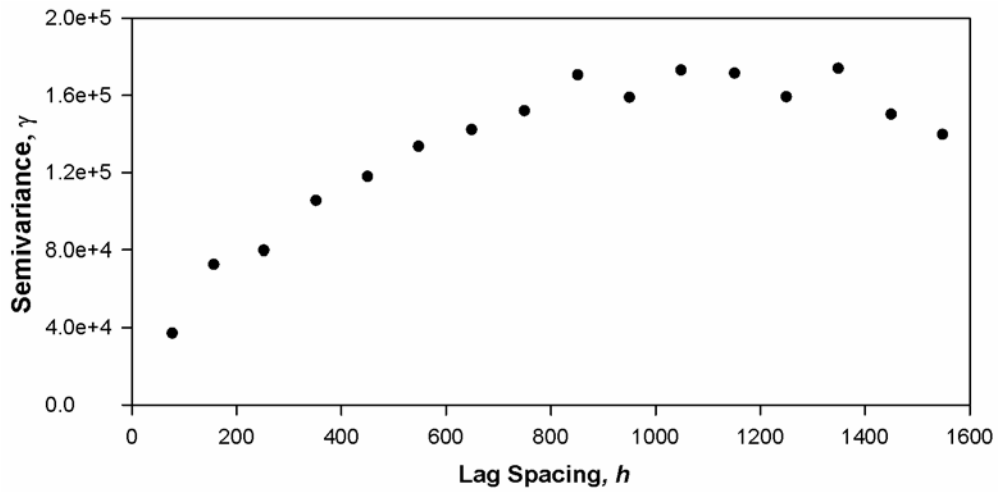

Figure 2.7 Zinc concentration empirical semivariogram.

The selection of lag spacing, *h*, will influence the number of semivariance values that can be calculated; the larger the lag spacing, the smaller the count of

semivariance values that are calculated. Consequently, the amount of data points available for the empirical semivariogram will decrease. The lag spacing for a given data set should be adjusted using judgment and experience until a meaningful empirical semivariogram is established, for which a theoretical semivariogram model can be fitted.

Figure 2.8 shows three different empirical semivariograms for zinc concentration data from the Meuse data set (Pebesma, 2004). The only difference between Figures 2.8a, 2.8b, 2.8c, and 2.8d is that the lag spacing was decreased for each successive semivariogram. The lag spacing values are 500, 100, 50, and 10, respectively. It is clear that the empirical semivariogram shown in Figure 2.8a does not have adequate data points to be fitted with a model; this is because the selected lag spacing of 500 is too large. The empirical semivariograms with a lag spacing of 100, 50, and 10 (Figures 2.8b, 2.8c, 2.8d) each provide enough resolution for model fitting. However, if the lag spacing is too small then the resulting empirical semivariogram will produce a large number of data points, causing a scattered or "cloudy" plot, as shown in Figure 2.8d. Fortunately, this scatter will not significantly affect the fitted theoretical semivariogram model; however, it does tend to make visual assessment of the model fit more difficult. Although a smaller lag spacing will allow for a more "true" fit of a theoretical model, lag spacings beyond a certain "critical" value tend to not significantly alter the model fit parameters that are selected using traditional model fitting approaches.

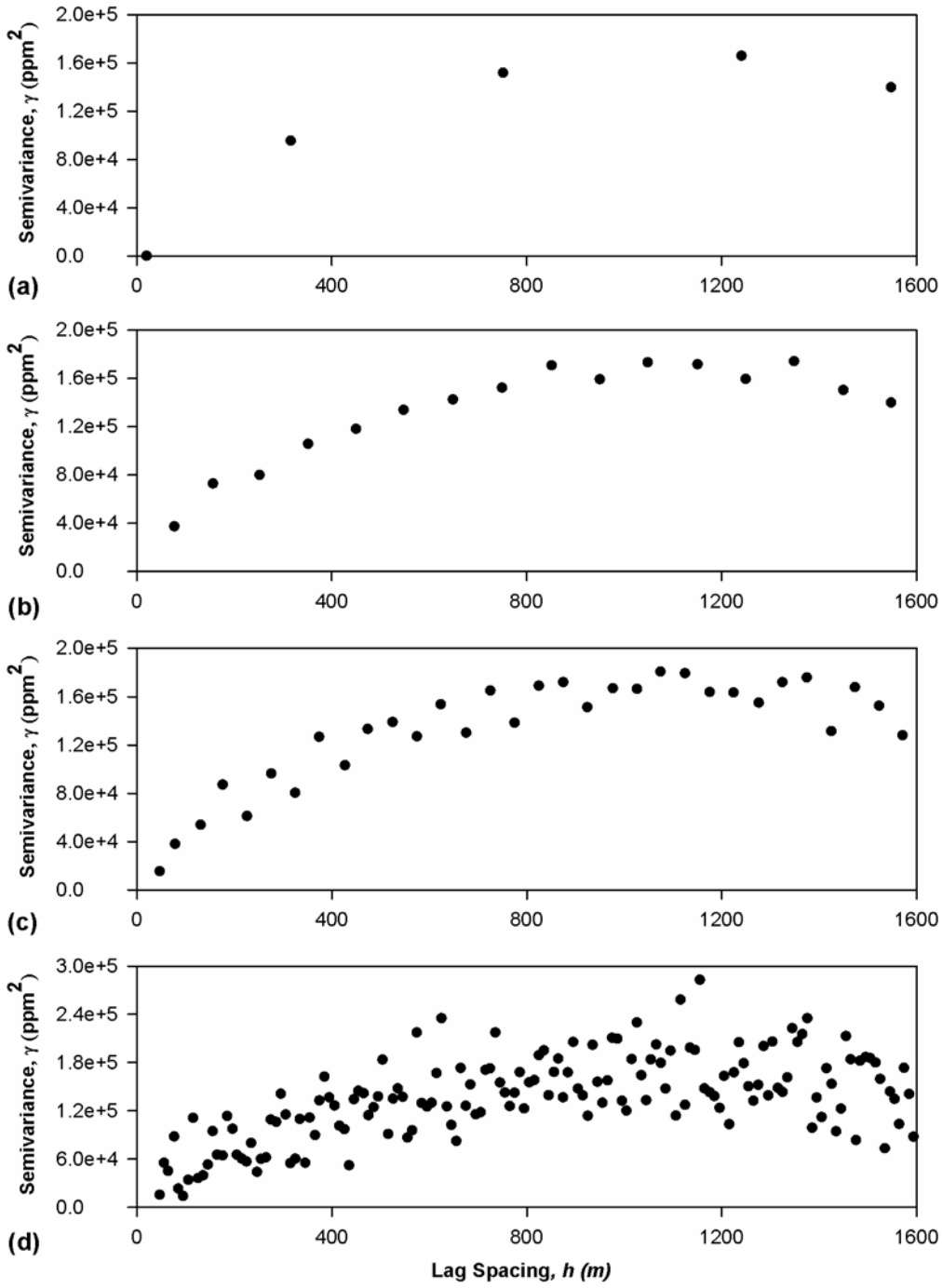

Figure 2.8 Zinc concentration empirical semivariograms: (a) lag spacing = 500 m, (b) lag spacing = 100 m, (c) lag spacing = 50 m, and (d) lag spacing = 10 m (data from Pebesma, 2004, R Development Core Team 2012).

Empirical semivariogram plots, as shown in Figures 2.7 and 2.8, are typically used to develop the weighting functions for kriging. Following conventional practice, a theoretical model $\gamma'(h, \theta)$ is fit to the empirical semivariogram $\gamma(h)$ data; this theoretical model is then used to determine the appropriate kriging weighting functions (e.g., Isaaks and Srivastava 1989, Cressie 1993, Clark and Harper 2002). A variety of theoretical semivariogram models are commonly used with ordinary kriging. For geospatial predictions, the four most common models are probably the linear, spherical, exponential, and Gaussian models (e.g., Isaaks and Srivastava 1989, Cressie 1993, Clark and Harper 2002). The mathematical expressions for the four common models previously mentioned are shown in Table 2.5. The "best" model for use with a given data set may be chosen by one of the three following methods:

1) Visual inspection through trial and error (Goovaerts 1997)

2) Weighted least squares (Jian et al. 1996)

3) Maximum likelihood (Kitanidis 1997)

The implementation of these selection methods will not be discussed herein, the reader may refer to the respective references for more details on the selection process.

Table 2.5 Mathematical Expressions for Semivariogram Models

Model Name	Mathematical Expression
Linear	$\gamma'(h,\theta) = \begin{cases} 0 & , \quad h = 0 \\ \theta_n + bh & , \quad h \neq 0 \end{cases}$
Spherical	$\gamma'(h,\theta) = \begin{cases} 0 & , \quad h = 0 \\ \theta_n + \theta_s\left(\frac{3h}{2\theta_r} + \frac{h^3}{2\theta_r{}^3}\right) & , \quad 0 < h < \theta_r \\ \theta_n + \theta_s & , \quad h \geq \theta_r \end{cases}$
Exponential	$\gamma'(h,\theta) = \begin{cases} 0 & , \quad h = 0 \\ \theta_n + \theta_s\left(1 - \exp\left(-\frac{h}{\theta_r}\right)\right) & , \quad h \neq 0 \end{cases}$
Gaussian	$\gamma'(h,\theta) = \begin{cases} 0 & , \quad h = 0 \\ \theta_n + \theta_s\left(1 - \exp\left(-\frac{h^2}{\theta_r{}^2}\right)\right) & , \quad h \neq 0 \end{cases}$

Note: h = spatial distance; b = slope of the line; θ_r = range; θ_n = nugget; $\theta_n + \theta_s$ = sill.

In addition to the spatial (lag) distance h, which is present in all of the models shown in Table 2.5; the model $\gamma'(h, \theta)$ may contain all or some of the following three parameters: the range (θ_r), the nugget (θ_n), and the sill ($\theta_n + \theta_s$), as shown in Figure 2.9. The range is the spatial distance at which measured values will no longer influence the prediction of an unknown value. In a simplistic semivariogram model, the range is defined as the distance h at which the model reaches the maximum semivariance or sill. The exponential and Gaussian models reach their sill asymptotically (as $h \rightarrow \infty$) and, therefore, never reach a true numerical range. For these models, the "effective range" is the distance where the variogram reaches 95% of the sill. The "effective range is $3\theta_r$ and $\sqrt{3}\theta_r$ for the exponential and Gaussian models, respectively (e.g., Journel and Huijbregts 1978; Christakos 1992; Deutsch and Journel

1992). The nugget effect corresponds to the discontinuity that can be present at the origin of the semivariogram. In theory, $\theta_n = 0$, but in reality due to micro scale variation a discontinuity at the origin leads to $\theta_n > 0$ (Cressie 1993). The possible reasons for this discontinuity are measurement errors and error as a result of rounding spatial distances between pairs of points to the nearest lag distance that is used to define the semivariogram. The sill, which is the sum of θ_n and the partial sill θ_s, is equal to the maximum semivariance of the model. If the semivariance increases asymptotically, then the sill of the semivariogram is the *h* value that corresponds to the asymptote. (Dučinskas and Šaltytė–Benth 2003).

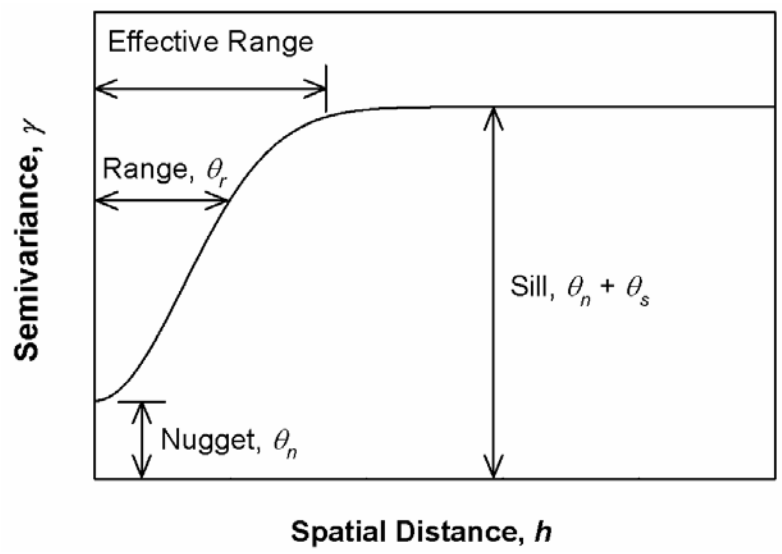

Figure 2.9 A typical theoretical semivariogram.

In order to perform kriging, theoretical prediction models derived from empirical isotropic semivariograms are needed, as discussed above. As part of the

development of the proper kriging models, it is necessary to assess whether the data that is being analyzed is isotropic or anisotropic in nature. For isotropic data sets, it is necessary to account for only the magnitude of the distance between points when creating the empirical semivariogram, while anisotropic empirical semivariograms require the use of techniques that account for both the magnitude and direction of the distance between data points (e.g., Isaaks and Srivastava 1989). Theoretical variogram models for kriging are based on isotropic models, so correction for anisotropy, if it exists, is necessary to perform kriging interpolation.

2.8.4.2 Anisotropy

The previous discussion relies on the assumption that the spatial correlation of the variable is the same in all directions, thus isotropic. For the isotropic case, omnidirectional semivariograms are used, which depend only on the magnitude of the lag spacing vector $h = |\mathbf{h}|$ and not the direction. Thus, the empirical semivariogram is computed by nesting data pairs separated by the appropriate lag distances with no regard for direction.

However, if different correlations exist in different spatial directions, then the data set is considered anisotropic. There are two types of anisotropy, *geometric anisotropy* and *zonal anisotropy* (Budrikaite and Ducinskas 2005). Geometric anisotropy exists when varying directional semivariograms have different range values. Alternatively, if the sill significantly changes between varying directional semivariograms, then zonal anisotropy exists (Budrikaite and Ducinskas 2005).

2.8.4.2.1 Directional Semivariograms

A simple method for evaluating anisotropic behavior is to compare the ranges and sills of different directional semivariograms (Budrikaite and Ducinskas 2005). If there is a significant difference in the range or sill values as the direction changes, this is evidence that the spatial data has a directional or zonal dependence. In order to create the directional semivariogram, the semivariance values for data pairs falling within a certain direction and lag spacing limits must be calculated. These data pairs must fall within the specified directional band determined by a given azimuthal direction ψ, angular tolerance, and bandwidth as shown in Figure 2.10 (Olea 1999).

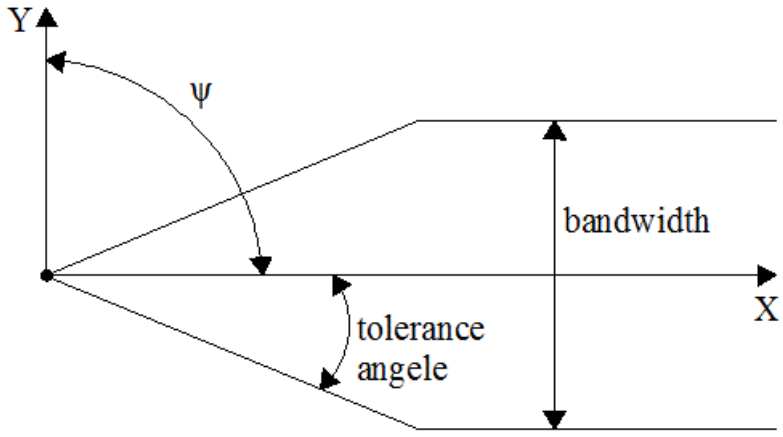

Figure 2.10 Directional band for directional semivariograms (modified after Olea 1999).

The azimuth direction ψ is measured from the *Y* axis and defines the direction of the semivariogram. Typically, when evaluating different directional semivariograms, a tolerance angle of 22.5° is implemented (e.g., Budrikaite and Ducinskas 2005). The bandwidth must be selected by the user to ensure that the directional band is scaled with respect to the spatial area of the measurements.

2.8.4.2.2 Geometric Anisotropy

Geometric anisotropy exists when there is a stronger influence in a single direction of the spatial data in comparison to other directions. Visually, if the range of each of the directional semivariograms were plotted on a two-dimensional plot, an ellipse (Figure 2.11) would form where the major and minor axes of the ellipse would correspond to the maximum and minimum ranges of the directional semivariograms (Budrikaite and Ducinskas 2005). Geometric anisotropy can also exist in three-dimensions, but only the two-dimensional case will be discussed herein.

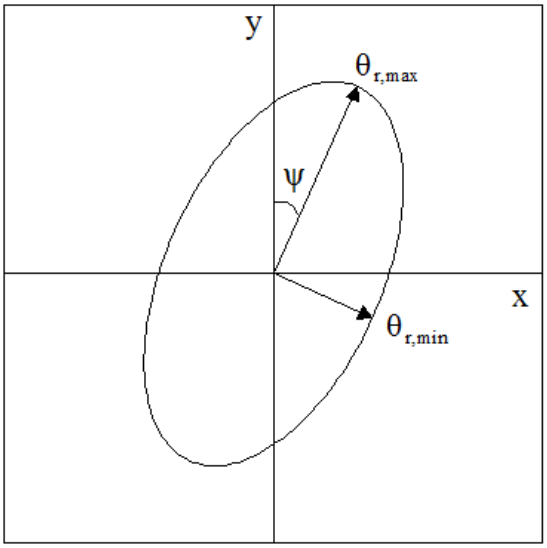

Figure 2.11 Ranges of directional semivariograms.

In Figure 2.11, ψ is the angle from the *y*-axis to the major axis of the ellipse and $\theta_{r,\min}$ and $\theta_{r,\max}$ are the minimum and maximum ranges of the directional semivariograms, respectively.

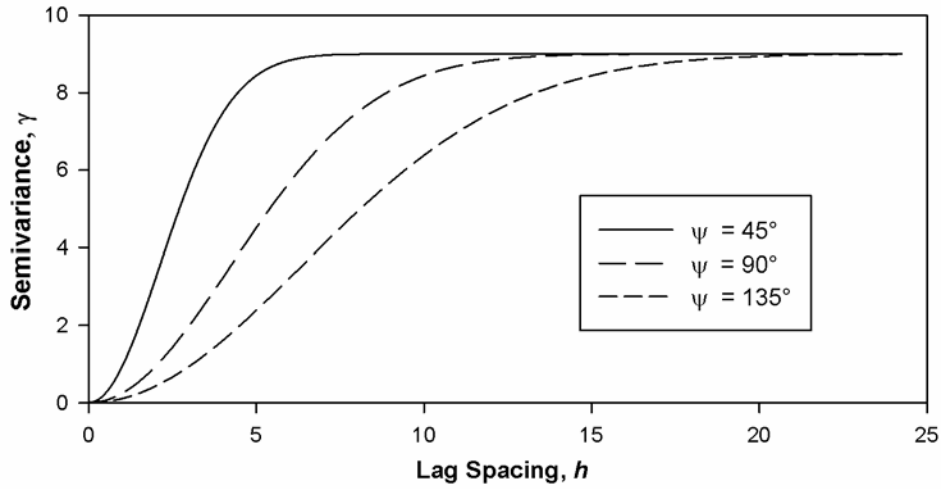

Figure 2.12 Directional semivariograms displaying geometric anisotropy.

A simplistic way to identify geometric anisotropy is to plot the semivariograms in various directions. If the ranges are different for different directional semivariograms, then there is likely geometric anisotropy (e.g. Figure 2.12). A common approach to modeling geometric anisotropy is to find the ranges $\theta_{r,\min}$ and $\theta_{r,\max}$ in the principal, orthogonal, directions of the ellipse and transform the two-dimensional lag spacing vector **h** = (h_{min}, h_{max}) into an equivalent isotropic lag spacing vector using the following equation (Budrikaite and Ducinskas 2005):

$$h = \sqrt{\left(\frac{h_{\min}}{\theta_{r,\min}}\right)^2 + \left(\frac{h_{\max}}{\theta_{r,\max}}\right)^2} \qquad (2.9)$$

where h_{min} and h_{max} are the lag spacing vectors of the directional semivariograms in the principal directions of the geometric anisotropy ellipse, as shown in Figure 2.11.

2.8.4.2.3 Geometric Anisotropic Model Determination (Gaussian Example)

In order to better understand the development of the geometric anisotropic model that is used as the weighting function for kriging interpolation, an example using the Gaussian model will be shown. The general form for the geometrical anisotropic Gaussian model is shown in Equation 2.10.

$$\gamma'(h,\theta) = \theta_{n,geo} + \theta_{s,geo}\left(1 - \exp\left(-\frac{h^2}{\theta_{r,geo}{}^2}\right)\right) \tag{2.10}$$

where h = spatial distance, $\theta_{r,geo}$ = anisotropic range, θ_n = nugget, and $\theta_{n,geo} + \theta_{s,geo}$ = anisotropic sill.

When geometric anisotropy exists in the data set, the directional semivariogram that corresponds to the major and minor axis must be determined. Theoretical models must be fit to the directional semivariograms to determine the range of the major axis semivariogram ($\theta_{r,\max}$) and the range of the minor axis semivariogram ($\theta_{r,\min}$) (Equation 2.11). Note that the difference in the nugget and the sill between the directional variograms are considered insignificant, by definition of geometric anisotropy, and they are therefore considered equivalent in all directions (Equations 2.12 and 2.13).

$$\theta_{r,\max} \neq \theta_{r,\min} \tag{2.11}$$

$$\theta_{n,\max} = \theta_{n,\min} \tag{2.12}$$

$$\theta_{s,\max} = \theta_{s,\min} \tag{2.13}$$

The geometric anisotropic range $\theta_{r,geo}$ that corresponds to the semivariogram created from the equivalent lag spacing vector *h* shown in Equation 2.9 can be calculated as follows:

$$\theta_{r,geo} = \theta_{r,\min} \sqrt{\frac{1}{\cos^2(\psi - \beta)k^2 + \sin^2(\psi - \beta)}} \tag{2.14}$$

where ψ is the angle between the major axis of the ellipse and the *Y*-axis, *k* is the anisotropy ratio (Equation 2.15), and β is an angle that defines the argument of the spatial distance.

$$k = \frac{\theta_{r,\min}}{\theta_{r,\max}} < 1 \tag{2.15}$$

The explanation above provides the step by step process for determining the geometrical anisotropic semivariogram model that is necessary to perform kriging interpolation. Computer based programs such as R (R Development Core Team 2012) provide geostatistical tools that will perform geometrical anisotropic kriging interpolation; specifically, the *gstat* R package (Pebesma 2004). These geostatistical tools typically assume that: 1) the direction of the minimum and maximum range is perpendicular, 2) the type of theoretical model is the same in all directions, and 3) the sills of the theoretical models are equal in all directions (e.g., Olea 2006).

2.8.4.2.4 Zonal Anisotropy

Similar to geometric anisotropy, zonal anisotropy occurs in spatial data where there is strong directional influence. In contrast to geometric anisotropy, pure zonal anisotropy will produce semivariogram plots in varying directions that have equal ranges, but have different sills (Figure 2.13a). Typically, in practice, pure zonal isotropy does not exist. Zonal isotropy usually exists in combination with geometric anisotropy, as shown in Figure 2.13b (Budrikaite 2005).

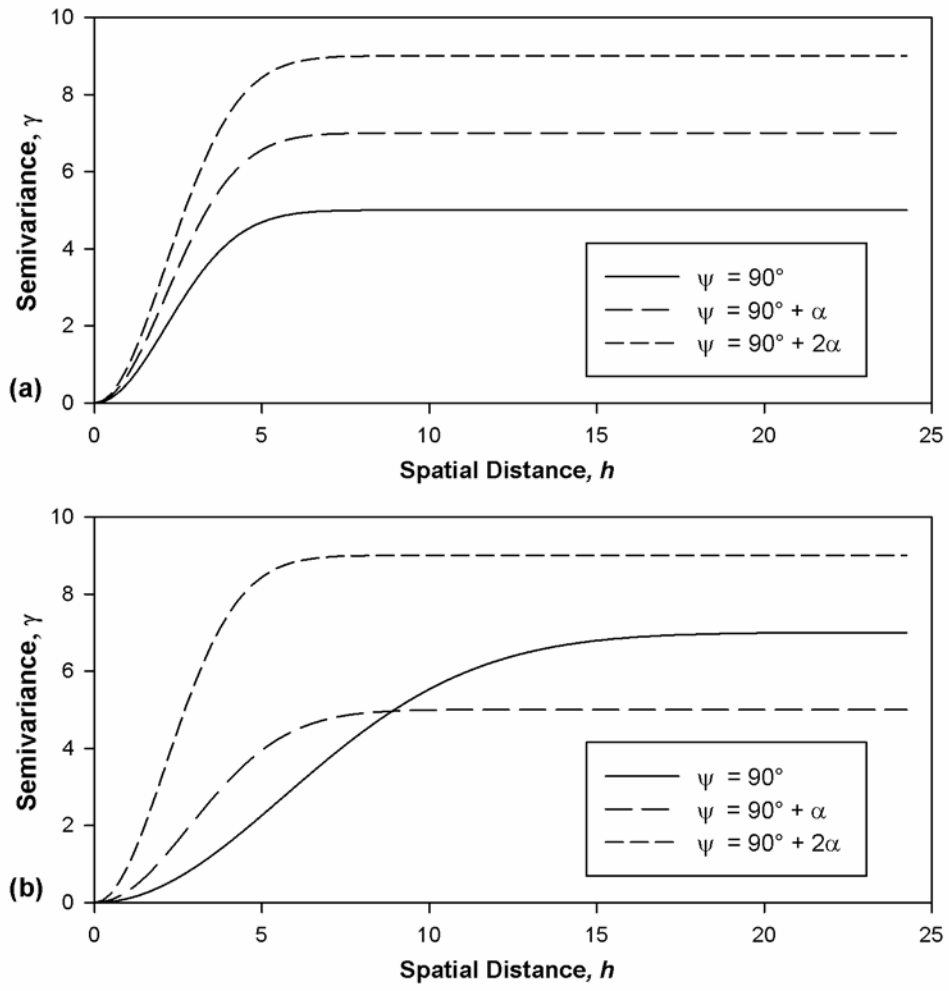

Figure 2.13 Zonal anisotropy: (a) pure zonal anisotropy; (b) a combination of zonal and geometric anisotropy.

If zonal anisotropy exists in a data set, the kriging process is more difficult than what is encountered when performing isotropic kriging or geometric anisotropic kriging methods, which can generally be easily performed with computer-based programs. The difficulty with kriging a zonal anisotropic data set lies in the determination of an equivalent isotropic semivariogram model that properly accounts for the changes in the range and sill for different directional semivariograms. A nesting process is required to determine the zonal anisotropic semivariogram model. The zonal anisotropic model is determined by taking a weighted sum of the directional semivariogram models that are scaled by the respective model ranges. The selection of weights is performed through trial and error with the requirement that the summation of the weights is equivalent to the sill of the zonal anisotropic model (Budrikaite 2005). A more expansive explanation on this process is provided below.

In order to determine the zonal anisotropic model, the directional semivariograms with the maximum and minimum continuity must first be identified and fitted independently with a theoretical model (Budrikaite 2005). The maximum and minimum directions of continuity typically correspond to the principal directions of geometric anisotropy. From this point on, the directional semivariogram values for the maximum and minimum continuity will be denoted as $\gamma'(h_{max})$ and $\gamma'(h_{min})$ respectively, where the subscripts *max* and *min* represent the two main directions of anisotropy.

The zonal anisotropic model has two components: 1) the isotropic semivariogram model $\gamma'(h)$ (model fit to the omnidirectional semivariogram), and 2) the zonal anisotropic component (Equations 2.16 & 2.17).

$$\gamma'\left(h_{\max}, h_{\min}\right) = \gamma'\left(\sqrt{h_{\max}{}^2 + h_{\min}{}^2}\right) + \gamma'\left(h_{\min}\right) \tag{2.16}$$

where the sill of the zonal anisotropic component is the difference between the sill of the main direction semivariogram models. Since the isotropic component $\gamma'\left(\sqrt{h_{\max}{}^2 + h_{\min}{}^2}\right)$ is equal to the omnidirectional semivariogram model $\gamma'(h)$, the overall model may be rewritten as:

$$\gamma'\left(h_{\max}, h_{\min}\right) = \gamma'\left(h\right) + \gamma'\left(h_{\min}\right) \tag{2.17}$$

where the sill of the zonal anisotropic component is the difference of the sills in the main directions of continuity. The overall semivariogram model determined through Equation 2.17 is an accurate model that can be used for kriging interpolation to account for geometric and zonal anisotropy (Budrikaite 2005).

2.8.4.2.5 Zonal Anisotropic Model Determination (Gaussian Example)

In order to better understand the development of the zonal anisotropic model that is used as the weighting function for kriging interpolation, an example using the Gaussian model will be shown. The general form for the zonal anisotropic Gaussian model which adequately considers all directional influences in the form of Equation 2.17 is shown in Equation 2.18.

$$\gamma'(h,\theta) = \left[\theta_{n,iso} + \theta_{s,iso}\left(1 - \exp\left(-\frac{h^2}{\theta_{r,iso}{}^2}\right)\right)\right] + \left[\theta_{n,zon} + \theta_{s,zon}\left(1 - \exp\left(-\frac{h^2}{\theta_{r,zon}{}^2}\right)\right)\right] \tag{2.18}$$

where h = spatial distance; $\theta_{r,iso}$, $\theta_{n,iso}$, and $\theta_{n,iso} + \theta_{s,iso}$ are the range, nugget, and sill of the isotropic semivariogram model fit to the omnidirectional semivariogram; $\theta_{r,zon}$, $\theta_{n,zon}$, and $\theta_{n,zon} + \theta_{s,zon}$ are the range, nugget, and sill of the zonal anisotropic component of the model. The zonal component accounts for both zonal and geometric anisotropy since, typically, pure zonal anisotropy does not exist in practice. When zonal anisotropy exists in the data set the directional semivariograms that correspond to maximum and minimum variability must be determined. The anisotropic component of the model is then determined based on differences in the selected directional semivariogram. The directional semivariogram with the largest range $\theta_{r,\max}$ and the smallest range $\theta_{r,\min}$ are typically selected as the directions of maximum and minimum variability. If the range does not change for different directional semivariograms, then the difference in sills must be examined to determine the directions of maximum and minimum variability.

Unlike the geometric model where only the range values changed for different directional semivariograms, the zonal anisotropic component of the model will have a range and sill that are dependent on the parameters of the models that correspond to the semivariograms in the direction of the maximum and minimum variability. As in the geometric anisotropic case, the differences in the nugget are considered negligible. The equations that summarize the discussion of the parameters above are shown in Equations 2.19, 2.20, and 2.21.

$$\theta_{r,\max} \neq \theta_{r,\min} \tag{2.19}$$

$$\theta_{n,\max} = \theta_{n,\min} \tag{2.20}$$

$$\theta_{s,\max} \neq \theta_{s,\min} \tag{2.21}$$

The calculation of the range $\theta_{r,zon}$ for the anisotropic component of the model shown by Equation 2.18 can be found in Equation 2.22 (Budrikaite and Ducinskas 2005).

$$\theta_{r,zon} = \theta_{r,\min} \tag{2.22}$$

The calculation of the sill for the anisotropic component of the model shown by Equation 2.22 can be found in Equation 2.23 (Budrikaite and Ducinskas 2005).

$$\theta_{s,zon} = \theta_{s,\max} - \theta_{s,\min} \tag{2.23}$$

The explanation above provides the step by step process for determining the zonal anisotropic semivariogram model necessary to perform zonal anisotropic kriging interpolation. Computer based programs that provide solutions for zonal anisotropic kriging are, to the author's knowledge, not readily available.

Chapter 3

PROJECT DESCRIPTION

3.1 Introduction

In July of 2008 at the Burrice Borrow Pit (Figure 3.1) located in Odessa, Delaware, an experimental field study was performed to examine the effectiveness and reliability of continuous compaction control (CCC) technology for use as quality assurance (QA) compaction verification tool under real field construction conditions. The field project involved the construction of a small-scale embankment using conventional earth moving and compaction equipment. To assess the capabilities of CCC technology, a number of conventional in situ test compaction control tests were performed within the compaction area in conjunction with CCC measurements. This process allowed for comparisons between in situ test method results and CCC roller measured values (MV). This chapter provides a summarization of the field study that was performed, using information that has been compiled from previous publications in this area; a more detailed in-depth discussion of the field study may be found in Tehrani (2009).

Figure 3.1 Location of the field study: Burrice Borrow Pit, Odessa, Delaware (Tehrani 2009).

3.2 Embankment Construction

A 61 m long by 6 m wide (200 ft by 20 ft) embankment was constructed using conventional earth moving equipment, following Delaware general specifications for road sub-base construction (DelDOT 2001). The soil that was used to construct the embankment was generally uniform (Tehrani 2009, Meehan and Tehrani 2011), falling at the boundary between two USCS soil classifications: a poorly graded sand with silt (SP-SM) and a silty sand (SM) (ASTM D 2487). The fill material that was used is fairly common for Delaware Department of Transportation (DelDOT) projects, and it generally conforms to DelDOT class G borrow material specifications, Grades V and VI (Figure 3.2).

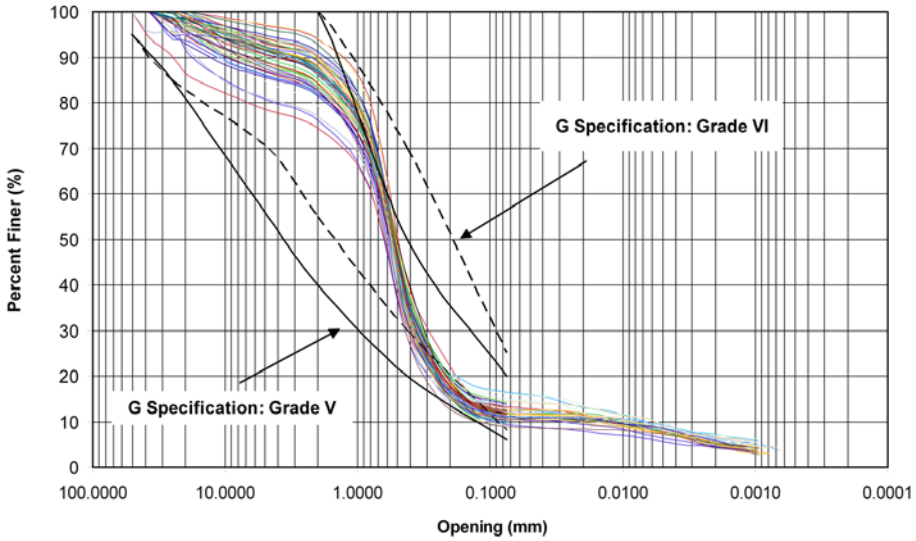

Figure 3.2 Gradation results for field samples taken from in situ test locations (Tehrani 2009).

The embankment was constructed to an approximate total final height of 0.9 m (3.0 ft), by compacting five 20.3 cm (8 in.) loose lift layers, following Delaware general specifications for road sub-base construction (DelDOT 2001). (This was the general loose-lift thickness target value, more discussion on actual lift thicknesses after compaction is presented in Chapter 4). To construct each lift, a Caterpillar 980H bucket loader was used to place fill for spreading by an on-site bulldozer (Figure 3.3).

Figure 3.3 Placing the fill material with a Caterpillar 980H bucket loader (Tehrani 2009).

To spread the material to an approximate loose-lift thickness of 20.3 cm (8 in), a Caterpillar D6K dozer was utilized (Figure 3.4). For some of the lifts that were spread, a global positioning system (GPS) was mounted on the Caterpillar D6K dozer, allowing the material to be placed at a relatively uniform and consistent thickness.

Figure 3.4 Spreading the fill material with a Caterpillar D6K bulldozer (Tehrani 2009).

Prior to roller compaction of the material, a water truck (Figure 3.5) was driven over the compaction area with its sprayers on, to increase the moisture content of the fill material to bring it into a more desirable range (to help achieve more optimum soil compaction).

Figure 3.5 Moisture content conditioning of fill material before compaction (Tehrani 2009).

3.2.1 Compaction of the Embankment Using a CCC Instrumented Roller

After completion of soil placement and moisture adjustment, each soil lift was compacted using a Caterpillar CS56 smooth drum vibratory roller (Figure 3.6). This instrumented roller could perform real-time CCC measurements using a Machine Drive Power (MDP) and Compaction Meter Value (CMV) approach. An on-board *real time kinematic-global positioning system* (RTK-GPS) was used to determine the location of the instrumented roller in real-time, while it was recording CCC measurements and roller operational parameters. The CS56 had a roller drum that was 2.1 m (7 ft) wide, and the machine had an overall operating weight of ≈11,400 kg (25,100 lb). During compaction, the roller speed was kept relatively constant, at around 3.25 km/h (2.02 mph). CCC roller MV and three-dimensional position measurements were recorded simultaneously, approximately every 0.20 m (8 in.), on average, in the direction of roller travel (along the length of the embankment).

Figure 3.6 Caterpillar CS56 vibratory smooth drum roller (Tehrani 2009).

Using the CS56 compactor, each lift was compacted in a series of passes using three side-by-side lanes, with approximately 15 cm (6 in) of overlap at the edges of each compacted soil lane. For a given lift, between six and nine roller passes were performed. Specific information on the roller passes and material lifts is present in Table 3.1.

Table 3.1 General Information about the Compaction Lifts and Passes (Tehrani 2009)

Lift	Number of Passes Performed	Pass Number where Data was Recorded	Date	Start Compaction	End Compaction
Lift 0 (Base Layer)	2	2	7/21/2008	14:18	14:29
Lift 1	6	NA	7/22/2008	NA	NA
Lift 2	6	6	7/22/2008	18:16	18:22
Lift 3	8	8	7/23/2008	11:30	11:36
Lift 4	9	9	7/23/2008	16:22	16:28
Lift 5	7	1	7/24/2008	11:08	11:18
		2	7/24/2008	12:14	12:20
		3	7/24/2008	13:14	13:22
		4	7/24/2008	14:51	14:57
		5	7/24/2008	15:07	15:13
		7	7/24/2008	16:22	16:28

As shown in Table 3.1, the CCC data that was recorded for Lift 1 was lost because of a technical issue related to data storage and download from the CCC equipment. For the sake of time, Lift 5 was the only lift for which CCC measurements

were taken on successive passes for comparison with in situ test results. On all other lifts, CCC measurements were only recorded for the final passes for each lift.

3.2.2 In Situ Test Methods

As an aid to determine if the compaction acceptance level had been reached for a given lift, several conventional quality assurance compaction verification in situ test methods were performed. The in situ test measurements from these tests could then be used for comparison with the CCC roller MV, as is discussed in detail in Chapters 5 and 6. The in situ test methods utilized included the nuclear density gauge test, sand cone test, plate load test, light weight deflectometer test, falling weight deflectometer test, dynamic cone penetrometer test, and soil stiffness gauge test. These six in situ test methods were performed at 19 discrete (X, Y) locations spaced at approximately 3 m (10 ft) intervals along the centerline of the embankment for the base layer and the final passes of each engineered lift. In addition, in situ test measurements were recorded for all passes of Lift 5; however, to expedite compaction, a lower frequency of testing was performed for the earlier passes (prior to the final pass). The location of each in situ test measurement was measured using a GPS rover unit. Additional information on the in situ testing plan can be found in Tehrani (2009).

Chapter 4

MONITORING FIELD LIFT THICKNESS USING COMPACTION EQUIPMENT WITH GLOBAL POSITIONING SYSTEM (GPS) TECHNOLOGY

4.1 Introduction

Researchers are currently exploring the appropriate specification approaches to use for incorporating Continuous Compaction Control (CCC) and Intelligent Compaction (IC) technologies into a quality assurance / quality control (QA/QC) framework for compaction verification (Floss et al. 1983; Samaras et al. 1991; Brandl and Adam 1997; Thompson and White 2008; Meehan and Tehrani 2011; Cacciola et al. 2013). Previous studies in this area have primarily focused on the development of engineering parameter correlations between CCC/IC roller measurements and those from more traditional in situ moisture-density tests such as the sand cone or nuclear density gauge test (e.g., Floss et al. 1983; Samaras et al. 1991; Thompson and White 2008). More recent work has also looked at development of correlations between CCC/IC roller measurements and those from modulus-based in situ compaction control tests (e.g.,; Brandl and Adam 1997; White and Thompson 2008; Vennapusa et al. 2010).

In this thesis, similar correlation relationships between CCC measurements and density-based and modulus-based in-situ test results are developed in Chapter 5, and the associated application of these correlations is presented in Chapter 6. In addition to the in situ soil moisture content and density (or unit weight, relative compaction,

modulus, etc.) criteria that are used to ensure optimum soil densification, most current compaction QA/QC specifications have a maximum lift thickness requirement that must be monitored by the Field Inspector.

This maximum lift thickness requirement is equally as important as the other requirements that are stipulated for performing adequate QA/QC of compacted soil lifts. It is important largely because the compactor energy penetration is less effective for thicker lifts, and the resulting quality of the compacted soil is, therefore, less. Additionally, for compaction verification purposes, if the soil layer is thicker than the depth of influence of the compaction verification tool, then the materials outside of this zone cannot be verified.

There are currently two methods that are commonly used for monitoring field lift thickness. The most common is visual inspection and field measurement by a Field Inspector. This method, although effective with respect to the cost and time involved, is extremely unreliable and can easily result in non-uniform soil lifts, especially if the Field Inspector is not continually present on a given job site. The second method is to perform field surveying during the compaction process. This method is fairly uncommon, especially on smaller projects, due to the associated surveying costs and time delays.

To date, the potential use of CCC technology for monitoring field lift thickness of compacted soil lifts has been largely overlooked. In addition to recording soil vibratory response and other machine parameters, all CCC equipment also records three-dimensional position measurements using an affixed real time kinematic-global positioning system (RTK-GPS). These frequent position measurements offer a

potential mechanism for field engineers to monitor the soil compaction process and resulting lift thickness for the entire compaction area.

This chapter presents a framework for using the *X*-*Y*-*Z* position measurements that are made by RTK-GPS instrumentation that is deployed on CCC equipment to monitor the lift thickness of compacted soils during construction of a roadway embankment. The practical issues associated with using RTK-GPS position measurements for monitoring of lift thickness is assessed using data collected from the field study that is described in Chapter 3. The use of both simple and complex geospatial statistical analysis techniques are examined for interpolation of CCC measured field data onto a uniform grid to allow for lift thickness assessment. The procedure that is presented can be used to build spatial maps of compacted soil lift thickness in real time, a procedure which can be used by field engineers who are trying to ensure the quality of compacted soil lifts. The proposed method is more advantageous than current methods, in that it can be conducted from remote locations, without the added costs and delays.

4.2 An Approach for Monitoring Field Lift Thickness

The approach that is proposed in this chapter is fairly simple. It involves taking the elevation (*Z*-value) measurements from the RTK-GPS for one soil lift, and comparing those values to the elevation measurements from the previous lift. The difference between two elevation measurements at the same location is the lift thickness at that location. In practice, however, this exact process is not possible without geospatial statistical analysis techniques, because the CCC equipment never records data at the same two locations in space (the same *X* and *Y* coordinates) from lift to lift. In order to bypass this problem, a fixed-position (*X*, *Y*) coordinate grid must

be determined. The RTK-GPS measured elevation values can then be used to predict the corresponding elevations at each of the grid points. The lift thickness at each grid point location can then be calculated by taking the difference in elevation from successive layer grids. This process is then repeated for each grid point over the entire area of compaction, to build a spatial map of lift thickness. This process is demonstrated in more detail in this chapter.

4.3 Using RTK-GPS Measurements to Monitor Compactor Location

As discussed in Chapter 3, during the field study a full scale embankment was constructed and compacted in five soil lifts. Each lift required several roller passes to achieve the required soil density. For purposes of the lift thickness monitoring approach described in this chapter, the final pass from each of the soil lifts will be used to assess the thickness of each compacted "dense" lift.

Typical surveying convention yields compactor position data recorded in Northings and Eastings via the RTK-GPS measurement system. To simplify the gridding process it is ideal to work with a local *X*-*Y* coordinate system that corresponds to the longitudinal and transverse directions of the roadway that is being analyzed. Therefore, in this study, the global *X′*-*Y′* coordinate system is converted to a local *X*-*Y* coordinate system where *X* is the longitudinal direction of the embankment (roller travel direction) and *Y* is the transverse direction of the embankment (perpendicular to roller travel direction). The elevation data values (*Z*) correspond to an arbitrary local datum and, thus, are the same for both the global and local coordinate systems. The global *X′*-*Y′* position measurements were converted to the local *X*-*Y* coordinate system using the transformation matrix shown in Equation 4.1.

$$\begin{bmatrix} X \\ Y \end{bmatrix} = \begin{bmatrix} \cos\alpha & -\sin\alpha \\ \sin\alpha & \cos\alpha \end{bmatrix} \begin{bmatrix} X' \\ Y' \end{bmatrix} \tag{4.1}$$

where α is the rotation angle between the local coordinate system and the northing-easting coordinate system.

From this point, for the entirety of this thesis document, all field measurements will be presented in the local *X*-*Y* coordinate system. The position measurements from the RTK-GPS for the final passes of each of the five soil lifts are shown in Figure 4.1. Figure 4.1a shows the roller position measurements for each lift in plan view. It should be noted that position measurements are not presented for Lift 1 due to a malfunction in the data acquisition system at the time of compaction. Additionally, Lift 0 corresponds to the final roller pass of the existing subgrade material before the placement of the first engineered soil lift. Figure 4.1b shows the profile view for roller elevation measurements (*Z*) that correspond to the center line of the roller drum for each of the soil lifts and the respective roller compaction lanes. The large gap in Figure 4.1b between Lift 0 and Lift 2 can be associated with the difference in elevation that occurs between the two compacted soil lifts, due to the missing Lift 1 elevation measurements.

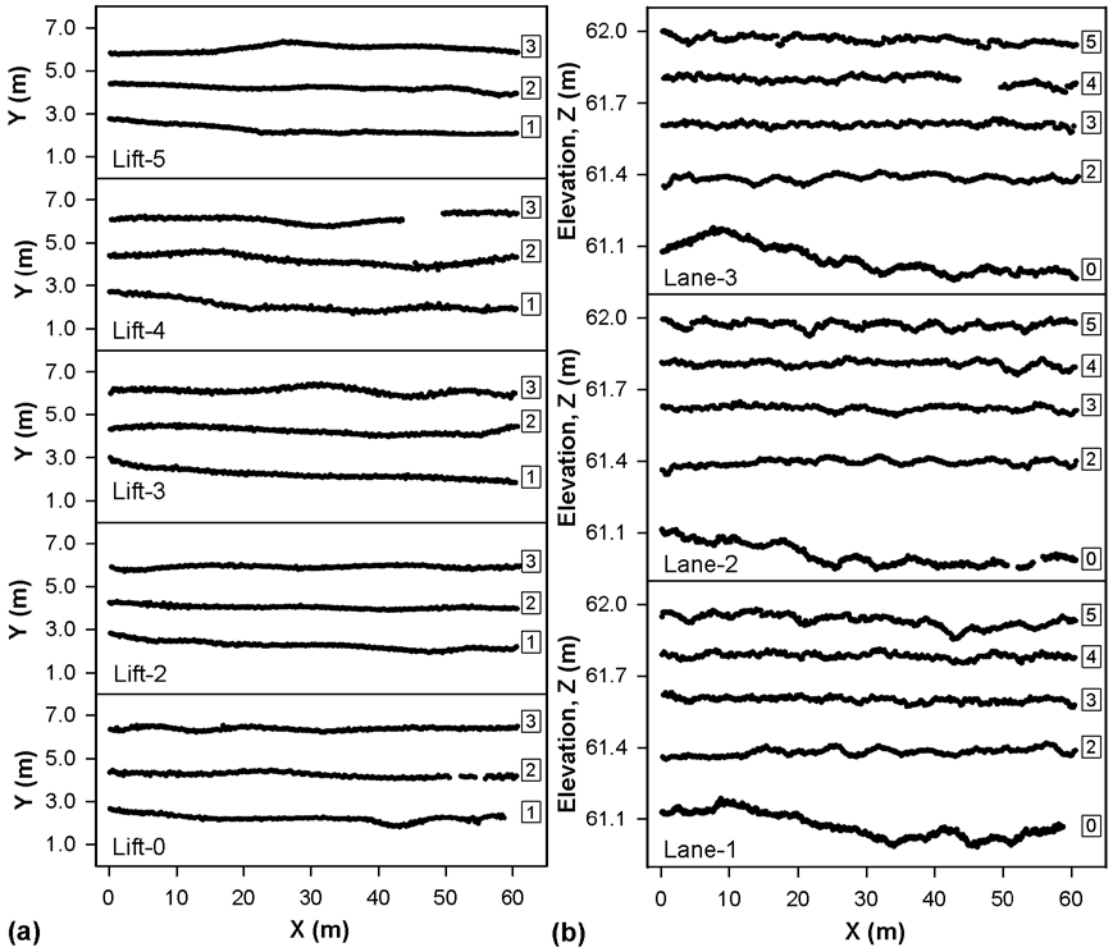

Figure 4.1 RTK-GPS data measured by CCC equipment for five overlying lifts of compacted soil, with three lanes of compaction for each lift: (a) plan view, and (b) profile view.

The data shown in Figure 4.1 supports the author's initial claim that the compactor can be in somewhat different locations from lift to lift. Additionally, it shows that there can sometimes be gaps or jumps in the data that is recorded. This undesirable phenomenon may be observed for a variety of reasons on a real project site. Therefore, it is imperative that the measured position data be interpolated onto a

uniform coordinate grid so that point to point comparisons can be made from lift to lift.

4.4 Establishing a Uniform Grid for Thickness Map Creation

As previously mentioned, the CCC measurements are recorded at arbitrary locations and thus may vary from lift to lift, especially for larger areas of compaction. Proper evaluation of soil lift thickness requires elevation measurements be located in generally the same *X*-*Y* locations from lift to lift. Since this is not always practical to do with conventional CCC equipment, it is necessary to interpolate from a high-density data set of recorded measurements onto an artificial grid. The effect of the grid point spacing of the artificial grid is evaluated within this section and then a recommendation is made for grid spacing selection.

Typical CCC compaction methods result in a large variability in the resolution of measured values in the *X* and *Y* directions. Reasons for this include the speed and direction of the compactor, and the frequency with which data is acquired by the CCC equipment. Figure 4.2 shows the cumulative distribution functions of the point spacings in the *X* and *Y* directions for each of the five lifts. In the current study, the mean grid point spacing of the measured location values is 0.18 m in the *X* direction and 1.95 m in the *Y* direction. These values fall within the range of typical CCC projects that have been previously performed (e.g., Facas et al. 2010).

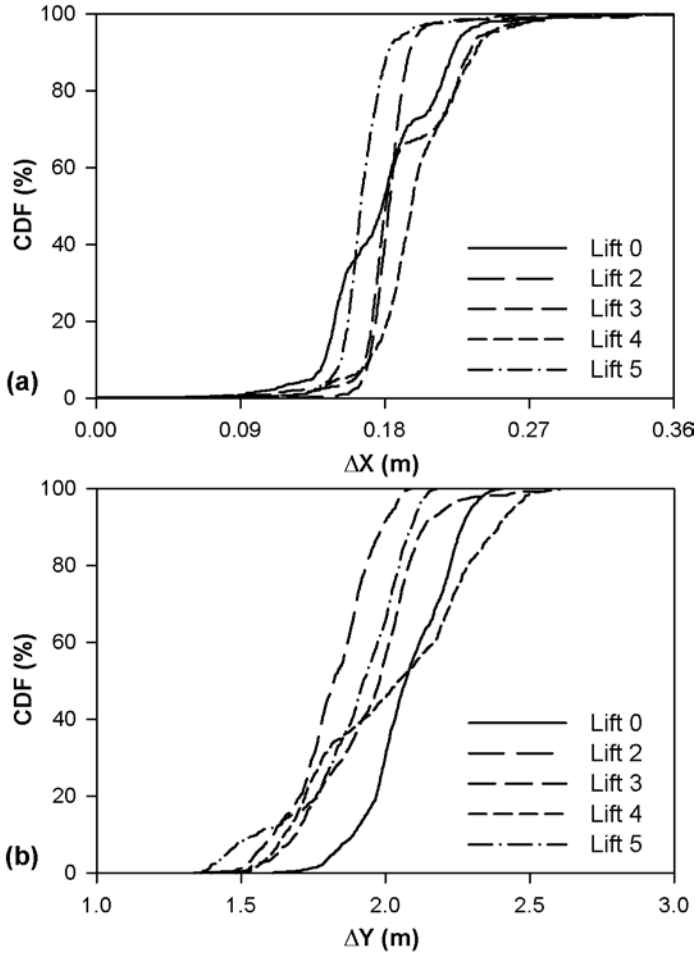

Figure 4.2 Cumulative distribution functions of the point-to-point spacings in the *X* and *Y* directions for five lifts of compacted soil.

A thorough sensitivity analysis was performed to determine the proper geospatial grid for prediction. First, isotropic grids with equal spacing in the *X* and *Y* directions of 0.01 m, 0.05 m, 0.1 m, 0.5 m, and 1.0 m were evaluated. It was observed that isotropic prediction grids with spacing greater than 0.1 m had a significant effect on the analysis results. At isotropic grid spacings smaller than and equal to 0.1 m the results converged, and the effect of grid spacing on the analysis results was negligible.

From this sensitivity analysis, an isotropic grid with point spacings of 0.1 m would be selected because it is the most computationally efficient without having a noticeable effect on the prediction results.

However, due to the nature of typical CCC patterns of compaction, point measurements are typically recorded in an anisotropic fashion, as can be observed in Figures 4.1 and 4.2. Thus, an anisotropic grid with point spacings in the *X*-direction that are not equivalent to the *Y*-direction, was evaluated for several different point spacing configurations. Included in this analysis was an anisotropic grid with 0.1 m *X*-spacing and a 1.0 m *Y*-spacing to simulate the 1:10 ratio of the field measured values. It was determined that the differences between isotropic and anisotropic grids on the prediction results were negligible. This evaluation of grid spacing showed that the most important factor in the selection of gird point spacings is that the artificial grid point spacings be smaller than the corresponding field measured point spacings. Although coarser grid spacings could be used without a significant effect on the results, since the computational power of a standard computer can handle the finer grid point spacings, there is no reason not to use the more refined grids. Consequently, an isotropic grid spacing of 0.1 m was arbitrarily selected and used for all of the analyses in the remainder of this chapter.

4.5 Ordinary Kriging Method for Lift Thickness Predictions

In this section, the ordinary kriging method is used for spatial interpolation of roller measured values (*MV*) of elevation to predict unknown values onto a uniform grid for each lift of the constructed embankment to allow for determination of lift thickness. The uniform grid spacing selected is 0.1 m in both the *X* and *Y* directions, as discussed in Section 4.4. Generalized step by step procedures for using the ordinary

kriging method have been provided in Chapter 2. Within this section, the roller-measured elevation values for each of the five lifts will individually be interpolated onto the established grid.

4.5.1 Determination of Weighting Functions for the Ordinary Kriging Method

The first step in the ordinary kriging method is to establish the empirical semivariograms of the spatially oriented data and, then, fit the weighting models to these semivariograms. At this step, the presence of geometric anisotropy, zonal anisotropy, or both will be investigated. If the spatial data set does not show a directional influence then isotropic kriging methods utilizing omnidirectional semivariograms can be used.

First the directional semivariograms will be presented to assess any anisotropy. The lag spacing for the respective empirical semivariograms has been selected by the author according to the process described in Chapter 2. Due to the nature of the data that is acquired by the CCC rollers, the resolution in some directions, specifically the *Y*-direction, will be much lower than in others. The minimum required lag spacing to develop adequate empirical semivariograms in the direction of the lowest resolution of measured values, the *Y*-directional semivariogram, was determined to be $h = 0.05$ m. Since decreasing the lag spacing did not impact the nature of the other directional semivariograms, for consistency purposes, a lag spacing of $h = 0.05$ m will be used for all empirical semivariograms developed in this chapter.

Once proper empirical semivariograms have been created, in order to properly assess the anisotropy of the semivariograms, the theoretical model type must be selected from the various model options that are presented in Table 2.1. Based on a

combination of the visual inspection method (Goovaerts 1997) and a weighted least squares assessment (Jian et al. 1996), the Gaussian model has been selected as the "best fit" for the majority of the theoretical semivariograms for the elevation measured values. In order to keep the analysis consistent, all theoretical semivariograms in this chapter will be fitted with the Gaussian model.

The empirical semivariograms in this chapter were generated using the R package *gstat* (Pebesma, 2004, R Development Core Team 2012). The package requires an input of the measured values and respective X and Y locations and, then, requires the user to specify the lag spacing h of the semivariogram. As previously mentioned, a lag spacing of h = 0.05 m was specified by the author for semivariograms generated in this chapter. If the user requires the generation of directional semivariograms, the angle corresponding to the direction of the semivariogram, ψ, measured from the Y-axis and the tolerance angle must be specified. A tolerance angle of 45 degrees is used for all directional semivariograms presented in this chapter, as this is a typical value used for this application (e.g., Budrikaite and Ducinskas 2005).

Additionally, the *gstat* package includes a code that will "fit" a theoretical semivariogram model to the generated empirical semivariograms. The code requires that the user input the empirical semivariogram data and, then, specify the model type (e.g. Linear, Exponential, Gaussian, or Spherical). The code then will fit the selected model type using weighted least squares fit similar to the method used by Jian et al. (1996).

Typical investigation of anisotropic behavior usually necessitates that directional semivariograms corresponding to ψ angles of 0°, 45°, 90°, and 135° be

considered (Budrikaite and Ducinskas 2005). The author has opted to perform a more thorough analysis of the data, and therefore examined directional semivariograms corresponding to ψ angles of 0°, 30°, 60°, 90°, 120°, and 150°. It should be noted that an angle ψ = 0° corresponds to the semivariogram in the *Y*-direction, whereas, the angle ψ = 90° represents the *X*-directional semivariogram. Due to the nature of the acquisition of the elevation measured values it is expected that the *X*-axis will correspond to the major axis of the anisotropy ellipse. The inherit assumption of geometrical anisotropy, which allows for kriging interpolation, requires that the minor axis of the ellipse be perpendicular to the major axis. Presentation of the directional semivariograms for each lift elevation data will confirm that the *X*-axis is, in fact, the major axis of anisotropy because the ψ = 90° semivariograms have the largest range values. Thus, the minor axis of the ellipse, which will correspond to the smallest range value, is by default the *Y*-axis (ψ = 0°).

In order to perform anisotropic kriging, empirical semivariograms must be developed in the directions of the major and minor axis of anisotropy so that the associated anisotropic weighting functions can be determined. As will be shown, for all of the elevation measurements in this study, the roller direction, ψ = 90°, corresponds to the major axis of anisotropy. As a result, the direction perpendicular to the roller travel direction, ψ = 0°, is the minor axis of anisotropy. Due to the nature of the compaction process, the density of recorded data in the *X* direction is significantly higher than in the *Y* direction. It is for this reason that the *X* direction will be the major axis of anisotropy. Unfortunately, a byproduct of this artificially induced anisotropy of measurement locations is that the density of recorded elevations in the *Y* direction is too low to develop empirical semivariograms. This deficiency will be confirmed

within this chapter. Subsequently, only isotropic weighting function will be developed for the kriging interpolation of measured elevation values onto an isotropically spaced 0.1 m grid.

4.5.1.1 Lift 0 Elevation Data Weighting Functions

The empirical directional semivariograms for the elevation data of Lift 0 are presented in Figures 4.3 and 4.4, and Table 4.1.

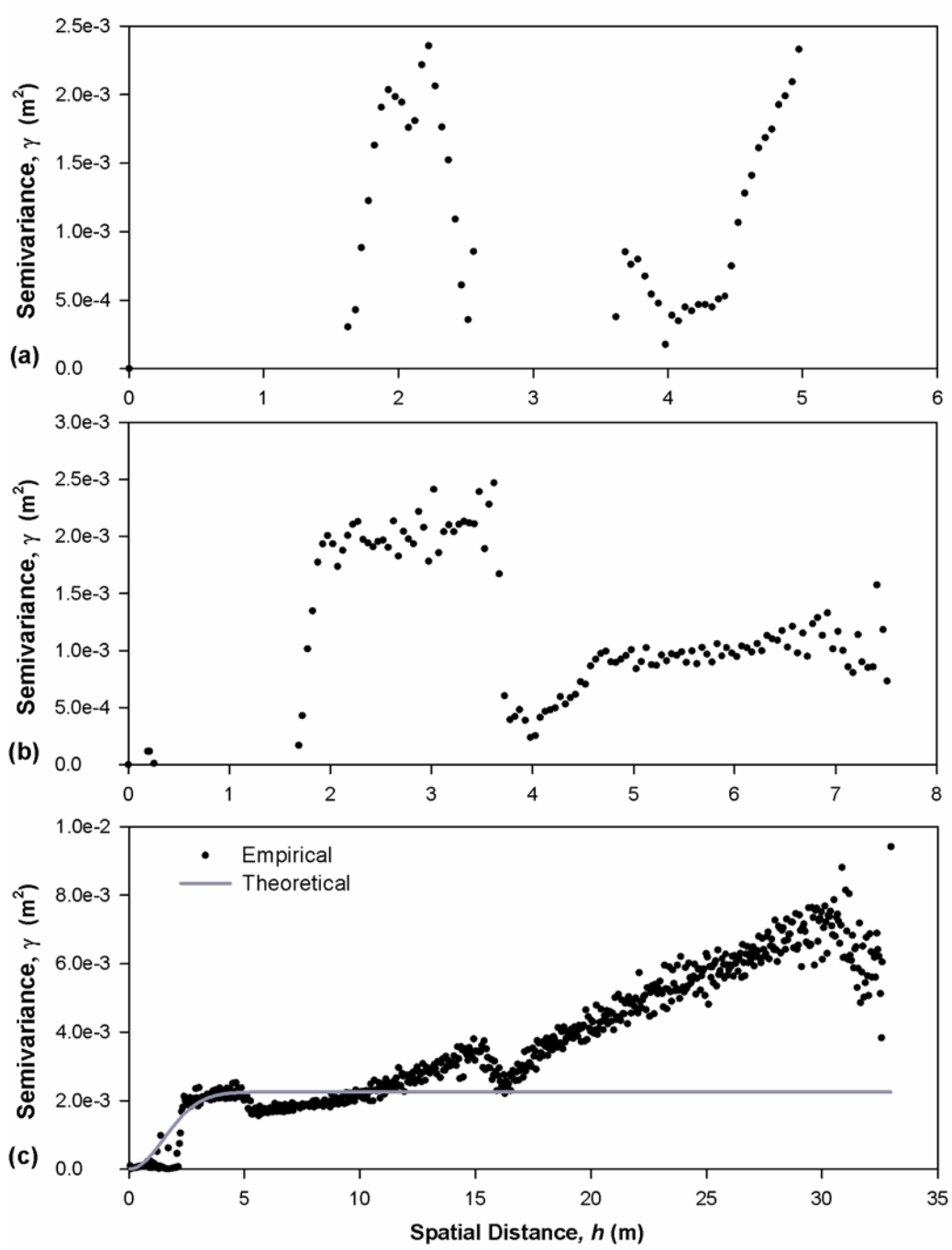

Figure 4.3 Lift 0 elevation empirical semivariograms: a) ψ = 0 degrees; b) ψ = 30 degrees; c) ψ = 60 degrees.

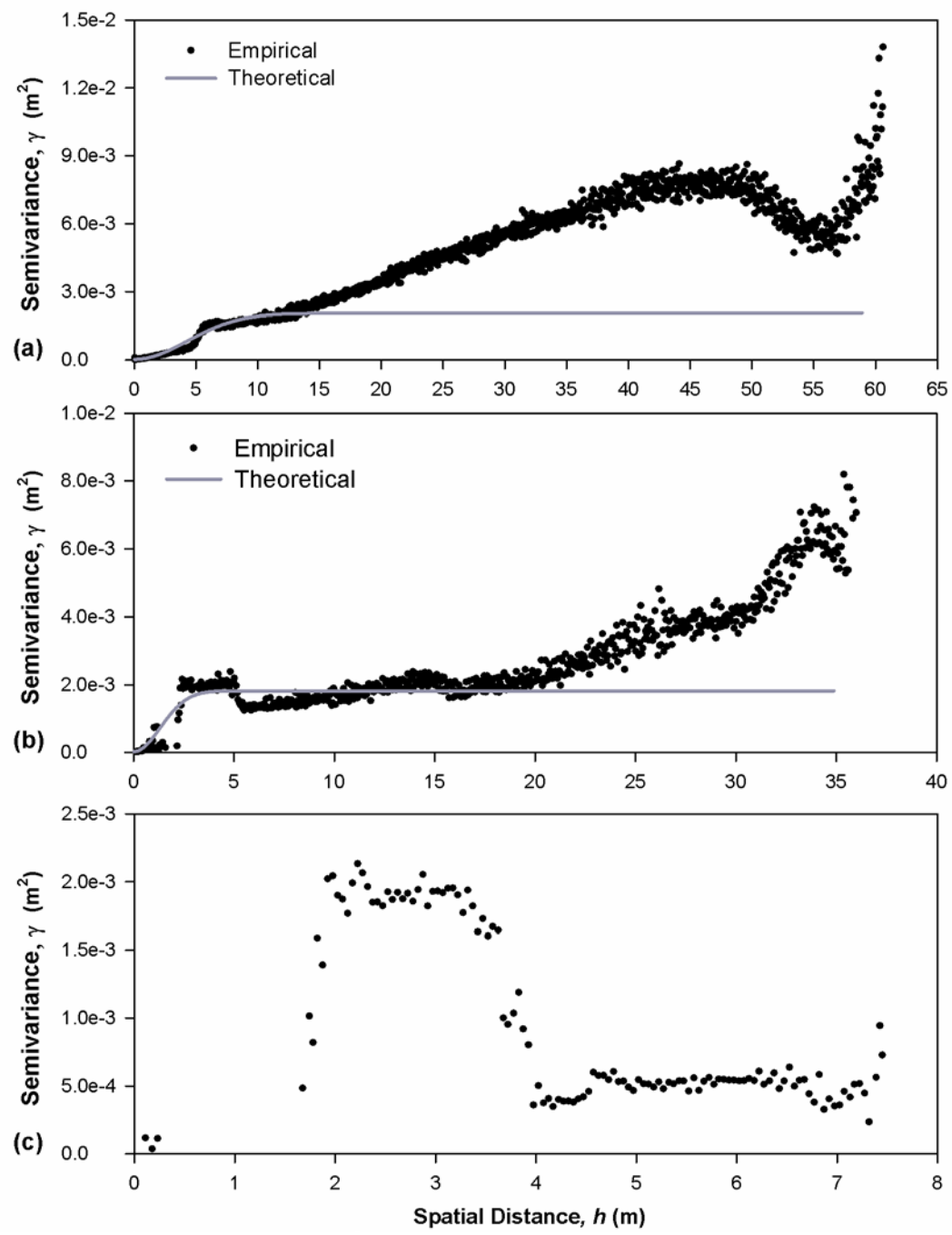

Figure 4.4 Lift 0 elevation empirical semivariograms: a) ψ = 90 degrees; b) ψ = 120 degrees; c) ψ = 150 degrees.

Visual inspection of the empirical semivariograms (Figures 4.3 and 4.4) shows a varying density of data points depending on the angle ψ. The *X*-directional (ψ = 90°) semivariogram has the largest number of data points, while the number of data points decreases as the directional semivariograms moves further away from the *X*-direction. This is a direct result of the density of data recorded in the *X*-direction compared to the *Y*-direction, which has been previously discussed and can be seen in Figure 4.1. Consequently, theoretical semivariogram models were not able to be fit to the empirical semivariograms for ψ angles of 0°, 30°, and 150°.

Observation of Figures 4.3, 4.4 and Table 4.1 show that the range is largest for the *X*-directional theoretical semivariogram model (ψ = 90°). This supports the author's previous assessment that the *X* direction corresponds to the major axis of anisotropy. This is problematic because, as previously mentioned, in order to perform anisotropic kriging, theoretical semivariogram models must be developed in both the major and minor direction of anisotropy. Since there is not enough data to generate a theoretical semivariogram model in the *Y*-direction, anisotropy cannot be properly assessed and anisotropic kriging interpolation cannot be performed. Consequently, isotropic kriging will be used for interpolation of measured elevation data onto a uniform grid for Lift 0.

Table 4.1 Lift 0 elevation theoretical semivariogram model parameters

Angle, ψ (°)	Nugget (m)	Sill (m^2)	Range (m)
60	6.668E-06	0.002245	2.122013
90	2.889E-05	0.002019	6.024451
120	2.712E-05	0.001793	1.887319

In order to perform isotropic kriging, isotropic weighting functions must be determined based on the theoretical omnidirectional semivariograms. The omnidirectional semivariogram for Lift 0 elevation measurements (both the empirical semivariogram and theoretical model fit) are shown in Figure 4.5; the corresponding theoretical model parameters are provided in Table 4.2.

Table 4.2 Lift 0 Elevation Theoretical Semivariogram Model Parameters

Nugget (m)	Sill (m^2)	Range (m)
4.13E-07	0.001764097	2.480211

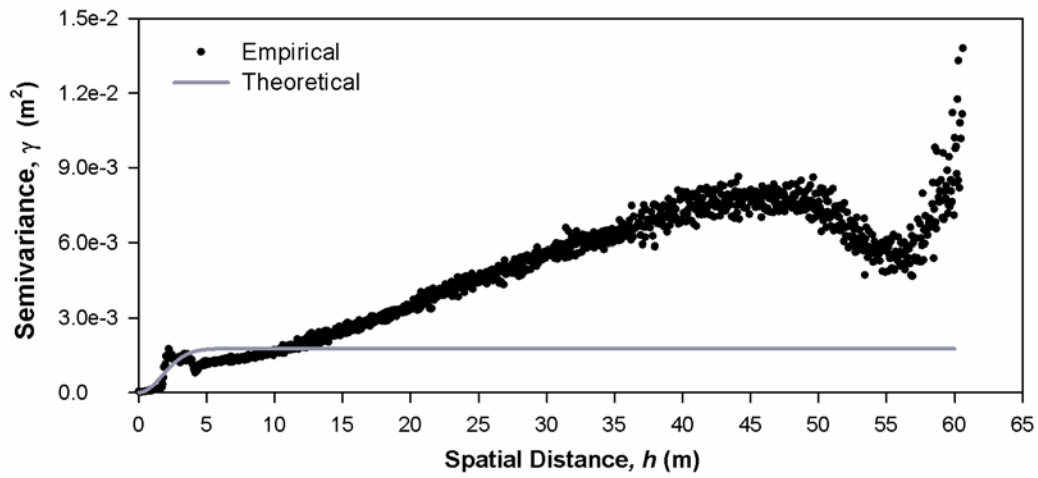

Figure 4.5 Lift 0 elevation omnidirectional semivariogram.

The Gaussian weighting function may now be developed for the Lift 0 elevation data. This function will follow the form of Equation 2.6. The weighting function for ordinary kriging of Lift 0 elevation measurements is the Gaussian isotropic function shown below:

$$\gamma'(h,\theta) = 4.13*10^{-7} + 0.00176\left(1-\exp\left(-\frac{h^2}{2.48^2}\right)\right) \tag{4.3}$$

4.5.1.2 Lift 2, 3, 4, and 5 Elevation Data Weighting Function Determination

Following Section 4.5.1.1, this section will show the examination of anisotropy and selection of isotropic ordinary kriging interpolation functions for Lifts 2, 3, 4, and 5. These Lifts have been grouped together to conserve space within the chapter because they all follow the same trend and process that was observed for Lift 0, as described in Section 4.5.1.1. Figures 4.6 through 4.13 show the directional semivariograms of elevation data for Lifts 2, 3, 4, and 5, at angles ψ of 0°, 30°, 60°, 90°, 120°, and 150°. Table 4.3 shows the theoretical model parameters corresponding to the directional semivariograms. As previously stated, the *X* direction (ψ = 90°) corresponds to the major axis of anisotropy, forcing the minor axis of anisotropy to be along the *Y* axis (ψ = 0°). As was observed for the Lift 0 elevation measurement semivariograms, theoretical semivariogram models cannot be determined in the *Y*-direction due to the low density of elevation measurements. Therefore, anisotropic kriging is not possible and isotropic weighting functions will be used for the gridding of elevation measurements for all of the lifts.

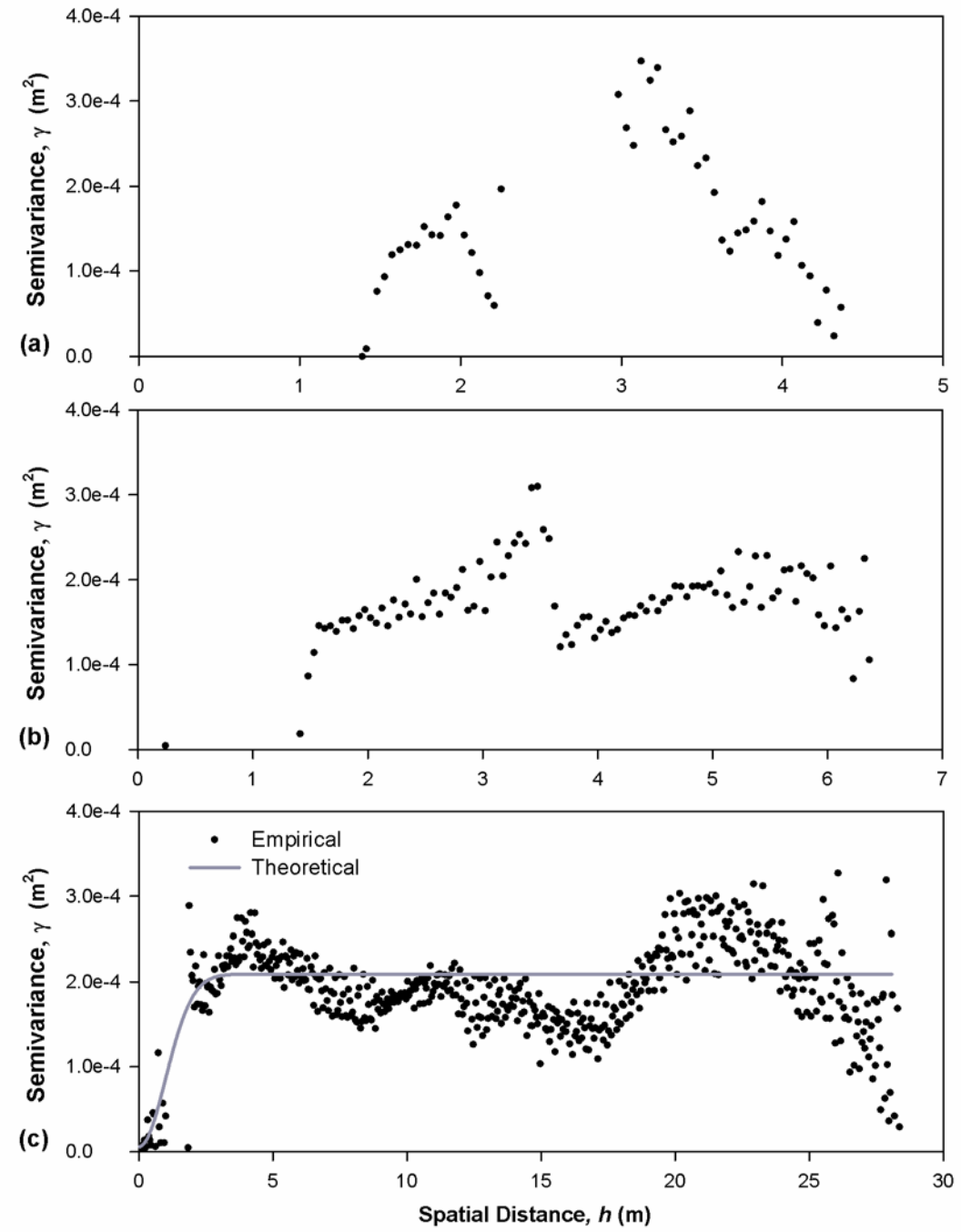

Figure 4.6 Lift 2 elevation empirical semivariograms: a) ψ = 0 degrees; b) ψ = 30 degrees; c) ψ = 60 degrees.

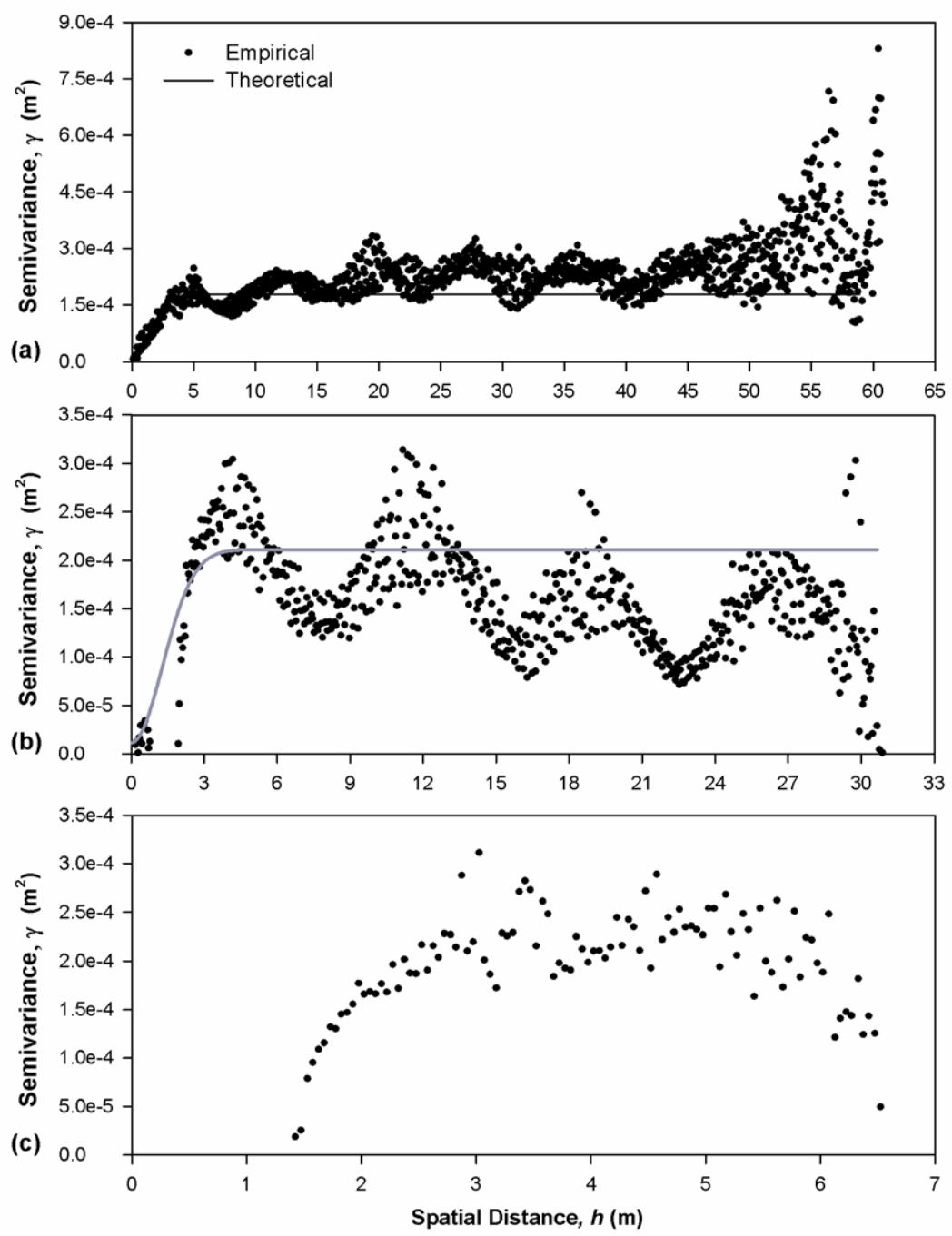

Figure 4.7 Lift 2 elevation empirical semivariograms: a) ψ = 90 degrees; b) ψ = 120 degrees; c) ψ = 150 degrees.

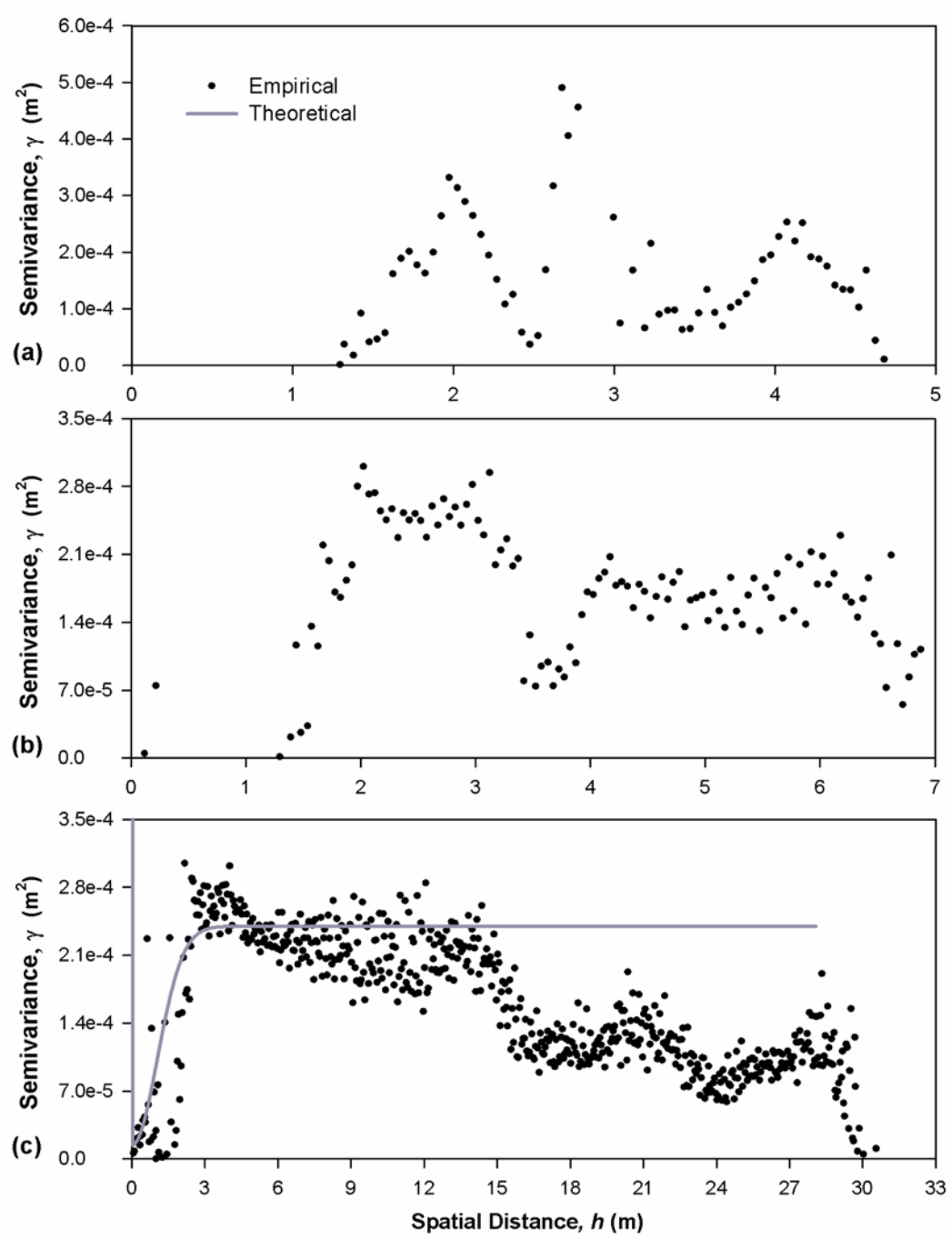

Figure 4.8 Lift 3 elevation empirical semivariograms: a) ψ = 0 degrees; b) ψ = 30 degrees; c) ψ = 60 degrees.

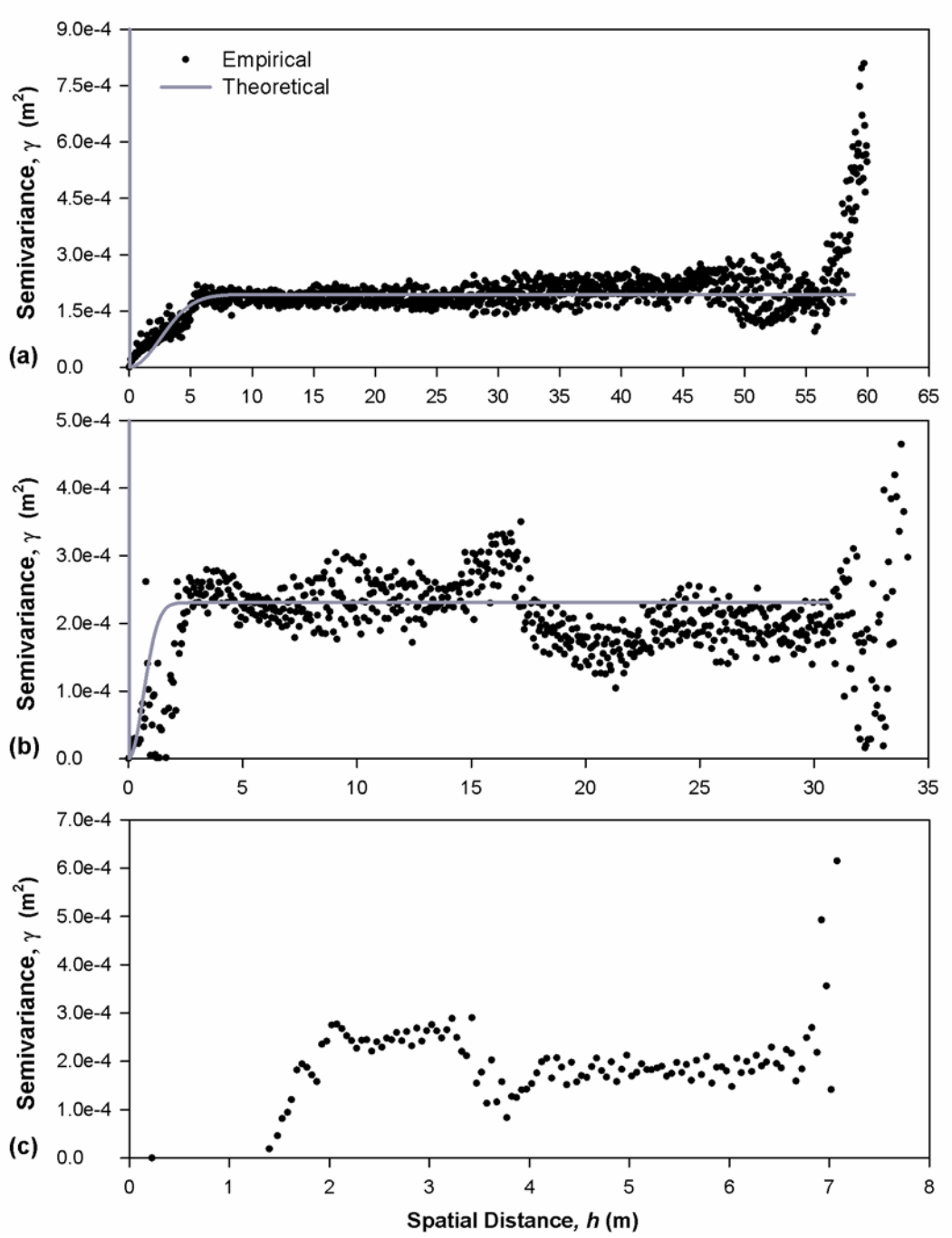

Figure 4.9 Lift 3 elevation empirical semivariograms: a) ψ = 90 degrees; b) ψ = 120 degrees; c) ψ = 150 degrees.

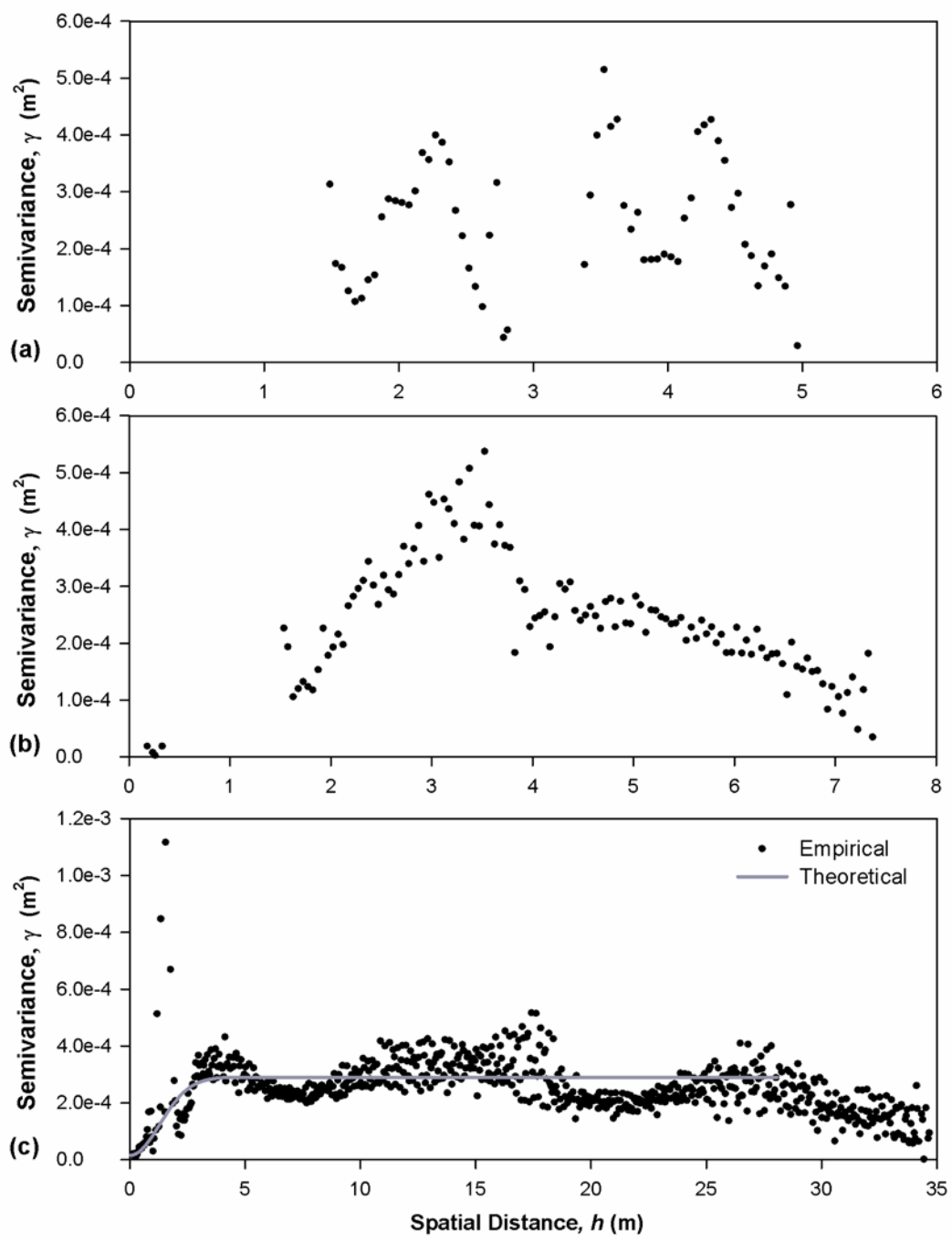

Figure 4.10 Lift 4 elevation empirical semivariograms: a) ψ = 0 degrees; b) ψ = 30 degrees; c) ψ = 60 degrees.

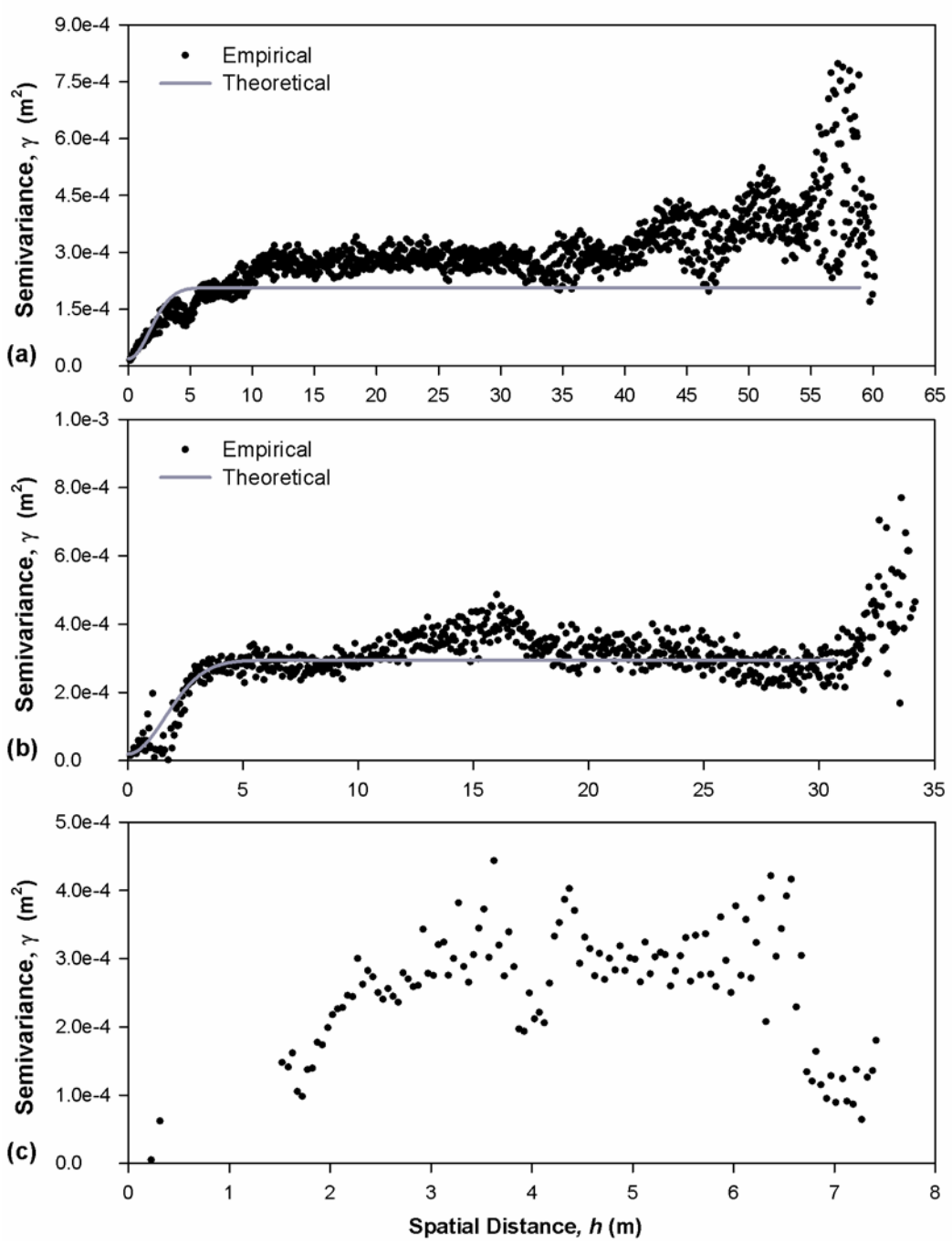

Figure 4.11 Lift 4 elevation empirical semivariograms: a) ψ = 90 degrees; b) ψ = 120 degrees; c) ψ = 150 degrees.

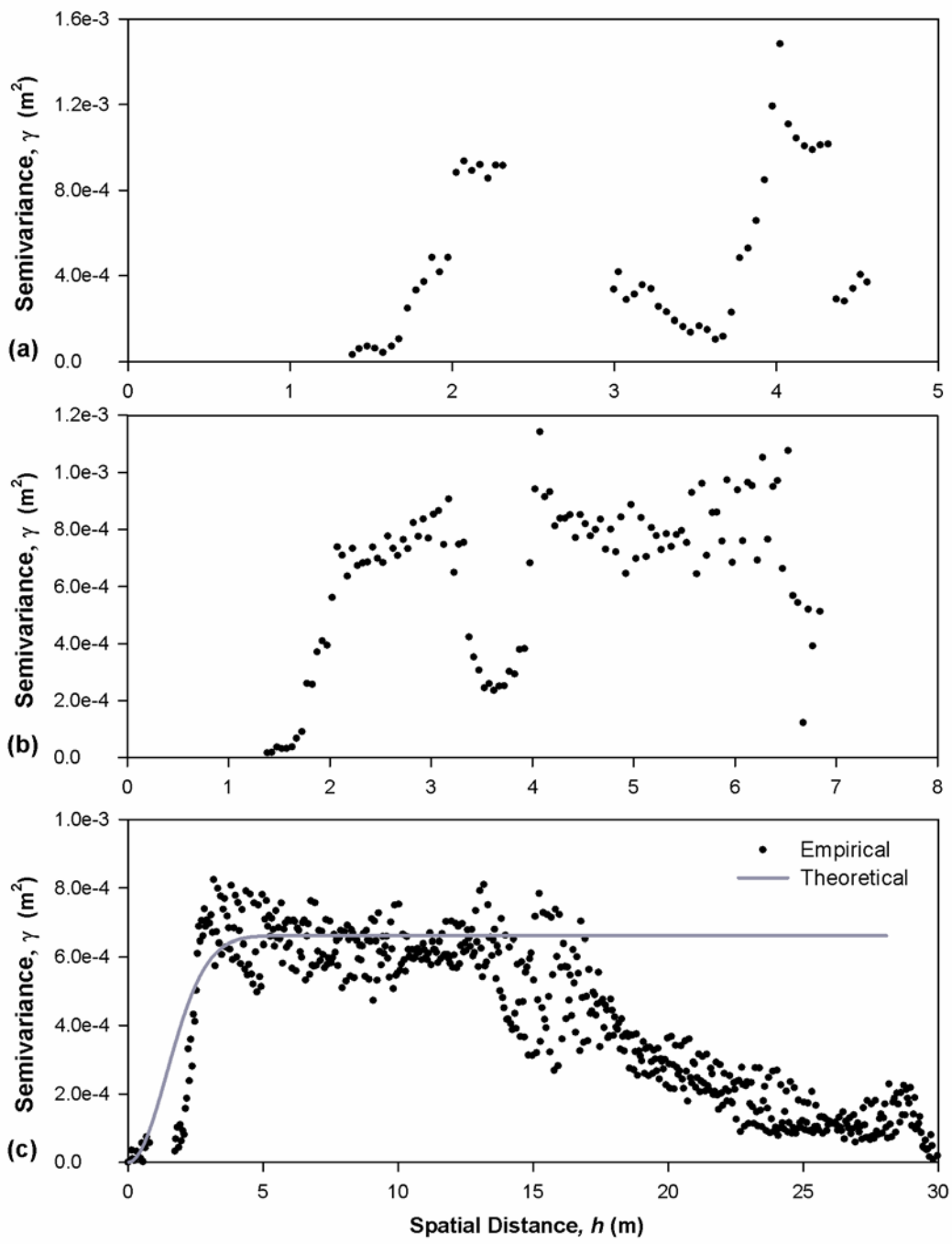

Figure 4.12 Lift 5 elevation empirical semivariograms: a) ψ = 0 degrees; b) ψ = 30 degrees; c) ψ = 60 degrees.

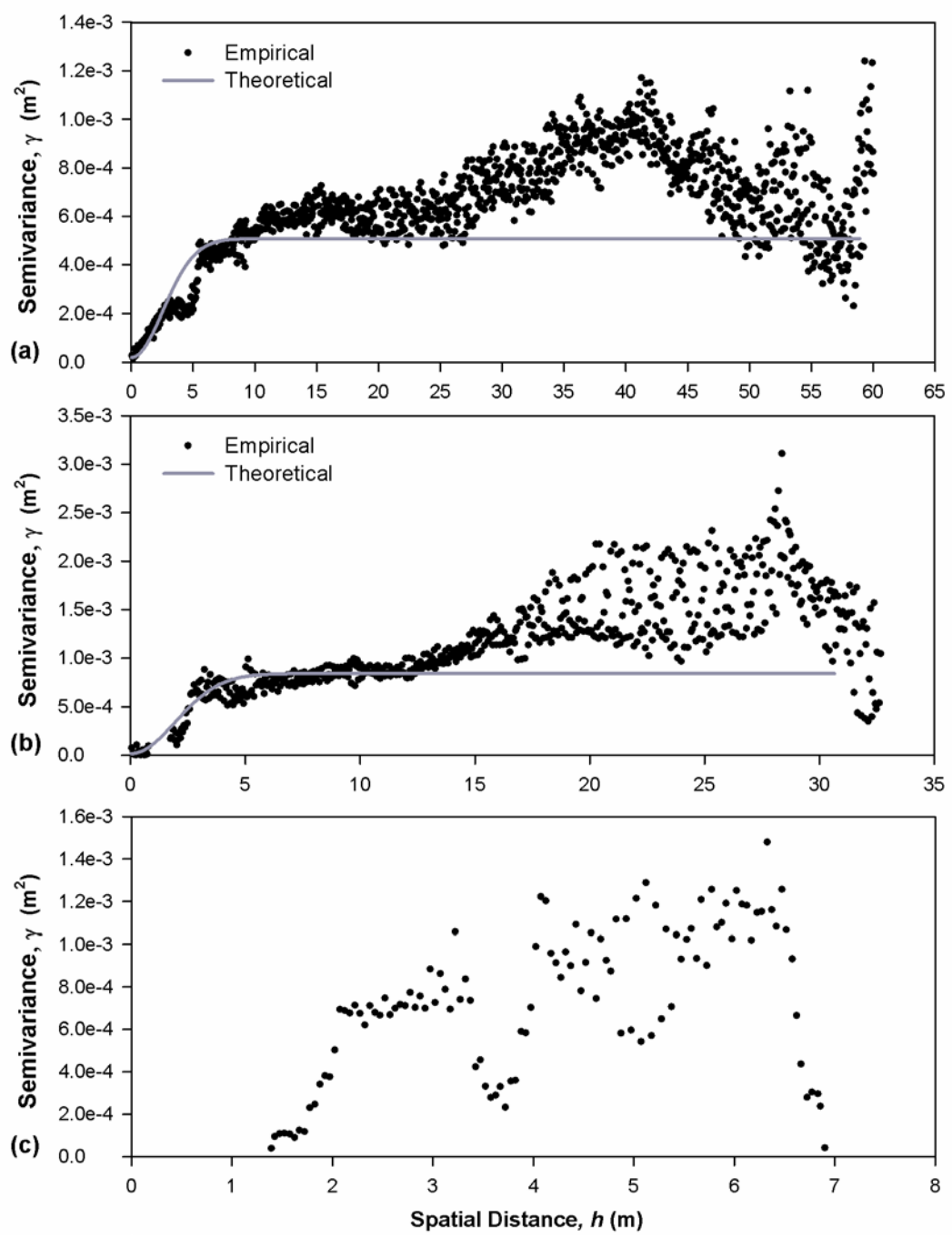

Figure 4.13 Lift 5 elevation empirical semivariograms: a) ψ = 90 degrees; b) ψ = 120 degrees; c) ψ = 150 degrees.

Table 4.3 Lifts 2, 3, 4, and 5 Theoretical Directional Semivariogram Model Parameters

Lift	Angle, ψ(°)	Nugget (m)	Sill (m^2)	Range (m)
Lift 2	60	4.96E-06	0.000203063	1.409765
	90	8.07E-06	0.000169021	**2.003681**
	120	1.15E-05	0.000199548	1.810719
Lift 3	60	1.39E-05	0.000225851	1.478259
	90	1.63E-06	0.000192617	**3.59367**
	120	8.61E-08	0.000230472	0.903505
Lift 4	60	1.49E-05	0.000275318	1.823161
	90	1.91E-05	0.000187508	**2.44502**
	120	1.91E-05	0.000275029	2.309626
Lift 5	60	9.47E-08	0.000660782	2.022746
	90	2.11E-05	0.000487266	**3.636002**
	120	1.66E-05	0.00082515	2.747053

It should be noted that the maximum range value for each lift that is shown in bold text in Table 4.3 indicates that the *X* direction (ψ = 90°) is the major axis of anisotropy for all of the compacted soil lifts. For each of these lifts, the corresponding range of the theoretical *Y*-directional semivariogram could not be determined, making anisotropic geometric kriging impossible. Consequently an isotropic kriging approach employing omnidirectional semivariograms was used for each of the compacted soil lifts.

Determination of the isotropic kriging functions requires fitting of theoretical semivariogram models to the empirical omnidirectional semivariograms. The empirical omnidirectional semivariograms of elevation measurements for Lifts 2, 3, 4, and 5 are presented in Figure 4.14.

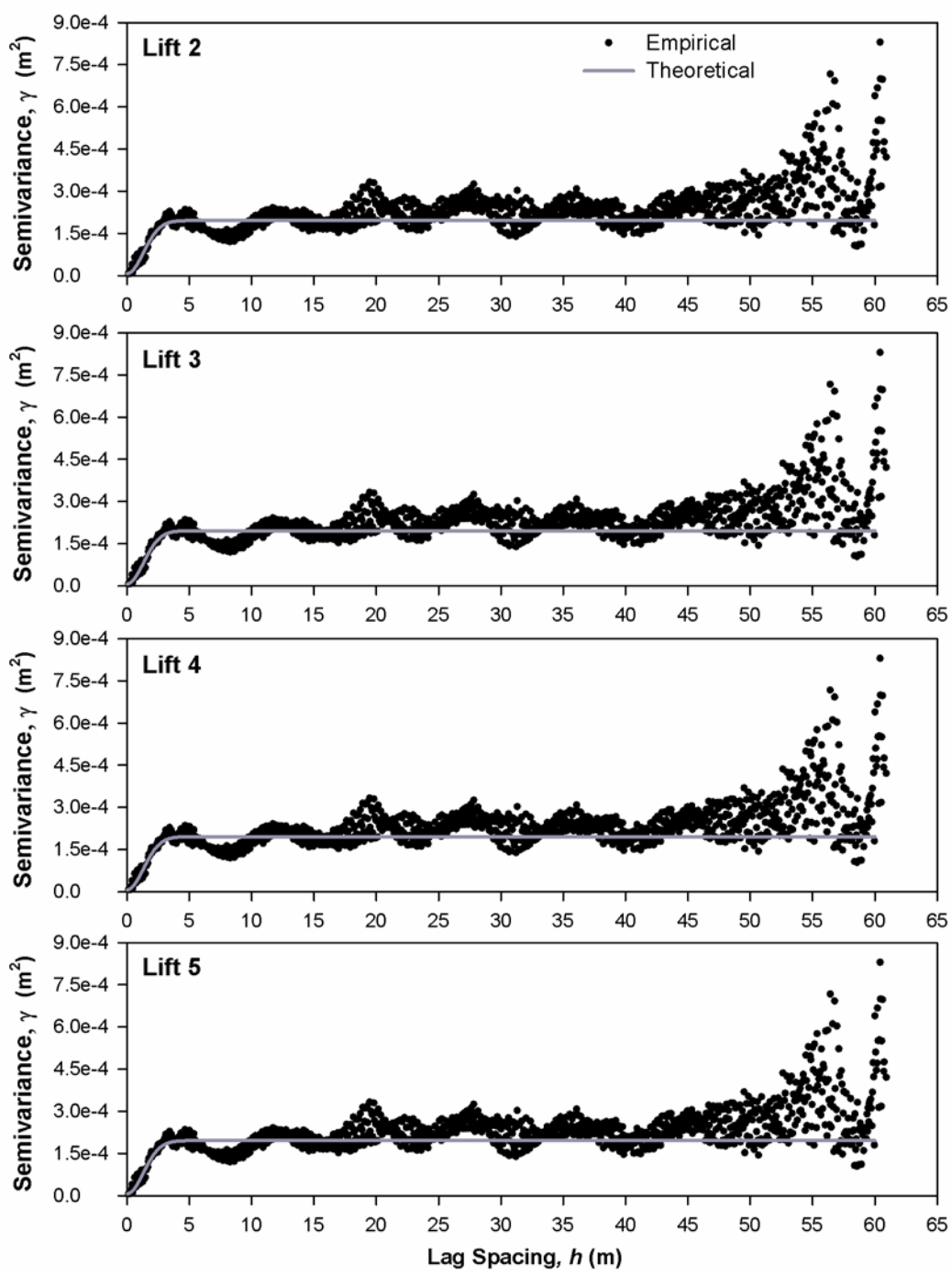

Figure 4.14 Elevation omnidirectional semivariograms for Lifts 2, 3, 4, and 5.

The Gaussian theoretical omnidirectional semivariogram model parameters will be used to determine the weighting functions for isotropic kriging; the associated model parameters for all lifts are summarized in Table 4.4.

Table 4.4 Elevation Theoretical Omnidirectional Semivariogram Model Parameters for All Lifts

Lift	Nugget (m)	Sill (m^2)	Range (m)
Lift 0	4.13E-07	0.001764097	2.480211
Lift 2	6.80E-06	0.000188689	1.858034
Lift 3	6.75E-07	0.000182551	1.246738
Lift 4	1.58E-05	0.000240893	2.04910
Lift 5	1.91E-06	0.000611068	2.08811

It is important to remember that Lift 0 is the only lift that was not "engineered"; instead, this lift is the natural foundation soil of the embankment. The differences between the semivariograms of Lift 0 when compared to the other lifts can be attributed to differences that would be expected between this "natural" soil layer versus a "man-made" soil layer phenomenon. The most noticeable difference that can be seen is in the sill parameter of the semivariogram models. The sill of the Gaussian models for Lift 0 is an order of magnitude greater than that of the subsequent lifts. It is reasonable to expect that the variability of elevation measured values for the "natural" layer will be higher than for elevation measured values of carefully constructed "engineered" lifts. This higher variability could account for the larger semivariances and sill seen in the Lift 0 semivariogram.

Using the omnidirectional parameters presented in Table 4.4, the Gaussian isotropic weighting functions have been generated following the form of Equation 2.6, and are presented in Table 4.5.

Table 4.5 Isotropic Gaussian weighting functions for all lifts

Lift	Isotropic Weighting Function
Lift 0	$\gamma'(h,\theta) = 4.13*10^{-7} + 0.00176\left(1-\exp\left(-\frac{h^2}{2.48^2}\right)\right)$
Lift 2	$\gamma'(h,\theta) = 6.80*10^{-6} + 0.000189\left(1-\exp\left(-\frac{h^2}{1.86^2}\right)\right)$
Lift 3	$\gamma'(h,\theta) = 6.75*10^{-7} + 0.000183\left(1-\exp\left(-\frac{h^2}{1.25^2}\right)\right)$
Lift 4	$\gamma'(h,\theta) = 1.58*10^{-5} + 0.000241\left(1-\exp\left(-\frac{h^2}{2.05^2}\right)\right)$
Lift 5	$\gamma'(h,\theta) = 1.91*10^{-6} + 0.000611\left(1-\exp\left(-\frac{h^2}{2.09^2}\right)\right)$

4.5.2 Lift Thickness Predictions Using the Ordinary Kriging Method

The final compacted thickness of each soil lift can be determined by comparing the interpolated elevation value at each grid point location with the interpolated value at the same grid point location for the underlying lift. Taking the difference in elevation values from lift to lift at each of the grid point locations allows a spatial map of lift thickness to be built.

Final compacted thicknesses of each soil lift are presented as determined by the isotropic ordinary kriging method (Figure 4.15). The isotropic soil lift thicknesses were predicted using the isotropic weighting functions presented in Table 4.5. Table 4.6 offers an explanation of the notation for layer numbering by showing the successive lifts that correspond to Layers 1, 2, 3, and 4.

Table 4.6 Layer Notations

Layer Name	Corresponding Lifts
Layer 1	Lift 2 - Lift 0
Layer 2	Lift 3 - Lift 2
Layer 3	Lift 4 - Lift 3
Layer 4	Lift 5 - Lift 4

For easy assessment of the distribution of the lift thickness results, histograms are presented in Figure 4.15. Additionally, the mean lift thickness of each layer (μ), standard deviation (σ), and coefficient of variation (COV) for each layer are displayed on the respective histograms.

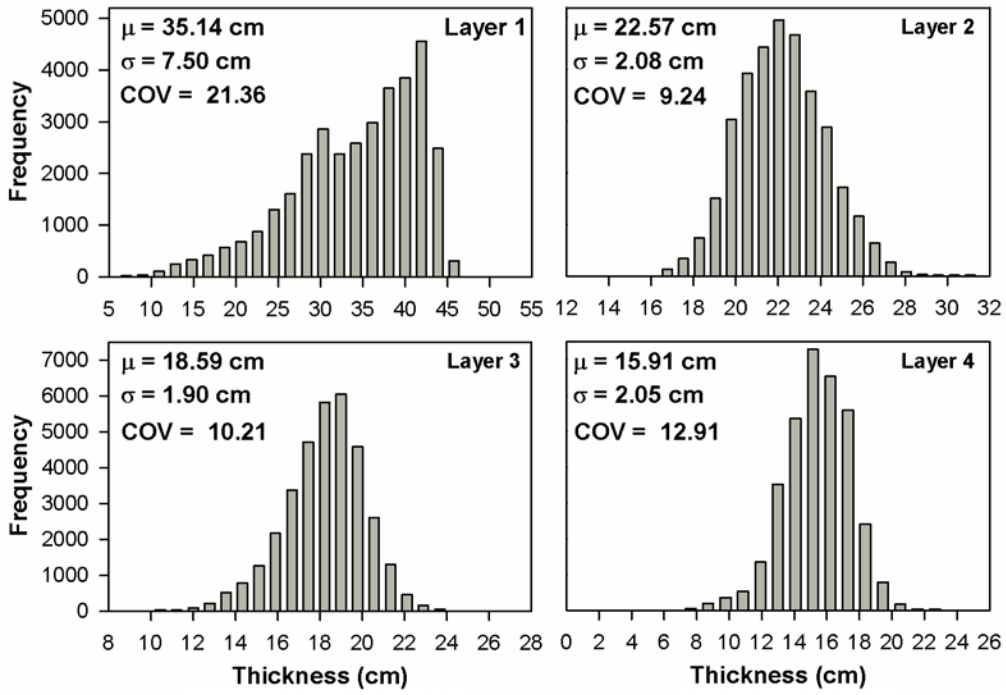

Figure 4.15 Isotropic kriging predictions of lift thickness.

When examining the lift thickness data, it should be noted that the Layer 1 data corresponds to the thickness of two compacted soil lifts, due to a field malfunction with the data acquisition system during the placement of the first lift (Lift 1). Consequently, the thickness measurements for Layer 1 are much larger than those for the other lifts. Also, it should be noted that Lifts 1 and 2 (Layer 1) were spread manually by a bulldozer operator, while Lifts 3-5 (Layers 2, 3, and 4) were placed using the same bulldozer with GPS-control on the blade of the bulldozer. Furthermore, when placing the base lift in the field, it was also observed that the bulldozer operator tended to fill low areas with thicker soil lifts to achieve a more uniform pad for soil compaction; this is reflected in the data shown in Figure 4.15, and is likely the reason that the standard deviation for Layer 1 is much larger than what was observed for Layers 2-4. Table 4.7 provides the mean, standard deviation, and coefficient of variation values for the thickness of each layer.

As previously mentioned in Chapter 3, the goal of this project was to build a road subbase embankment to an approximate total final height of 0.9 m (3.0 ft), by compacting five 20.3 cm (8 in.) loose-lift layers. However, actual QA/QC monitoring of loose-lift thickness in the field was much more casual, as is typical of many real field projects – there was simply too much going on to keep track of spreading and loose-lift placement operations at all times, even with a number of experienced field personnel (and most typical sites this size would only have one or two field engineers). However, by examining the mean compacted lift thickness data shown in Table 4.7, it can generally be observed that the mean after-compaction lift thicknesses were fairly reasonable for the current project. (It should be noted, however, that this observation

requires a bit of judgment, as the loose-lift and compacted-lift thickness values are different measures of thickness).

Table 4.7 Summary Statistics of Layer Thickness for Isotropic Kriging

Layer	Mean (cm)	Standard Deviation (cm)	COV (%)
1	35.14	7.50	21.36
2	22.57	2.08	9.24
3	18.59	1.90	10.21
4	15.91	2.05	12.91

The data presented in Figure 4.15 and Table 4.7 offers a good understanding of the overall data set base on the summary statistics (e.g. mean, standard deviation, and coefficient of variation). However, in a specifications framework, the engineer would also be concerned with the specific locations of the “thicker areas” and “thinner-areas” within the compaction area. Contour plots of the isotropic kriging lift thickness results for each of the four layers are presented in Figure 4.16 to allow for assessment of location-specific differences in thickness throughout each compacted layer.

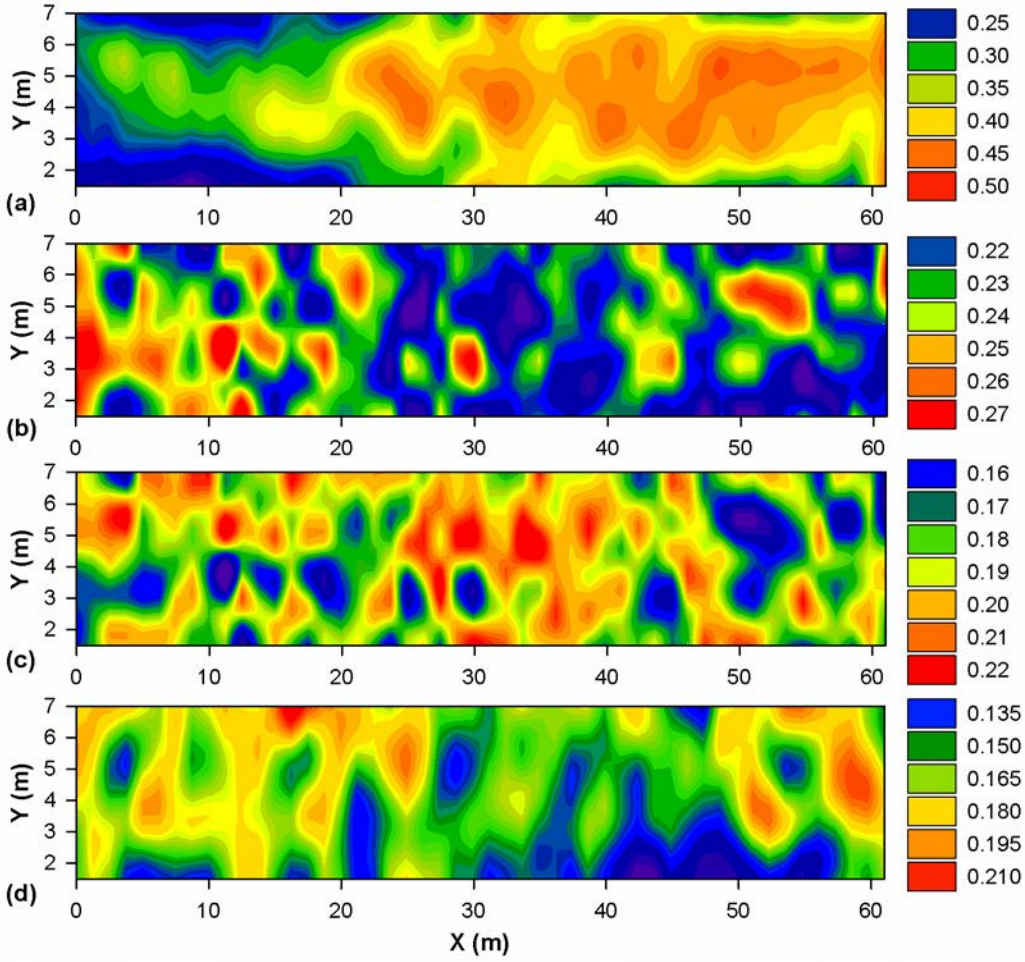

Figure 4.16 Contour plots of lift thickness determined using an isotropic kriging approach: (a) Layer 1; (b) Layer 2; (c) Layer 3; and (d) Layer 4 (contour intervals shown are in m).

For this specific data set, the isotropic ordinary kriging approach has proven acceptable for interpolating measured elevation values onto a uniform grid. This approach can then be used to build spatial thickness maps that provide a contractor or field QA/QC personnel with feedback about areas where overly thick soil lifts have been placed. Future studies using a data set that is more balanced in the *X*- and *Y*-

directions are recommended for assessing whether or not an anisotropic kriging approach is more appropriate for roller-measured RTK-GPS data.

4.6 Limitations to Using a Kriging Approach in a Specification Framework

Kriging methods have been widely used as the state of the art for prediction of CCC measured values due to their ability to consider both the distance and degree of variation between measured values for predictions resulting in the best linear unbiased prediction (BLUP). However, the complexity of this method requires significant computational effort and a strong background in statistics. The use of kriging methods for determination of lift thickness may not be the best technique for deployment of geospatial interpolation tools in a specification (QA/QC) framework. This is particularly true because field engineers or engineering technicians will need to perform these elevation predictions in real time in the field during the compaction process.

An additional drawback to using kriging methods is that they require some judgment-based decisions which can significantly influence the kriging prediction results. The determination of the empirical and theoretical semivariograms is judgment-based and presents repeatability problems. Additionally, evaluation of directional semivariograms must be performed to assess the magnitude of anisotropy that is present for a given data set. This includes the fitting of models to the data to create theoretical models needed for comparison of range values and kriging predictions. As mentioned previously, there are a variety of different models to choose from and each one of them requires user determination of the input parameters (e.g. range, sill, and nugget). These examples represent only a few of the many complexities of kriging which have been discussed throughout the chapter.

The variety of judgment-based factors that are needed when performing kriging can make user-to-user analysis of a given data set fairly variable. This potentially opens room for conflicts between the owner and contractor if this procedure is to be used as part of a field QA/QC specification framework. Consequently, it is worth exploring the use of simpler interpolation techniques for predicting elevation values at grid point locations.

4.7 Inverse Distance Weighting (IDW) Method for Lift Thickness Prediction

Although, there are several types of more sophisticated weighted neighborhood approaches that can be employed within an inverse distance weighting (IDW) interpolation framework (e.g., Shepard's 1968 method), a relatively simplistic isotropic IDW approach was utilized in the current study. The reason for this was to provide a simple, repeatable interpolation method that is easily understandable for field engineers and technicians, with little room for debate between contractors and owners. If a more sophisticated interpolation approach is needed, it is recommended that the kriging techniques that are previously discussed be utilized.

For the roller data that was recorded in this study, the IDW method was applied to the elevation data, with four different exponent values being assessed: p = 1, p = 2, p = 4, and p = 64 (Figures 4.17 and 4.18). Selection of the correct exponent value is a critical step in performing IDW interpolation. An increase of the exponent value results in a diminishing "smoothing" effect on the measured data. The most common choice for the exponent value is p = 2, however, p = 4 is also common, especially when utilizing Shepard's method for IDW (Shepard 1968). Although p = 1 and p =64 are acceptable exponent values from a mathematical respect, they represent the two extreme cases of the "smoothing" effect for this particular elevation data set.

Through observation of Figure 4.17 it is clear that an exponent value of $p = 1$ is not suitable for this data set since due to the excessive smoothing. An exponent vale of p = 64 shows the opposite effect and is also not suitable (Figure 4.18). Observation of the contour plots leads the author to believe that IDW interpolation with an exponent value of either $p = 2$ or $p = 4$ may potentially prove as adequate alternatives to the ordinary kriging method.

In addition to this visual assessment of the IDW exponent value selection, there is a mathematical way to assess which exponent value is appropriate. Based on the assumption that the isotropic kriging prediction results are the "best" possible predictions, the IDW prediction results that match the most closely with the kriging results can be considered to be the most accurate. In order to utilize this approach, the point-to-point error must be compared between the kriging results and the various IDW results.

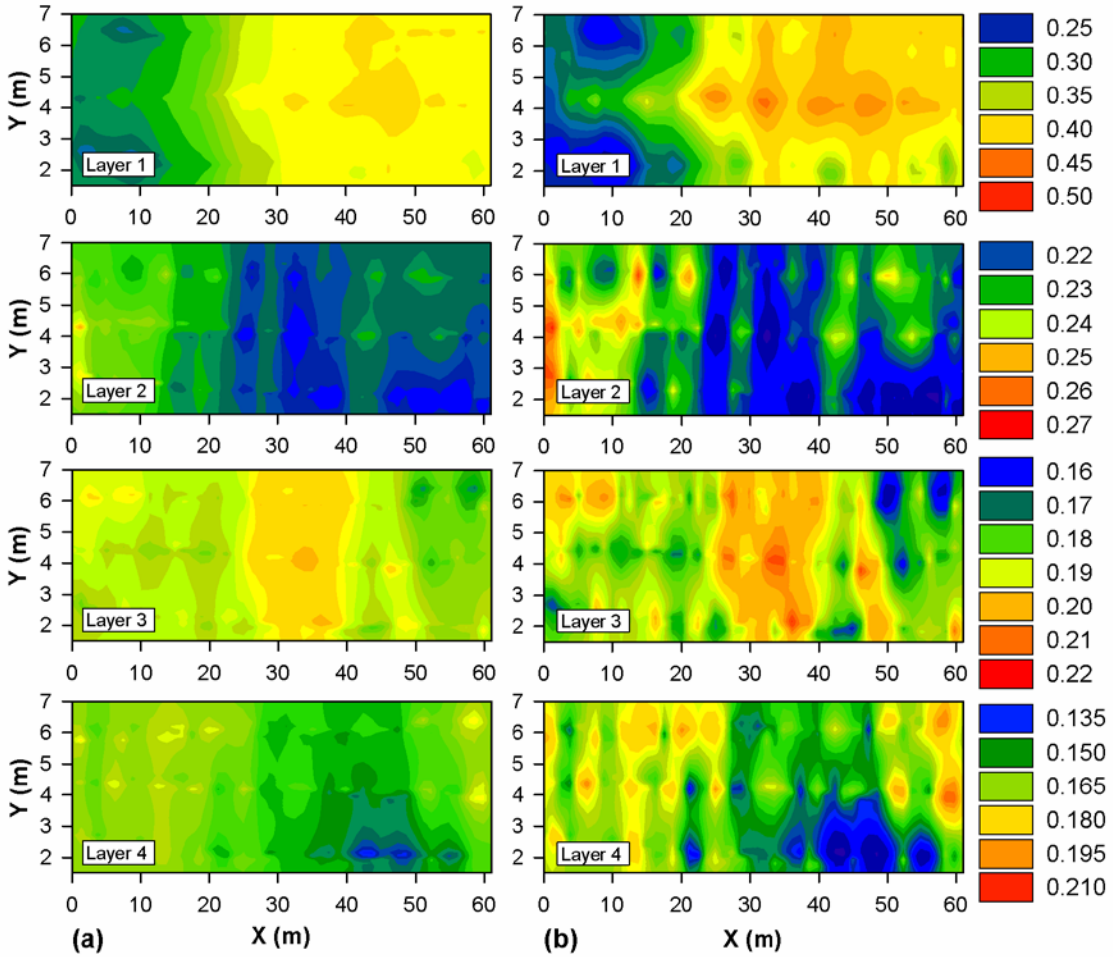

Figure 4.17 Contour plots of lift thickness (m): a) IDW *p* = 1; b) IDW *p* = 2.

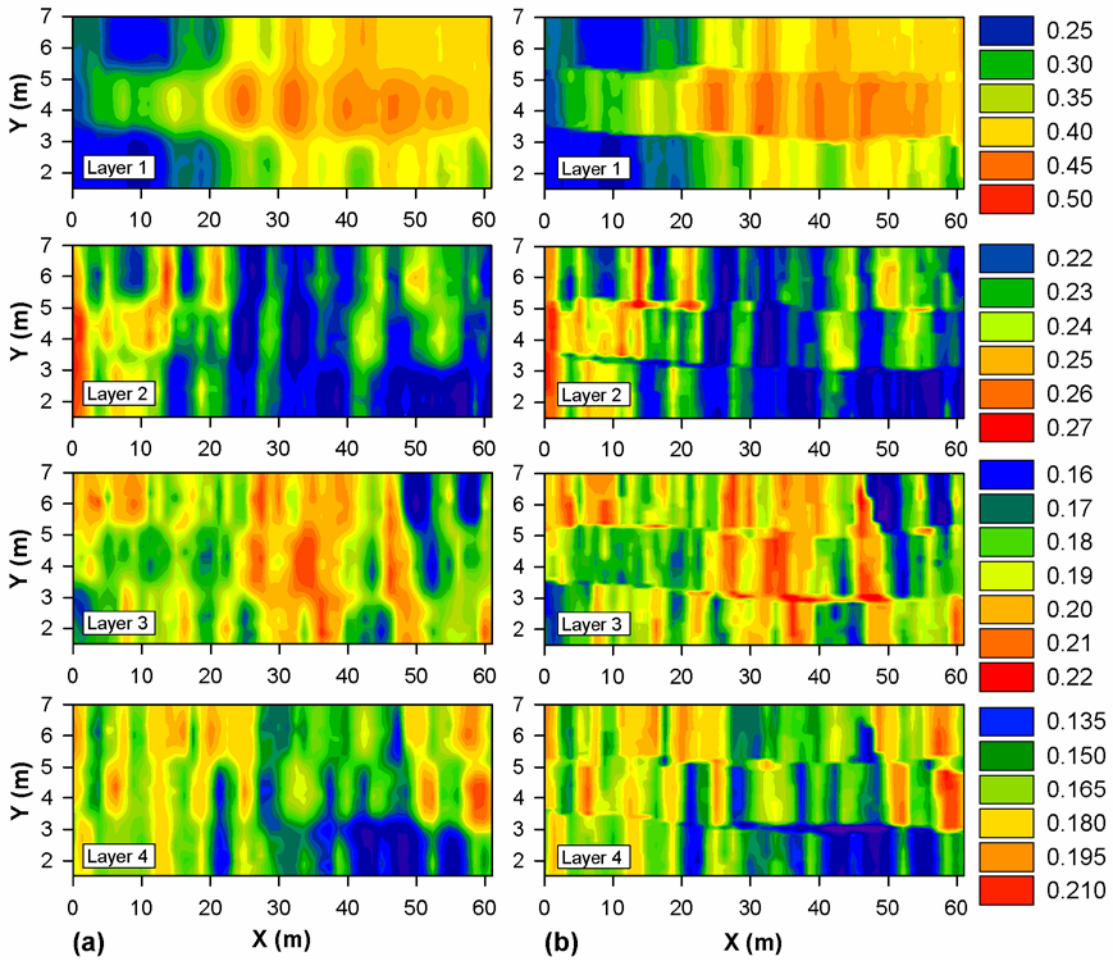

Figure 4.18 Contour plots of lift thickness (m): a) IDW *p* = 4; b) IDW *p* = 64.

A mathematical approach for assessing the point-to-point error between "observed" (kriged) and "predicted" (IDW) values is to calculate the root mean square error (RMSE). The calculation for RMSE is shown in Equation 4.2.

$$RMSE = \sqrt{\frac{1}{N}\sum_{i=1}^{N}(y_i - \hat{y}_i)^2} \qquad (4.2)$$

where N is the total number of observed values, y is the observed value, and $\hat{y}$ is the predicted value. In this case, the smaller the RMSE value, the better the ability of the interpolation method to predict results that match the results of the kriging prediction of CCC measurements. The resulting RMSE values for comparison of the four IDW exponent values in question and the isotropic kriging layer thickness predictions are summarized in Table 4.8.

Table 4.8 RMSE between Predicted Elevation Values Determined Using an Isotropic Kriging Approach and an IDW Approach with Various Exponent Values

Layer	IDW (p = 1)	IDW (p = 2)	IDW (p = 4)	IDW (p = 64)
1	0.0382	0.0212	**0.0164**	0.0195
2	0.0110	0.0057	**0.0043**	0.0072
3	0.0098	0.0057	**0.0053**	0.0086
4	0.0146	0.0084	**0.0071**	0.0111

Observation of Table 4.8 shows that the IDW lift thickness prediction results using an exponent value of p = 4, exhibited the least amount of point-to-point variation when compared to the isotropic lift thickness predication results. Before declaring that IDW p = 4 interpolation is a suitable alternative to kriging, there are a few other practical concerns that must be investigated. First the general summary statistics (mean, standard deviation, and coefficient of variation) for the prediction results from the two techniques should be compared. The summary statistics are provided in Table 4.9.

Table 4.9 Summary Statistics of Layer Thickness Summary Statistics for Anisotropic Kriging and IDW (p = 4)

Layer	Isotropic Kriging			Inverse Distance Weighting, p = 4		
	Mean (cm)	Standard Deviation (cm)	COV (%)	Mean (cm)	Standard Deviation (cm)	COV (%)
1	35.00	6.75	19.29	34.67	6.55	18.88
2	22.46	1.56	6.97	22.46	1.58	7.05
3	18.70	1.29	6.87	18.71	1.32	7.05
4	15.84	1.92	12.10	15.84	1.92	12.15

Observation of Table 4.9 shows that the summary statistics of the two resulting layer thickness data sets are very similar, further supporting the selection of IDW p = 4 as an alternative to ordinary isotropic kriging.

The last check that should be performed before IDW p = 4 is declared as an acceptable alternative is to compare contour plots of layer thickness predictions for IDW p = 4 and kriging side-by-side to access the local spatial agreement (Figure 4.19). This is of significant importance if this framework is to be used as a QA/QC tool, since field engineers will need to be able to identify the “thinner” and “thicker” areas within the compaction area. Observation of Figure 4.19 offers confirmation that there is good agreement of the “thinner” and “thicker” areas between the two interpolation techniques.

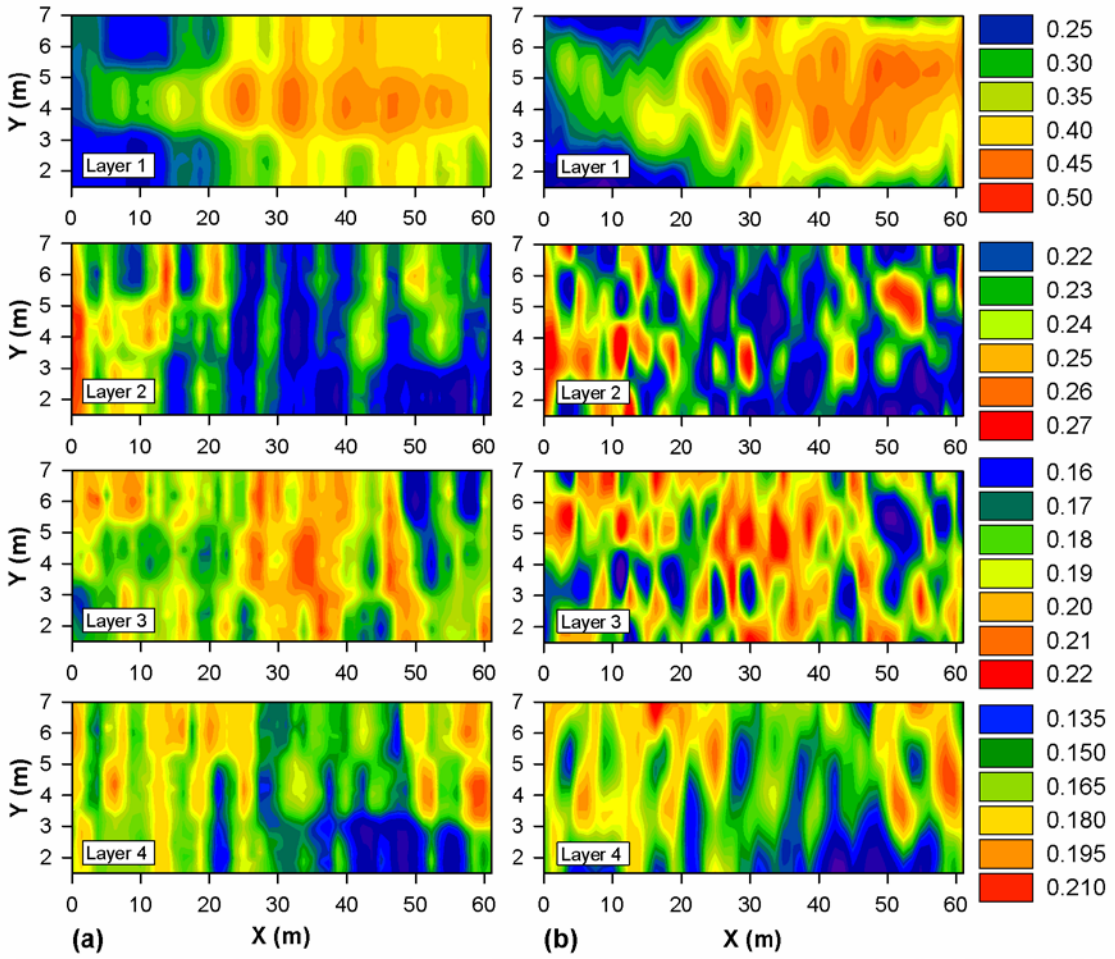

Figure 4.19 Contour plots of lift thickness a) IDW p = 4; b) Isotropic Kriging.

A comparison of the RMSE values in Table 4.8, the summary statistic values shown in Table 4.9, the "smoothness" effect observed in Figures 4.26 and 4.27, and the identification of "thicker-areas" and "thinner-areas" in Figure 4.19 generally support the conclusion that the IDW method with p = 4 may be an acceptable substitute for ordinary isotropic kriging, for prediction of "typical resolution" RTK-GPS elevation data. Further studies are needed to support this conclusion, as it is not yet clear if this trend will be consistent across other data sets. Side-by-side results

presented using isotropic kriging and an IDW approach with $p = 4$ allow the reader to make their own assessment and comparisons of these two approaches.

4.8 A Discussion of Thickness Measurements, Their Accuracy, and the Effect of this Accuracy on Specification Implementation

The QA/QC procedure that is proposed within this chapter utilizes RTK-GPS measured position values and grid point interpolation to construct spatial maps of soil lift thickness. The proposed technique has the potential for use in in monitoring the lift thickness specification criterion during earthwork compaction projects. The technique has the potential for use to monitor both “loose lift” and “compacted lift” specifications. The technique demonstrated throughout this chapter is for compacted soil lifts. Based upon experience from the current study, it is the author’s recommendation that this QA/QC technique be used to assess the thickness of compacted soil lifts. The necessary RTK-GPS position data is best obtained from QA/QC roller measurements that are made during the final pass of compaction for each lift, as was done in the current study.

Essentially, this procedure proposes the use of RTK-GPS equipment to perform field surveying of soil lift elevation. It is essential that there be discussion on the accuracy of the RTK-GPS to evaluate the possible effects of measurement uncertainty, due to the effect that this factor can have on implementation of this technique within a specification framework.

A detailed discussion of the accuracy of the RTK-GPS equipment and the resulting implications on the proposed QA/QC technique is provided in Meehan et al. 2013. The following excerpt provides this discussion (Meehan et al. 2013):

"Conventional RTK-GPS manufacturer specifications cite nominal accuracy for their dual-frequency GPS systems that are on the order of ±(1 cm + 2 ppm) for horizontal position measurements and ±(2 cm + 2ppm) for vertical position measurements; independent verification of these accuracy levels has shown that they are generally correct within reasonable survey distances from the base station unit (e.g., Lemmon and Gerdan 1999). Many vendors also indicate that the more satellites that are being received, the better the measurement accuracy will be, which seems logical given the general operating principles of GPS technology. Interestingly, Lemmon and Gerdan (1999) reported that, for field surveys conducted where the GPS satellite counts ranged between 5 and 9, an increase in satellites made no significant contribution to the accuracy of the RTK positions (although the reliability of the ambiguity resolution process did improve).

With RTK-GPS systems, a secondary receiving station is set up in the near vicinity of the survey area. This receiving station, which is typically called a "base station", is set up over a known, surveyed point, and its primary function is to eliminate survey errors caused by the earth's atmosphere. As the base station receives GPS satellite information, it compares that data to its known location and continually transmits correction data to the "roving" GPS receivers and GPS machine control units that are located at the job site. This local correction data allows the roving units to calculate their "relative" position often to an accuracy level of a few millimeters.

In general, the "relative" position accuracy of various roving units that are measured with an RTK-GPS unit that has a base station setup has not been as well quantified by manufacturers or researchers, as the accuracy of relative position measurements is more difficult to directly ascertain. However, most manufacturers

and researchers generally agree that local coordinate measurements made by RTK-GPS systems (e.g., relative position measurements) are generally more accurate than the absolute accuracy values that are quoted by GPS manufacturers. In general, the absolute accuracy of RTK-GPS measurements is also limited by the accuracy of the field survey that was used to determine the position of the base station.

In any case, it is not overly productive to get caught up in a detailed discussion of whether the accuracy level of RTK-GPS systems is a few millimeters or a few centimeters. RTK-GPS systems are generally accepted to be accurate enough for "rough" survey control. Moreover, the approach that is proposed herein is significantly more accurate than the current state of practice for field QA/QC of lift thickness.

If the agency or agent responsible for QA/QC has concerns about how the potential measurement accuracy of RTK-GPS systems could be drawn into a contentious debate between an owner and contractor, or how this discussion of uncertainty error might play out in a penalty or incentive framework (or worse yet, in a courtroom setting), the solution is a fairly simple one: If you want an 18 cm thick lift at the end of compaction, only penalize the contractor for areas of the lift that are thicker than 20 or 21 cm. Also, in the specification, be sure to specify a minimum number of satellites that must be maintained (5 seems reasonable, corresponding to the observations made by Lemmon and Gerdan 1999), and require that the data acquisition system actively record the number of satellites for each position point measurement that is made. This takes the question of accuracy off the table, while keeping the big picture in mind – after all what is the real goal here? To catch lifts that are being placed at 150% or 200% of their maximum specified lift thickness, not

105% - e.g., the "bad offenders" in the soil compaction process that will likely lead to performance-related problems in the long-term.

If nothing else, perhaps the most important point to make here is that, if deployed properly, the methodology that is proposed here will "do no harm". That is, we now have a tool that could be used to identify potential problem areas, particularly areas that are in gross violation of lift thickness placement requirements. If there is a real concern about the accuracy of the RTK-GPS equipment, once these problem areas are identified, other more traditional tools (manual measurements, high-accuracy field surveying, etc.) can be deployed to assess the significance of the problem."

4.9 Summary and Conclusions

In this chapter, a framework is presented for using field RTK-GPS position measurements made by CCC or IC equipment to monitor and control the thickness of compacted soil lifts during construction of a roadway embankment.

The QA/QC procedure that is proposed involves the following steps:

(1) During the compaction process, continuously record compactor position information (*X*, *Y*, and elevation data) for at least two successive compacted soil lifts. Typical CCC procedures require collection of position data for each compactor pass in a given lift. However, for the proposed monitoring procedure, it is only necessary to compare data collected from the final pass of compaction for two consecutive soil lifts.

(2) Select a "projection grid" that is consistent from lift to lift to enable comparison of elevation measurements for two consecutive lifts, for determination of lift thickness. According to the current study, the "projection grid" should be isotropic,

with a grid point spacing that is near the lower bound of the measured point spacing distances in the roller travel direction (the *X*-direction).

(3) Predict elevation values at each of the grid point locations of the "projection grid", using the measured elevation (*Z*) data from the final pass of compaction for each lift. Based upon the results from the current chapter, either an ordinary isotropic kriging approach or an inverse distance weighting (IDW) approach with an exponent value of $p = 4$ may be utilized for this purpose. The author strongly recommends the IDW method, as it is simpler and less user sensitive, and the results from this study did not differ substantially from the more sophisticated ordinary kriging approach.

(4) Determine the spatial lift thickness of each compacted soil lift by taking the difference in elevation values from lift to lift at each of the "projection grid" point locations. Calculate the mean lift thickness and a statistical measure of its variability (standard deviation and/ coefficient of variation). Additionally, generate spatial maps of the lift thickness to identify "thinner" and "thicker" areas; this can be done with contour plots. In the event that the mean is larger than specified or the variability is higher than desired, the spatial maps can be used to identify problem areas for the contractor to address, in an attempt to meet the specification requirements, prior to moving on to the next lift.

As demonstrated in this paper with data collected from a full-scale field study, this proposed QA/QC technique can be effectively used to monitor compacted soil lift thicknesses. Additional research using CCC rollers is needed to determine acceptable target levels for "good construction practices" and "bad construction practices", prior to development of specifications that utilize this approach. Further research is also

needed to develop a better understanding of the effect that RTK-GPS measurement accuracy has on lift thickness measurements. Once target levels of acceptability for “good construction practices” and “bad construction practices” have been defined and the effect of measurement error on the device results is better understood, incentives and penalties can be built in to the specification framework to ensure good construction practices (Meehan et al. 2013).

Chapter 5

RELATIONSHIPS BETWEEN CONTINUOUS COMPACTION CONTROL ROLLER MEASUREMENTS AND IN SITU TEST METHOD MEASUREMENTS

5.1 Introduction

Since the introduction of continuous compaction control (CCC) and intelligent compaction (IC) technologies, significant research has been performed to correlate the results from in situ spot testing to the different types of measurements that are made by CCC and IC equipment (e.g., Floss et al. 1983; Samaras et al. 1991; Brandl and Adam 1997; Thompson and White 2008; Tehrani 2009). Accurate comparison of in situ spot testing measurements (e.g. sand cone, nuclear density gauge, lightweight deflectometer, etc.) and CCC measurements requires that the measurements be recorded at identical field locations. Unfortunately, this location-specific agreement is difficult to achieve during normal field operations, and the locations of measured CCC values often do not correspond exactly to the in situ spot testing locations. If data for CCC and in situ spot testing measured values share the same location, then a direct comparison may be made. However, in most CCC field studies, the CCC measured values need to be estimated at the locations of the in situ spot testing locations. (It is also possible to estimate in situ test results at each of the CCC field locations for comparison purposes, however this approach is typically not utilized, given the typically large spatial coverage of CCC data sets relative to their in situ testing counterparts). The adopted interpolation technique for this process is typically the

kriging method (e.g., Brandl and Adam 2004, Thompson and White 2007, Petersen et al. 2007, Tehrani 2009).

Within this chapter, CCC values will be predicted using the ordinary kriging method, at the location of the in situ measured values. Then, univariate and multivariate regression analysis will be performed to explore and understand the relationships that exist between the CCC measured values and the in situ measured values.

5.2 Ordinary Kriging Method for CCC Roller Measurement Predictions

In this section, the ordinary kriging method will be used for spatial interpolation of roller measured values (MV) of MDP and CMV at each of the in situ spot testing locations, for various lifts and passes of compaction for the embankment that was constructed. The short-hand notation that is to be used to describe each lift and pass for which data is collected for the constructed embankment is shown in Table 5.1. In order to expedite construction of the embankment, CCC measurements were not recorded for successive passes for Lifts 0-4, instead CCC and in situ measurements were only taken during the final pass of the lifts. As mentioned previously, due to problems with the field data acquisition system, there is no recorded CCC data for Lift 1. Within this section, CCC measured values recorded for the final pass of Lifts 0-4 and successive passes for Lift 5 will be used to interpolate the corresponding CCC values that would be expected at each of the in situ spot testing locations for each lift and pass of interest, so that regression analysis may then be performed.

Table 5.1 Description of Notation Used in Kriging Interpolation of CCC Measured Values for the Constructed Embankment

CCC Measurement Notation	Description
Lift 0	Final roller pass of base layer (2/2)
Lift 2	Final roller pass of Lift 2 (6/6)
Lift 3	Final roller pass of Lift 3 (8/8)
Lift 4	Final roller pass of Lift 4 (9/9)
Lift 5 Pass 1	First roller pass of Lift 5 (1/7)
Lift 5 Pass 2	Second roller pass of Lift 5 (2/7)
Lift 5 Pass 3	Third roller pass of Lift 5 (3/7)
Lift 5 Pass 4	Fourth roller pass of Lift 5 (4/7)
Lift 5 Pass 5	Fifth roller pass of Lift 5 (5/7)
Lift 5 Pass 7	Final roller pass of Lift 5 (7/7)

As mentioned in Section 2.5.3 of Chapter 2, the CMV values collected during compaction may be unreliable if the roller is in the double jump, rocking motion, and/or chaotic motion modes of operation. Typically, resonant meter value (RMV) data is collected in conjunction with CMV data and used to indicate the roller mode of operation. A sudden increase in RMV data observed alongside a decrease in CMV data often indicates that an undesirable mode of operation has occurred; in this case, the CMV data collected during that time must either be removed or adjusted. The CMV data sets used in this study were carefully examined along with the RMV data sets, and it has been determined that the operation mode of the roller remained within acceptable limits for the vast majority of the compaction process. This desirable pattern of behavior was likely due to the relatively low vibratory amplitude values that were applied by the roller during the compaction process (Table 7.1). Consequently,

the CMV data sets that were recorded during the current study did not need to be adjusted to account for undesirable modes of operation.

5.2.1 Determination of Weighting Functions for the Ordinary Kriging Method

As mentioned in Chapter 2, the first step in the ordinary kriging method is to establish the empirical semivariograms of the spatially oriented data, which are then used to develop theoretical semivariogram models that are used to define the weighting functions for the kriging process. At this step, the presence of anisotropy will be investigated. If the spatial data set does not show a directional influence then isotropic kriging methods utilizing omnidirectional semivariograms will be used.

First, the directional semivariograms must be evaluated to assess any anisotropy. The lag spacing for the respective empirical semivariograms has been selected by the author following the process that is described in Chapter 2. Due to the nature of the data acquisition system that is connected to the RTK-GPS on the CCC rollers, the resolution in some directions, specifically the *Y*-direction, will be much lower than in others. The minimum required lag spacing to develop adequate empirical semivariograms in the direction of the lowest resolution of measured values (the *Y*-directional semivariogram) was determined to be $h = 0.05$ m. Since decreasing the lag spacing will not impact the nature of the other directional semivariograms, for consistency purposes, a lag spacing of $h = 0.05$ m will be used for all empirical semivariograms developed in this chapter.

Once proper empirical semivariograms have been created, in order to properly assess the anisotropy of the semivariograms, the theoretical model type must be selected. For the theoretical semivariogram models that were assessed in the current study (Linear, Spherical, Gaussian, and Exponential), the Exponential model was

selected as the one that tended to yield the "best fit" to the empirical MDP and CMV semivariogram data. These results are consistent with previous work that was performed on this data set using a different spatial analysis kriging approach (Tehrani 2009). In order to keep the analysis consistent, all theoretical semivariograms in this chapter will be fitted with the exponential model.

The empirical semivariograms in this chapter were generated using the gstat package (Pebesma 2004) in the R statistics platform (R Development Core Team 2011). The code requires an input of the measured values and their respective *X* and *Y* locations, and then requires the user to specify the lag spacing of the semivariogram. As previously mentioned, a lag spacing of 0.05 m was specified by the author for the semivariograms generated in this chapter. If directional semivariograms are desired, the angle corresponding to the direction of the semivariogram measured from the *Y*-axis (ψ) and the tolerance angle must be specified. A tolerance angle of 45 degrees is used for all of the directional semivariograms that are presented in this chapter.

Additionally, the "gstat" package (Pebesma 2004) includes a code that will "fit" a theoretical semivariogram model to the generated empirical semivariograms. The code requires that the user input the empirical semivariogram data and the desired theoretical semivariogram model type (e.g., Linear, Exponential, Gaussian, or Spherical). The code then will fit the selected model type using a weighted least squares fitting approach. It should be noted that the gstat package (Pebesma 2004) forces the nugget to be zero when fitting exponential models. Consequently, the weighting functions presented in this chapter will only have two parameters (sill and range), as opposed to the weighting functions presented in Chapter 4 that had three parameters (nugget, sill, and range).

Typical investigation of anisotropic behavior will review the directional semivariograms corresponding to ψ angles of 0°, 45°, 90°, and 135°. The author has selected to perform a more thorough analysis of the data and, therefore, has selected to study directional semivariograms corresponding to angles ψ of 0°, 30°, 60°, 90°, 120°, and 150°. It should be noted that an angle $\psi = 0°$ represents the semivariogram in the *Y*-direction, whereas, the angle $\psi = 90°$ represents the *X*-directional semivariogram.

Due to the nature of the acquisition of the CCC measured values, it is expected that the *X*-axis will correspond to the major axis of the anisotropy ellipse. The inherit assumption of geometrical anisotropy, which allows for kriging interpolation, requires that the minor axis of the ellipse be perpendicular to the major axis. If examination of the directional semivariograms for each lift and pass shows that the 90° semivariograms have the largest range values, then the *X*-axis is, in fact, the major axis of anisotropy. However, in order to perform anisotropic kriging interpolation, it is also necessary to find the range of the directional variogram corresponding to the minor axis. If the nature of the data acquisition results in insufficient data for development of the minor axis direction variogram, then, anisotropic kriging cannot be used and, by default, isotropic kriging methods must be used.

If anisotropy exists and the models have been selected and fit to the directional semivariograms, then, the anisotropy ratio *k* can be determined. At this point the gstat package be used to perform ordinary kriging interpolation using the fitted models as the weighting functions; more discussion of this process can be found in Chapter 2. The code requires that the user input the fitted model for the omnidirectional semivariogram and then specify the anisotropy ratio *k*. If performing isotropic kriging, $k = 1$, otherwise, $0 < k < 1$ for anisotropic kriging (Pebesma 2004).

5.2.1.1 Investigation of Anisotropy in CCC Measured Values

The MDP and CMV data for all the lift and passes of the embankment were examined using the process described in Chapter 2 and Section 5.2.1 above. Insufficient data in the *Y*-direction did not allow for the development of a wide range of directional semivariogram models and, therefore, the true major and minor axis of anisotropy could not be determined. Consequently, only isotropic ordinary kriging can be used for interpolation. The determination of the isotropic weighting functions for respective lift and pass data will be presented in following sections.

5.2.1.2 Determination of Weighting Functions

In this section, the process for determining the weighting functions for isotropic ordinary kriging will be shown using MDP and CMV data from Lift 0. The resulting weighting function parameters will then be shown in summary Tables 5.3 and 5.4. The unique empirical semivariograms and theoretical semivariogram model equations for all other lifts are presented in Appendix A.

The omnidirectional semivariograms for the CCC data of Lift 0 are presented in Figure 5.1. The theoretical semivariogram models produced by the gstat package are shown on the figure to allow for visual verification of the selected models.

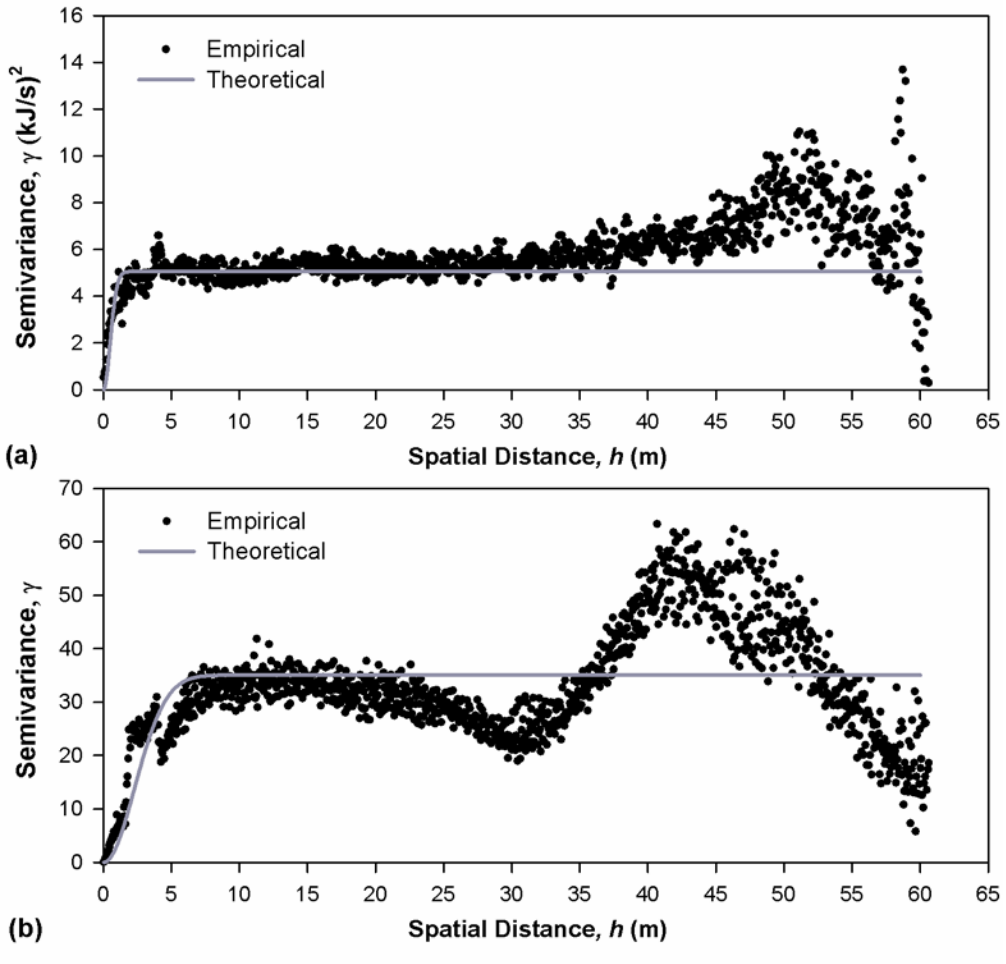

Figure 5.1 Lift 0 CCC isotropic semivariograms: a) MDP; b) CMV.

The values of the sill and range corresponding to the selected theoretical exponential models for the MDP and CMV data sets are provided in Table 5.2.

Table 5.2 Lift 0 CCC Theoretical Isotropic Semivariogram Model Parameters

CCC Measurement	Sill	Range
MDP	5.05065 $(kJ/s)^2$	0.69870 m
CMV	35.0775	3.22487 m

The exponential weighting functions may now be developed for the Lift 0 CCC data. The functions will follow the form of the exponential mathematical expression shown in Table 2.1. The resulting weighting functions for isotropic ordinary kriging of the MDP and CMV Lift 0 data are provided in Equations 5.1 and 5.2, respectively.

$$\gamma'(h,\theta) = 5.05\left(1 - \exp\left(-\frac{h}{0.70}\right)\right) \tag{5.1}$$

$$\gamma'(h,\theta) = 35.08\left(1 - \exp\left(-\frac{h}{3.22}\right)\right) \tag{5.2}$$

The process shown above, for Lift 0 data, is the method for determination of the isotropic weighting functions for kriging interpolation of MDP and CMV values. The resulting theoretical isotropic semivariogram model parameters for MDP and CMV for all lifts and passes for which data was assessed are presented in Tables 5.3 and 5.4, respectively.

Table 5.3 Theoretical Isotropic Semivariogram Model Parameters (MDP)

Lift/Pass	Sill $(kJ/s)^2$	Range (m)
Lift 0	5.05065	0.6987
Lift 2	3.01366	0.42015
Lift 3	8.57653	0.62732
Lift 4	7.87483	0.97623
Lift 5 Pass 1	5.86992	0.65154
Lift 5 Pass 2	2.79728	0.45731
Lift 5 Pass 4	2.48635	0.71695
Lift 5 Pass 5	2.00821	0.70273
Lift 5 Pass 7	1.62237	0.57548

Table 5.4 Theoretical Isotropic Semivariogram Model Parameters (CMV)

Lift	Sill	Range (m)
Lift 0	35.0775	3.22487
Lift 2	16.2647	2.07007
Lift 3	14.2811	2.22519
Lift 4	15.9249	2.30816
Lift 5 Pass 1	9.81336	0.76514
Lift 5 Pass 2	14.8977	1.08072
Lift 5 Pass 4	17.0005	1.31186
Lift 5 Pass 5	14.7449	1.44228
Lift 5 Pass 7	14.5383	1.47182

5.3 Regression Analysis

In order for CCC technology to be used as a compaction verification tool in a specification framework, a correlation must exist between current in situ method

measurements (i.e., soil density or modulus) and the measurements made by CCC rollers. During this study, both CCC measurements (i.e., MDP and CMV) and common in situ testing methods (i.e., NDG, LWD, SSG, etc.) were used as part of the compaction verification process for construction of the embankment. This chapter will attempt to find correlations between the CCC measurements and the in situ method measurements.

Regression analysis is one of the most commonly used statistical methods for investigation of correlations between variables. Univariate regression analysis is performed between a dependent variable and a single independent variable. Multivariate regression is the analysis of a dependent variable and multiple independent variables (Draper and Smith 1998). These tools can be used to access the strength of the relationship between variables and develop numerical models to predict the dependent variable. The previous section in this chapter describes the process (the ordinary kriging method) by which CCC measurements were predicted at the locations of the in situ method measurement locations. This is necessary to ensure that the CCC and in situ measured values are representative of the same soil.

The ordinary least squares (OLS) regression method will be used in this study. The model used for OLS regression is shown in Equation 5.3 below.

$$Y = \beta X + \varepsilon \tag{5.3}$$

where Y is a vector of the actual values of the response (dependent) variables, β is a vector of regression coefficients, X is the matrix of the predictor variables, and ε is the error of the model. The following assumptions must be made when performing OLS regression analysis: (1) the errors are normally distributed with a mean equal to zero and a constant variance; (2) errors are independent of each other; (3) the

independent variables are measured without error. If each of these assumptions is satisfied, the OLS regression models will provide coefficients with the minimum variance of all linear unbiased estimators. However, when the assumptions are not satisfied and/or there are many outliers that influence the model, then the coefficients produced by the models may not predict a response variable that accurately represents the collected data. For purposes of this study, it is assumed that the CCC and in situ data meet all of the requirements of OLS regression analysis. Additionally, the error of the models ε will be ignored when developing the mathematical regression equations.

As previously discussed, in situ data was collected along with CCC data for the final passes of each lift and for all successive passes of Lift 5, as shown in Table 5.1. Data for Lift 1 does not exist due to data acquisition problems during construction. Additionally, the Lift 5, Pass 1 CMV data will not be included in the regression analysis. This is because, during construction, the amplitude of the vibratory roller was increased during the first pass of each lift to expedite the compaction process. For all other passes the amplitude during compaction was returned the normal value and kept constant. Since the calculation of CMV is a function of the amplitude, as shown in Chapter 2, the data cannot be used during the regression analysis.

Throughout this chapter, regression analysis will be performed on five different subsets of the CCC and in situ data. The data sets are as follows: (1) *all lifts and passes*; (2) *all lifts and passes excluding the base layer*; (3) *final passes*; (4) *final passes excluding the base layer*; and (5) *Lift 5 passes*. The reasons for sub-sampling the data in this way will be discussed within the chapter. For each data set, the CCC data will be compared to each of the following in situ test method measurements: GeoGauge E, LWD 300 E, LWD 200 E, $DCPI_M$ E, $DCPI_A$ E, and NDG γ_d. An in-

depth explanation of each of the in situ test methods and their respective measurements can be found in Chapter 2 and will not be discussed here. In addition to comparisons of CCC measurements to in situ measurements, the two CCC measurements (MDP and CMV) will be compared to each other. For univariate regression analysis, CCC measurements will be compared to laboratory moisture content values (lab ω) and nuclear density gauge measured moisture content values (NDG ω). For multivariate regression analysis moisture content will be introduced as the second independent variable. Further explanation of the regression models used will follow within the chapter.

Figures will be provided for all regressions to visually assess the scatter of the original data and the fit of the selected models. The coefficient of determination (R^2) will be presented on each figure and also presented in summary tables, to assess the strength of the correlation between the CCC measured values and the in situ measured values. In addition, the significance of each model to accurately represent the data has been determined by examining the significance probability (p-value) of the generated models. The p-value represents the probability that an effect at least as extreme as the current observation has occurred by chance (Schervish 1996). Statisticians generally have accepted a p-value of 0.05 as the maximum value for acceptance of the fitted model (Schervish 1996). In the summary tables for coefficient of determination values provided within this chapter, all models which do not meet this criteria (models with p-value greater than 0.05) will be denoted with an asterisk (*). It is the opinion of the author that while suitable for most mathematical applications, an acceptance limit p-vale equal to 0.05 may be too restrictive for geotechnical applications. However, the reader may make their own assessment by viewing the figures and tables provided

within this chapter. In order to enable better visual assessment of the data, the author has decided not to present the mathematical expressions representing the fitted models on the figures. Instead the coefficients for the models will be provided in summary tables located in Appendix B.

5.3.1 Univariate Regression Analysis of Individual CCC Kriging Predictions versus In Situ Testing Data

Simple univariate regression analyses were performed to look for a direct relationship between CCC measurements, or roller-recorded values (*RRV*), and in situ method measurements (*ITM*). Two different univariate regression forms were used throughout the univariate analysis. The first approach that was utilized is a linear regression model (Equation 5.4) which is shown as a solid line on the figures.

$$ITM_i = C_0 + C_1 RRV_i \tag{5.4}$$

where C_0 is the *y*-intercept, and C_1 is the univariate regression coefficient for RRV_i. The notation of R^2_1 on the figures and in the summary tables will refer to the coefficient of determination for the fitted linear regression models. The second approach that was utilized is a second-degree polynomial model (Equation 5.5) which is denoted as a dashed line on the figures.

$$ITM_i = C_0 + C_1 RRV_i + + C_2 RRV_i^2 \tag{5.5}$$

where C_0 is the *y*-intercept, and C_1 and C_2 are the univariate regression coefficients for the respective terms. Similarly, the notation of R^2_2 on the figures and in the summary tables will refer to the coefficient of determination for the fitted second-degree polynomial regression models. Additionally, the measured CCC and in situ data will

be shown in the figures (denoted as solid dots) so that the overall scatter of the data and fit of the model may be visually examined.

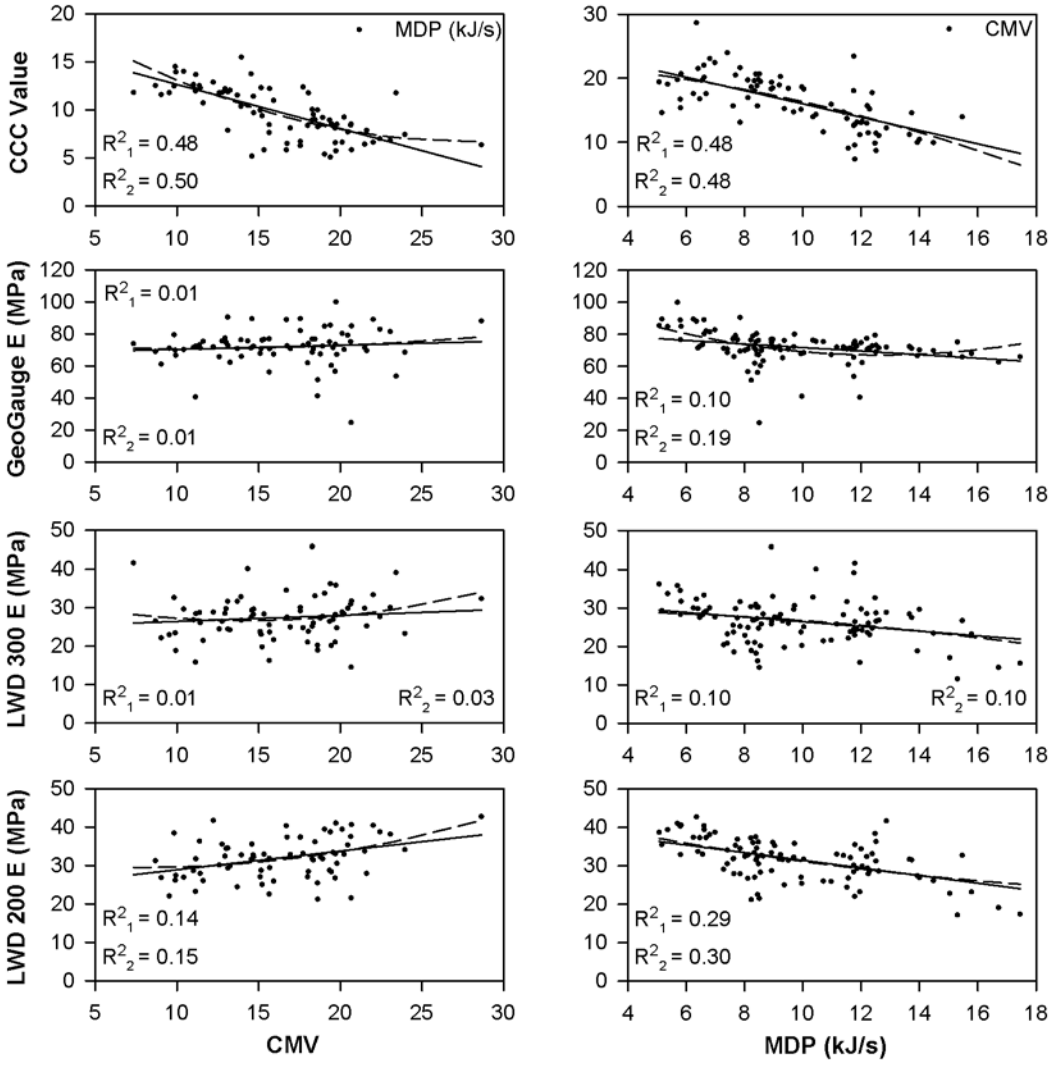

Figure 5.2 Univariate regression analyses of CCC, GeoGauge, and LWD measured values, vs. kriged MDP and CMV measurements for all lifts and passes.

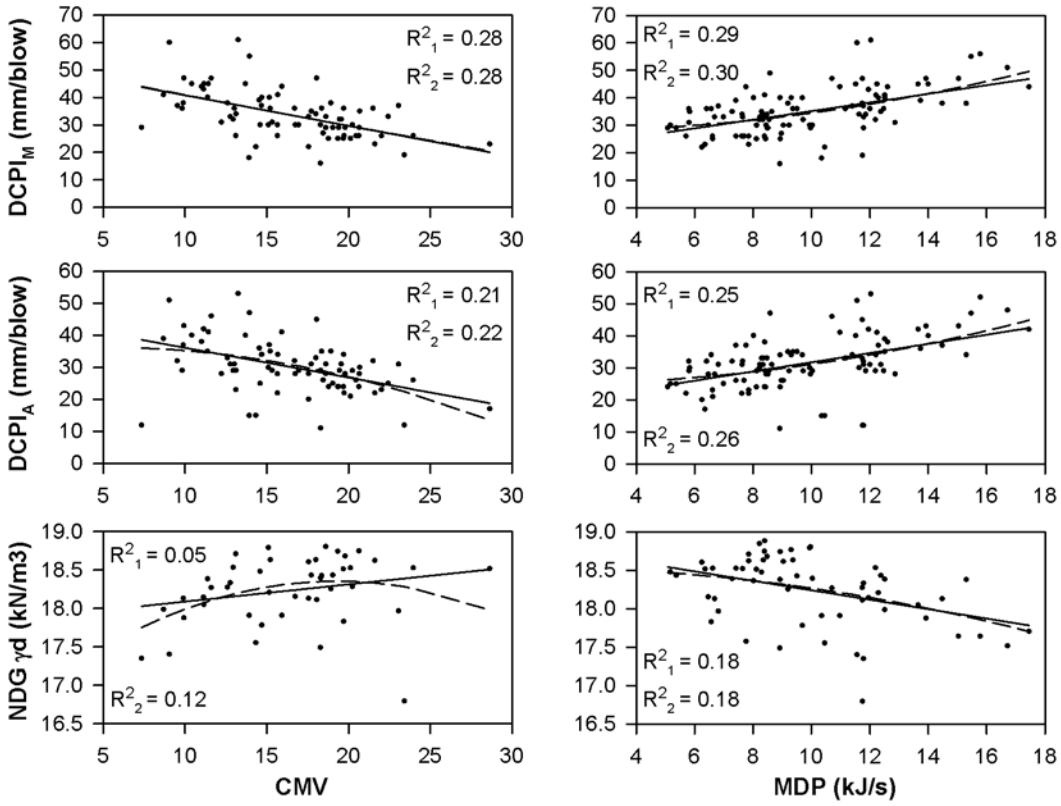

Figure 5.3 Univariate regression analyses of DCP and NDG measured values, vs. kriged MDP and CMV measurements for all lifts and passes.

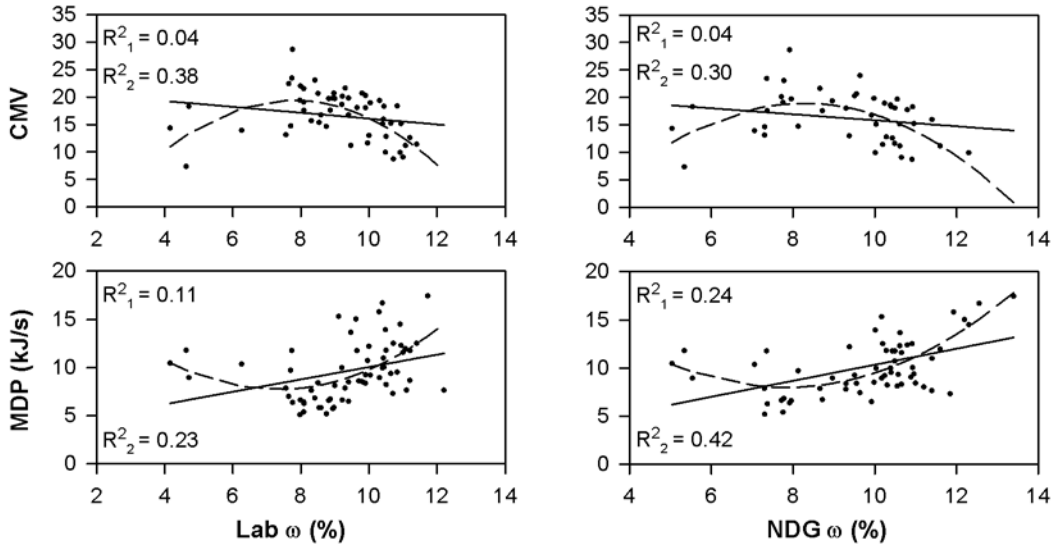

Figure 5.4 Univariate regression analyses of Lab and NDG water contents, vs. kriged MDP and CMV measurements for all lifts and passes.

The univariate regression models for the data set of *all lifts and passes* are shown in Figures 5.2 through 5.4. Examination of the figures reveals that there is not a strong linear or second-degree polynomial correlation between the CCC measured values and the in situ measured values. Additionally, there is not a significant improvement in correlation for the second-degree polynomial model, with the exception of the moisture content data. Both sets of moisture content data show that although there is not a strong second-degree polynomial correlation with the CCC data, it is much better than the linear model.

Since this data set includes measurements from all passes of all of the lifts there may be some underlying factors which could negatively influence the correlations. One of these factors could be the influence of the measured data from the base layer of the embankment. While Lifts 1 through 5 were “man-made” lifts, the base layer soils were “naturally existing”, and were only proof-rolled prior to the start

of construction; as a result, it is reasonable to expect that their behavior may be different than what would be observed for well-compacted engineered soil lifts. In order to determine if the base layer measurements had an effect on the correlations, univariate regressions analysis was also performed for *all lifts and all passes excluding the base layer*; the results are shown in Figures 5.5 through 5.7.

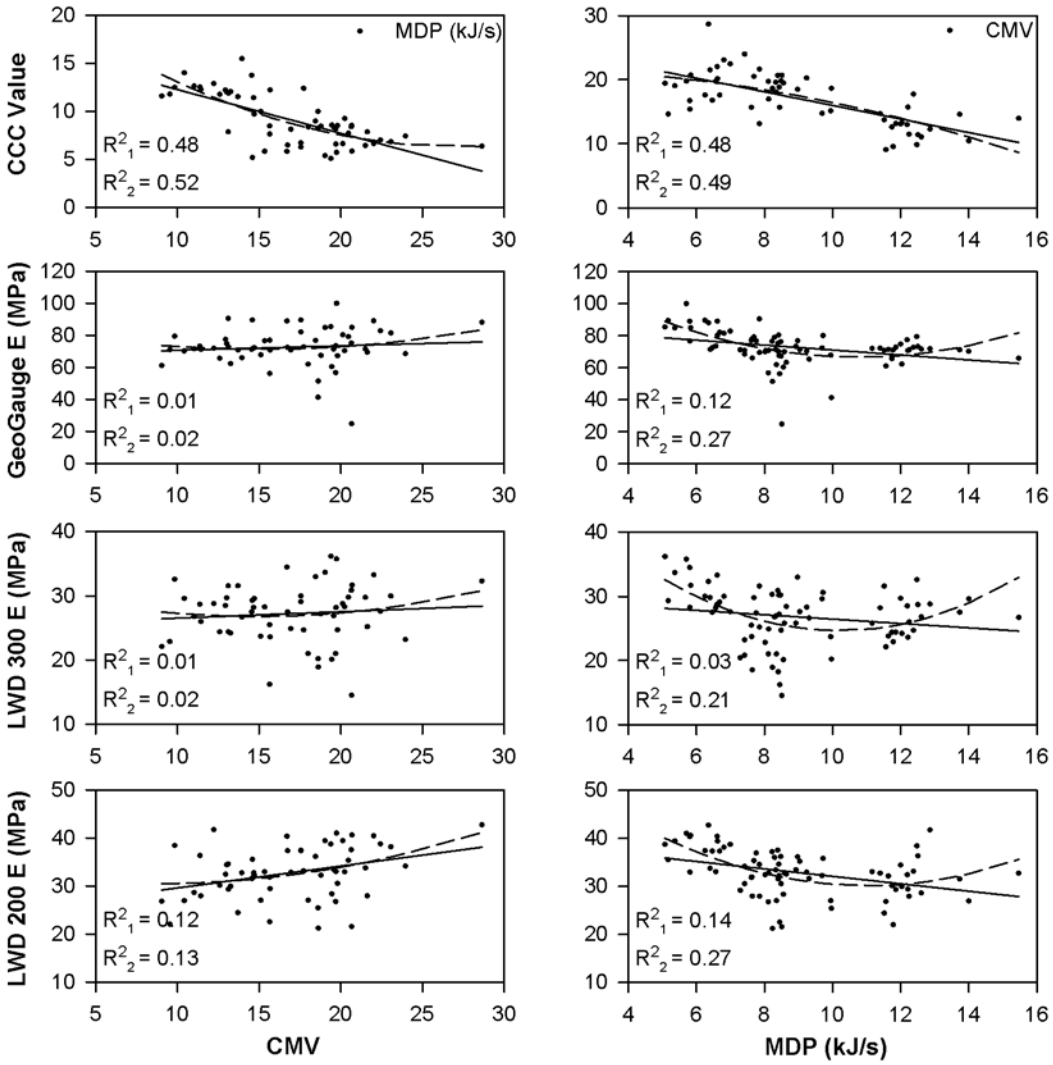

Figure 5.5 Univariate regression analyses of CCC, GeoGauge, and LWD measured values, vs. kriged MDP and CMV measurements for all lifts and passes, excluding the base layer.

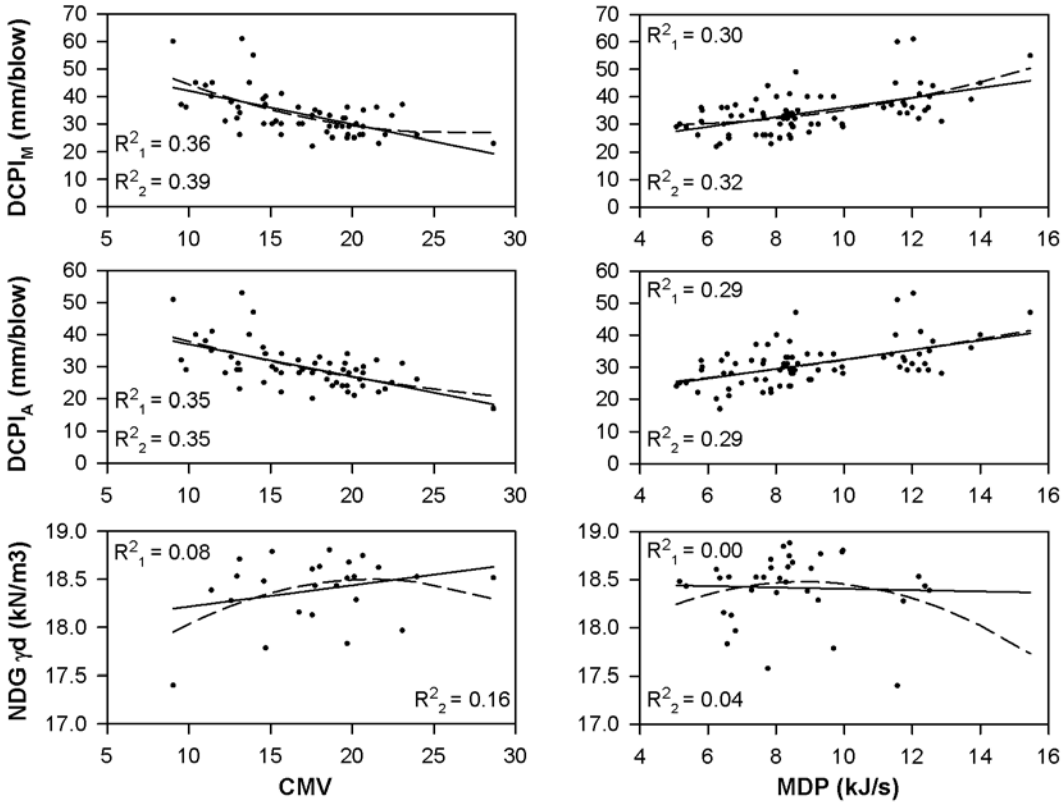

Figure 5.6 Univariate regression analyses of DCP and NDG measured values, vs. kriged MDP and CMV measurements for all lifts and passes, excluding the base layer.

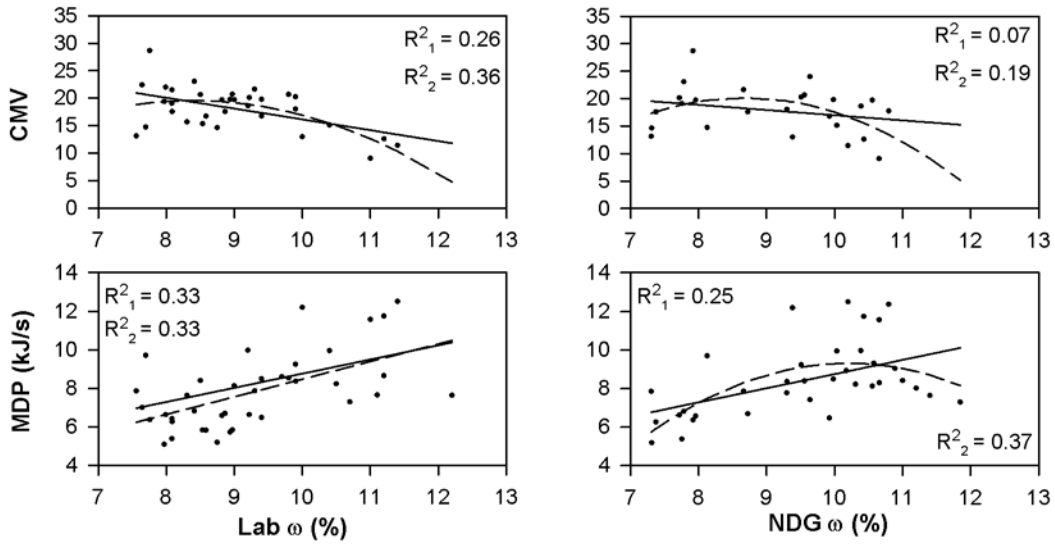

Figure 5.7 Univariate regression analyses of Lab and NDG water contents, vs. kriged MDP and CMV measurements for all lifts and passes, excluding the base layer.

Observation of the results provided in Figures 5.6 through 5.7 shows that the correlations slightly improve by eliminating the base layer measured values; however, the resulting correlations are still not strong. Additionally, the polynomial models do not offer much improvement over the linear models, with the exception of the MDP versus the modulus-based in situ methods (GeoGauge and LWD) and, again, the moisture content values.

Another factor which may affect the strength of the correlations could be the "relative compaction" range of the values in the correlation. By performing the univariate regression analysis on only the final pass measurements, the range of the data will be minimized. This is true because the final pass of each lift represents "dense" soil which has passed other more traditional QA/QC compaction verification standards. The Lift 5 pass 1, 2, 3, 4, and 5 data is representative of less "dense"

material than the final pass data (pass 7), thus, removal of these measurements reduces the range of the measurements. Univariate regression results performed on the *all final passes* data set are presented in Figures 5.8 through 5.10.

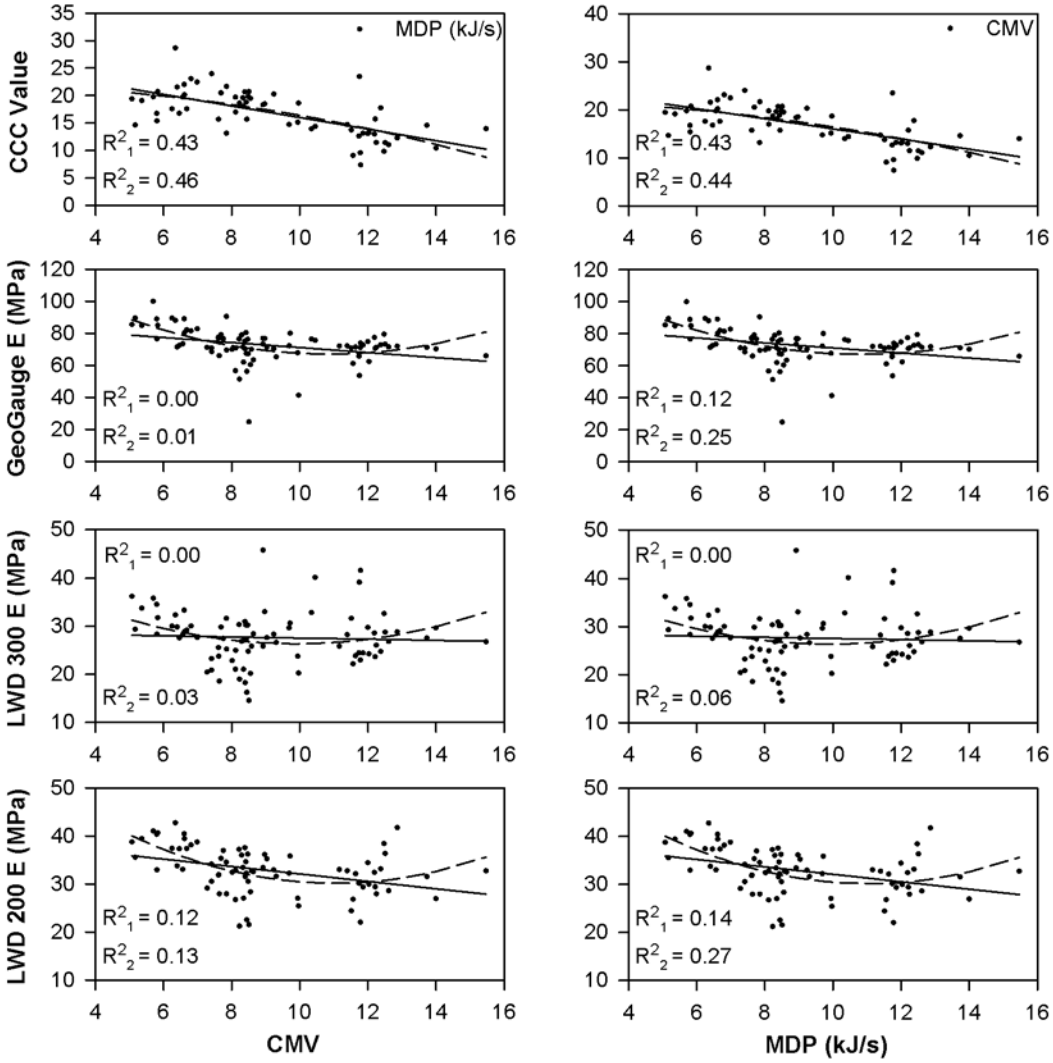

Figure 5.8 Univariate regression analyses of CCC, GeoGauge, and LWD measured values, vs. kriged MDP and CMV measurements for all final passes.

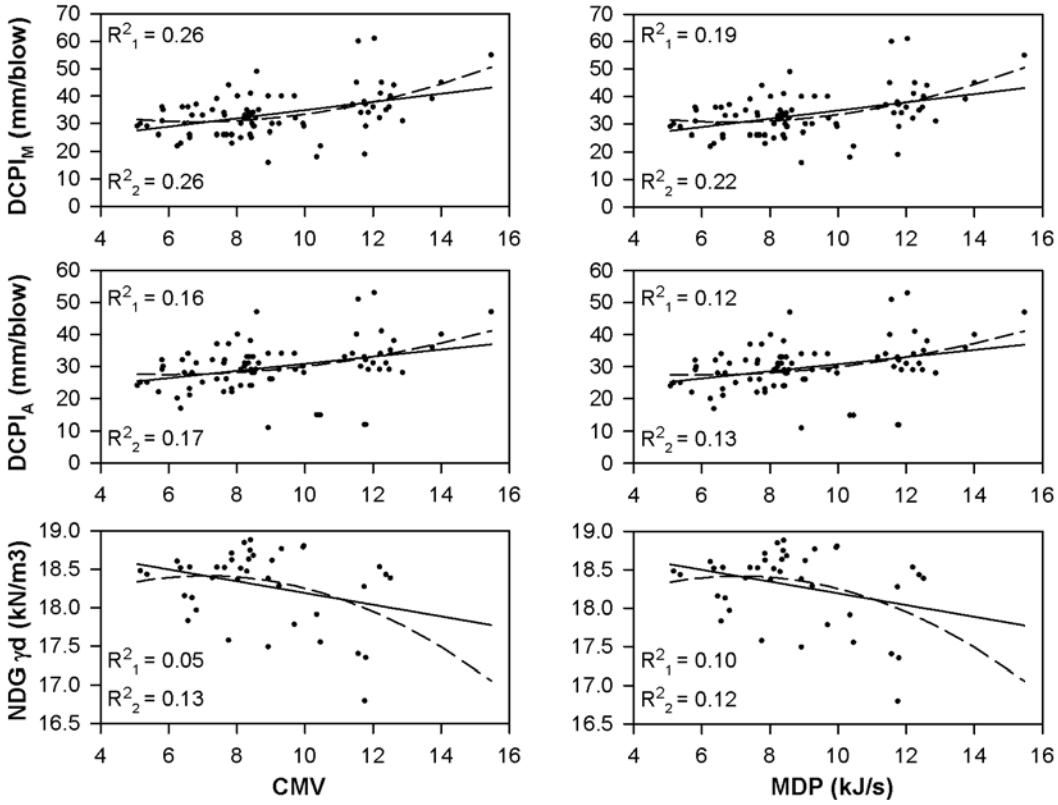

Figure 5.9 Univariate regression analyses of DCP and NDG measured values, vs. kriged MDP and CMV measurements for all final passes.

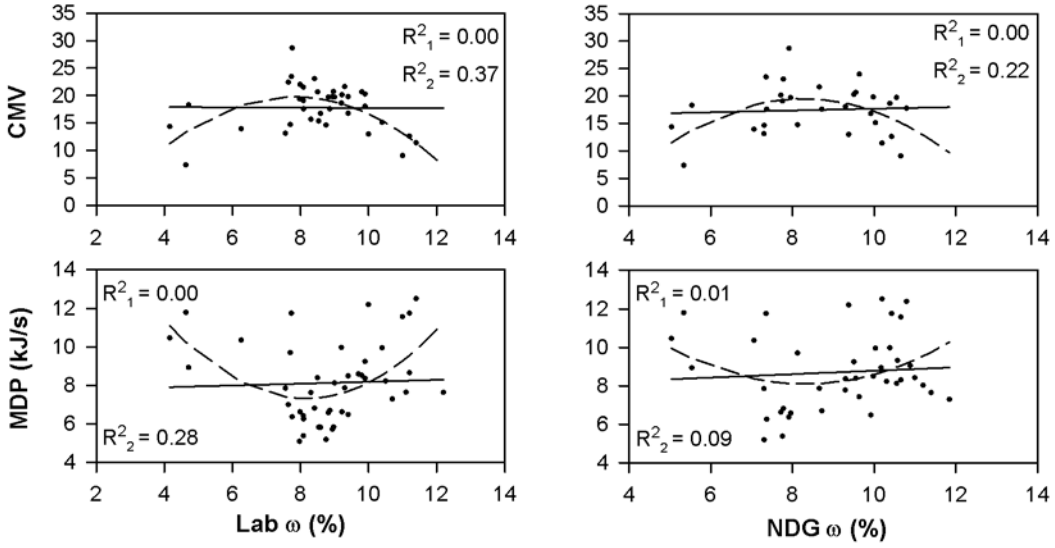

Figure 5.10 Univariate regression analyses of Lab and NDG water contents, vs. kriged MDP and CMV measurements for all final passes.

As shown in Figures 5.16 through 5.18, the quality of the correlations tends to slightly decrease when only data from the final passes of each lift is considered in the regression process. Similarly, the polynomial models do not offer much improvement over the linear models, with the exception of the MDP versus the modulus-based in situ methods (GeoGauge and LWD) and, again, the moisture content values.

As was assessed previously, the influence of the base layer on the correlation results is examined for the final pass data. The univariate regression analysis results for the *all final passes excluding the base layer* data set are shown in Figures 5.11 through 5.13.

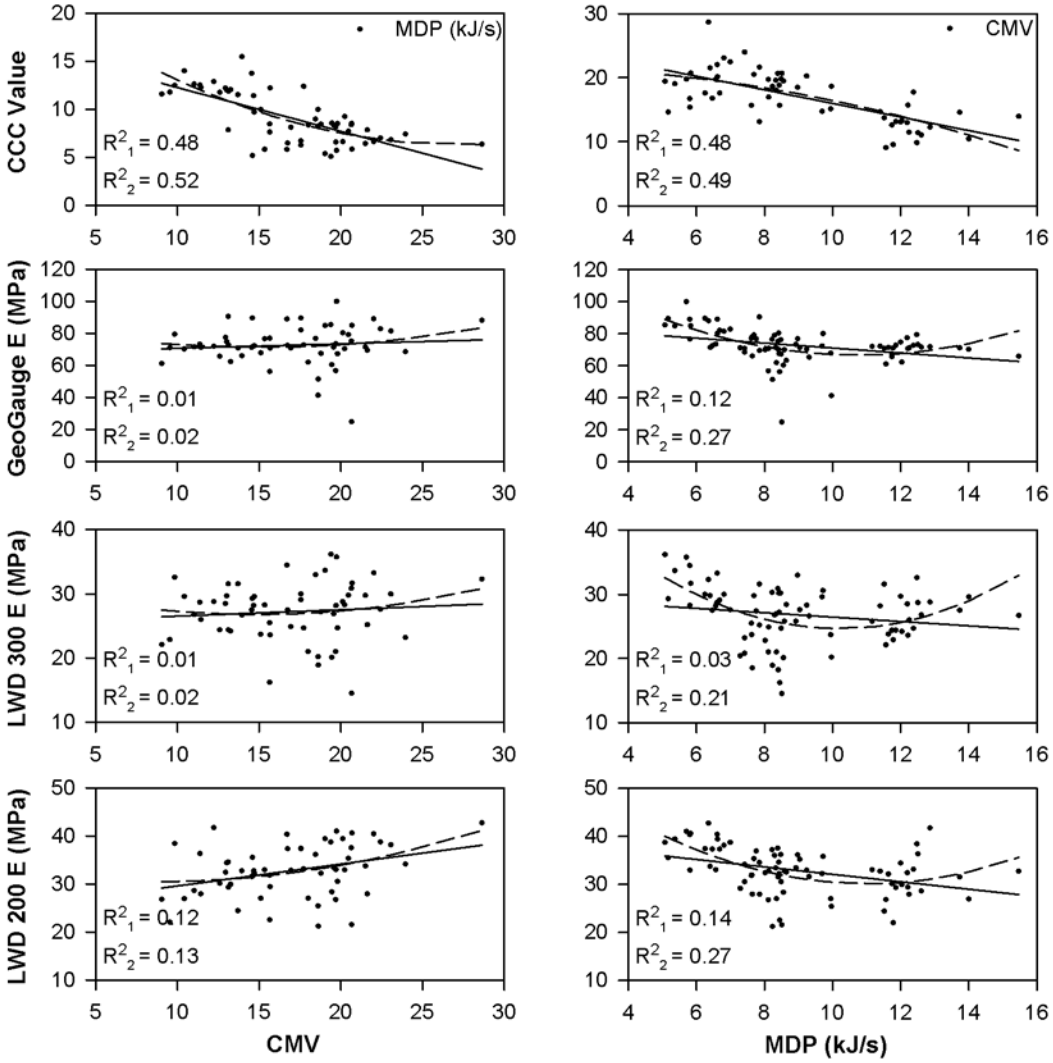

Figure 5.11 Univariate regression analyses of CCC, GeoGauge, and LWD measured values, vs. kriged MDP and CMV measurements for all final passes, excluding the base layer.

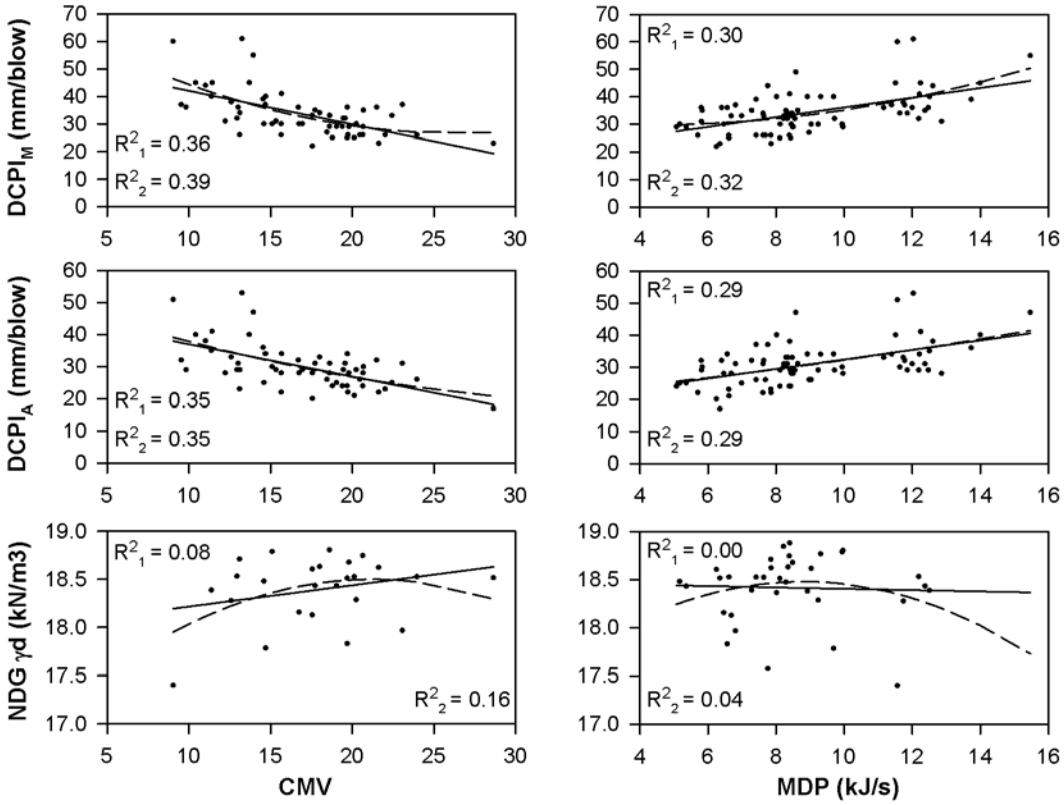

Figure 5.12 Univariate regression analyses of DCP and NDG measured values, vs. kriged MDP and CMV measurements for all final passes, excluding the base layer.

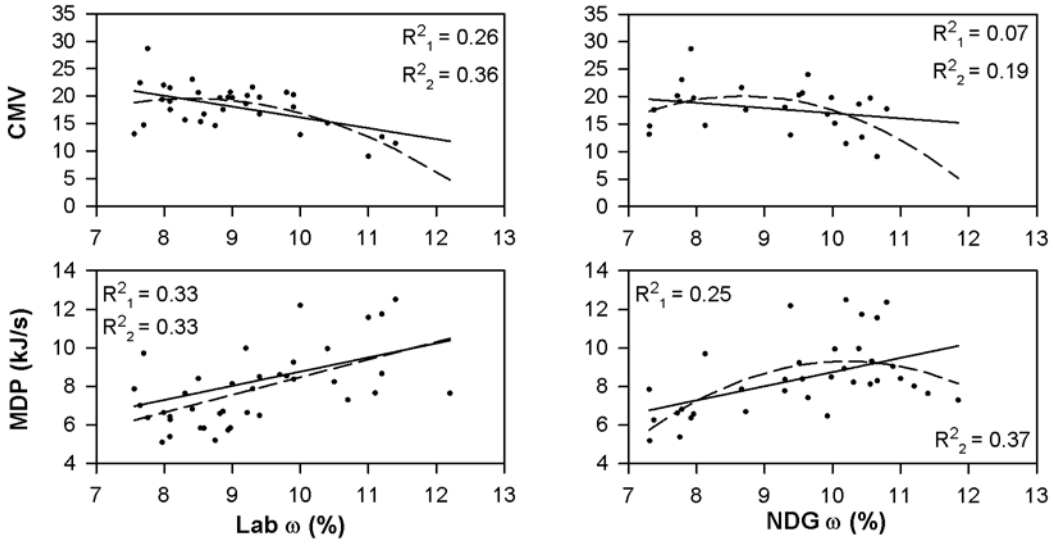

Figure 5.13 Univariate regression analyses of Lab and NDG water contents, vs. kriged MDP and CMV measurements for all final passes, excluding the base layer.

Similar to excluding the base layer from the entire data set, Figures 5.19 through 5.21 show a slight improvement for omitting the base layer from the final pass analysis. However, the correlations that are presented are generally still weak and worse than that of the entire data set. Again, the polynomial models do not offer much improvement over the linear models, with the exception of the MDP versus the modulus-based in situ methods (GeoGauge and LWD) and the moisture content values.

For the final univariate regression sample, only measurements from Lift 5 will be used in the analysis. Although sieve analysis was performed at each in situ test location and the soils were generally classified as extremely similar, it is not unreasonable to expect the soil from lift to differ slightly in gradation and/or moisture content in comparison to other lifts. To investigate the influence of these factors the

univariate regression analysis results for the *Lift 5 pass* measurements are shown in Figures 5.14 through 5.16.

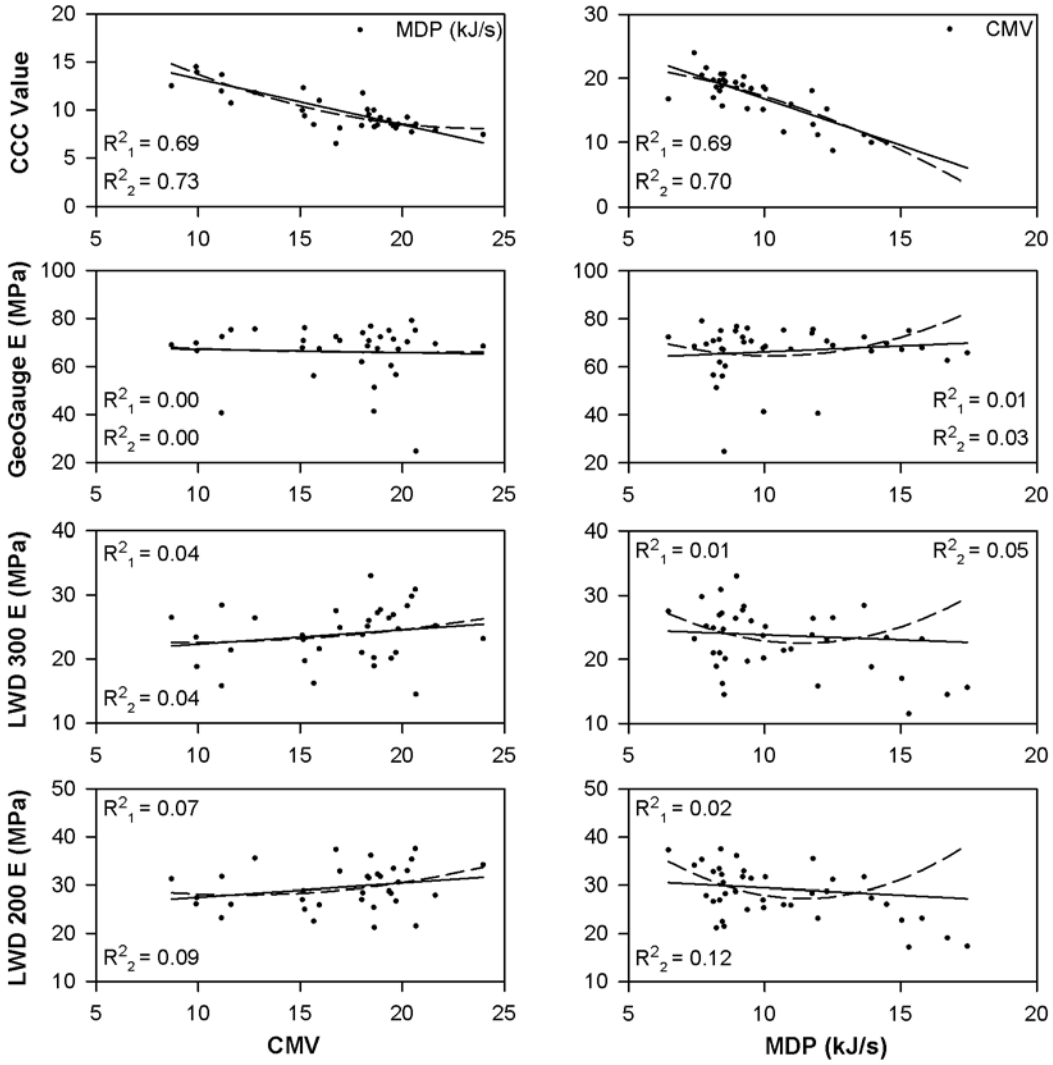

Figure 5.14 Univariate regression analyses of CCC, GeoGauge, and LWD measured values, vs. kriged MDP and CMV measurements for Lift 5.

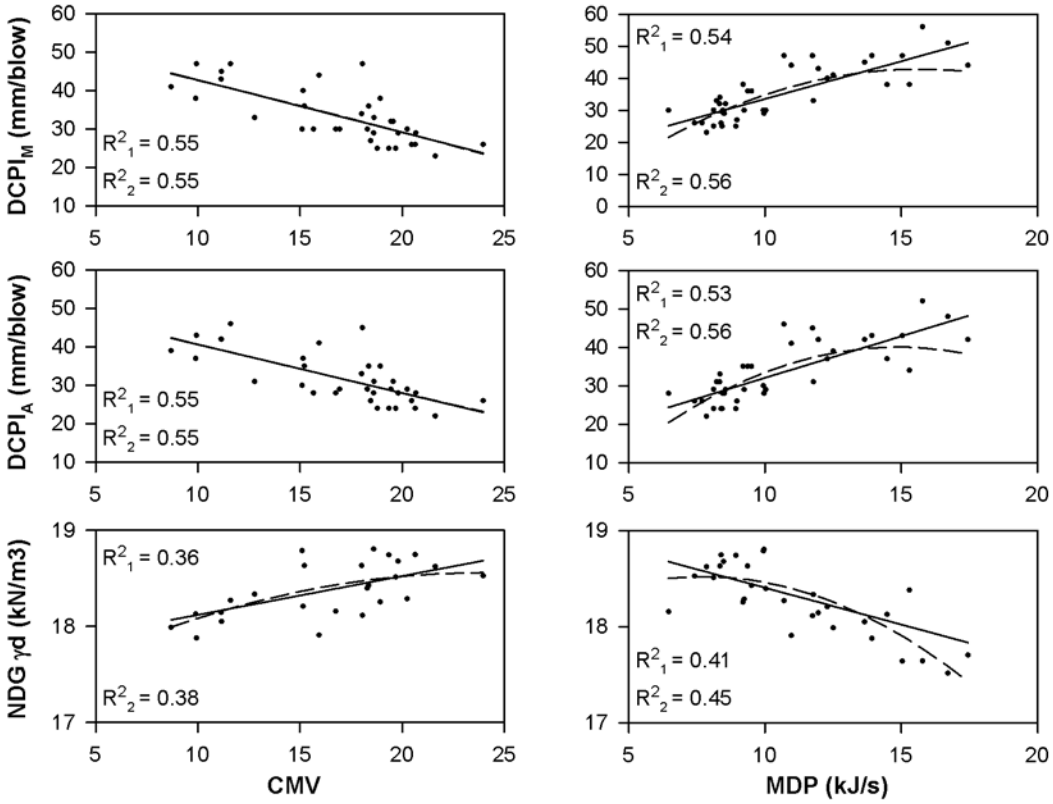

Figure 5.15 Univariate regression analyses of DCP and NDG measured values, vs. kriged MDP and CMV measurements for Lift 5.

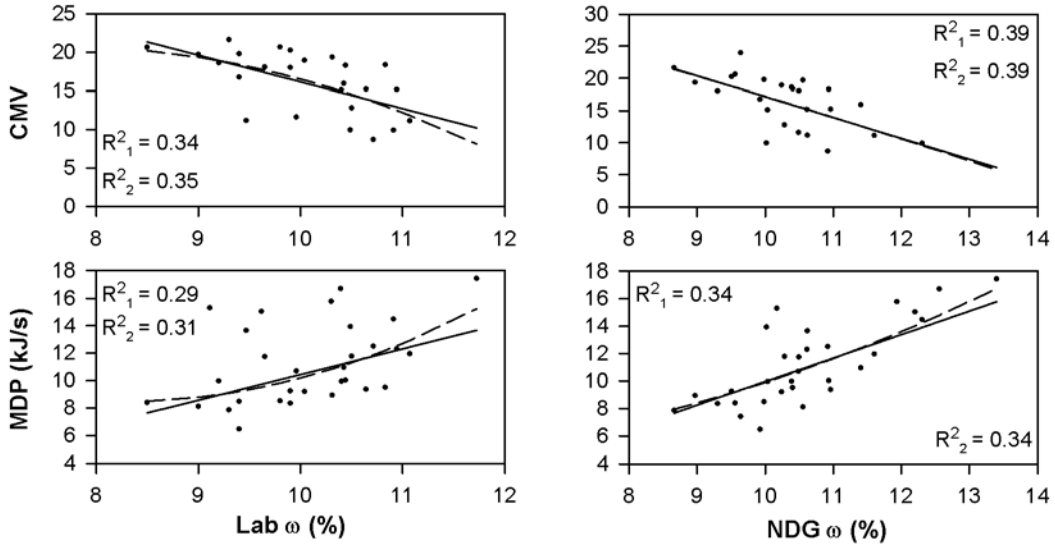

Figure 5.16 Univariate regression analyses of Lab and NDG water contents, vs. kriged MDP and CMV measurements for Lift 5.

As seen in Figures 5.22 through 5.24, the correlations remain fairly weak for the modulus-based in situ test methods (GeoGauge and LWD), however, the MDP versus CMV (and vice versa) correlations are very strong in comparison to all the analysis done to this point. In addition, the correlations between the CCC measurements and the DCP and NDG test measurements are higher than the strongest correlations that were previously observed when examining the entire data set excluding the base layer measurements. For this case, the polynomial models do not offer a significantly better fit than the linear models, even for the moisture content data which did show significant differences between coefficients of determination for all the other data sets.

To allow for easy comparison of the five different data sets used in the regression analysis, all of the coefficient of determination values are summarized in Tables 5.5 and 5.6. As previously mentioned, the regression models that have a p-

value greater than 0.05 will be denoted with an asterisk (*). The coefficient of determination values for the linear models are presented in the R^2_1 columns (shaded in grey), and the coefficient of determination values for the second-degree polynomial models are presented in the R^2_2 columns.

Table 5.5 Coefficients of Determination from the Univariate Regression Analyses that were Performed on Individual Data Points (In Situ Data as Dependent Variable)

Variables	All		All Excluding Base Layer		Finals		Finals Excluding Base Layer		Lift 5	
	R^2_1	R^2_2	R^2_1	R^2_2	R^2_1	R^2_2	R^2_1	R^2_2	R^2_1	R^2_2
MDP (kJ/s) vs. CMV	0.48	0.50	0.53	0.55	0.43	0.46	0.48	0.52	0.69	0.73
Geogauge *E* (MPa) vs. CMV	0.01*	0.01*	0.02*	0.03*	0.00*	0.01*	0.01*	0.02*	0.00*	0.00*
LWD 300 *E* (MPa) vs. CMV	0.01*	0.03*	0.04*	0.04*	0.00*	0.03*	0.01*	0.02*	0.04*	0.04*
LWD 200 *E* (MPa) vs. CMV	0.14	0.15	0.14	0.15	0.12	0.13†	0.12	0.13†	0.07*	0.09*
$DCPI_M$ (mm/blow) vs. CMV	0.28	0.28	0.38	0.39	0.26	0.26	0.36	0.39	0.55	0.55
$DCPI_A$ (mm/blow) vs. CMV	0.21	0.22	0.38	0.38	0.16	0.17	0.35	0.35	0.55	0.55
NDG γ_d (kN/m^3) vs. CMV	0.05*	0.12*	0.17	0.23	0.05*	0.13*	0.08*	0.16*	0.36	0.38
CMV vs. MDP (kJ/s)	0.48	0.48	0.53	0.54	0.43	0.44	0.48	0.49	0.69	0.70
Geogauge *E* (MPa) vs. MDP (kJ/s)	0.10	0.19	0.12	0.21	0.12	0.25	0.12	0.27	0.01*	0.03*
LWD 300 *E* (MPa) vs. MDP (kJ/s)	0.10	0.10	0.18	0.18	0.00*	0.06*	0.03*	0.21	0.01*	0.05*
LWD 200 *E* (MPa) vs. MDP (kJ/s)	0.29	0.30	0.33	0.33	0.14	0.27	0.14	0.27	0.02*	0.12*
$DCPI_M$ (mm/blow) vs. MDP (kJ/s)	0.29	0.30	0.40	0.41	0.19	0.22	0.30	0.32	0.54	0.56
$DCPI_A$ (mm/blow) vs. MDP (kJ/s)	0.25	0.26	0.42	0.42	0.12	0.13	0.29	0.29	0.53	0.56
NDG γ_d (kN/m^3) vs. MDP (kJ/s)	0.18	0.18	0.25	0.32	0.10*	0.12*	0.00*	0.04*	0.41	0.45

*: Models that have a p-value greater than 0.05

†: Models that have a p-value between 0.01 and 0.05

Table 5.6 Coefficients of Determination from the Univariate Regression Analyses that were Performed on Individual Data Points

Variables	All		All Excluding Base Layer		Finals		Finals Excluding Base Layer		Lift 5	
	R^2_1	R^2_2	R^2_1	R^2_2	R^2_1	R^2_2	R^2_1	R^2_2	R^2_1	R^2_2
CMV vs. Lab ω	0.04*	0.38	0.33	0.38	0.00*	0.37	0.26	0.36	0.34	0.35
CMV vs. NDG ω	0.04*	0.30	0.21	0.27	0.00*	0.22†	0.07*	0.19*	0.39	0.39
MDP (kJ/s) vs. Lab ω	0.11*	0.23*	0.32*	0.33*	0.00*	0.28*	0.33*	0.33*	0.29*	0.31*
MDP (kJ/s) vs. NDG ω	0.24*	0.42*	0.48*	0.50*	0.01*	0.09*	0.25*	0.37*	0.34*	0.34*

*: Models that have a p-value greater than 0.05
†: Models that have a p-value between 0.01 and 0.05

As shown in the summary tables, the removal of data from the base layer results in slightly stronger univariate correlations for both the overall data set and the final passes data set. This is likely due to the fact that the base layer was not an "engineered" lift (it was not mixed like the other layers, sampled to confirm uniformity with the other soil types, moisture conditioned, or sufficiently compacted). Consequently, the author has decided to exclude the regression figures for the two data sets that include the base layer data for all further regression analysis in this chapter.

In evaluation of the remaining three data sets which exclude the base layer, the *Lift 5* data set has, in general, a stronger univariate correlation followed by the *all excluding base layer* data set and then the *finals excluding base layer*, which has only slightly lower correlation values. The data sets for only the final passes were evaluated in an attempt to improve upon the correlations seen in the data sets which included all the passes for each lift, however, in general, the correlations became weaker when evaluating only the final pass data. Consequently, the author has decided to exclude

the regression figures for *finals excluding base layer* for all further regression analysis in this chapter.

Unfortunately, there is not a strong linear or second-degree polynomial univariate regression relationship between individual in situ test measurements and the corresponding CCC measurements for the majority of the data. Previous research done with CCC technology has exhibited consistent observations to those presented here (e.g. Kröber et. al. 2001, White and Thompson 2008). It is clear that a point-by-point comparison of in situ measurements and the corresponding kriged CCC measurements does not result in a strong relationship; therefore, another approach must be used to achieve better correlations between measured in situ test results and CCC measurements. Previous researchers have attempted to smooth the data sets, in order to remove point-to-point discrepancies in the data, by performing regression analysis of average lift and pass data. The smoothing process and resulting regression analysis for the average data sets will be presented in the following section.

5.3.2 Univariate Regression Analysis of Average CCC Kriging Predictions versus Average In Situ Testing Data

In an attempt to achieve a stronger univariate regression relationship between in situ test method results and kriged CCC measurements, the average in situ test value and the corresponding average CCC measurement value for each lift and pass were calculated. Univariate regression analysis was then performed on the resulting data set of average in situ measurement values and the average CCC measurement values. Just as in Section 5.3.1, two different univariate regression forms are used throughout the univariate analysis. The first is a linear regression model which is shown as a solid line on the figures. The notation of R^2_1 on figures and in summary tables will refer to

the coefficient of determination for the fitted linear regression models. The second is a second-degree polynomial model which is denoted as a dashed line on the figures. Similarly, the notation of R^2_2 on figures and in summary tables will refer to the coefficient of determination for the fitted second-degree polynomial regression models. Additionally, the measured CCC and in situ data will be shown in the figures (denoted as solid dots) so that the overall scatter of the data and fit of the model may be visually examined.

As previously discussed, the exclusion of the base layer data is justifiable because it is not an "engineered lift" and its removal improves the regression correlations. Additionally, the examination of only the final pass data did not offer improvement in coefficient of determination values and, therefore, is not presented in this analysis. Consequently, univariate regression analysis of average data will only be performed on two of the five original subsets of the CCC and in situ data. The data sets are as follows: (1) *all lifts and passes excluding the base layer*; and (2) *Lift 5*. The univariate regression analysis results are presented in Figures 5.17 to 5.19.

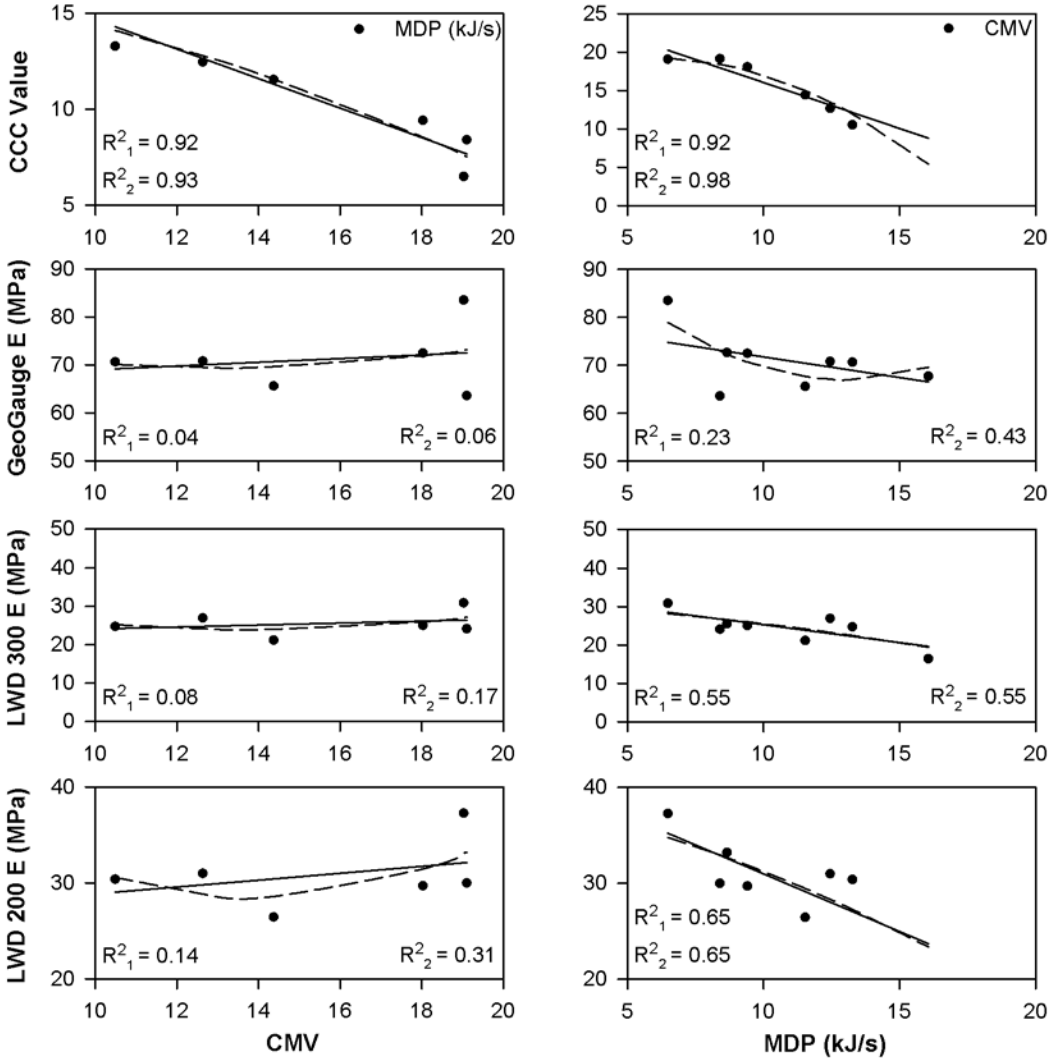

Figure 5.17 Univariate regression analyses of average CCC, GeoGauge, and LWD measured values, vs. kriged MDP and CMV measurements for all lifts and passes, excluding base layer.

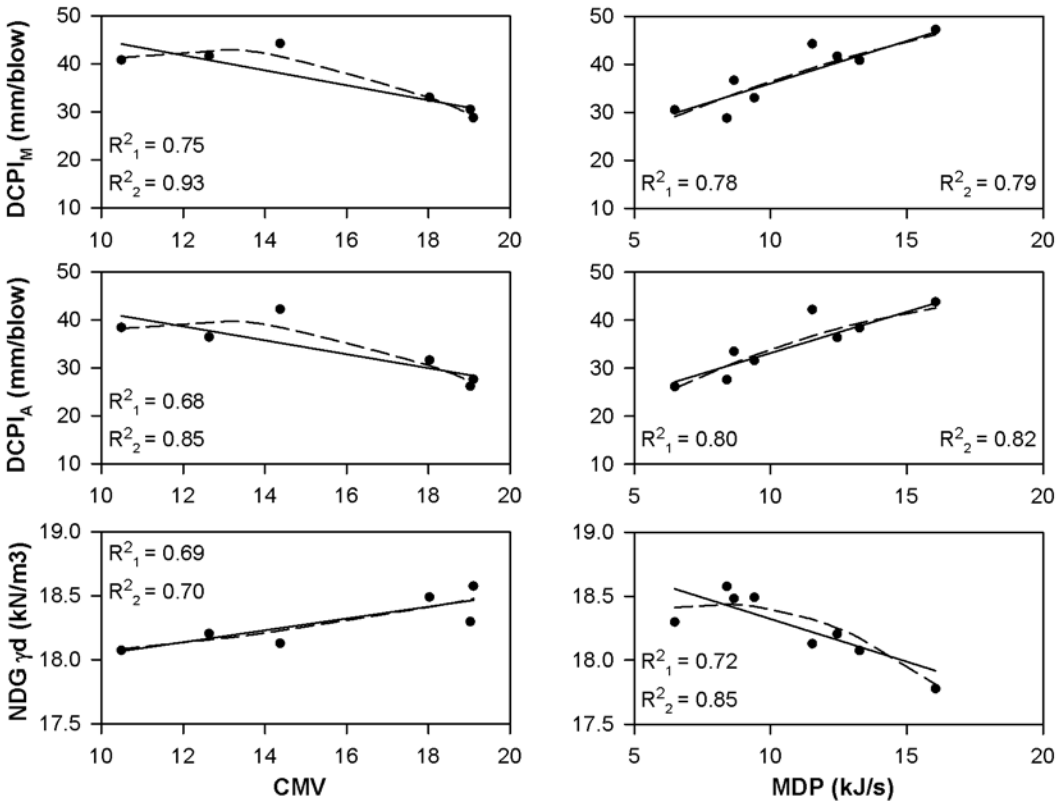

Figure 5.18 Univariate regression analyses of average DCP and NDG measured values, vs. kriged MDP and CMV measurements for all lifts and passes, excluding base layer.

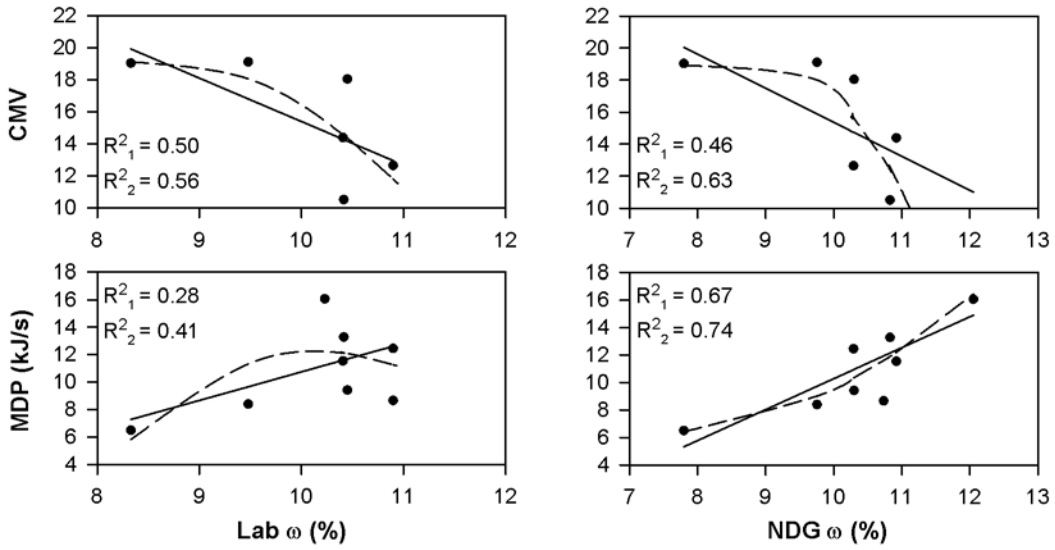

Figure 5.19 Univariate regression analyses of average Lab and NDG water contents, vs. kriged MDP and CMV measurements for all lifts and passes, excluding base layer.

As shown in Figures 5.17 through 5.19, the coefficients of determination, in general, greatly improve compared to the univariate regression models developed from the analysis of individual data points (Figures 5.5 through 5.7). The results shown here are consistent with those noted by other researchers that have also used regression analysis of CCC measurements (Thompson and White 2008). These results show that univariate regression analysis of average lift and pass data may be a suitable method for determining correlations between CCC measurements and in situ test method measurements.

Examination of Figures 5.17 through 5.19 reveals that there is a strong linear and second-degree polynomial correlation between the CCC measured values and the in situ measured values for the DCPI and NDG, where both the MDP and CMV models show similar R^2 values. The regression models for the GeoGauge and LWD

results show a much stronger relationship with MDP measurements than with the CMV measurements. Additionally, all of the data show that there is a stronger second-degree polynomial correlation with the CCC data than the linear model, although the differences vary.

For the next univariate regression sample, only measurements from Lift 5 will be used in the analysis. The results for Lift 5 measurements are shown in Figures 5.20 through 5.22.

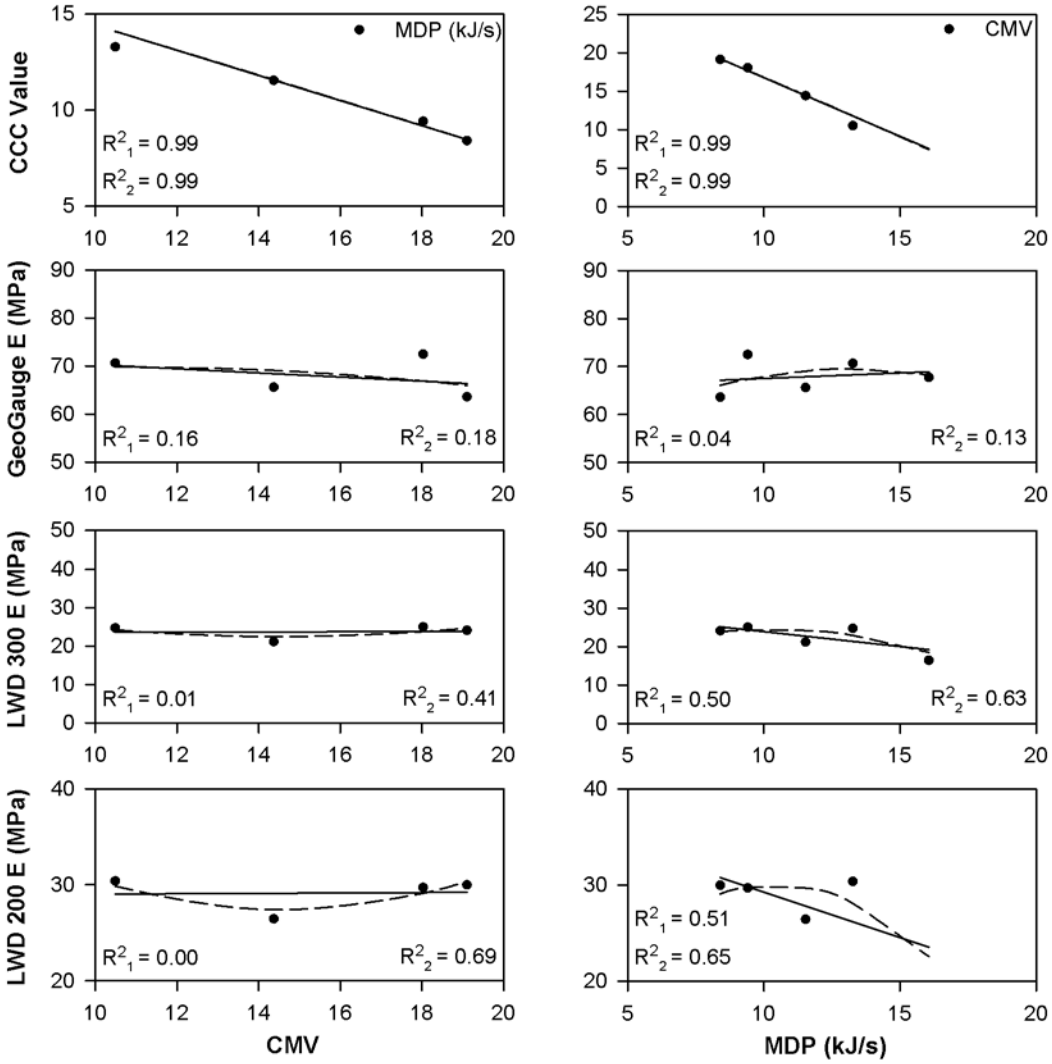

Figure 5.20 Univariate regression analyses of average CCC, GeoGauge, and LWD measured values, vs. kriged MDP and CMV measurements for Lift 5.

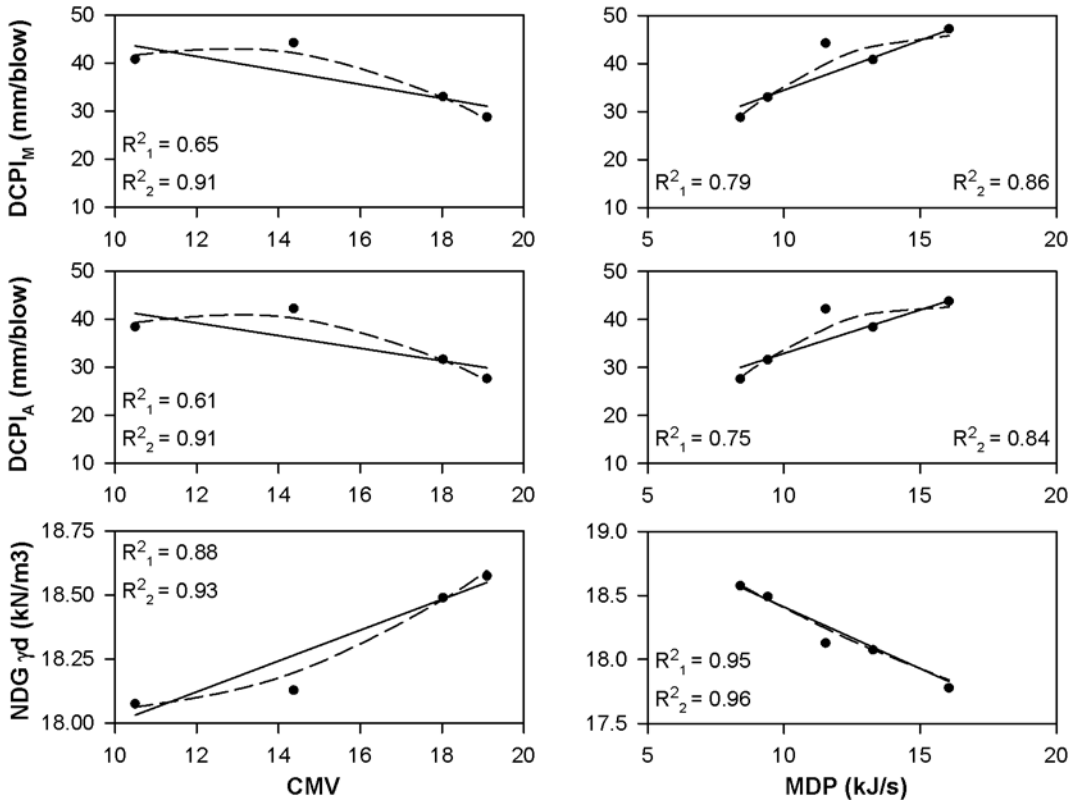

Figure 5.21 Univariate regression analyses of average DCP and NDG measured values, vs. kriged MDP and CMV measurements for Lift 5.

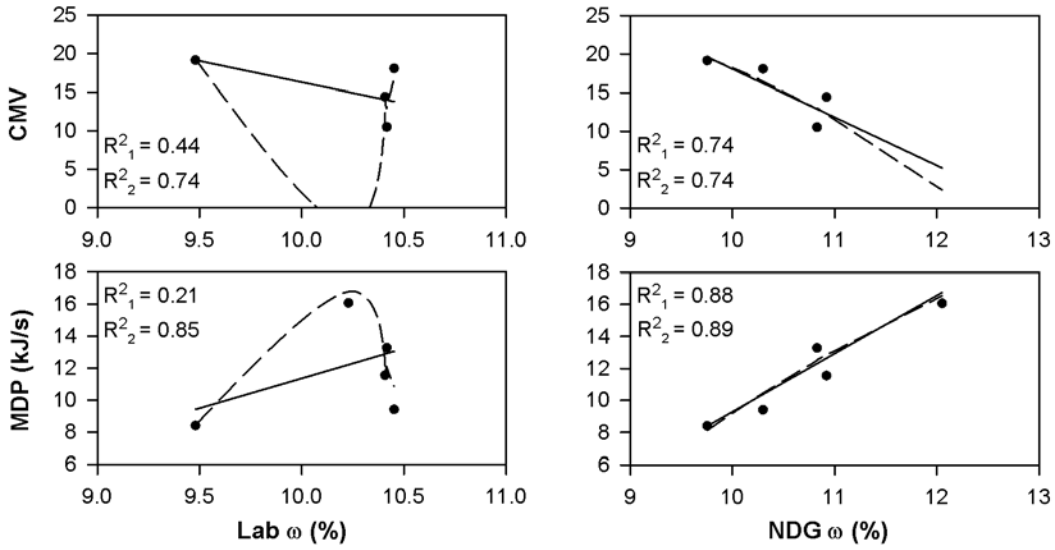

Figure 5.22 Univariate regression analyses of average Lab and NDG water for Lift 5.

As shown in Figures 5.20 through 5.22, the coefficients of determination, in general, greatly improve compared to the univariate regression models developed from the analysis of individual data points (Figures 5.2 through 5.16), as was observed when examining the *all lifts and all passes* data set. This is further confirmation that univariate regression analysis of average lift and pass data is a suitable method for determining correlations between CCC measurements and in situ test method measurements.

Figures 5.20 through 5.22 reveal that there is a strong linear and second-degree polynomial correlation between the CCC measured values and the in-situ measured values for the DCPI and NDG, where both the MDP and CMV models show similar R^2 values. The regression models for the GeoGauge and LWD results show a much stronger relationship with MDP measurements when compared to the relationship with the CMV measurements. Additionally, all of the data show that there is a stronger

second-degree polynomial correlation with the CCC data than the linear model, although the differences vary.

To allow for easy comparison of the five different data sets used in the regression analysis, all of the coefficient of determination values are summarized in Tables 5.7 and 5.8. As previously mentioned, the regression models that have a p-value greater than 0.05 will be denoted with an asterisk (*). The coefficient of determination values for the linear models are presented in the R^2_1 columns (shaded in grey), and the coefficient of determination values for the second-degree polynomial models are presented in the R^2_2 columns.

Table 5.7 Coefficients of Determination from the Univariate Regression Analyses that were Performed on Average Data (In Situ Data as Dependent Variable)

Variables	All		All Excluding Base Layer		Finals		Finals Excluding Base Layer		Lift 5	
	R^2_1	R^2_2	R^2_1	R^2_2	R^2_1	R^2_2	R^2_1	R^2_2	R^2_1	R^2_2
MDP (kJ/s) vs. CMV	0.92	0.92	0.92	0.93†	0.87*	0.88*	0.86*	*1.00**	0.99	0.99*
Geogauge *E* (MPa) vs. CMV	0.04*	0.05*	0.04*	0.06*	0.01*	0.05*	0.01*	*1.00**	0.16*	0.18*
LWD 300 *E* (MPa) vs. CMV	0.01*	0.09*	0.08*	0.17*	0.06*	0.97*	0.00*	*1.00**	0.01*	0.41*
LWD 200 *E* (MPa) vs. CMV	0.14*	0.31*	0.14*	0.31*	0.11*	*1.00**	0.11*	*1.00**	0.00*	0.69*
$DCPI_M$ (mm/blow) vs. CMV	0.35*	0.35*	0.75†	0.93†	0.18*	0.93*	0.99†	*1.00**	0.65*	0.91*
$DCPI_A$ (mm/blow) vs. CMV	0.21*	0.24*	0.68†	0.85*	0.04*	0.98*	0.96*	*1.00**	0.61*	0.91*
NDG γ_d (kN/m^3) vs. CMV	0.19*	0.38*	0.69†	0.70*	0.25*	0.99	0.54*	*1.00**	0.88*	0.93*
CMV vs. MDP (kJ/s)	0.92	0.97	0.92	0.98	0.87*	0.94*	0.86*	*1.00**	0.99	0.99*
Geogauge *E* (MPa) vs. MDP (kJ/s)	0.23*	0.41*	0.23*	0.43*	0.21*	0.61*	0.21*	0.74*	0.04*	0.13*
LWD 300 *E* (MPa) vs. MDP (kJ/s)	0.23*	0.31*	0.55†	0.55*	0.02*	0.03*	0.12*	0.93*	0.50*	0.63*
LWD 200 *E* (MPa) vs. MDP (kJ/s)	0.65†	0.65*	0.65†	0.65*	0.43*	0.78*	0.43*	0.78*	0.51*	0.65*
$DCPI_M$ (mm/blow) vs. MDP (kJ/s)	0.46†	0.49*	0.78	0.79†	0.08*	0.29*	0.72*	0.73*	0.79†	0.86*
$DCPI_A$ (mm/blow) vs. MDP (kJ/s)	0.36*	0.38*	0.80	0.82†	0.01*	0.15*	0.78*	0.79*	0.75*	0.84*
NDG γ_d (kN/m^3) vs. MDP (kJ/s)	0.29*	0.29*	0.72	0.85	0.18*	0.19*	0.19*	0.94*	0.95	0.96†

Italics: Models that have too many coefficients for the number of data points

*: Models that have a p-value greater than 0.05

†: Models that have a p-value between 0.01 and 0.05

Table 5.8 Coefficients of Determination from the Univariate Regression Analyses that were Performed on Average Data

Variables	All		All Excluding Base Layer		Finals		Finals Excluding Base Layer		Lift 5	
	R^2_1	R^2_2	R^2_1	R^2_2	R^2_1	R^2_2	R^2_1	R^2_2	R^2_1	R^2_2
CMV vs. Lab ω	0.08*	0.55*	0.50*	0.56*	0.02*	0.91*	0.75*	*1.00**	0.44*	0.74*
CMV vs. NDG ω	0.13*	0.61*	0.46*	0.63*	0.01*	0.66*	0.38*	*1.00**	0.74*	0.74*
MDP (kJ/s) vs. Lab ω	0.08*	0.20*	0.28*	0.41*	0.01*	0.62*	0.61*	0.61*	0.21*	0.85*
MDP (kJ/s) vs. NDG ω	0.30*	0.72*	0.67*	0.74*	0.01*	0.34*	0.44*	0.49*	0.88*	0.89*

Italics: Models that have too many coefficients for the number of data points
*: Models that have a p-value greater than 0.05
†: Models that have a p-value between 0.01 and 0.05

While performing the univariate regression analysis on the average data sets, a simple statistical problem arose. The reduction of the data into average values for each lift and pass resulted in data sets that have a small number of data points. When the number of data points approaches the number of coefficients in a fitted model, the coefficient of determination value of the model will increase and ultimately reach the maximum value of $R^2 = 1.00$, showing a false strong correlation.

Due to this problem it is important not to solely rely on the coefficient of determination value when evaluating the suitability of the regression models. A simple way to identify and disregard the models with too few data points is to use the p-value criteria, previously discussed throughout this chapter, which will determine the model's significance. As previously discussed, from a purely statistically standpoint, the p-value criteria alone would be adequate; however, it is the opinion of the author that from a geotechnical engineering perspective, the use of the standard p-value limits

of 0.01 and/or 0.05 may be too restrictive. Therefore, to further distinguish the regression models that are unacceptable, from a statistical and geotechnical perspective due to lack of an adequate number of data points, the regression coefficients of determination will be italicized in summary Tables 5.7 and 5.8 and on any figures if necessary. The regression models that are unreliable based on the coefficients of the model and number of data points will be easily recognizable because the coefficient of determination will always be precisely *1.00* and italicized.

As shown in the Tables 5.7 and 5.8, consistent with the analysis of individual points, the removal of data from the base layer results in slightly stronger univariate correlations for both the overall data set and the final passes data set. Additionally, strong correlations are seen between CCC measurement values and the DCPI, NDG, and Moisture content values. For a number of the models, a higher correlation was seen with the MDP measurements than with the CMV measurements. In addition, the second-degree polynomial regression model improved R^2 values when compared to the linear models.

It is important to note that just as in the analysis of individual data points, the analysis of the average data points show strong correlations between moisture content and CCC measurements. This is expected since moisture content has largely been considered a significant factor that influences the mechanical properties of compacted soils (Adam 1997, White et al. 2007). To investigate the influence of moisture content in more detail, multivariate regression analysis was performed introducing moisture content as an additional independent variable in the regression model, and the associated results are shown in Section 5.4 of this chapter.

5.4 Multivariate Regression Analysis of CCC Kriging Predictions versus In Situ Testing Data

In the previous section, univariate regression analysis was performed on individual and average data sets of CCC measurements and in situ test method measurements. The average data sets showed significant improvement in correlations when compared to the individual data sets, likely due to the fact that point-to-point discrepancies were removed as a result of this "smoothing" process. In addition, it was shown that evaluation of only the final pass of each lift did not offer a significant improvement in correlations when compared to the data sets that included additional passes. In contrast, it was shown that the exclusion of the base layer data resulted in a stronger relationship between CCC measurements and in situ test measurements. This observation is consistent with the fact that the base layer was not an engineered lift, meaning that it potentially had significantly more variability in soil characteristics since the soil was not mixed, spread, and compacted as the other lifts were.

The strong relationship between moisture content and the CCC measurements for the univariate regression analysis warrants a further investigation of the effect of moisture content on the relationship between CCC measurements and in situ test method measurements. Therefore, multivariate regression analysis techniques will be used to develop correlations between the CCC measurements and in situ test measurements, including the corresponding moisture content as an additional independent variable. The same approach has been utilized by other researchers in this area (e.g., White et al. 2005, White and Thompson 2008, Tehrani 2009).

As previously mentioned, multivariate regression analysis uses multiple independent variables to predict the dependent variable. The multivariate regression analysis performed herein will follow the linear additive model, which is described in

Rawlings et al. (1998). The general form of the linear additive model that is used to relate a dependent variable to *p* independent variables is shown in Equation 5.6.

$$Y_i = \beta_0 + \beta_1 X_{i1} + \beta_2 X_{i2} + \cdots + \beta_p X_{ip} \varepsilon_i \tag{5.6}$$

where β_0 is the intercept, and the β_i's are the rate of change in the dependent variables (Y_i) per unit change in the independent variables (X_i's). The ε_i's are the random error associated with each independent variable.

The equation may be extended into matrix form, as shown in Equation 5.7.

$$\begin{bmatrix} Y_1 \\ Y_2 \\ \vdots \\ Y_n \end{bmatrix}_{nx1} = \begin{bmatrix} 1 & X_{11} & \cdots & X_{1p} \\ 1 & X_{21} & \cdots & X_{2p} \\ \vdots & \vdots & \ddots & \vdots \\ 1 & X_{n1} & \cdots & X_{np} \end{bmatrix}_{nxp} \begin{bmatrix} \beta_0 \\ \beta_1 \\ \vdots \\ \beta_p \end{bmatrix}_{px1} + \begin{bmatrix} \varepsilon_0 \\ \varepsilon_1 \\ \vdots \\ \varepsilon_p \end{bmatrix}_{nx1} \tag{5.7}$$

or, simply, as:

$$\mathbf{Y} = \mathbf{X\beta} + \boldsymbol{\varepsilon} \tag{5.8}$$

Solving Equation 5.8 will result in the prediction values of the dependent variable. Note that the independent variables (X_i's) can be a function of other variables. The adequacy of the resulting model fit can be evaluated using coefficients of determination and p-value significance criterion as discussed in Section 5.3.

5.4.1 Regression Models for Analysis

In order to include the influence of moisture, the multivariate regression analysis approach that was employed included a combination of roller-recorded values (*RRV*) and moisture content values (ω) as the two independent variables that were used to predict the value of the in situ test measurement (*ITM*), the dependent variable. Two different linear regression equation forms were employed herein. The first regression form is as follows:

$$ITM_i = C_0 + C_1 RRV_i + C_2 \omega_i \quad (5.9)$$

where C_0 is the y-intercept, and C_1 and C_2 are the multivariate regression coefficients for the respective terms.

The second regression model form introduces an interaction term. The interaction term is the product of *RRV* and ω, as shown in Equation 5.10.

$$ITM_i = C_0 + C_1 RRV_i + C_2 \omega_i + C_3 RRV_i \omega_i \quad (5.10)$$

where C_0 is the y-intercept, and C_1, C_2, and C_3 are the multivariate regression coefficients for the respective terms.

The NDG dry unit weight values and the modulus values of the GeoGauge, LWD's, and DCPI's were used separately as dependent variables for their respective models. The MDP and CMV values, predicted at the in situ testing locations using the ordinary kriging method described in Section 5.2, were used as the roller-recorded independent variables. The laboratory measured moisture content values taken at the in situ testing locations were utilized as the second independent variable in the regression models. Unfortunately, laboratory moisture content values were not available for all of the in situ testing locations; consequently, the number of points in the overall data sets will differ from the respective univariate regression analysis data sets that were previously analyzed and presented in this chapter.

Similar to the univariate regression analysis, figures of the generated models and summary tables containing the coefficient of determination values for each model will be presented. As mentioned, two different multivariate regression models were used in the analysis. The first is a linear regression model (Equation 5.23) which is shown as a solid line on the figures. The notation of R^2_1 on figures and in summary

tables will refer to the coefficient of determination for these fitted linear regression models. The second is a linear regression model containing an interaction term (Equation 5.24) which is denoted as a dashed line on the figures. Similarly, the notation of R^2_2 on figures and in summary tables will refer to the coefficient of determination for the fitted linear regression models containing the interaction term. Additionally, the measured CCC and in situ data will be shown in the figures (denoted as solid dots) so that the overall scatter of the data and fit of the model may be visually examined.

5.4.2 Multivariate Regression Analysis of Individual CCC Kriging Predictions versus In Situ Testing Data

The presentation of the multivariate regression analysis for the individual in situ test measurements versus the CCC measurements and corresponding moisture content will follow in suit with the presentation style for the univariate regression analysis shown in Section 3. Accordingly, multivariate regression analysis will be performed on five different subsets of the CCC and in situ data. The data sets are as follows: (1) *all lifts and passes*; (2) *all lifts and passes excluding the base layer*; (3) *final passes*; (4) *final passes excluding the base layer*; and (5) *Lift 5 passes*. The results are presented in Figures 5.23 through 5.32 and summary Table 5.9.

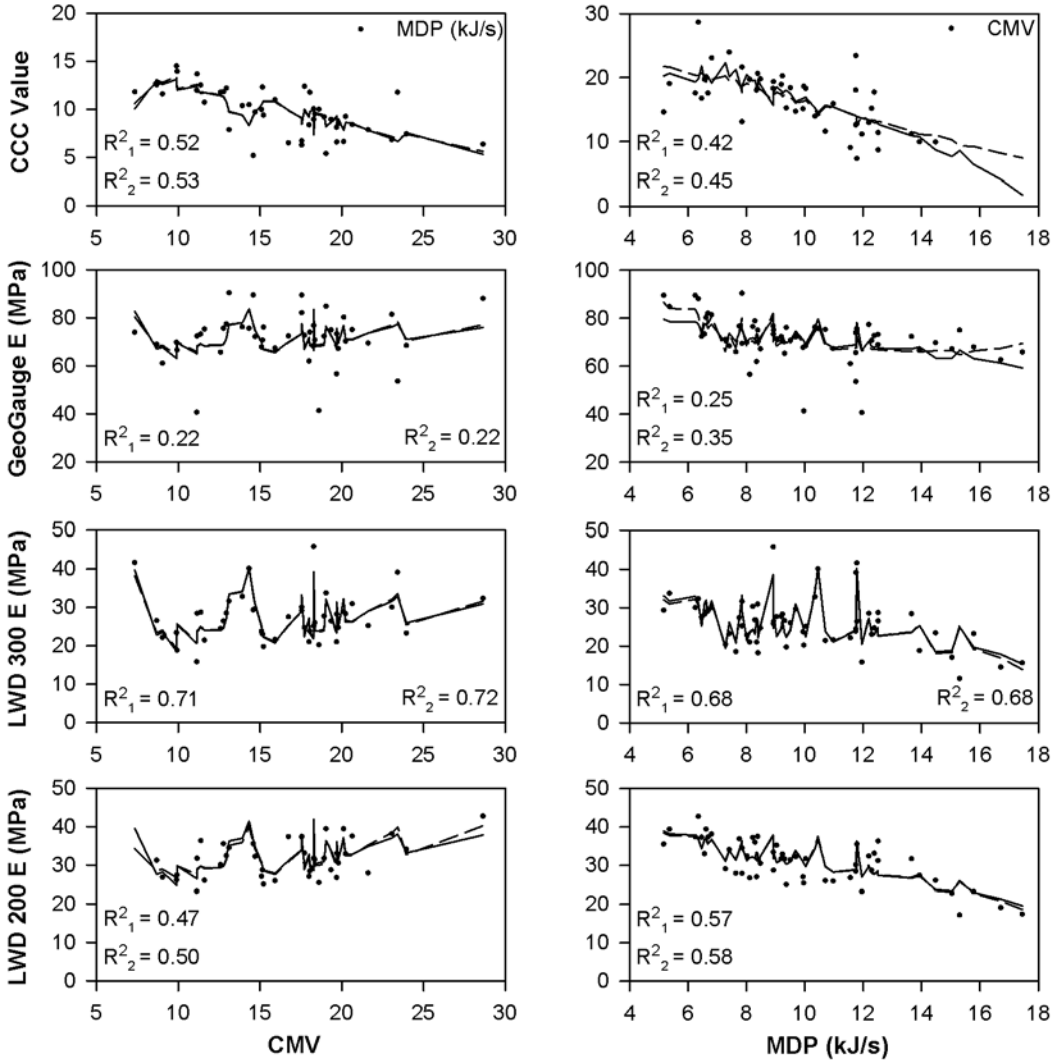

Figure 5.23 Multivariate regression analyses of CCC, GeoGauge, and LWD measured values, vs. kriged CCC measurements and moisture content for all lifts and passes.

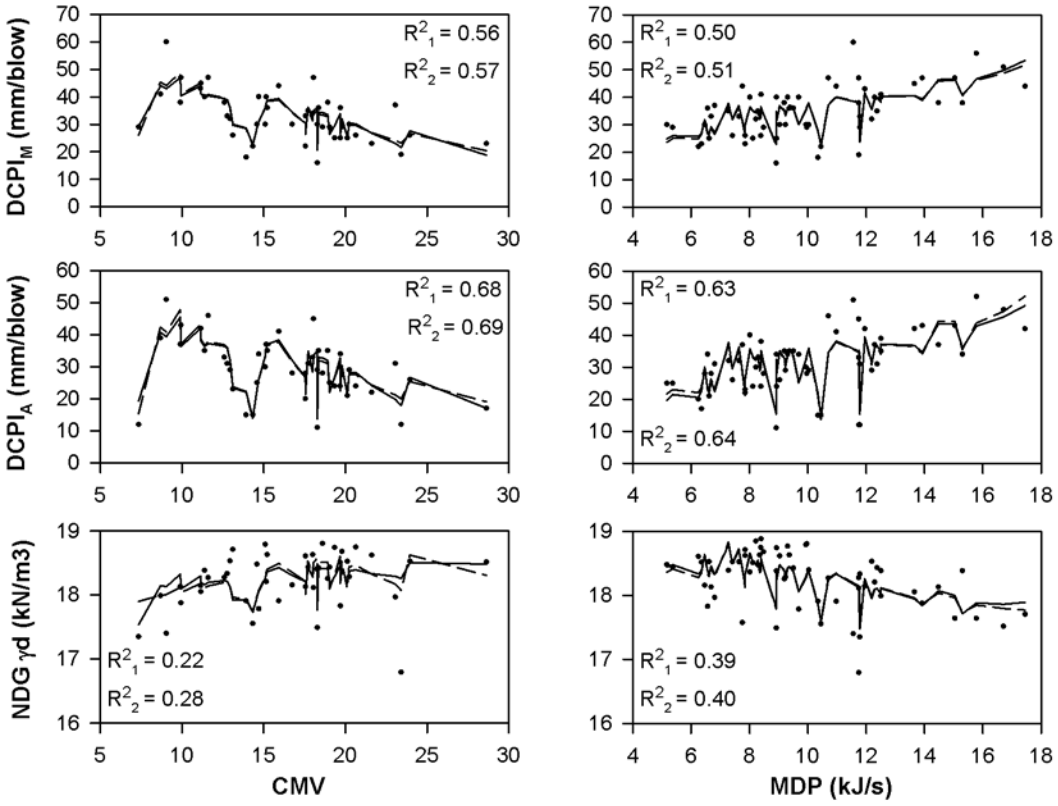

Figure 5.24 Multivariate regression analyses of DCP and NDG measured values, vs. kriged CCC measurements and moisture content for all lifts and passes.

As shown in Figures 5.31 and 5.32, there is significant improvement in the coefficient of determination values in comparison to the univariate regression models. However, the coefficient of determination values are still fairly low, meaning there is not a strong relationship between the in situ test values and the CCC measurements for the data set of *all lifts and all passes*.

The next data set that was analyzed removed the base layer measurements and the results are presented in Figures 5.25 and 5.26.

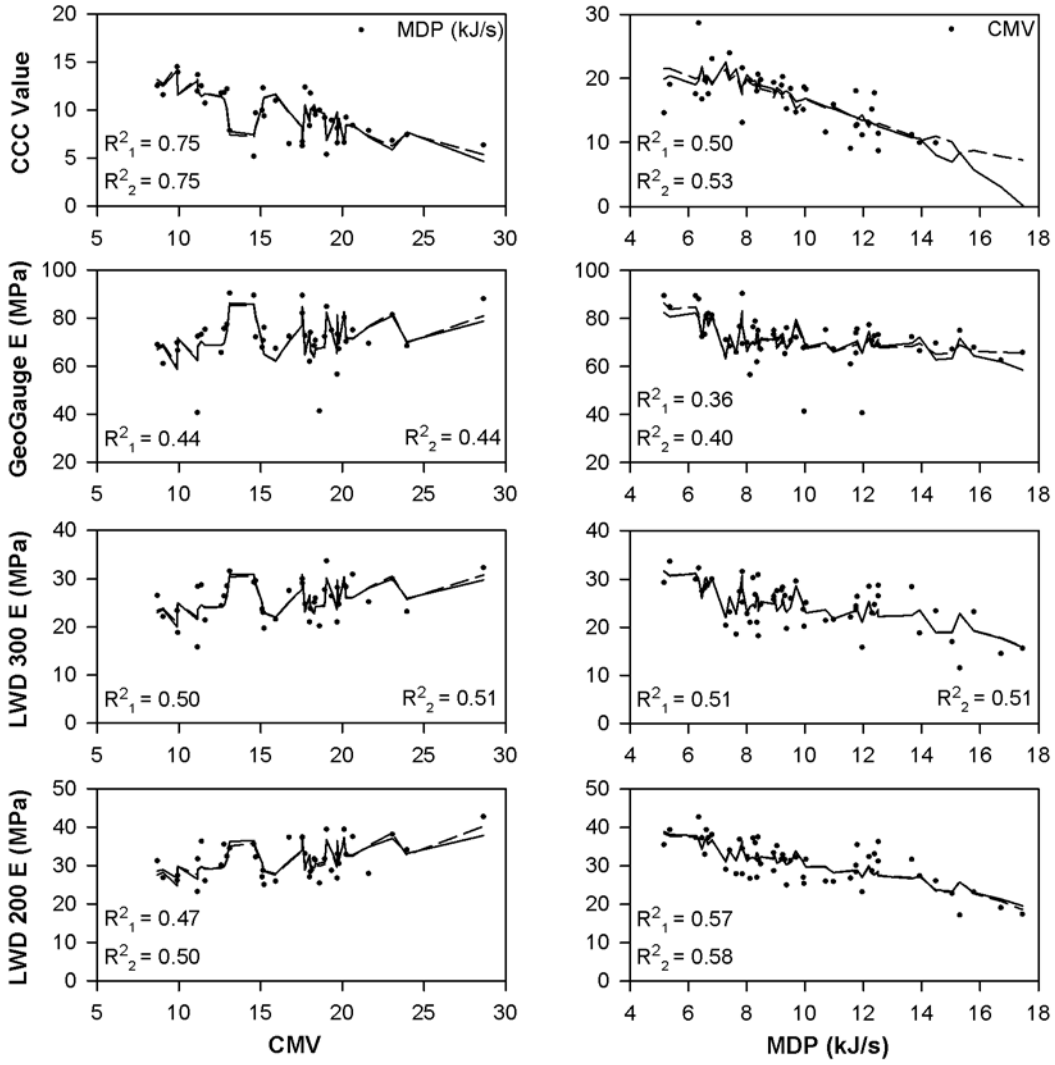

Figure 5.25 Multivariate regression analyses of CCC, GeoGauge, and LWD measured values, vs. kriged CCC measurements and moisture content for all lifts and passes, excluding the base layer.

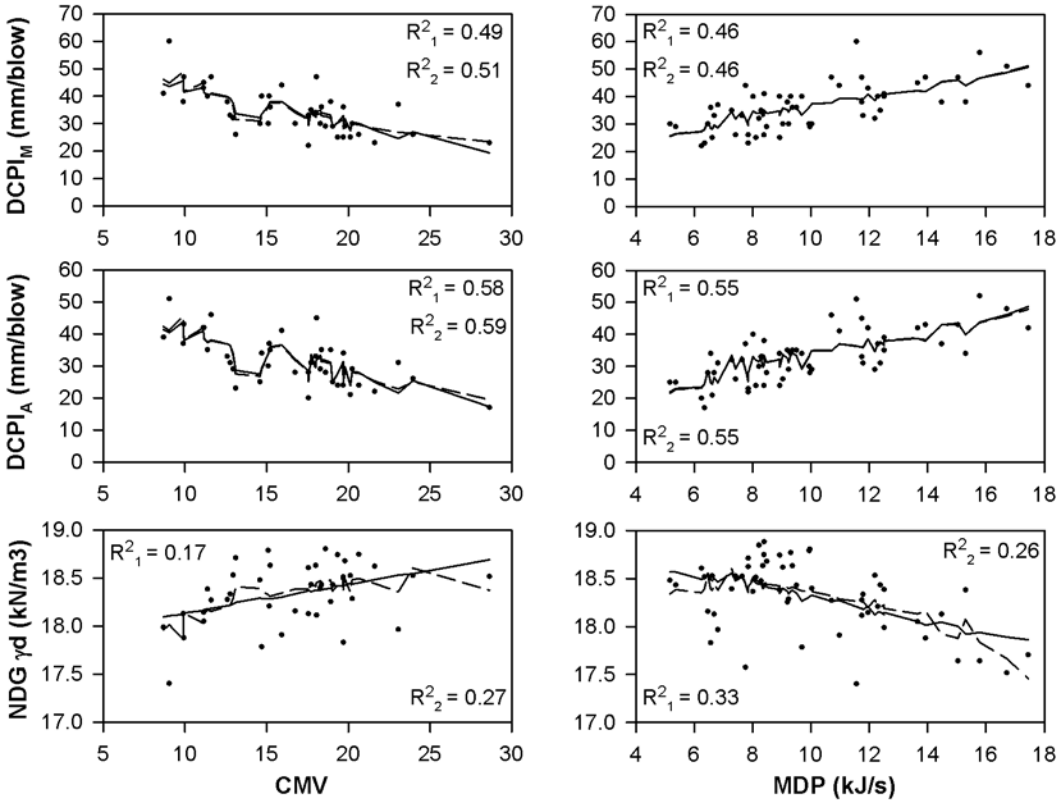

Figure 5.26 Multivariate regression analyses of DCP and NDG measured values, vs. kriged CCC measurements and moisture content for all lifts and passes, excluding the base layer.

In an attempt to strengthen correlations, multivariate regression analysis was performed on the data set of *all final passes*. The results are shown in Figures 5.27 and 5.28.

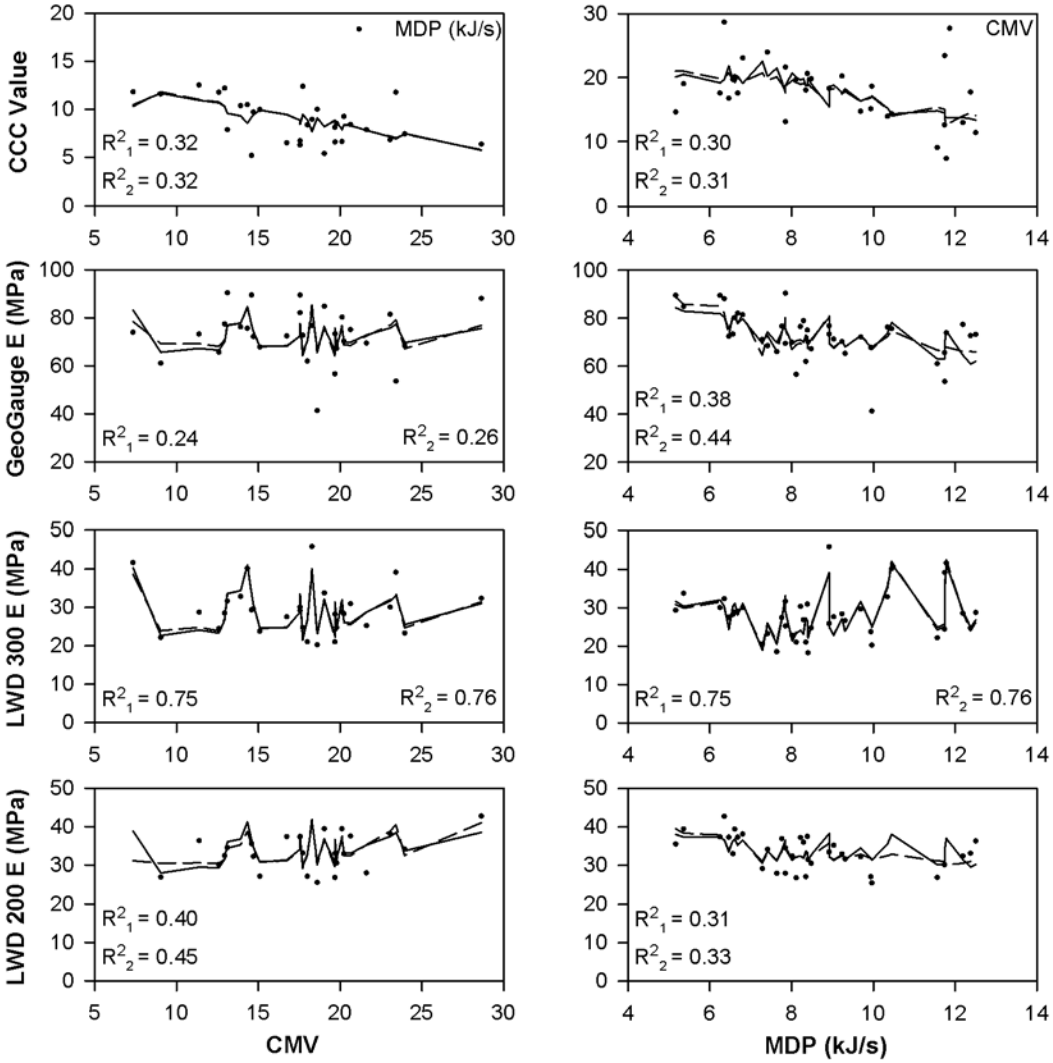

Figure 5.27 Multivariate regression analyses of CCC, GeoGauge, and LWD measured values, vs. kriged CCC measurements and moisture content for all final passes.

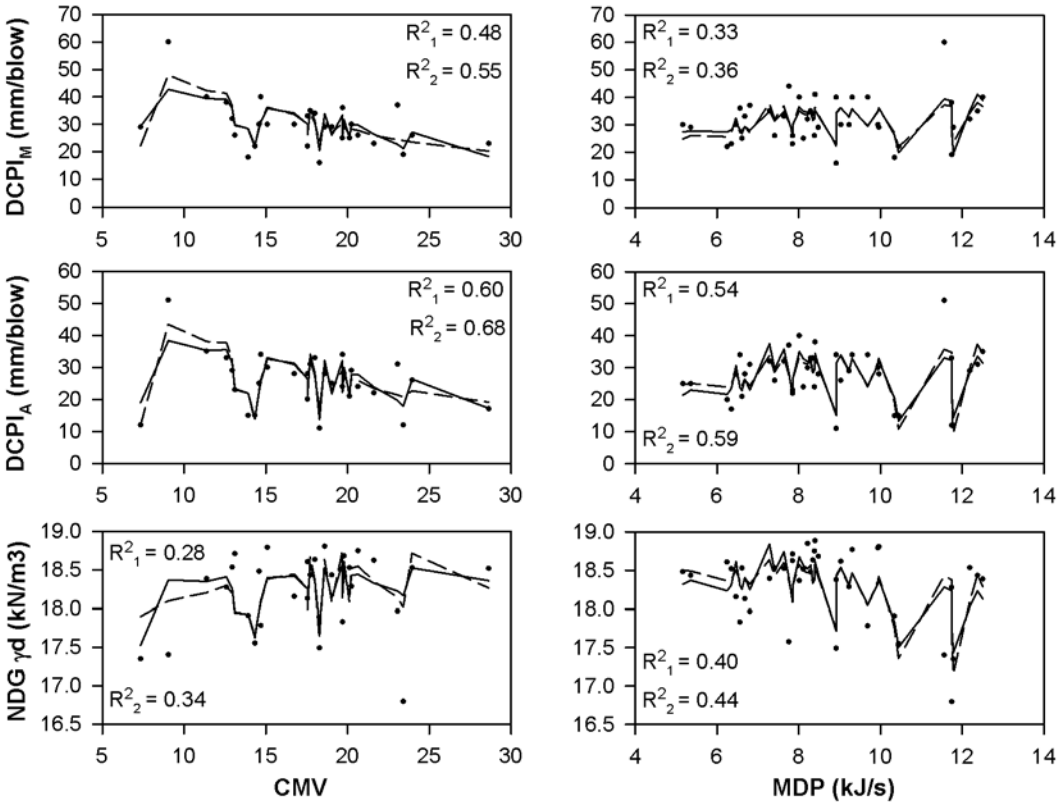

Figure 5.28 Multivariate regression analyses of DCP and NDG measured values, vs. kriged CCC measurements and moisture content for all final passes.

To further investigate the effect of the base layer measurements, multivariate regression analysis was performed on the data set of *all final passes excluding the base layer*. The resulting regression models are shown in Figures 5.29 and 5.30.

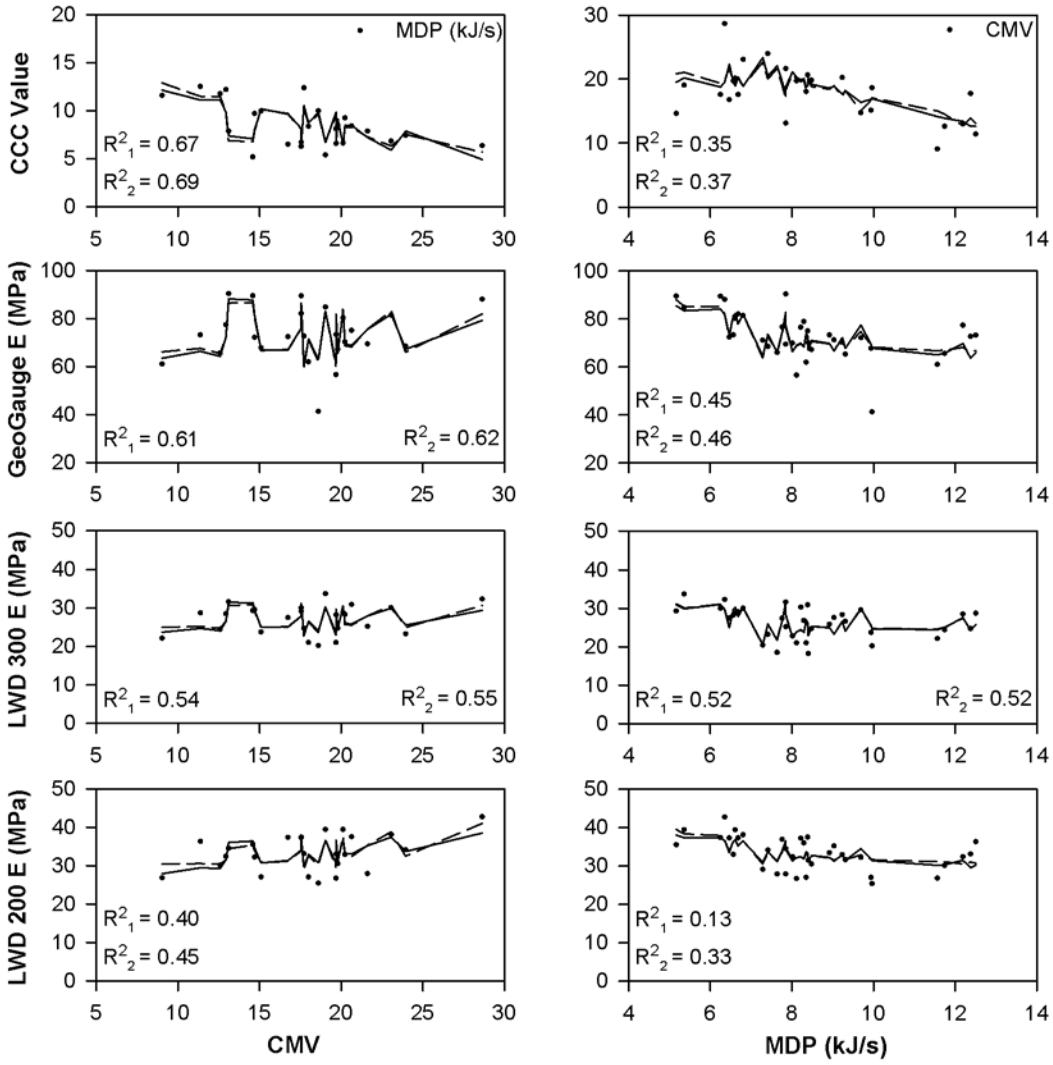

Figure 5.29 Multivariate regression analyses of CCC, GeoGauge, and LWD measured values, vs. kriged CCC measurements and moisture content for all final passes, excluding the base layer.

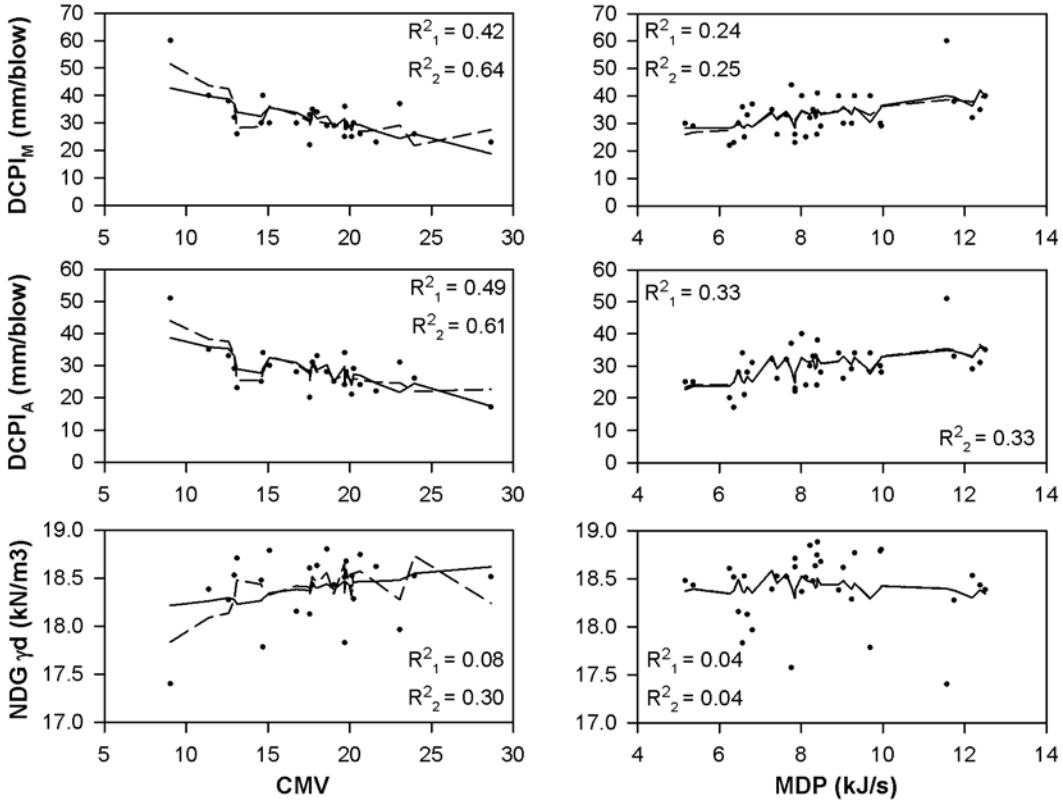

Figure 5.30 Multivariate regression analyses of DCP and NDG measured values, vs. kriged CCC measurements and moisture content for all final passes, excluding the base layer.

For comparison purposes, multivariate regression analyses were also performed on the data set of *Lift* 5 passes only, and the corresponding results are shown in Figures 5.31 and 5.32.

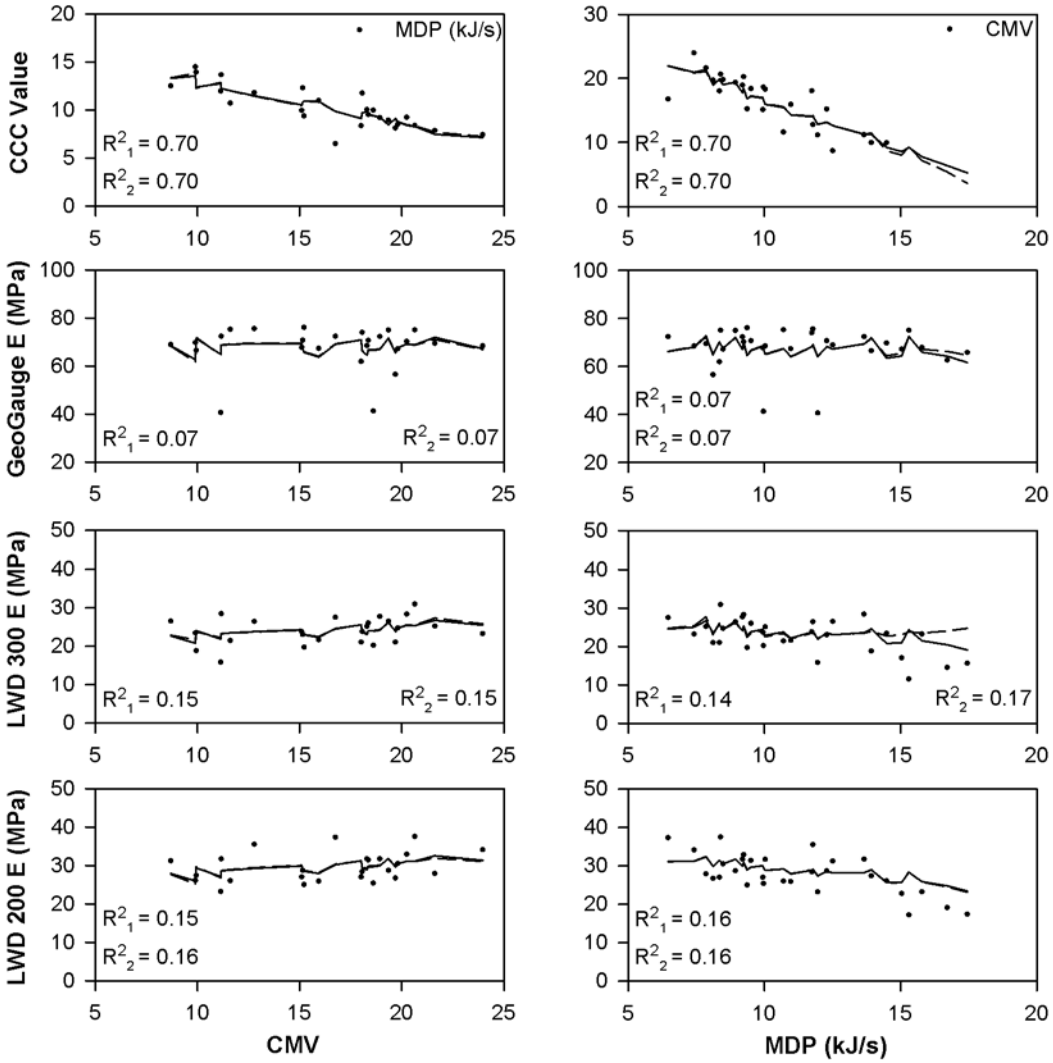

Figure 5.31 Multivariate regression analyses of CCC, GeoGauge, and LWD measured values, vs. kriged CCC measurements and moisture content for Lift 5.

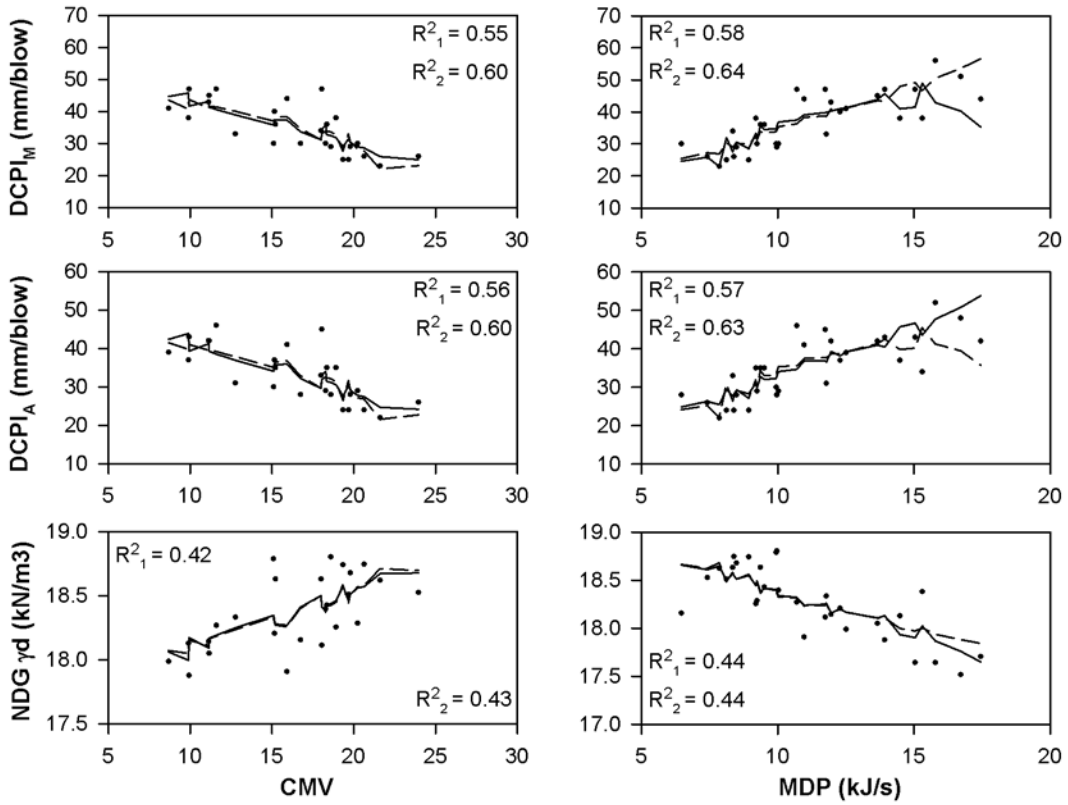

Figure 5.32 Multivariate regression analyses of DCP and NDG measured values, vs. kriged CCC measurements and moisture content for Lift 5.

To allow for easy comparison of the five different data sets used in the multivariate regression analysis, all of the coefficient of determination values are summarized in Table 5.9. As previously mentioned, the regression models that have a p-value greater than 0.05 will be denoted with an asterisk (*). The coefficient of determination values for the linear models without an interaction term are presented in the R^2_1 columns (shaded in grey), and the coefficient of determination values for the linear models with the interaction term presented in the R^2_2 columns.

Table 5.9 Coefficients of Determination from the Multivariate Regression Analyses that were Performed on Individual Data Points (In Situ Data as Dependent Variable)

Variables	All		All Excluding Base Layer		Finals		Finals Excluding Base Layer		Lift 5	
	R^2_1	R^2_2	R^2_1	R^2_2	R^2_1	R^2_2	R^2_1	R^2_2	R^2_1	R^2_2
MDP (kJ/s) vs. CMV	0.52	0.53	0.75	0.75	0.32	0.32†	0.67†	0.69*	0.70	0.70
Geogauge *E* (MPa) vs. CMV	0.22	0.22†	0.44	0.44	0.24†	0.26†	0.61	0.62	0.07*	0.07*
LWD 300 *E* (MPa) vs. CMV	0.71	0.72	0.50	0.51	0.75	0.76	0.54	0.55	0.15*	0.15*
LWD 200 *E* (MPa) vs. CMV	0.47	0.50	0.47	0.50	0.40	0.45	0.40	0.45	0.15*	0.16*
$DCPI_M$ (mm/blow) vs. CMV	0.56	0.57	0.49	0.51	0.48	0.55	0.42	0.64	0.55	0.60
$DCPI_A$ (mm/blow) vs. CMV	0.68	0.69	0.58	0.59	0.60	0.68	0.49	0.61	0.56	0.60
NDG γ_d (kN/m^3) vs. CMV	0.22	0.28	0.17†	0.27	0.28†	0.34†	0.08*	0.30*	0.42	0.43
CMV vs. MDP (kJ/s)	0.42	0.45	0.50	0.53	0.30	0.31†	0.35	0.37†	0.70	0.70
Geogauge *E* (MPa) vs. MDP (kJ/s)	0.25	0.35	0.36	0.40	0.38	0.44	0.45	0.46	0.07*	0.07*
LWD 300 *E* (MPa) vs. MDP (kJ/s)	0.68	0.68	0.51	0.51	0.75	0.76	0.52	0.52	0.14*	0.17*
LWD 200 *E* (MPa) vs. MDP (kJ/s)	0.57	0.58	0.57	0.58	0.31	0.33	0.31	0.33	0.16*	0.16*
$DCPI_M$ (mm/blow) vs. MDP (kJ/s)	0.50	0.51	0.46	0.46	0.33	0.36	0.24†	0.25†	0.58	0.64
$DCPI_A$ (mm/blow) vs. MDP (kJ/s)	0.63	0.64	0.55	0.55	0.54	0.59	0.33	0.33	0.57	0.63
NDG γ_d (kN/m^3) vs. MDP (kJ/s)	0.39	0.40	0.26	0.33	0.40	0.44	0.04*	0.04*	0.44	0.44

Italics: Models that have too many coefficients for the number of data points

*: Models that have a p-value greater than 0.05

†: Models that have a p-value between 0.01 and 0.05

As shown in Table 5.9, although the coefficient of determination values improved, consistent with the univariate regression analysis, there is not a strong relationship between the individual measured CCC values and in situ test method values. Additionally, there is no significant difference between the coefficients of determination of the two regression models employed. Maybe the most important observation is the result of excluding the base layer from the analyses of the entire data set and the data set of only the final passes. The result was a decrease in the coefficient of determination values, supporting the hypothesis that moisture content has a significant contribution in the correlation between CCC measurements and in situ testing measurements. Additionally, it supports the observation that the inclusion of the base layer measurements may have negatively affected correlations because of the drastically lower moisture content values associated with the measurements, and the fact that the base layer material was different than the fill material used for all other lifts of the embankment (as this layer was not an engineered lift).

5.4.3 Multivariate Regression Analysis of Individual CCC Kriging Predictions versus In Situ Testing Data

As a result of the observations shown by the univariate regression analysis in Section 5.3, multivariate regression analyses is performed on the average lift and pass measurements of the CCC values, in situ test values, and moisture content values. The same general procedure that was performed in Section 5.3.2 will be followed here. The results of this analysis are seen in Figures 5.33 through 5.42 and Table 5.10.

It is important to note that just as with the univariate regression analysis on the average data sets there will be cases were the number of data points in the data set will be equal to or less than the number of coefficients in the regression equations. As a

result, for a number of the models, the high correlation will need to be disregarded because it is falsely identifying an exact correlation between CCC measurements and the in situ test measurements when in reality the high correlation is a result of having an excessive number of regression model coefficients. These cases will be easily identifiable because $R^2 = \textit{1.00}$ for these models and the coefficient of determination will be italicized on the associated figures and in Table 5.10.

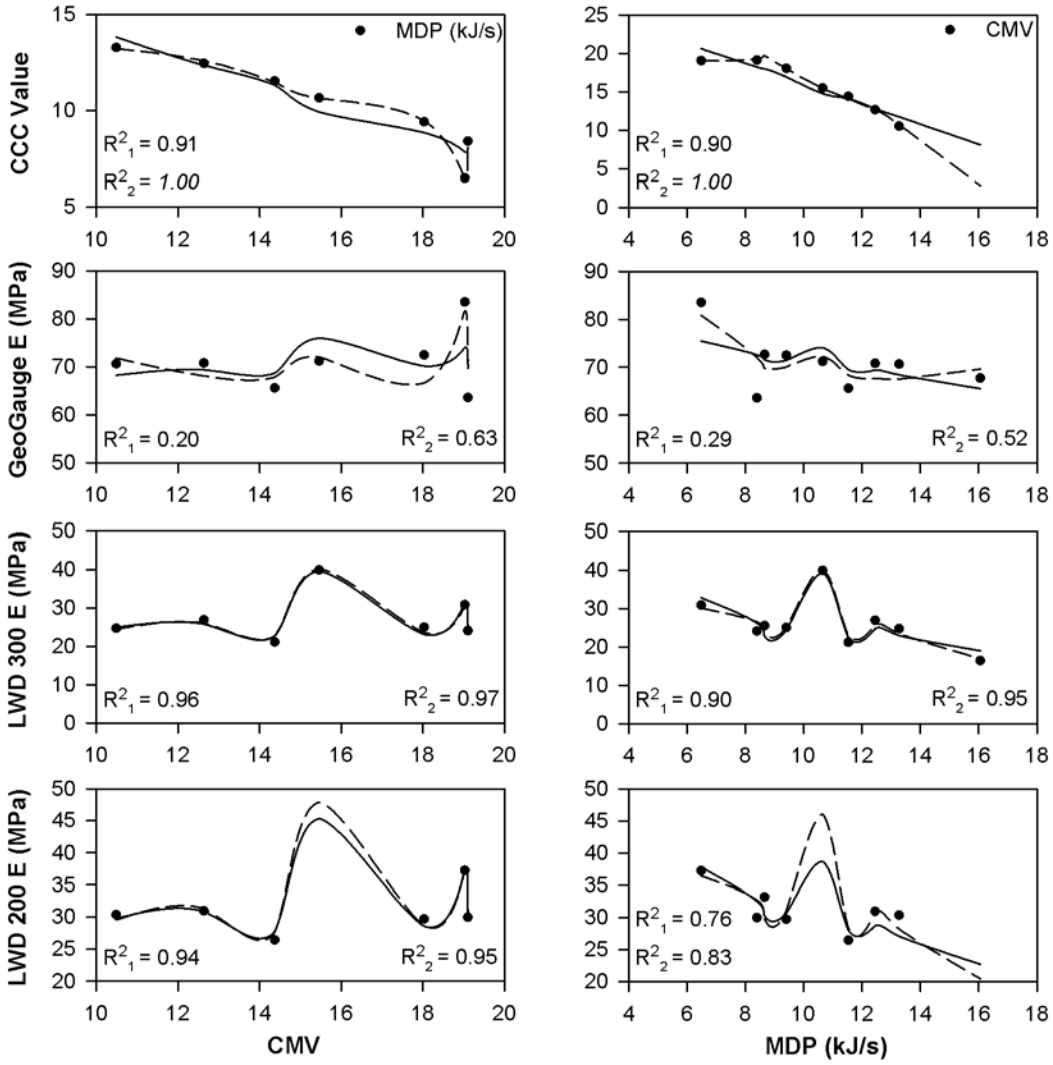

Figure 5.33 Multivariate regression analyses of average CCC, GeoGauge, and LWD measured values, vs. kriged CCC measurements and moisture content for all lifts and passes.

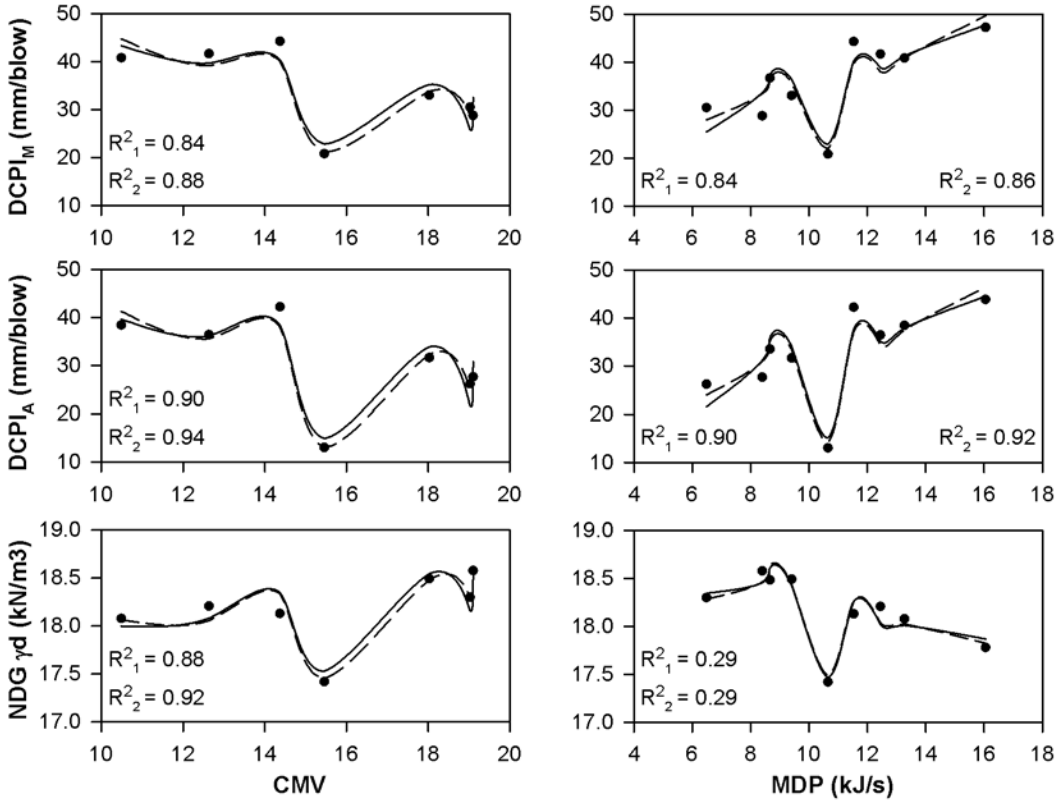

Figure 5.34 Multivariate regression analyses of average DCP and NDG measured values, vs. kriged CCC measurements and moisture content for all lifts and passes.

Observation of Figures 5.33 and 5.34 shows a strong correlation for all of the models, except for the GeoGauge models and the model of MDP values vs. NDG values.

For comparison, Figures 5.35 and 5.36 presented the results of the multivariate analyses after removing the base layer measurements.

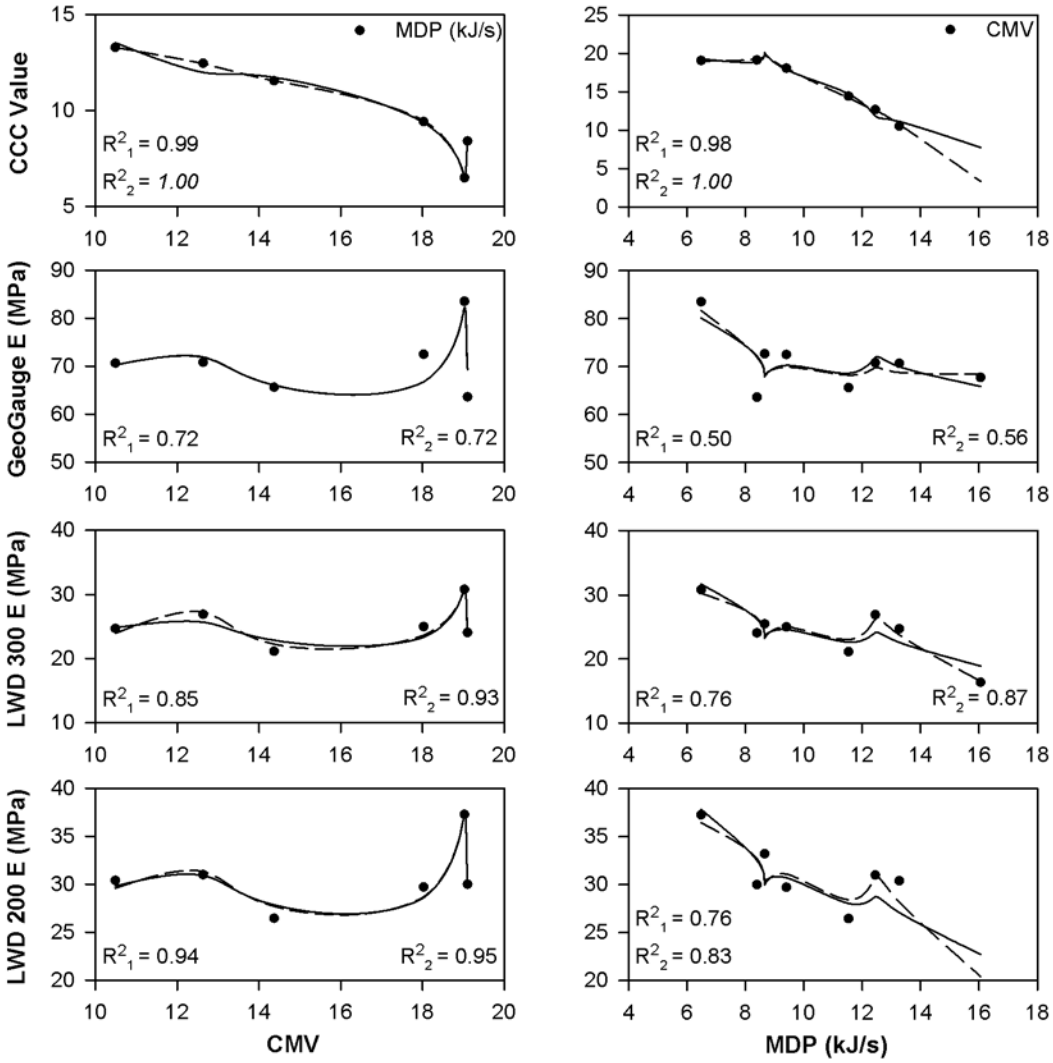

Figure 5.35 Multivariate regression analyses of average CCC, GeoGauge, and LWD measured values, vs. kriged CCC measurements and moisture content for all lifts and passes, excluding the base layer.

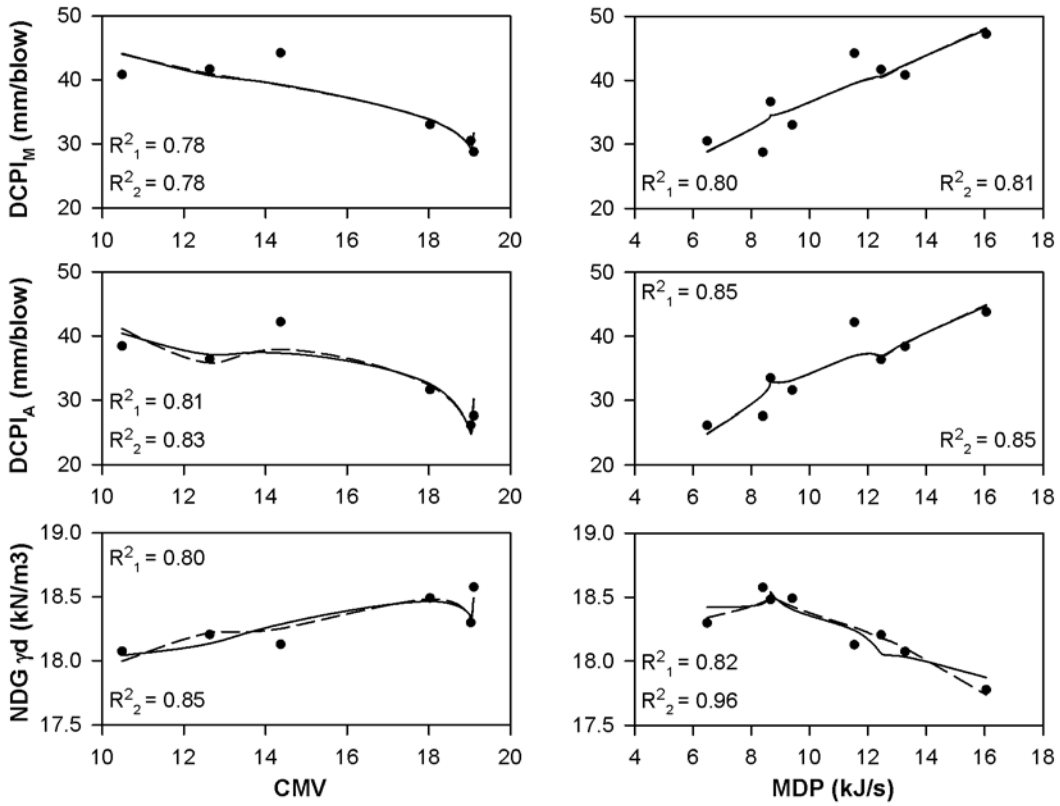

Figure 5.36 Multivariate regression analyses of average DCP and NDG measured values, vs. kriged CCC measurements and moisture content for all lifts and passes, excluding the base layer.

As shown in Figures 5.35 and 5.36, the coefficient of determination values decrease as a result of the exclusion of the base layer data, except for the models which showed poor correlations previously (i.e., the GeoGauge models and the MDP values versus NDG values model).

The next data set being analyzed is the *all final passes* data set, with results shown in Figures 5.37 and 5.38.

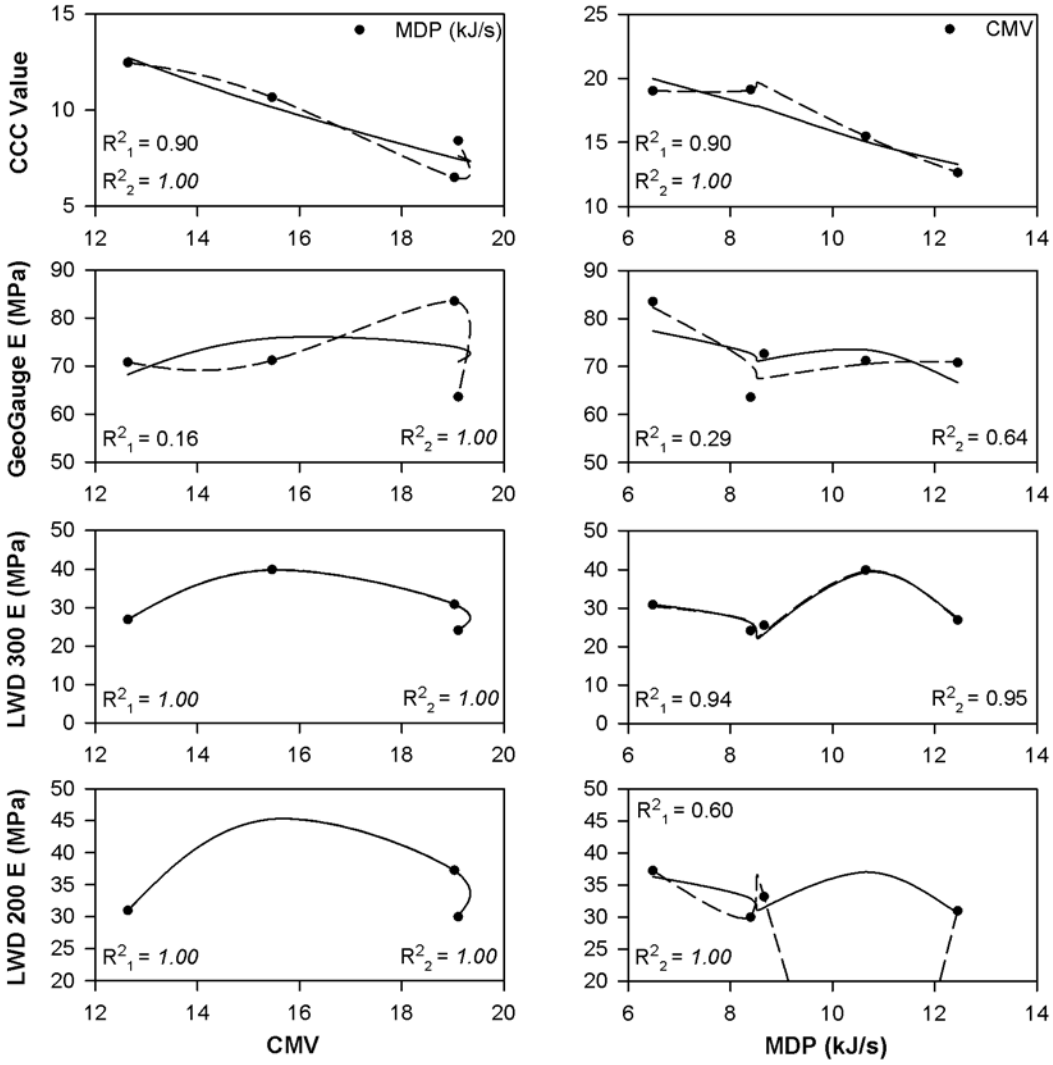

Figure 5.37 Multivariate regression analyses of average CCC, GeoGauge, and LWD measured values, vs. kriged CCC measurements and moisture content for all final passes.

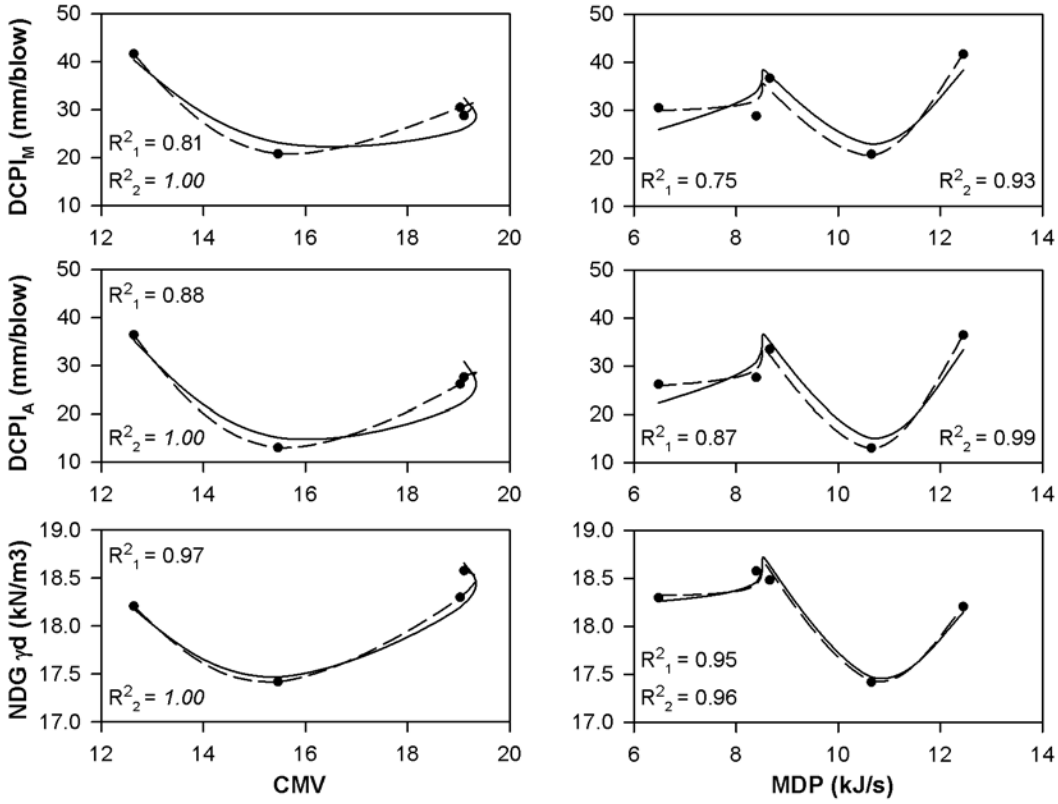

Figure 5.38 Multivariate regression analyses of average DCP and NDG measured values, vs. kriged CCC measurements and moisture content for all final passes.

Unfortunately, after observation of Figures 5.37 and 5.38, it can be seen that a number of the models do not have an adequate number of data points, as can be seen by the models with R^2=*1.00* on the figures above. This lack of data prevents a meaningful relationship from being determined.

For comparative purposes, multivariate regression analysis is performed on the data set of all final pass after the removal of the base layer, results shown in Figures 5.39 and 5.40.

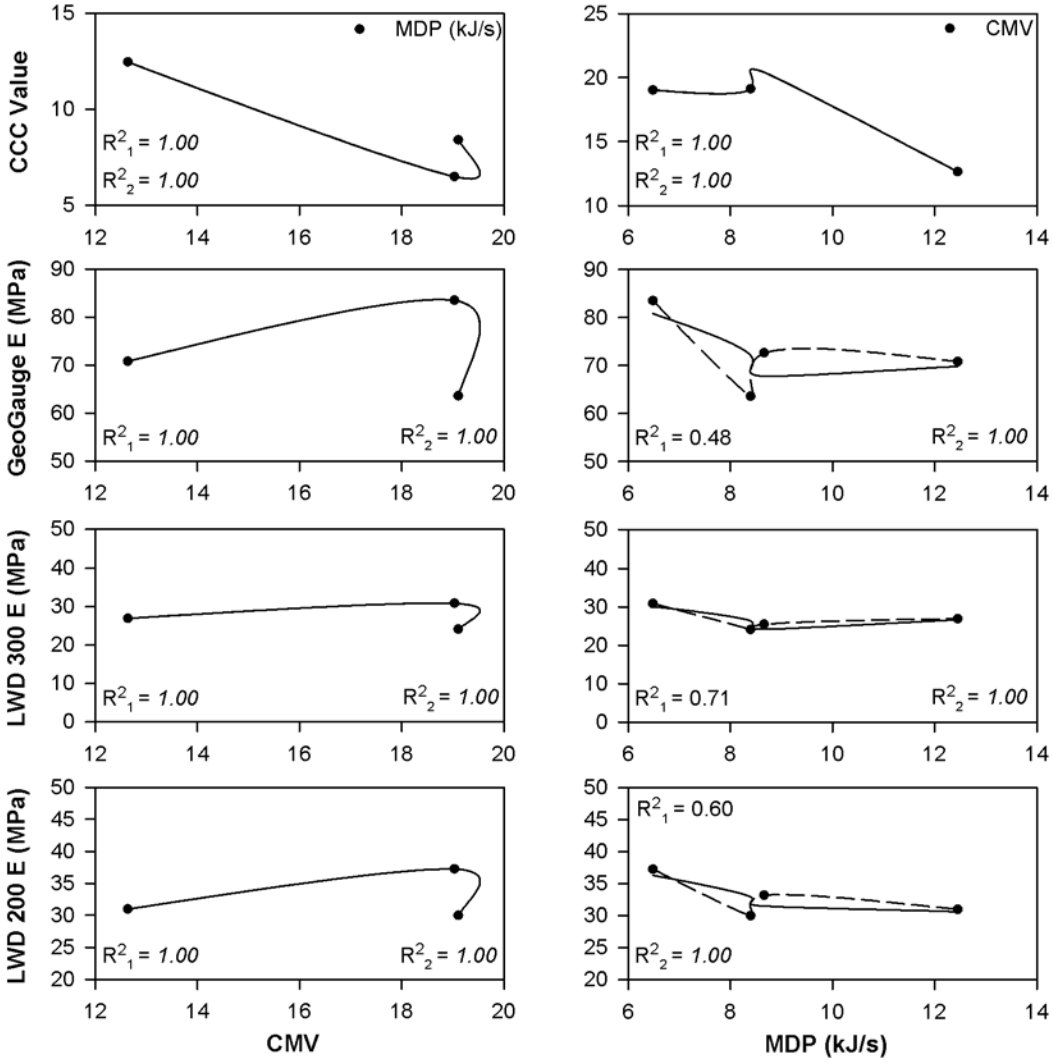

Figure 5.39 Multivariate regression analyses of average CCC, GeoGauge, and LWD measured values, vs. kriged CCC measurements and moisture content for all final passes, excluding the base layer.

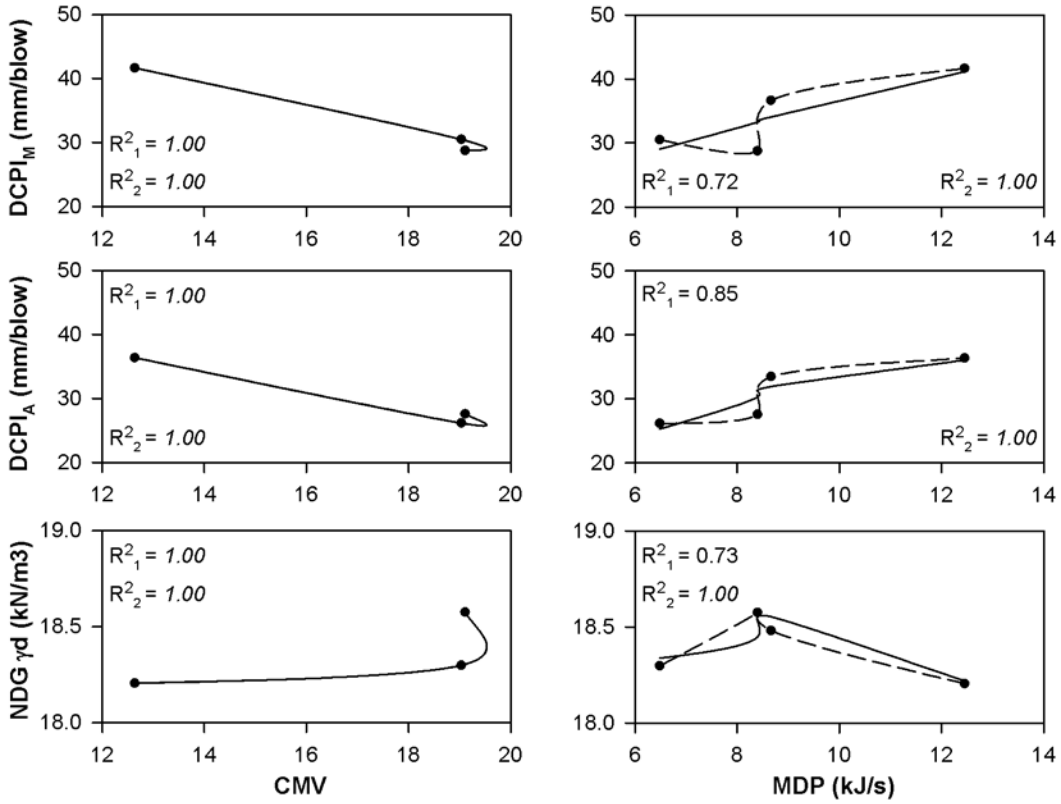

Figure 5.40 Multivariate regression analyses of average DCP and NDG measured values, vs. kriged CCC measurements and moisture content for all final passes, excluding the base layer.

As expected, since the removal of the base layer reduced the number of data points available for regression analysis, almost all of the models shown in Figures 5.39 and 5.40 lack the adequate number of data points to develop meaningful relationships between the average in situ test values and CCC measurements.

The final data set to be analyzed is the *Lift 5 passes* data set. The results are shown below in Figures 5.41 and 5.42.

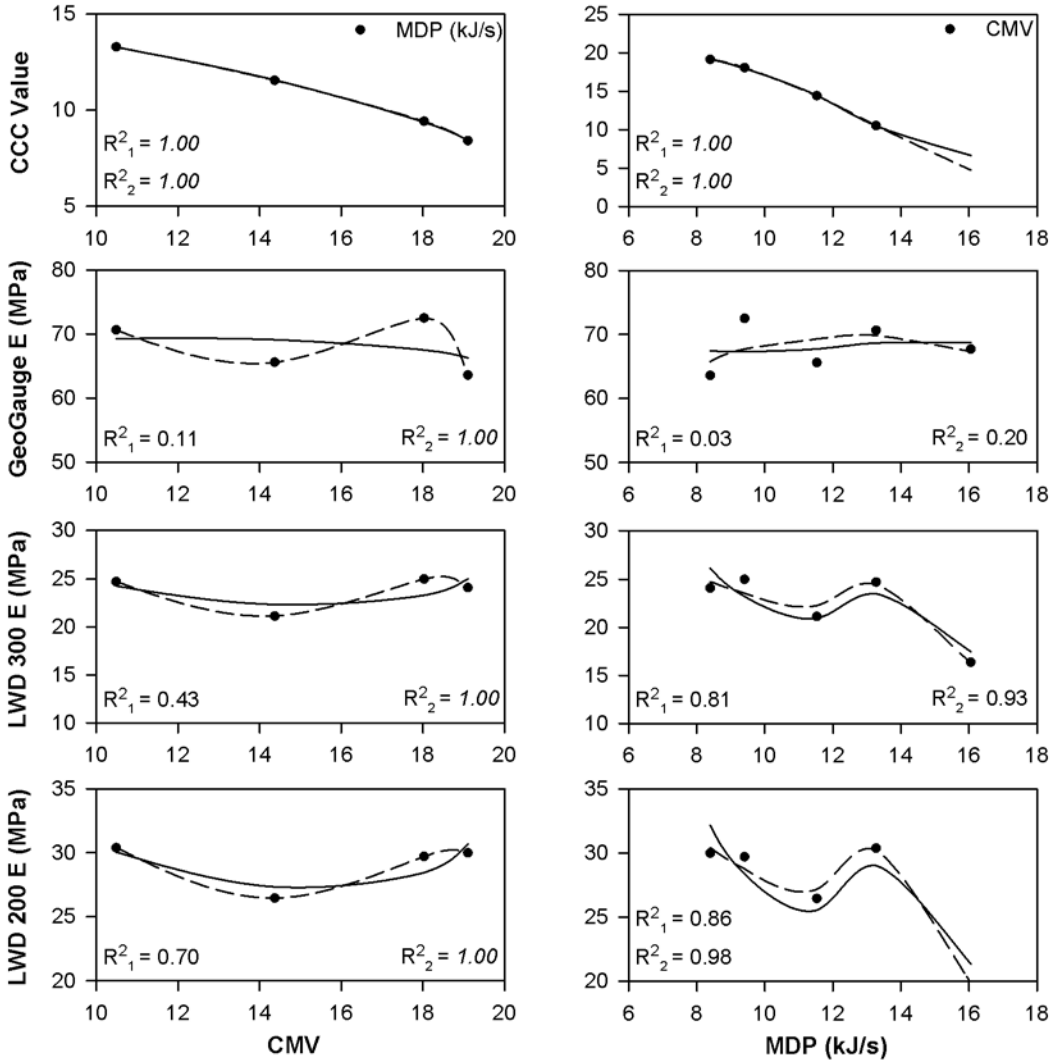

Figure 5.41 Multivariate regression analyses of average CCC, GeoGauge, and LWD measured values, vs. kriged CCC measurements and moisture content for Lift 5.

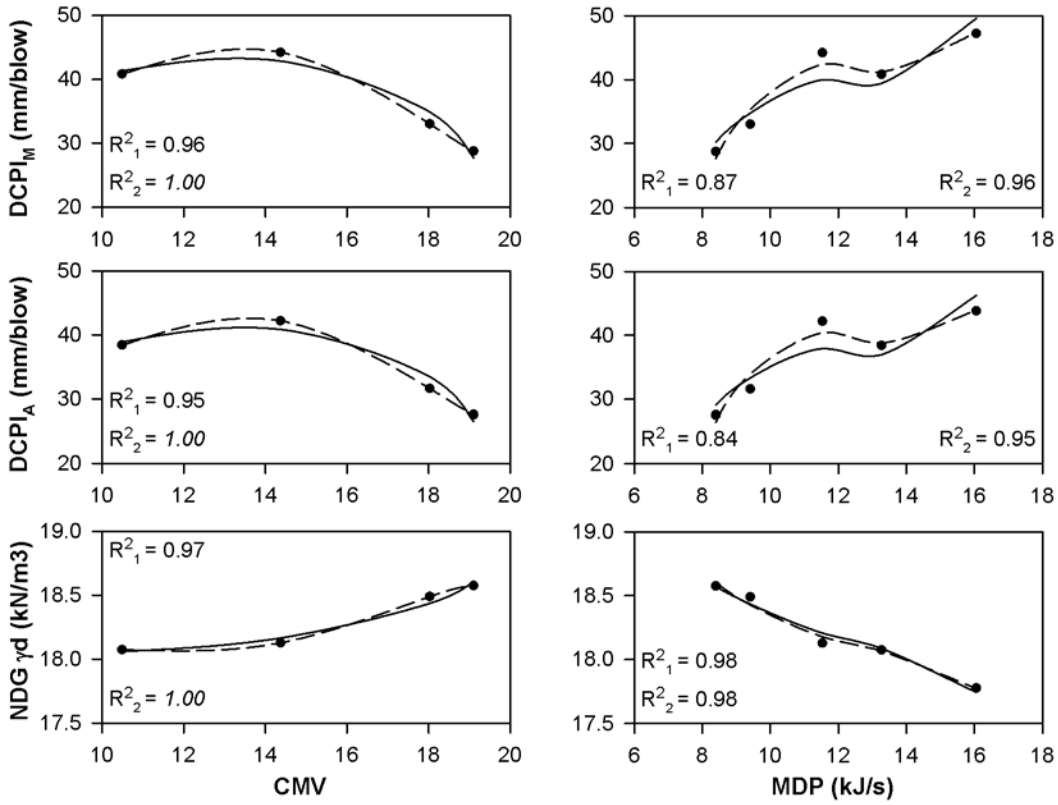

Figure 5.42 Multivariate regression analyses of average DCP and NDG measured values, vs. kriged CCC measurements and moisture content for Lift 5.

Inspection of Figures 5.50 and 5.51 shows that, again, many of the models lack the sufficient number of data points to develop meaningful relationships. However, when looking at the meaningful models for the *Lift 5 passes* data set, it is clear that the CCC measurements show the weakest correlations with the GeoGauge measured values.

For easy comparison, the coefficient of determination values from the multivariate regression analysis of the average data sets are summarized in Table 5.10.

Table 5.10 Coefficients of Determination from the Multivariate Regression Analyses that were Performed on Average Data (In Situ Data as Dependent Variable)

Variables	All		All Excluding Base Layer		Finals		Finals Excluding Base Layer		Lift 5	
	R^2_1	R^2_2	R^2_1	R^2_2	R^2_1	R^2_2	R^2_1	R^2_2	R^2_1	R^2_2
MDP (kJ/s) vs. CMV	0.91	*1.00*	0.99	*1.00*	0.90*	*1.00**	*1.00**	*1.00**	*1.00†*	*1.00**
Geogauge *E* (MPa) vs. CMV	0.20*	0.63*	0.72*	0.72*	0.16*	*1.00**	*1.00**	*1.00**	0.11*	*1.00**
LWD 300 *E* (MPa) vs. CMV	0.96	0.97	0.85*	0.93*	*1.00†*	*1.00**	*1.00**	*1.00**	0.43*	*1.00**
LWD 200 *E* (MPa) vs. CMV	0.94†	0.95*	0.94†	0.95*	*1.00**	*1.00**	*1.00**	*1.00**	0.70*	*1.00**
$DCPI_M$ (mm/blow) vs. CMV	0.84†	0.88*	0.78*	0.78*	0.81*	*1.00**	*1.00**	*1.00**	0.96*	*1.00**
$DCPI_A$ (mm/blow) vs. CMV	0.90	0.94†	0.81*	0.83*	0.88*	*1.00**	*1.00**	*1.00**	0.95*	*1.00**
NDG γ_d (kN/m^3) vs. CMV	0.88†	0.92†	0.80*	0.85*	0.97*	*1.00**	*1.00**	*1.00**	0.97*	*1.00**
CMV vs. MDP (kJ/s)	0.90	*1.00*	0.98	*1.00*	0.90*	*1.00**	*1.00**	*1.00**	*1.00†*	*1.00**
Geogauge *E* (MPa) vs. MDP (kJ/s)	0.29*	0.52*	0.50*	0.56*	0.29*	0.64*	0.48*	*1.00**	0.03*	0.20
LWD 300 *E* (MPa) vs. MDP (kJ/s)	0.90	0.95	0.76†	0.87†	0.94*	0.95*	0.71	*1.00**	0.81*	0.93
LWD 200 *E* (MPa) vs. MDP (kJ/s)	0.76*	0.83*	0.76†	0.83†	0.60*	*1.00**	0.60*	*1.00**	0.86*	0.98
$DCPI_M$ (mm/blow) vs. MDP (kJ/s)	0.84	0.86*	0.80†	0.81*	0.75*	0.93*	0.72*	*1.00**	0.87*	0.96
$DCPI_A$ (mm/blow) vs. MDP (kJ/s)	0.90	0.92	0.85	0.85†	0.87*	0.99*	0.85*	*1.00**	0.84*	0.95
NDG γ_d (kN/m^3) vs. MDP (kJ/s)	0.91	0.91*	0.82†	0.96†	0.95*	0.96*	0.73*	*1.00**	0.98†	0.98

Italics: Models that have too many coefficients for the number of data points

*: Models that have a p-value greater than 0.05

†: Models that have a p-value between 0.01 and 0.05

The results in Table 5.10 show that a large number of the models lacked a sufficient number of data points to develop meaningful relationships between CCC measurements and in situ test method measurements, as shown in italics in the table. Additionally, nearly all of the models did not meet the p-value criterion of 0.05. This may or may not be meaningful as the criterion may not be suitable for geotechnical engineering purposes.

In general, the second multivariate regression model showed higher coefficient of determination values. This is expected, since the introduction of the interaction term increased the number of coefficients for the predicting models. As seen in the analysis of the individual points, the removal of the base layer data resulted in decreased coefficient of determination values. Since this is the opposite of what occurred for the univariate analyses, it is believed that the low moisture content values of the base layer caused the problems for the univariate comparisons.

For the models which offer reliable coefficients of determination, it is clear that there is a strong multivariate relationship between the CCC measurements and the in situ test measurements (except for the GeoGauge) if the moisture content is considered.

5.5 Summary and Conclusions

In this chapter, possible relationships between CCC measurements and in situ test method measurements were explored using univariate and multivariate regression analysis. In order to perform the regression analysis, the CCC measurements needed to be predicted at the exact locations of the measured in situ testing data. Isotropic ordinary kriging interpolation was selected as the best method for the predications of the CCC data.

Two regression models were used for the univariate regression analysis: a linear model and a second-degree polynomial model. The univariate regression analyses were performed first on the data set of individual CCC measurements and the various in situ test method results. However, strong correlations were not observed in the point-to-point analysis of the CCC and in situ test method data sets. Consequently, univariate regression analyses were performed on average values for each lift and pass. The results of the univariate regression analyses resulted in the following observations:

- Comparisons of the individual values of CCC measurements and in situ test measurements at point-to-point locations showed weak correlations.
- Comparisons of the average values of CCC measurements and in situ test measurements at point-to-point locations yielded relatively strong correlations. However, a number of the average data sets did not have a sufficient number of data points; therefore, several of the models and corresponding coefficient of determination values were unreliable and should be ignored.
- For a number of the cases, the second-degree polynomial model showed significantly stronger correlations than the linear model (e.g., DCPI values, NDG dry unit weight values, and moisture contents).
- The removal of the base layer measurements from the respective data sets resulted in increased coefficients of determination. This phenomenon is likely due to the relatively low moisture content of the base layer in comparison to the “engineered” lifts, which indicates that

the moisture content had a significant influence on the density and modulus of the compacted soils.

- Examination of only the measurements collected on the final pass of each respective lift did not improve correlations; however examination of the Lift 5 data on its own did slightly improve correlations. This observation is likely due to the fact that the soil within a given lift is likely more uniform in soil gradation and moisture content in comparison to the soils from all five lifts and the base layer of the embankment.
- Generally, MDP measurements showed better correlations with the in situ test methods, in comparison to the CMV measurements. This is likely related to the different influence depths of the CCC measurements. The influence depth of MDP measurements is much closer to that of the in situ test methods which range from approximately 20 cm to 60 cm. In contrast, the influence depth of CMV measurements is roughly 80 cm to 150 cm, as noted in White and Thompson (2008).
- In general, the DCP indices show much stronger correlations with the CCC measurements, in comparison to the other in situ testing methods used in the study.
- In general, the GeoGauge moduli values showed the weakest correlations with the CCC measurements, in comparison to the other in situ testing methods used in the study.

- In general, both sets of moisture content values showed much stronger correlations with the CCC measurements, in comparison to the density-based and modulus-based in situ testing methods used in the study. This indicates that moisture content has a significant contribution to the density of compacted soils, which agrees with classic soil mechanics theory.

Examination of the univariate regression analyses results ultimately showed that, even when comparing the average CCC measurements and in situ test method measurements, the correlations were relatively weak indicating that there may not be a direct univariate relationship. Additionally, several observations indicated that the moisture condition of the soil may be a significant factor when measuring the modulus and dry unit weight of compacted soils. Therefore, multivariate regression techniques were examined so that influence of moisture content could be more thoroughly investigated.

Similar to the univariate regression analysis, for the multivariate regression analysis two regression models were used: a linear model without an interaction term and a linear model with an interaction term. The same procedure that was used for the univariate analyses was followed for the multivariate analyses. The multivariate regression analyses were performed first on the data set of individual CCC measurements and the various in situ test method results. Then, multivariate regression analyses were performed on average values for each lift and pass. The results of the multivariate regression analyses resulted in the following observations:

- Comparison of the individual values of CCC measurements and in situ test measurements at point-to-point locations showed improved

correlations compared to those seen in the univariate analyses, however, correlations were still relatively weak.

- Comparison of the average values of CCC measurements and in situ test measurements at point-to-point locations yielded very strong correlations. However, a majority of the average data sets did not have a sufficient number of data points; therefore, most of the models and corresponding coefficient of determination values were unreliable and needed to be ignored. To improve this, future studies should consider recording CCC and in situ test measurements for a significant number of passes and lifts of compacted soil, in order to create robust data set that does not have limitations due to a small amount of data.
- In general, the regression model with the interaction term resulted in slightly stronger coefficient of determination values. This observation is expected, considering that the additional term results in an additional regression model coefficient, which allows for a better fit model.
- The removal of the base layer measurements from the respective data sets resulted in decreased coefficient of determination values. This is contrary to the observation seen in the univariate analyses. This likely is an indication that the relatively low moisture content values of the base layer caused the measurements to be outliers in the univariate regression analyses. Since the multivariate regression analyses include the influence of moisture content in the models their inclusion in the data set did not negatively affect the correlations.

Overall examination of the regression results presented in this chapter shows that fairly strong relationships exist between average measurements of CCC values and in situ test method values. Unfortunately, point-to-point comparisons of individual CCC measurements and in situ testing measurements did not tend to yield good agreement in a regression framework; i.e., there tended to be a lot of data scatter about the trends that are predicted using a regression analysis approach. Additionally, it was determined that moisture content significantly affects the dry unit weight and modulus of compacted soils, validating the need to use multivariate regression analysis if the moisture content is not kept constant for all soils tested. As it is nearly impossible to keep uniform moisture content while compacting soil, it is the recommendation of the author that all further regression analyses performed comparing CCC measurements with in situ test method measurements use multivariate techniques to include moisture content as an additional independent variable in the regression models.

In this chapter, regression analyses were performed to compare in situ test measurements with predicted MDP and CMV values at the corresponding locations. As mentioned, the selected prediction method was isotropic ordinary kriging (anisotropic ordinary kriging could not be performed due to the nature of the collected data) largely because it has been the method of choice used previously in this research area for geospatial data (Brandl and Adam 2004, Thompson and White 2007, Petersen et al. 2007, Tehrani 2009). However, the ordinary kriging method is a complicated and nontrivial interpolation technique which requires significant user interpretation resulting in user sensitive results; evidence of this is displayed throughout this study, specifically in Chapter 2 and Section 5.2.

Later in this thesis, the framework for specifications of CCC equipment to be used for compaction verification will be presented and evaluated. Several of the methods rely in part on the relationship between CCC measurements and in situ method measurements. It is the belief of the author that the use of the ordinary kriging method for interpolation is not practical, due to its complexity, for practicing Geotechnical Engineers and Field Technicians to perform. Additionally, the user sensitivity of the interpolation technique does not allow for standardization in specifications which could ultimately result in litigation issues. Therefore, a simple, repeatable interpolation technique, that does not negativity affect the relationships between predicted CCC measurements and the corresponding in situ testing method measurements, must be found if CCC equipment is to be used in a compaction verification specification. Chapter 6 will examine the use of alternative interpolation techniques for the prediction of CCC measurements.

Chapter 6

EVALUATION OF ALTERNATIVE TECHNIQUES FOR INTERPOLATING CONTINUOUS COMPACTION CONTROL ROLLER MEASUREMENTS FOR COMPARISON WITH IN SITU TEST METHOD MEASUREMENTS

6.1 Introduction

For CCC and IC technologies to be adopted as a QA/QC compaction verification method, relationships must be shown between CCC measured values (e.g., MDP and CMV) and the in situ QA/QC testing methods currently used for this process. In Chapter 5, univariate and multivariate regression analyses were performed to compare interpolated CCC values to in situ test method measurements. A sophisticated geospatial interpolation technique, kriging, was used for predicting the expected CCC measurements at the in situ testing locations; this interpolation process was necessary to allow for direct comparisons between the data collected using these two approaches. This interpolation method has been used by a variety of others for this purpose in previous research (e.g., Brandl and Adam 2004, Thompson and White 2007, Petersen et al. 2007, Meehan et al. 2013). As shown in Chapter 5, the kriging method is extremely complex and precise repeatability from user to user is unlikely. The author does not believe the kriging method is a suitable interpolation technique to be used in a specification framework, where it is important that the methods be simple and repeatable. Other similar interpolation approaches are desirable to encourage adoption of CCC and IC technologies as a compaction verification technique in the United States.

In this chapter, alternative interpolation techniques which are simple in nature and repeatable will be investigated to predict CCC measurements of MDP and CMV. The interpolation techniques that will be examined are inverse distance weighting (IDW) and nearest neighbor (NN) interpolation. As a first step, the CCC measurements that are predicted using IDW and NN interpolation will be directly compared to the interpolated CCC values that are predicted using kriging, in an effort to find a simplistic technique that will provide comparable results to those that are yielded by the kriging process. After direct comparison of predicted CCC measured values, results that show strong agreement with the kriged predictions will be used in univariate and multivariate regression analyses, similar to those that are described in Chapter 5. The results of the regression analyses will be compared to the regression results from Chapter 5, to further verify if a simplistic interpolation technique can be used in place of the more sophisticated kriging method for QA/QC specification purposes.

6.2 Point-to-Point Comparison of Interpolation Techniques

Throughout this chapter, alternative interpolation techniques are compared to the isotropic kriging method which is explained in detail in Chapters 2, 4, and 5. The reason for this, as mentioned, is because kriging has been generally accepted as the best interpolation technique for this purpose (e.g., Brandl and Adam 2004, Thompson and White 2007, Petersen et al. 2007, Meehan et al. 2013). For this reason, the kriging predictions from the kriging method will be treated as the observed data set and all other predictions will be treated as estimated values. The two alternative interpolation techniques to be examined are NN and IDW. Each of these methods has been discussed in detail in Chapter 2.

The NN method simply selects the measured value that is closest in spatial distance to the prediction location and assigns that value as the interpolated value. The NN approach is extremely simple and has commonly been used by roller manufacturer software to provide spatial maps of CCC indicator value measurements (e.g., Facas et al. 2011). The inherent limitation with the NN method is that for data sets which show high measured value variability from point-to-point, the measured value closet in spatial distance may not be the most useful value. In other words, the NN method does not smooth the data in any way, which is not ideal, as CCC data sets tend to have high variability from point-to-point.

The IDW method uses a decaying weighting function that is based on spatial distance in conjunction with a series of existing measured values to make value predictions at other locations where measurements are not available. This method is less affected by point-to-point variations in measured values than the NN method. The IDW method requires that an exponent value be assigned to develop the inverse distance weighting function. A more detailed explanation of IDW may be found in Chapter 2.

For this study, predictions were made using NN interpolation and IDW interpolations with five different exponent values of p = 1, 2, 4, 8, and 64. The resulting predictions are compared to the kriging predictions in one-to-one plots, as shown in Figures 6.1 and 6.2. Hypothetically, if the results matched precisely, the data points would fall on the “line of equality”. This line is represented as a 45 degree line on each of the plots in Figures 6.1 and 6.2 and offers a way to visually assess the accuracy of the predictions being made.

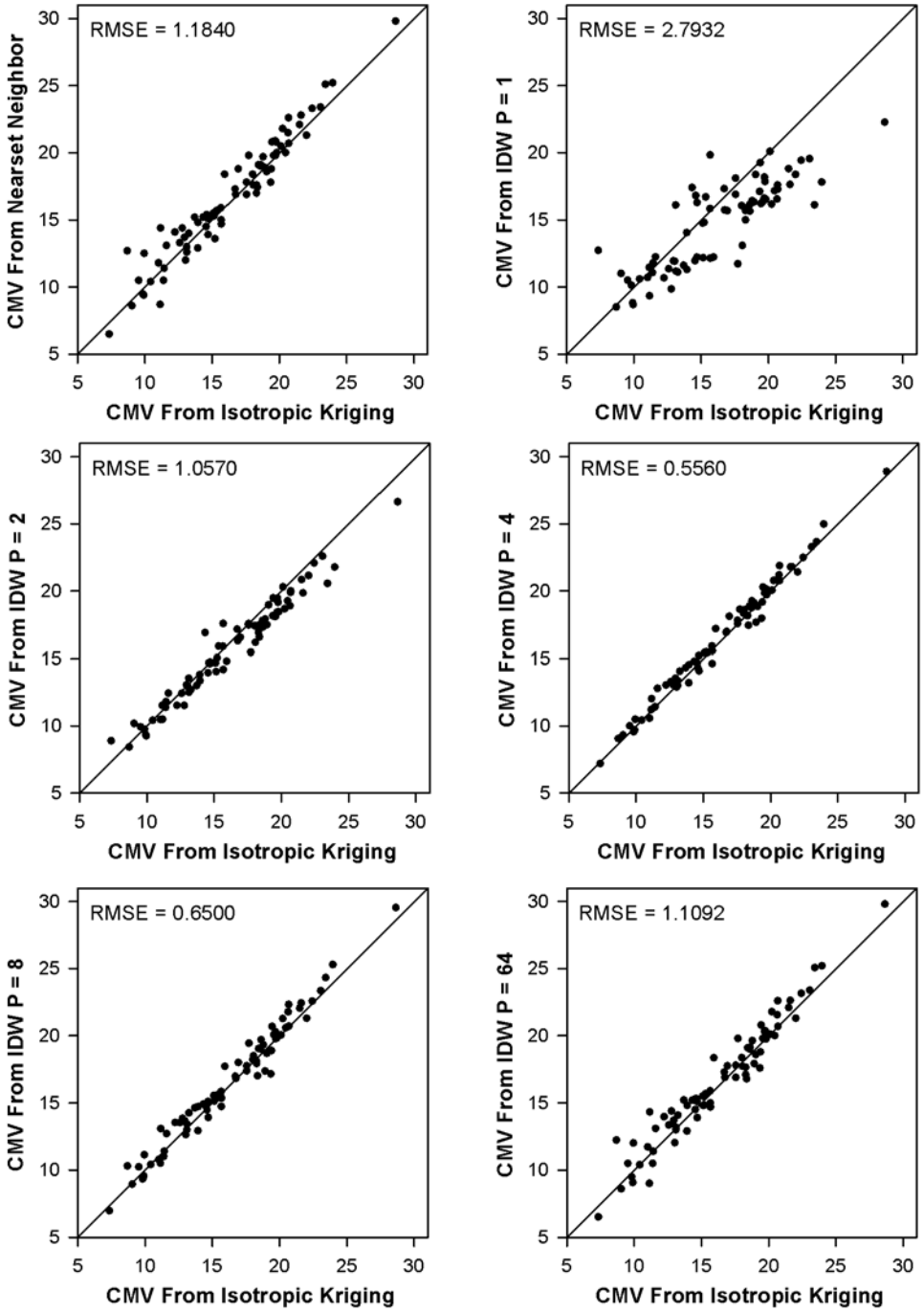

Figure 6.1 Comparison of CMV prediction results.

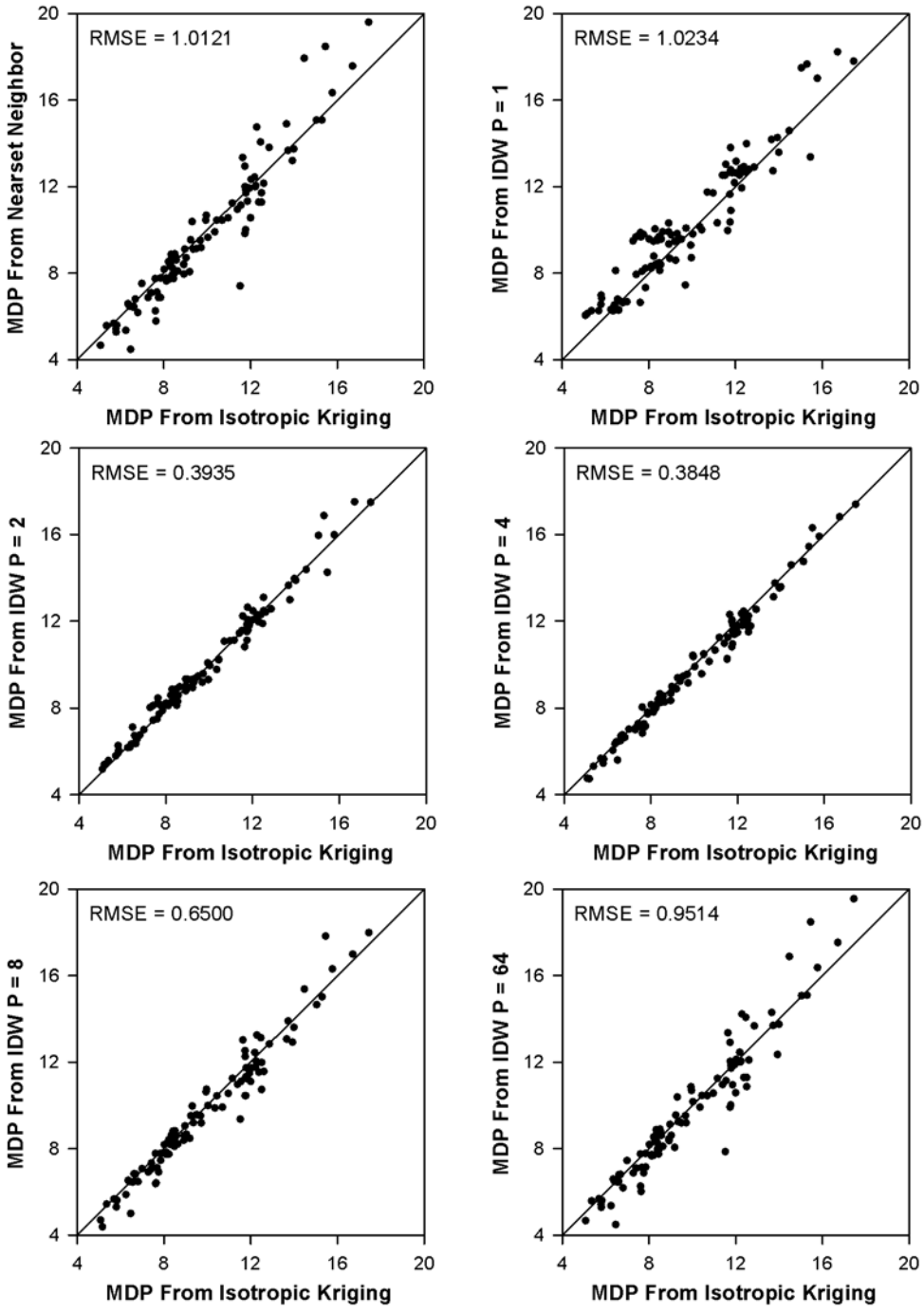

Figure 6.2 Comparison of MDP prediction results.

In a similar fashion as the assessment that was performed in Chapter 4, the point-to-point error between observed (kriged) and predicted (NN, IDW) values will be assessed using the associated root mean square error (RMSE). The calculation for RMSE is shown in Equation 4.2. In this case, the smaller the RMSE value, the better the ability of the interpolation method to predict results that match the results of the kriging prediction of CCC measurements.

Examination of Figures 6.1 and 6.2 shows agreement between the general trends that are observed in the MDP and CMV prediction results. The lowest RMSE value for both the MDP and CMV data sets, which corresponds to more precise predictions, is seen for the IDW method with an exponent value of $p = 4$. Therefore, predictions of CCC measurements using IDW with $p = 4$ most closely match the CCC prediction results from the ordinary kriging method. Coincidentally, as seen in Chapter 4, the exponent value of $p = 4$ also most closely matched the isotropic kriging results for elevation predictions. It is important to note that there is no convergence of RMSEs when increasing or decreasing the exponent value in the IDW method.

Additional review of Figures 6.1 and 6.2 shows that the CCC predictions made by the NN interpolation technique were the fifth least precise of the six interpolation techniques that were utilized. This would indicate that NN is, likely, not an accurate alternative to the isotropic kriging method. However, although this point-to-point assessment is excellent for initial comparisons, the change in the strength of correlations between the in situ test measurements and the CCC measurements is of more importance. Therefore, it is the author's decision to not rule out the NN interpolation method at this point. Consequently, the possibility of using the NN

method and the IDW p = 4 method as alternatives to the kriging method will be assessed from a regression correlation standpoint moving forward in this chapter.

6.3 Regression Analysis

In Chapter 5 (Section 5.3), regression analyses were performed on data sets of kriging predicted CCC values and in situ test measurements. As previously discussed, kriging has been established as the "state-of-the-art" interpolation technique for this purpose. Therefore, in this chapter, regression analyses will be performed on the resulting CCC measurements predicted from NN interpolation versus in situ test measurements, and IDW p = 4 interpolation versus in situ test measurements. The resulting correlations will be compared to the correlations that were previously developed using kriging interpolation. The intended goal is to find an alternative interpolation method to kriging that does not show a significantly lower quality of correlations with the in situ test measurements.

In Section 5.3, five different subsets of data were analyzed: (1) *all lifts and passes*; (2) *all lifts and passes excluding the base layer*; (3) *final passes*; (4) *final passes excluding the base layer*; and (5) *Lift 5 passes*. For purposes of comparison of interpolation methods, in this section, only the *all lifts and passes excluding the base layer* data set is evaluated. The reasoning for the selection of this subset is previously discussed in the conclusion of Chapter 5. The framework provided in Section 5.3 will still be followed. That is, four regression types will be performed: (1) univariate regression of individual data points, (2) univariate regression of the mean data for each lift and pass, (3) multivariate regression of individual data points, and (4) multivariate regression of the mean data for each lift and pass.

6.3.1 Univariate Regression Analysis of Individual CCC IDW & NN Predictions versus In Situ Testing Data

As in Section 5.3.1, two different univariate regression forms are used throughout the univariate analysis. The first is a linear regression model which is shown as a solid line on the figures. The notation of R^2_1 on figures and in summary tables will refer to the coefficient of determination for the fitted linear regression models. The second is a second-degree polynomial model which is denoted as a dashed line on the figures. Similarly, the notation of R^2_2 on figures and in summary tables will refer to the coefficient of determination for the fitted second-degree polynomial regression models. Additionally, the measured CCC and in situ data will be shown in the figures (denoted as solid dots) so that the overall scatter of the data and fit of the model may be visually examined.

Figures 6.3 through 6.8 show the univariate regression models for the NN prediction and IDW $p = 4$ data sets. Observation of the results shows that there is not a strong linear or second-degree polynomial correlation between the in situ test measurements and either of the predicted CCC values. Additionally, the polynomial models do not offer much improvement over the linear models with the exception of the CMV versus moisture content values.

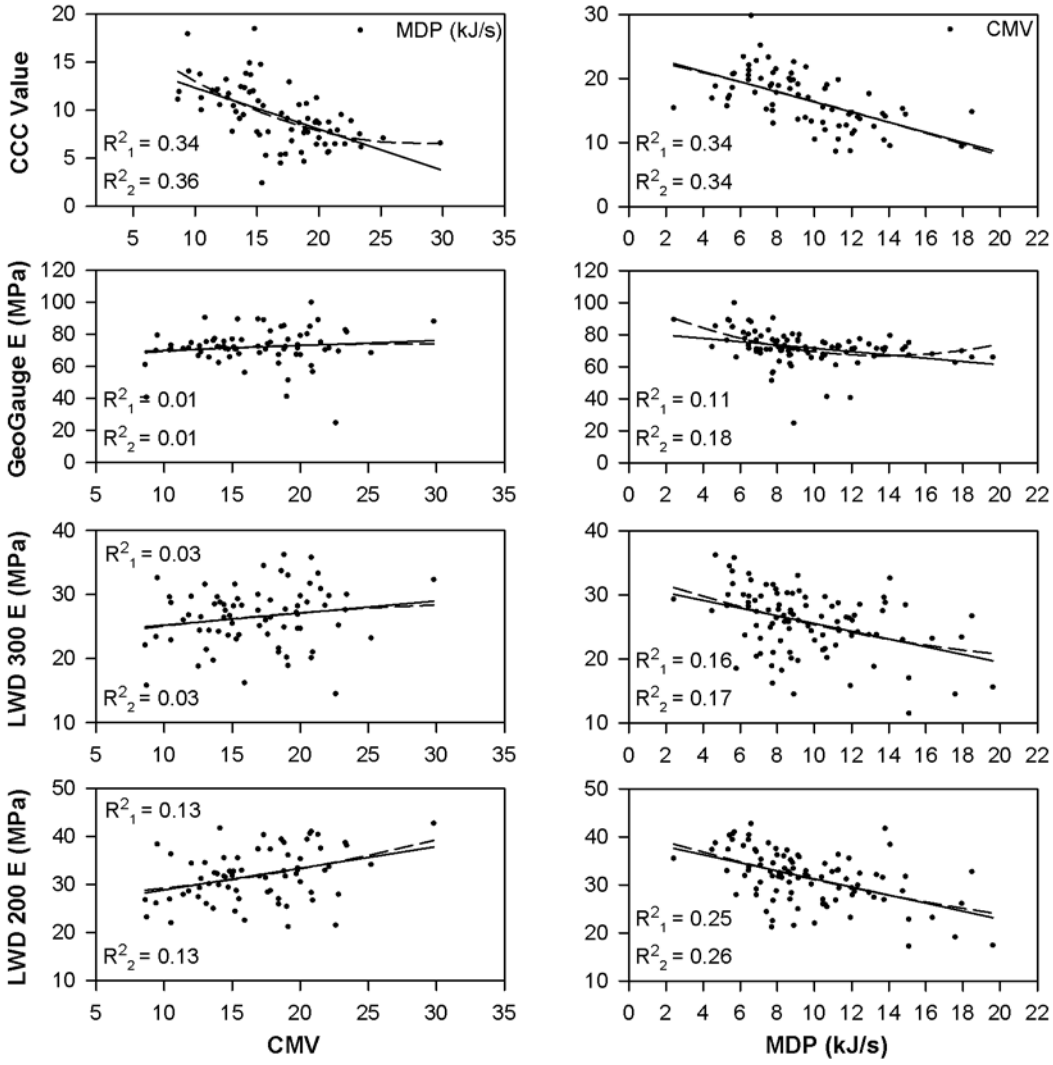

Figure 6.3 Univariate regression analyses of CCC, GeoGauge, and LWD measured values, vs. IDW *p* =4 predicted MDP and CMV measurements for all lifts and passes, excluding base layer.

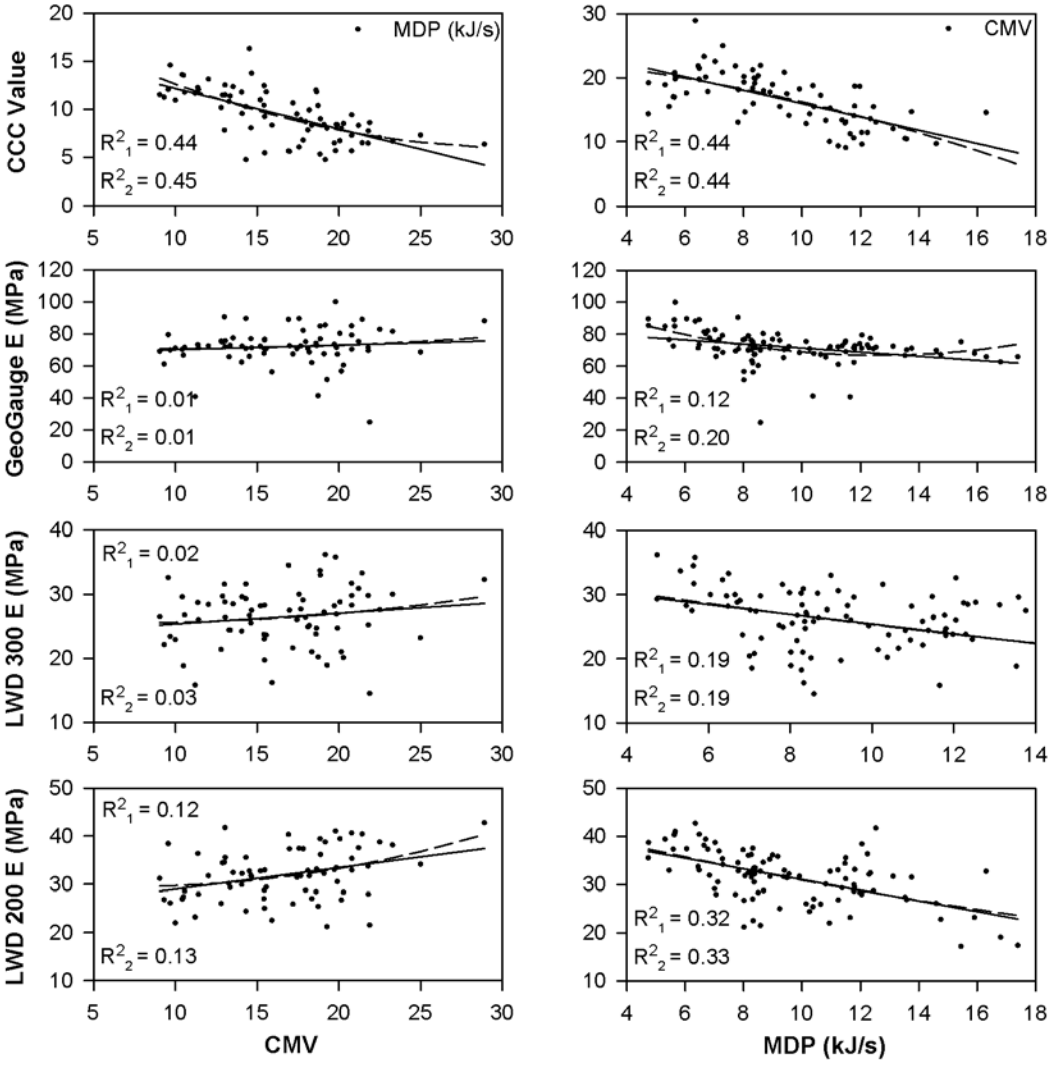

Figure 6.4 Univariate regression analyses of CCC, GeoGauge, and LWD measured values, vs. NN predicted MDP and CMV measurements for all lifts and passes, excluding base layer.

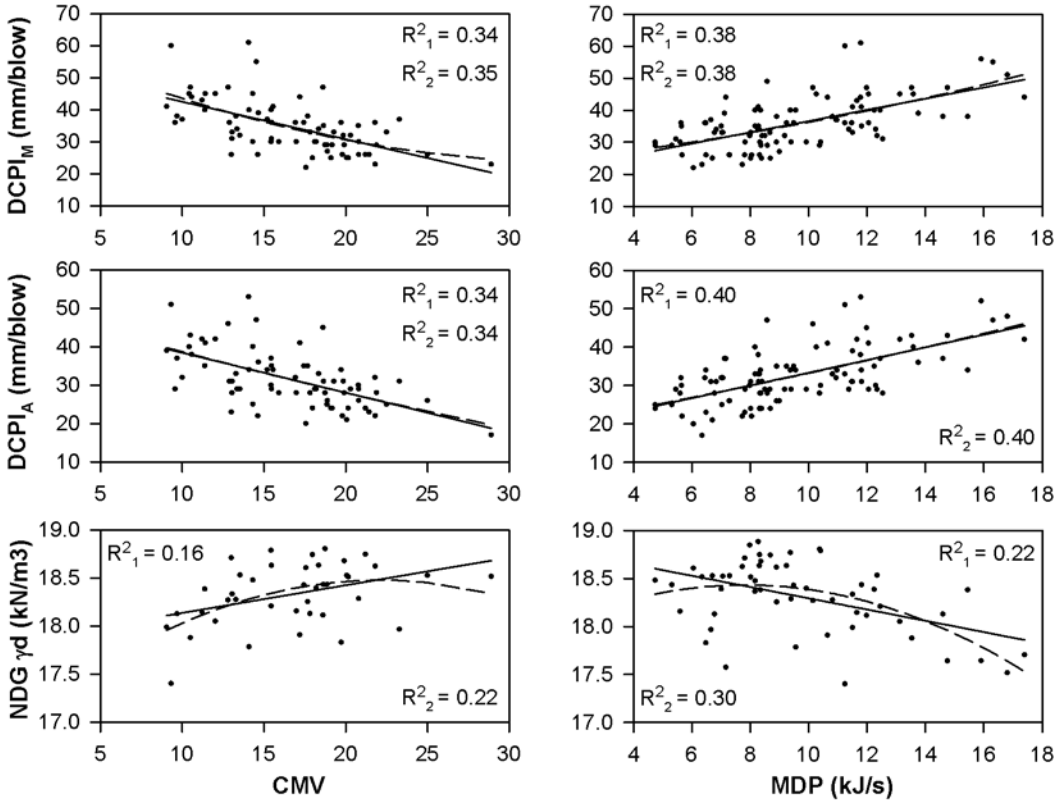

Figure 6.5 Univariate regression analyses of DCP and NDG measured values, vs. IDW *p* = 4 predicted MDP and CMV measurements for all lifts and passes, excluding base layer.

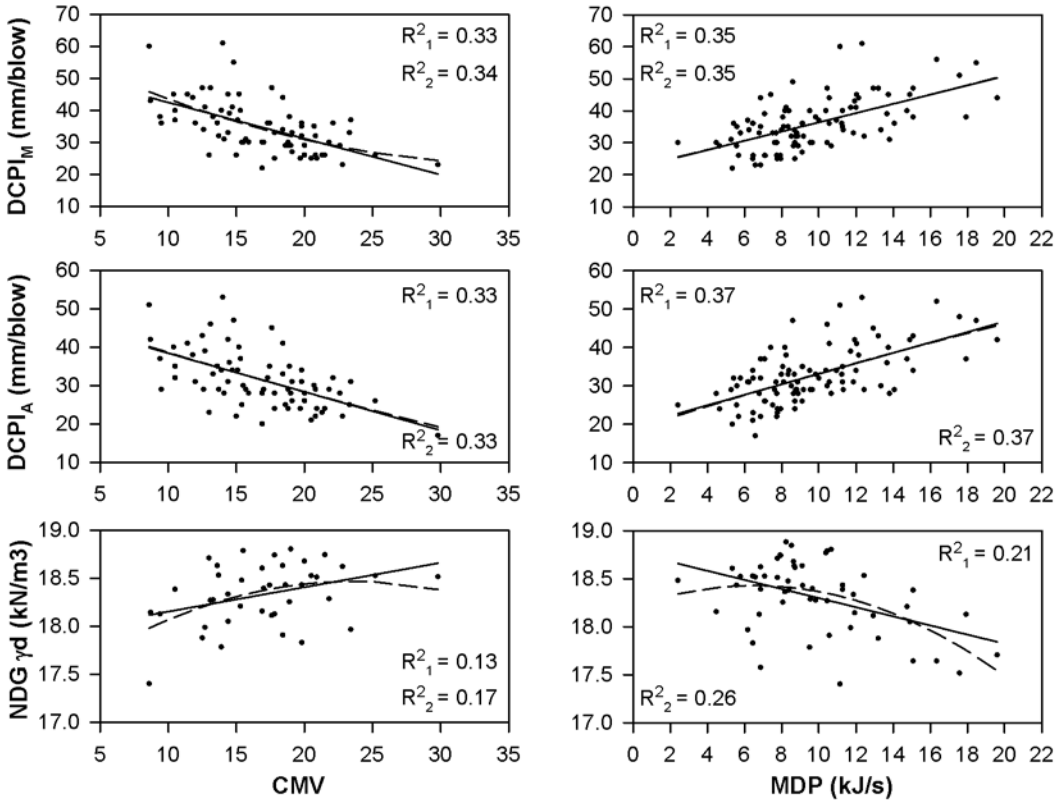

Figure 6.6 Univariate regression analyses of DCP and NDG measured values, vs. NN predicted MDP and CMV measurements for all lifts and passes, excluding base layer.

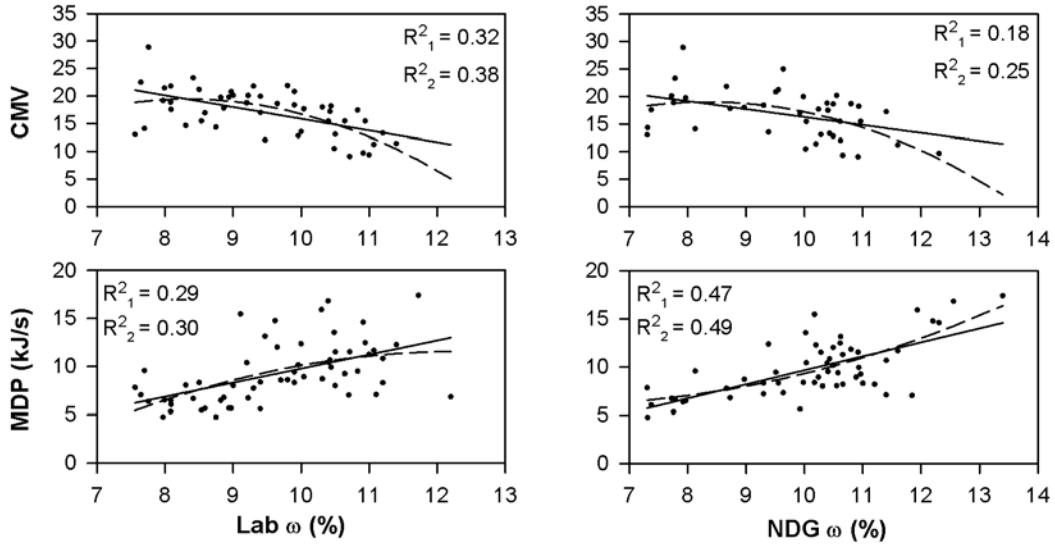

Figure 6.7 Univariate regression analyses of Lab and NDG water contents, vs. IDW p = 4 predicted MDP and CMV measurements for all lifts and passes, excluding base layer.

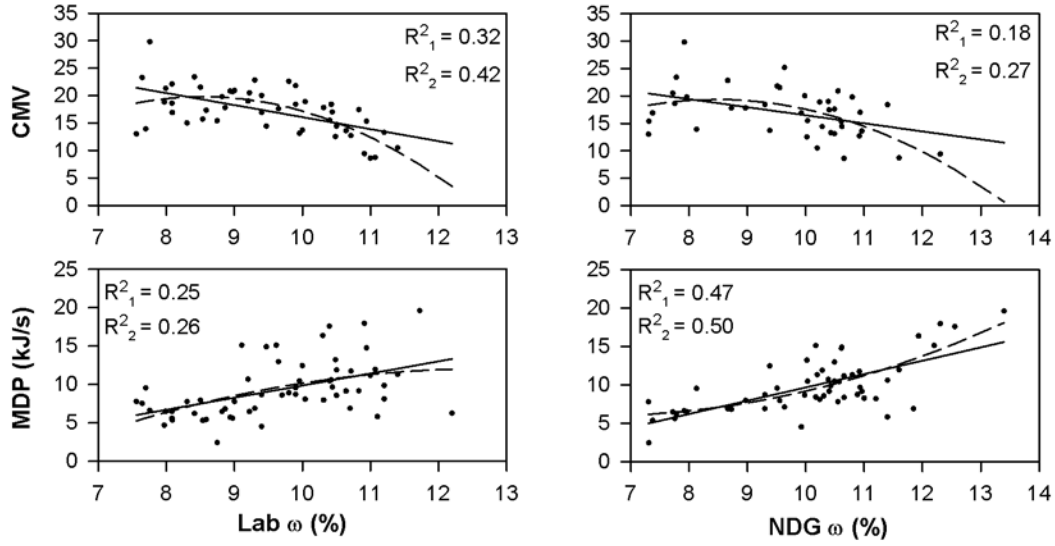

Figure 6.8 Univariate regression analyses of Lab and NDG water contents, vs. NN predicted MDP and CMV measurements for all lifts and passes, excluding base layer.

To allow for easy comparison of the results of the three different data sets (Kriging, IDW, NN) used in the regression analysis, all of the coefficient of determination values are summarized in Tables 6.1 and 6.2. As previously mentioned, the regression models that have a p-value greater than 0.05 will be denoted with an asterisk (*). The coefficient of determination values for the linear models are presented in the R^2_1 columns (shaded in grey), and the coefficient of determination values for the second-degree polynomial models are presented in the R^2_2 columns.

Table 6.1 R-Squared Values from the Univariate Regression Analyses that were Performed on Individual Data Points (In Situ Data as Dependent Variable)

Dependent Variable	Kriging		IDW P=4		NN	
	R^2_1	R^2_2	R^2_1	R^2_2	R^2_1	R^2_2
MDP (kJ/s) vs. CMV	0.53	0.55	0.44	0.45	0.34	0.36
Geogauge *E* (MPa) vs. CMV	0.02*	0.03*	0.01*	0.01*	0.01*	0.01*
LWD 300 *E* (MPa) vs. CMV	0.04*	0.04*	0.02*	0.03*	0.03*	0.03*
LWD 200 *E* (MPa) vs. CMV	0.14	0.15	0.12	0.13	0.13	0.13
$DCPI_M$ (mm/blow) vs. CMV	0.38	0.39	0.34	0.35	0.33	0.34
$DCPI_A$ (mm/blow) vs. CMV	0.38	0.38	0.34	0.34	0.33	0.33
NDG γ_d (kN/m^3) vs. CMV	0.17	0.23	0.16†	0.22	0.13†	0.17†
CMV vs. MDP (kJ/s)	0.53	0.54	0.44	0.44	0.34	0.34
Geogauge *E* (MPa) vs. MDP (kJ/s)	0.12	0.21	0.12	0.20	0.11	0.18
LWD 300 *E* (MPa) vs. MDP (kJ/s)	0.18	0.18	0.19	0.19	0.16	0.17
LWD 200 *E* (MPa) vs. MDP (kJ/s)	0.33	0.33	0.32	0.33	0.25	0.26
$DCPI_M$ (mm/blow) vs. MDP (kJ/s)	0.40	0.41	0.38	0.38	0.35	0.35
$DCPI_A$ (mm/blow) vs. MDP (kJ/s)	0.42	0.42	0.40	0.40	0.37	0.37
NDG γ_d (kN/m^3) vs. MDP (kJ/s)	0.25	0.32	0.22	0.30	0.21	0.26

*: Models that have a p-value greater than 0.05
†: Models that have a p-value between 0.01 and 0.05

Table 6.2 R-Squared Values from the Univariate Regression Analyses that were Performed on Individual Data Points (Moisture Content as Dependent Variable)

Dependent Variable	Kriging		IDW P=4		NN	
	R^2_1	R^2_2	R^2_1	R^2_2	R^2_1	R^2_2
Lab ω vs. CMV	0.33	0.38	0.32	0.38	0.32	0.42
NDG ω vs. CMV	0.21	0.27	0.18	0.25	0.18	0.27
Lab ω vs. MDP (kJ/s)	0.32*	0.33*	0.29*	0.30*	0.25*	0.26*
NDG ω vs. MDP (kJ/s)	0.48*	0.50*	0.47*	0.49*	0.47*	0.50*

*: Models that have a p-value greater than 0.05
†: Models that have a p-value between 0.01 and 0.05

Observation of summary Tables 6.1 and 6.2 show that in general the coefficient of determination trends that are seen in the Kriging results are also seen in IDW p = 4 and NN results. In general, the coefficient of determination values for IDW p = 4 are slightly lower than for kriging and the NN coefficient of determination values are slightly lower than that of the IDW p = 4. However, with the possible exception of the MDP vs. CMV results, the differences in the coefficient of determination values appear to be fairly insignificant between the different methods (a matter of a few hundredths or so change in R^2). Results from this analysis seem to support the conclusion that both IDW p = 4 and NN interpolation could be used as an alternative for the kriging method, with IDW p = 4 being the more accurate alternative.

6.3.2 Univariate Regression Analysis of Average CCC IDW & NN Predictions versus Average In Situ Testing Data

The same univariate regression analysis performed above will be followed in this section with the only exception being that the data sets here now consist of the average measurements for each lift and pass of compaction data. This is done in

attempt to “smooth” the data and remove the influence of any point-to-point discrepancies in the individual data. Consequently the number of data points is significantly reduced, therefore, the regression models must be inspected carefully to ensure that the coefficient of determination values accurately reflect the models and are not influenced by the small sampling size (sample sizes that are very small may result in high coefficient of determination values that do not appropriately portray the accuracy of the model fit for the data series).

Figures 6.9 through 6.14 show the univariate regression models for the NN prediction and IDW p = 4 average data sets. The data shown in Figures 6.9 through 6.14 indicates that there is generally a strong linear and second-degree polynomial correlation between the CCC measured values and the in situ measured values for DCPI and the NDG, where both the MDP and CMV models show similar R^2 values. The regression models for the GeoGauge, and LWD results show a much stronger relationship with MDP measurements when compared to the relationship with the CMV measurements. Additionally, all of the data show that there is a stronger second-degree polynomial correlation with the CCC data than the linear model, although the differences vary.

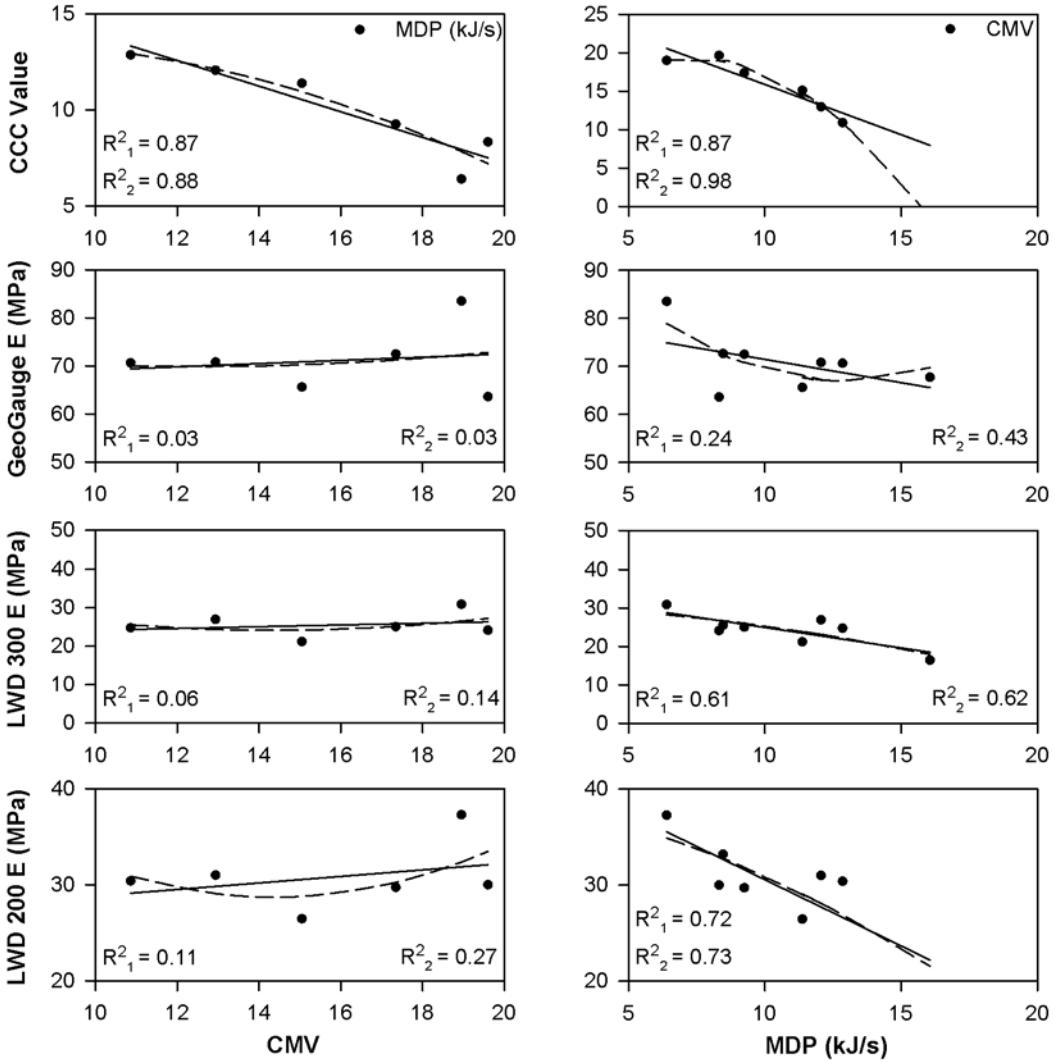

Figure 6.9 Univariate regression analyses of average CCC, GeoGauge, and LWD measured values, vs. IDW *p* = 4 predicted MDP and CMV measurements for all lifts and passes, excluding base layer.

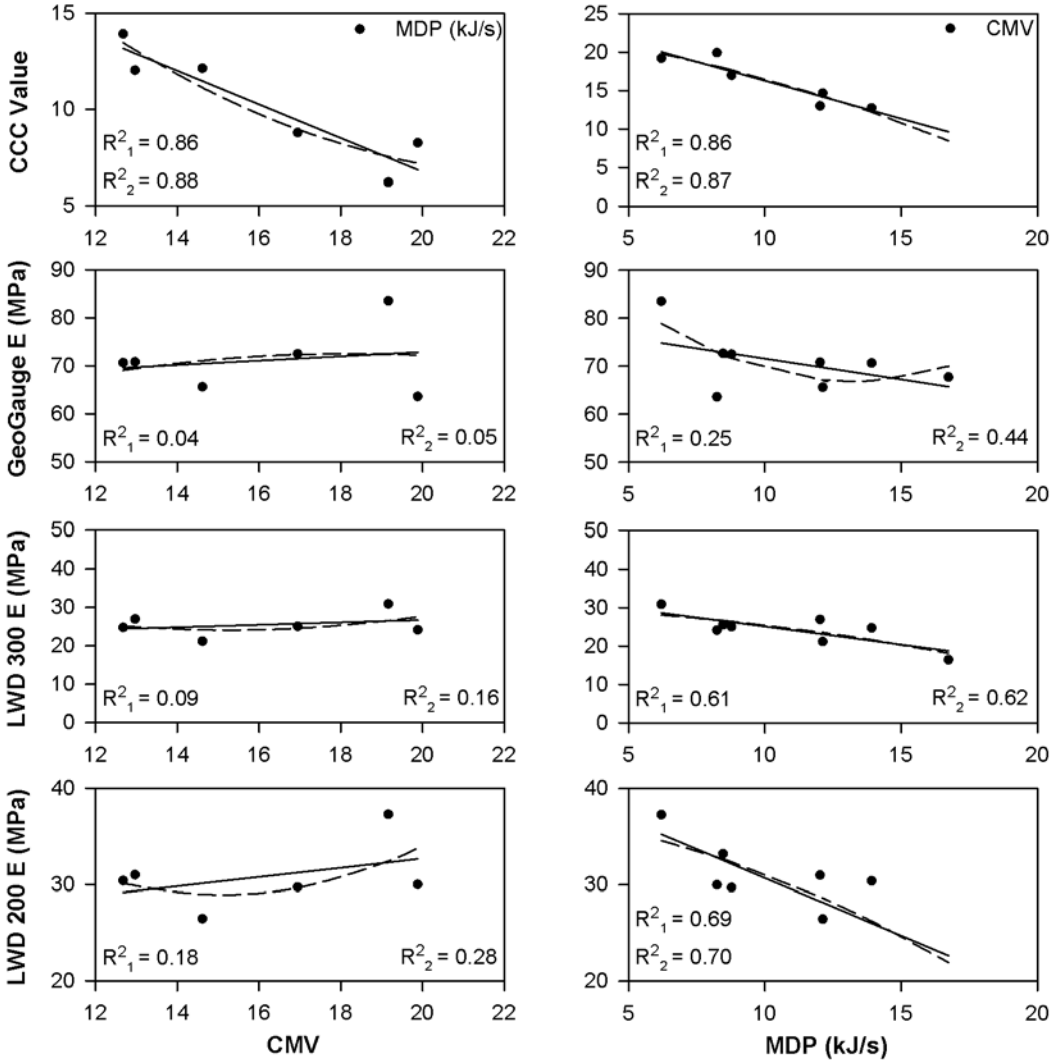

Figure 6.10 Univariate regression analyses of average CCC, GeoGauge, and LWD measured values, vs. NN predicted MDP and CMV measurements for all lifts and passes, excluding base layer.

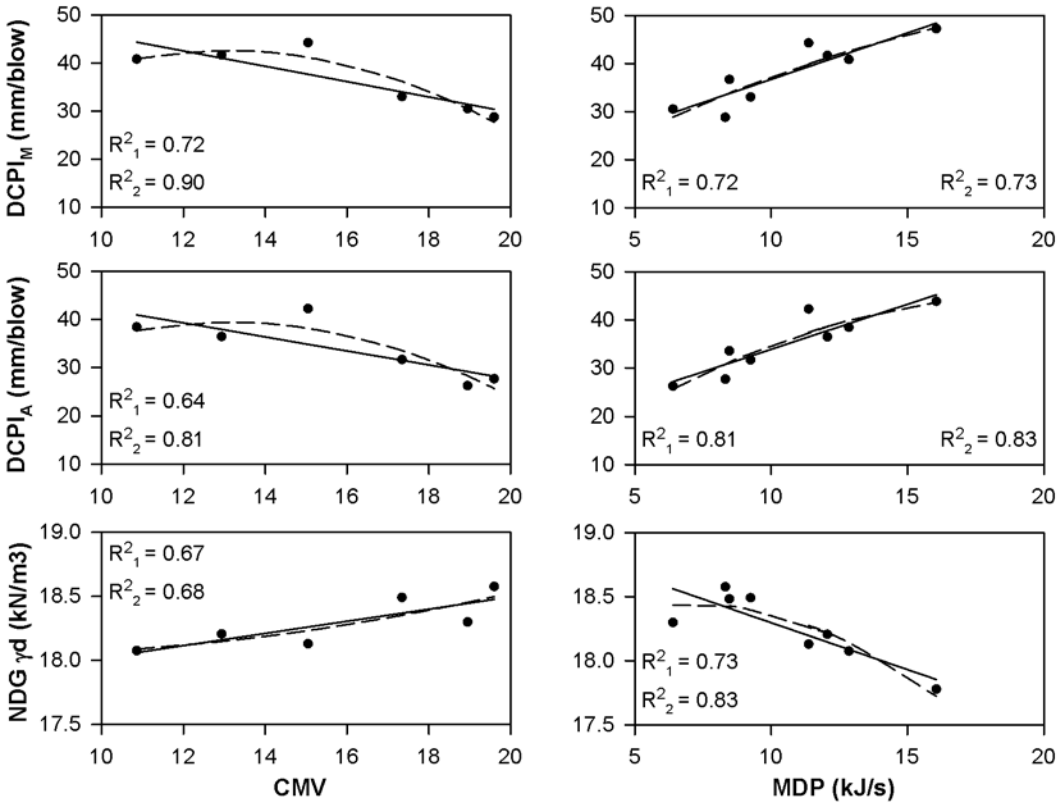

Figure 6.11 Univariate regression analyses of average DCP and NDG measured values, vs. IDW p = 4 predicted MDP and CMV measurements for all lifts and passes, excluding base layer.

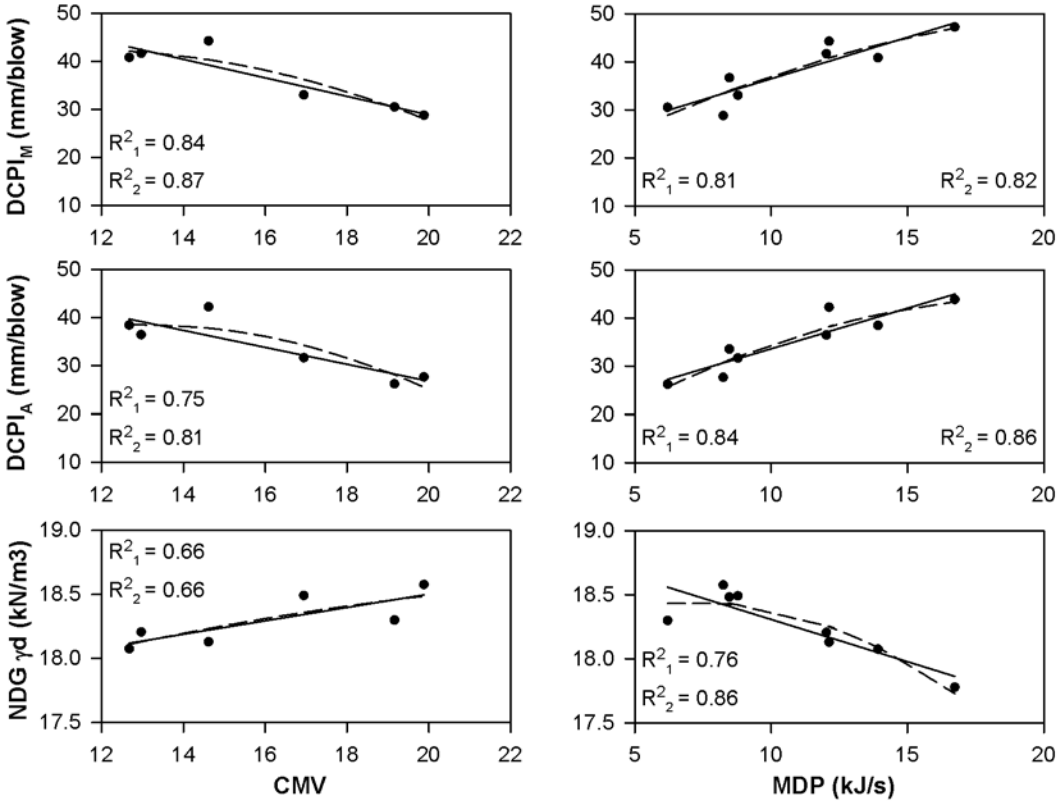

Figure 6.12 Univariate regression analyses of average DCP and NDG measured values, vs. NN predicted MDP and CMV measurements for all lifts and passes, excluding base layer.

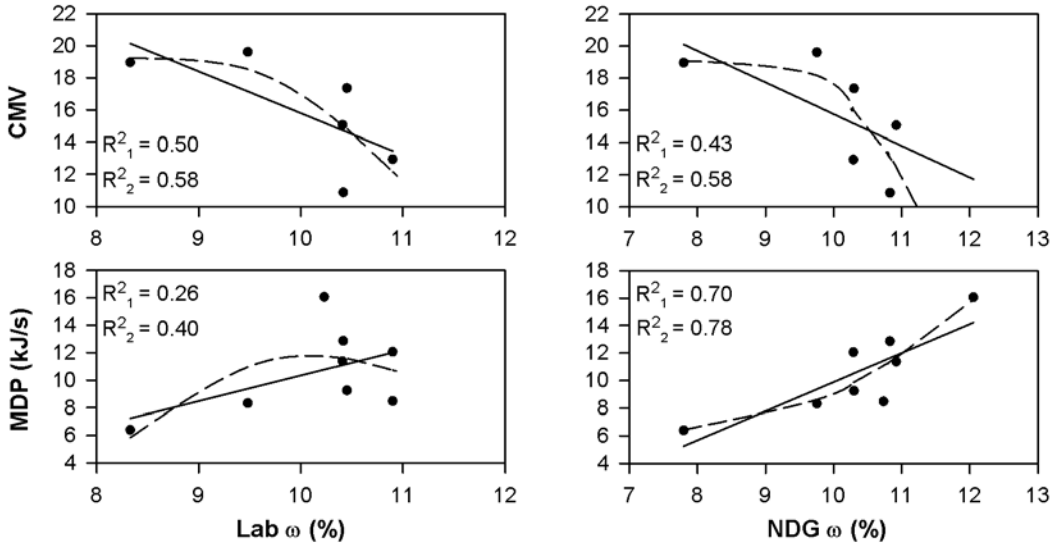

Figure 6.13 Univariate regression analyses of average Lab and NDG water contents, vs. IDW *p* = 4 predicted MDP and CMV measurements for all lifts and passes, excluding base layer.

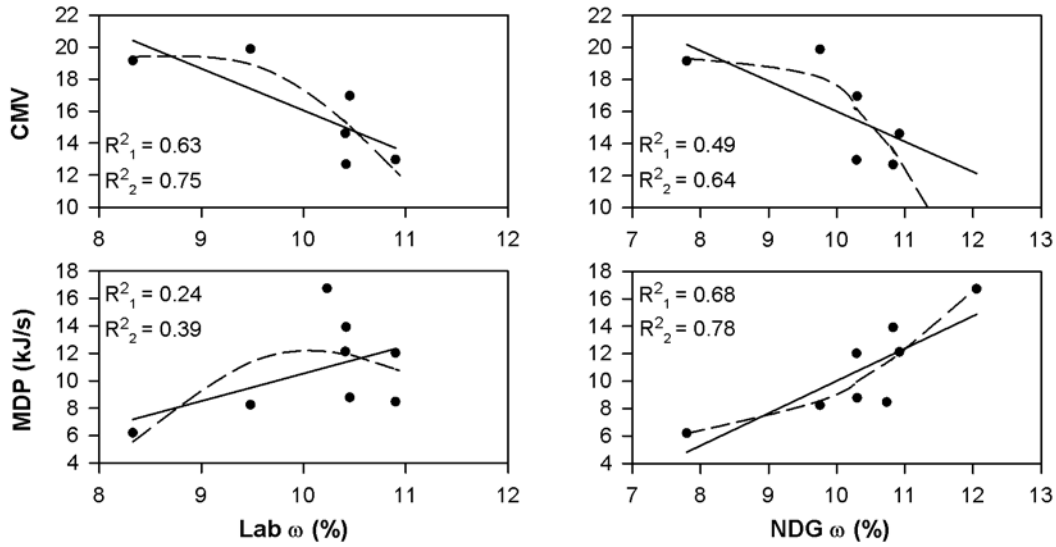

Figure 6.14 Univariate regression analyses of average Lab and NDG water contents, vs. NN predicted MDP and CMV measurements for all lifts and passes, excluding base layer.

To allow for easy comparison of the results of the three different average data sets (Kriging, IDW, NN) used in the regression analysis, all of the coefficient of determination values are summarized in Tables 6.3 and 6.4. As previously mentioned, the regression models that have a p-value greater than 0.05 will be denoted with an asterisk (*). The coefficient of determination values for the linear models are presented in the R^2_1 columns (shaded in grey), and the coefficient of determination values for the second-degree polynomial models are presented in the R^2_2 columns.

Table 6.3 R-Squared Values from the Univariate Regression Analyses that were Performed on Average Data (In Situ Data as Dependent Variable)

Dependent Variable	Kriging		IDW P=4		NN	
	R^2_1	R^2_2	R^2_1	R^2_2	R^2_1	R^2_2
MDP (kJ/s) vs. CMV	0.92	0.93†	0.87	0.88†	0.86	0.88†
Geogauge *E* (MPa) vs. CMV	0.04*	0.06*	0.03*	0.03*	0.04*	0.05*
LWD 300 *E* (MPa) vs. CMV	0.08*	0.17*	0.06*	0.14*	0.09*	0.16*
LWD 200 *E* (MPa) vs. CMV	0.14*	0.31*	0.11*	0.27*	0.18*	0.28*
$DCPI_M$ (mm/blow) vs. CMV	0.75†	0.93†	0.72†	0.90†	0.84	0.87†
$DCPI_A$ (mm/blow) vs. CMV	0.68†	0.85*	0.64*	0.81*	0.75†	0.81*
NDG γ_d (kN/m^3) vs. CMV	0.69†	0.70*	0.67†	0.68*	0.66*	0.66*
CMV vs. MDP (kJ/s)	0.92	0.98	0.87	0.98	0.86	0.87†
Geogauge *E* (MPa) vs. MDP (kJ/s)	0.23*	0.43*	0.24*	0.43*	0.25*	0.44*
LWD 300 *E* (MPa) vs. MDP (kJ/s)	0.55†	0.55*	0.61†	0.62*	0.61†	0.62*
LWD 200 *E* (MPa) vs. MDP (kJ/s)	0.65†	0.65*	0.72	0.73†	0.69†	0.70*
$DCPI_M$ (mm/blow) vs. MDP (kJ/s)	0.78	0.79†	0.80	0.80†	0.81	0.82†
$DCPI_A$ (mm/blow) vs. MDP (kJ/s)	0.80	0.82†	0.81	0.83†	0.84	0.86
NDG γ_d (kN/m^3) vs. MDP (kJ/s)	0.72	0.85	0.73	0.83†	0.76	0.86

*: Models that have a p-value greater than 0.05

†: Models that have a p-value between 0.01 and 0.05

Table 6.4 R-Squared Values from the Univariate Regression Analyses that were Performed on Average Data (Moisture Content as Dependent Variable)

Dependent Variable	Kriging		IDW P=4		NN	
	R^2_1	R^2_2	R^2_1	R^2_2	R^2_1	R^2_2
Lab ω vs. CMV	0.50*	0.56*	0.50*	0.58*	0.63*	0.75*
NDG ω vs. CMV	0.46*	0.63*	0.43*	0.58*	0.49*	0.64*
Lab ω vs. MDP (kJ/s)	0.28*	0.41*	0.26*	0.40*	0.24*	0.39*
NDG ω vs. MDP (kJ/s)	0.67*	0.74*	0.70*	0.78*	0.68*	0.78*

*: Models that have a p-value greater than 0.05
†: Models that have a p-value between 0.01 and 0.05

Observation of summary Tables 6.3 and 6.4 show that, in general, the coefficient of determination trends that are seen in the Kriging results are also seen in IDW p = 4 and NN results. It seems that the differences in coefficient of determination values for the three different interpolation technique results do not follow any pattern. For some analyses the kriging results have higher coefficient of determination value and for other the NN interpolation method has higher values. However, again, the differences in coefficient of determination values appear to be fairly insignificant (typically a matter of a few hundredths). The results from this analysis seem to support the conclusion that both IDW p = 4 and NN interpolation could be used as an alternative for the kriging method, for averaged data sets.

6.3.3 Multivariate Regression Analysis of Individual CCC IDW & NN Predictions versus In Situ Testing Data

The implementation of the multivariate regression analysis for the individual in situ test measurements versus the prediction results of CCC measurements and corresponding moisture content values will follow in suit with the presentation style for the multivariate regression analysis that is shown in Section 5.4.2. However, in the

current section, multivariate regression analysis will be performed on just one of the five different subsets of the CCC and in situ data, *all lifts and passes excluding the base layer*. The associated multivariate regression results are presented in Figures 6.15 through 6.18.

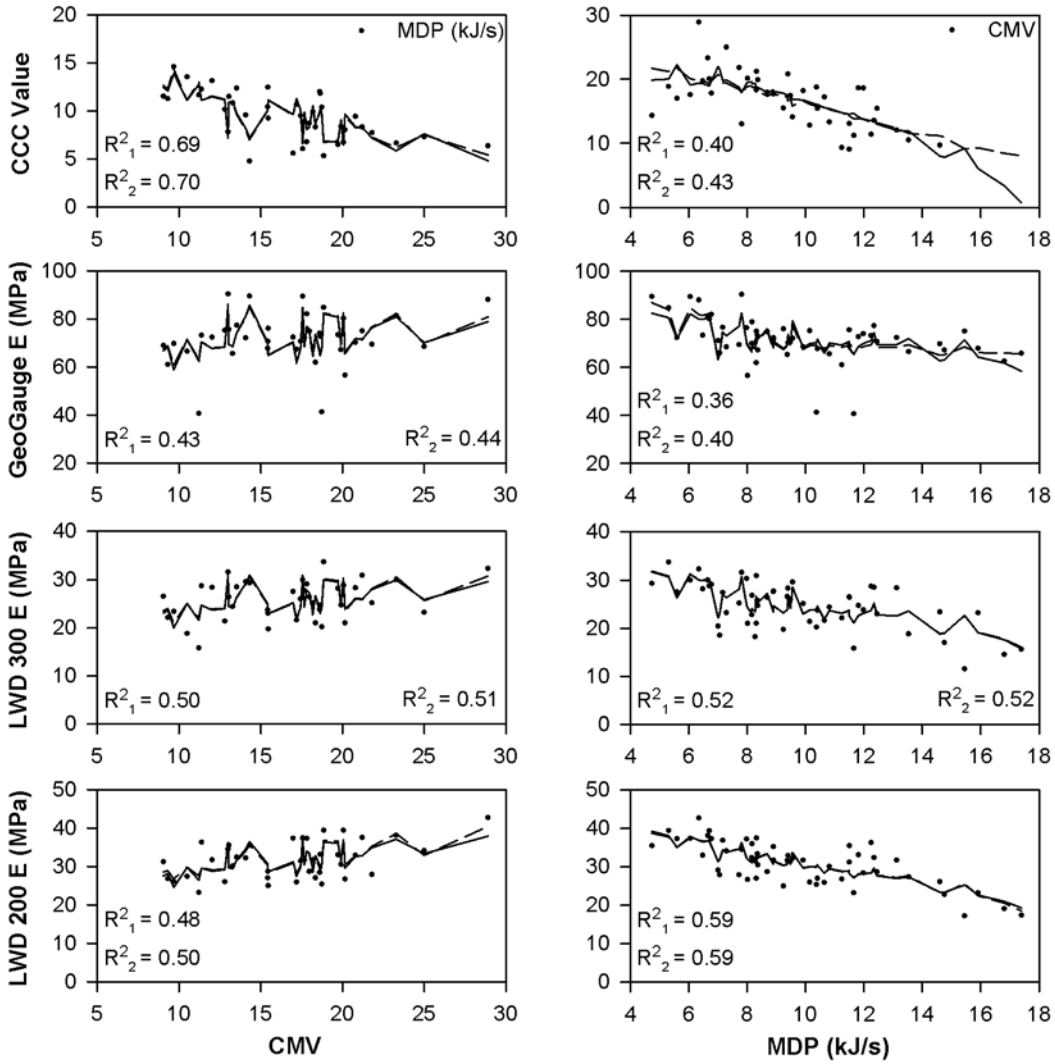

Figure 6.15 Multivariate regression analyses of CCC, GeoGauge, and LWD measured values, vs. IDW *p* = 4 predicted MDP and CMV measurements for all lifts and passes, excluding base layer.

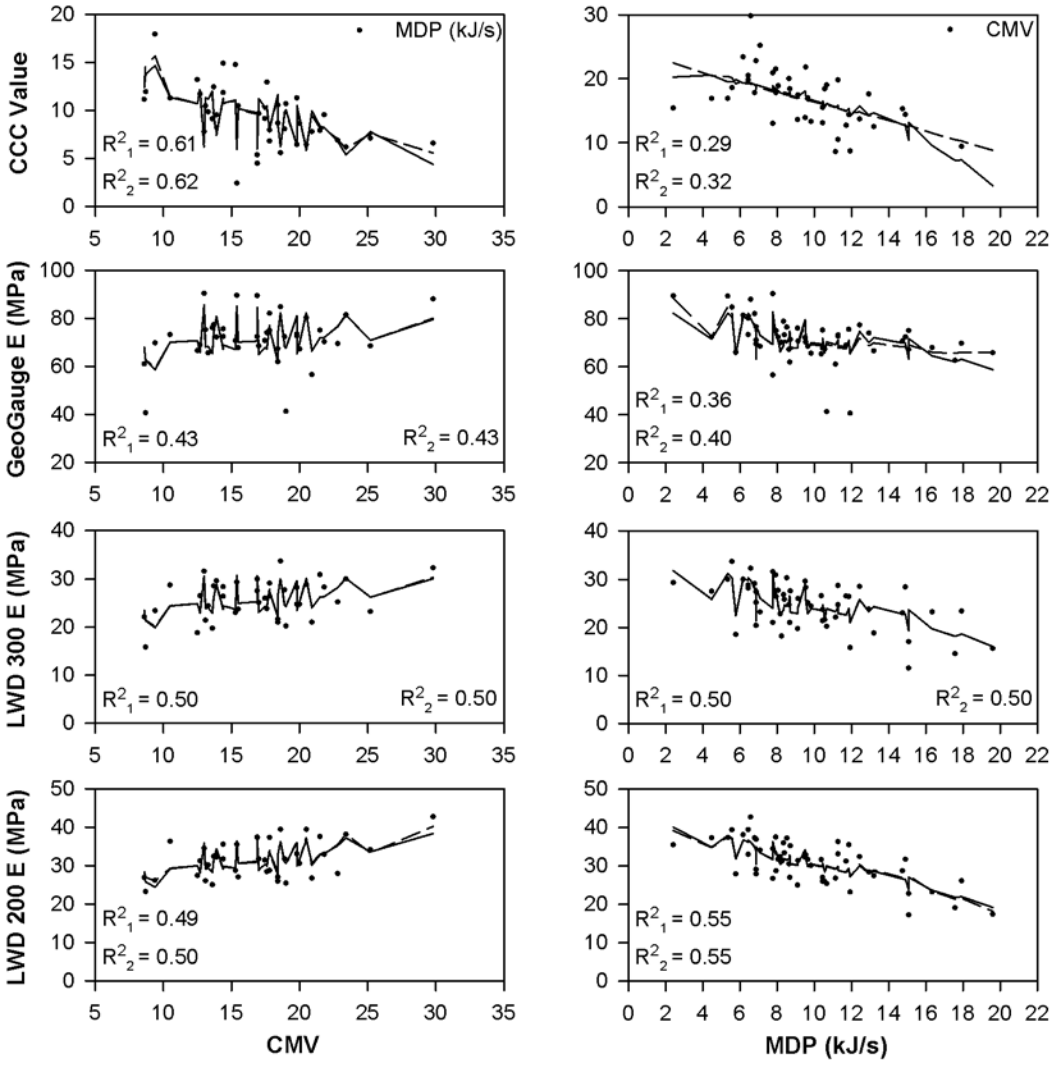

Figure 6.16 Multivariate regression analyses of CCC, GeoGauge, and LWD measured values, vs. NN predicted MDP and CMV measurements for all lifts and passes, excluding base layer.

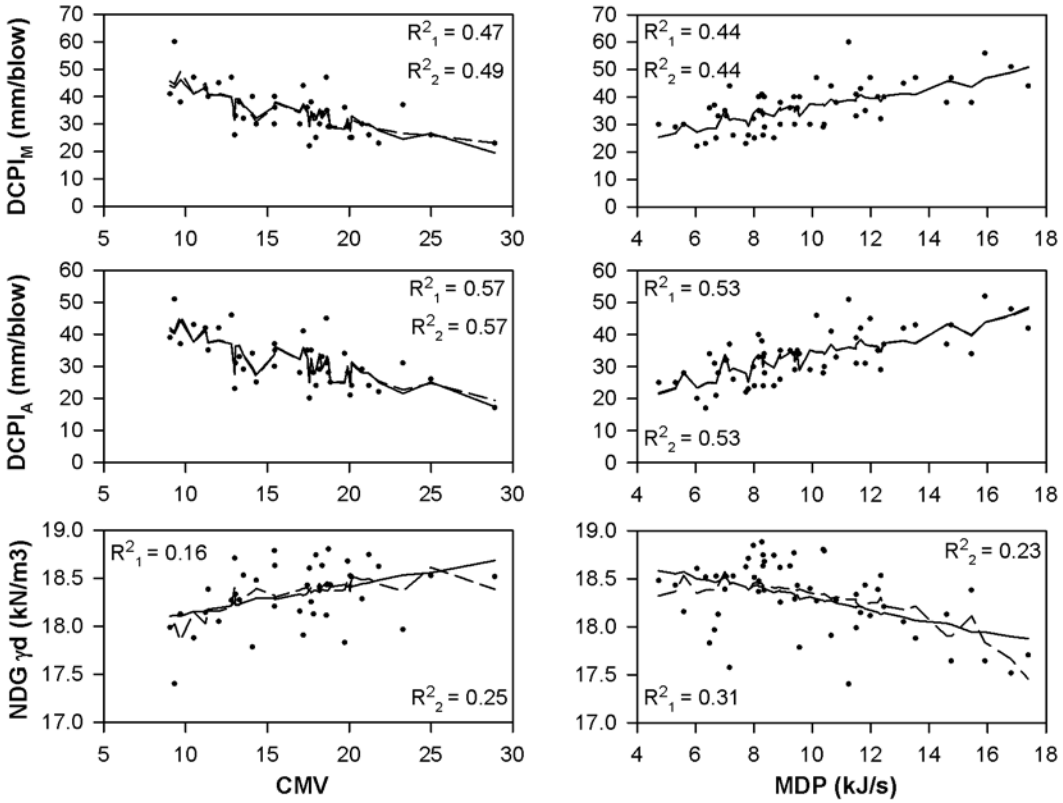

Figure 6.17 Multivariate regression analyses of DCP and NDG measured values, vs. IDW *p* = 4 predicted MDP and CMV measurements for all lifts and passes, excluding base layer.

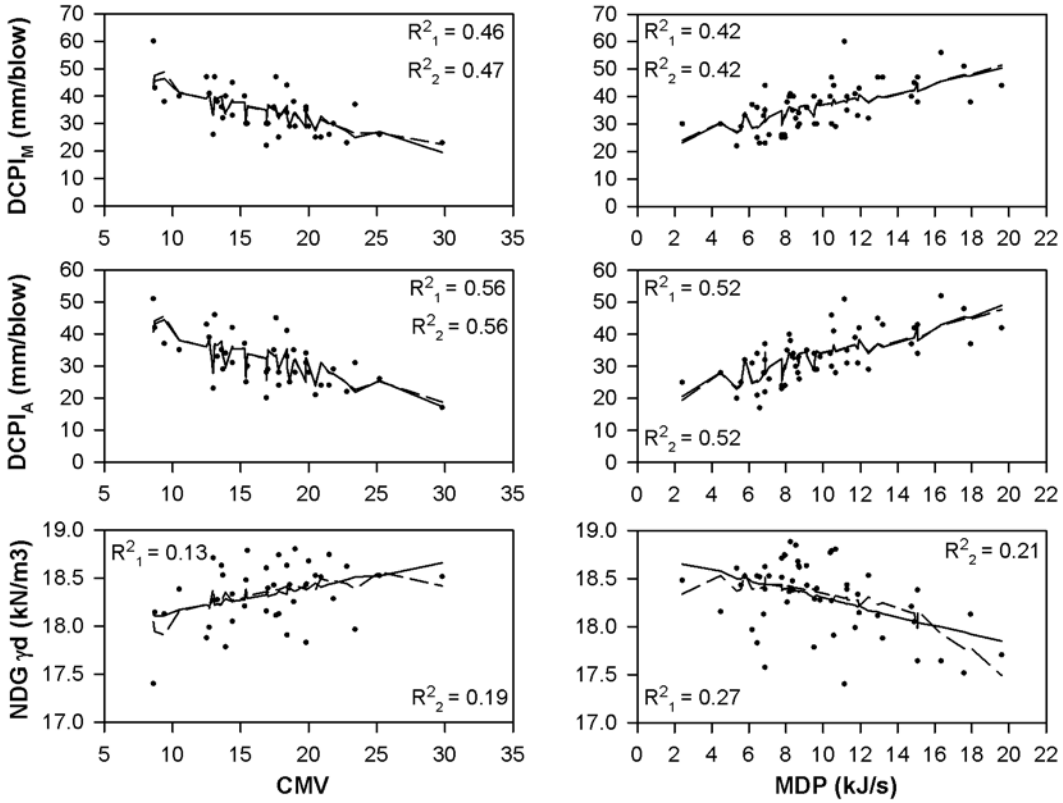

Figure 6.18 Multivariate regression analyses of DCP and NDG measured values, vs. NN predicted MDP and CMV measurements for all lifts and passes, excluding base layer.

The results shown in Figs. 6.15 through 6.18 are generally in agreement with the results of the multivariate analysis with kriging predictions presented in Section 5.4.2, where it was first shown that the introduction of moisture content as an additional independent variable greatly improves the strength of the correlations. To allow for easy comparison of the results of the three different average data sets (Kriging, IDW, NN) used in the regression analysis, all of the coefficient of determination values are summarized in Table 6.5. As previously mentioned, the regression models that have a *p*-value greater than 0.05 will be denoted with an

asterisk (*). The coefficient of determination values for the linear models are presented in the R^2_1 columns (shaded in grey), and the coefficient of determination values for the second-degree polynomial models are presented in the R^2_2 columns.

Table 6.5 R-Squared Values from the Multivariate Regression Analyses that were Performed on Individual Data Points (In Situ Data as Dependent Variable)

Dependent Variable	Kriging		IDW P=4		NN	
	R^2_1	R^2_2	R^2_1	R^2_2	R^2_1	R^2_2
MDP (kJ/s) vs. CMV	0.50	0.53	0.69	0.70	0.61	0.62
Geogauge *E* (MPa) vs. CMV	0.22	0.27†	0.43	0.44	0.43	0.43
LWD 300 *E* (MPa) vs. CMV	0.21†	0.22†	0.50	0.51	0.50	0.50
LWD 200 *E* (MPa) vs. CMV	0.24	0.24†	0.48	0.50	0.49	0.50
$DCPI_M$ (mm/blow) vs. CMV	0.45	0.47	0.47	0.49	0.46	0.47
$DCPI_A$ (mm/blow) vs. CMV	0.44	0.46	0.57	0.57	0.56	0.56
NDG γ_d (kN/m^3) vs. CMV	0.31	0.39	0.16†	0.25†	0.13*	0.19*
CMV vs. MDP (kJ/s)	0.75	0.75	0.40	0.43	0.29	0.32
Geogauge *E* (MPa) vs. MDP (kJ/s)	0.48	0.49	0.36	0.40	0.36	0.40
LWD 300 *E* (MPa) vs. MDP (kJ/s)	0.50	0.51	0.52	0.52	0.50	0.50
LWD 200 *E* (MPa) vs. MDP (kJ/s)	0.60	0.62	0.59	0.59	0.55	0.55
$DCPI_M$ (mm/blow) vs. MDP (kJ/s)	0.59	0.62	0.44	0.44	0.42	0.42
$DCPI_A$ (mm/blow) vs. MDP (kJ/s)	0.58	0.61	0.53	0.53	0.52	0.52
NDG γ_d (kN/m^3) vs. MDP (kJ/s)	0.58	0.64	0.23	0.31	0.21	0.27

*: Models that have a p-value greater than 0.05
†: Models that have a p-value between 0.01 and 0.05

Observation of summary Table 6.5 shows that the differences in the coefficient of determination values for the three different interpolation technique results do not follow any pattern. For several of the analyses the kriging results have higher coefficient of determination values, and for others the NN interpolation method has higher values. Still, in general, the differences in the coefficient of determination

values appear to be fairly insignificant (i.e., a matter of a few hundredths). However, there are a few exceptions were kriging analysis offer much stronger correlations (e.g., for the NDG vs. MDP and Geogauge vs. MDP data sets), and others where NN and IDW offer much stronger correlations (e.g. the Geogauge vs. CMV, LWD 300 vs. CMV, and LWD 200 vs. CMV data sets). In general, results from this analysis seem to support the conclusion that both IDW $p = 4$ and NN interpolation could be used as an alternative for the kriging method.

6.3.4 Multivariate Regression Analysis of Average CCC IDW & NN Predictions versus Average In Situ Testing Data

The same multivariate regression analysis performed above will be followed in this section, with the only exception being that the data sets here now consist of the average measurements for each lift and pass of compaction data. As mentioned in Section 6.3.2, this is done in attempt to "smooth" the data and remove the influence of any point-to-point discrepancies in the individual data. Consequently the number of data points is significantly reduced, therefore, the regression models must be inspected carefully to ensure that the coefficient of determination values accurately reflect the models and are not influenced by the small sampling size (sample sizes that are very small may result in high coefficient of determination values that are not reasonably representative of the data series).

Figures 6.19 through 6.22 show the multivariate regression models for the NN prediction and IDW $p = 4$ average data sets. Examination of Figures 6.19 through 6.22 reveals that, in general, there is a strong linear and second-degree polynomial correlation between the CCC measured values and the in situ measured values for all of the in situ test methods. Additionally, the CMV models show consistently higher R^2

values than the MDP models, with the exception of the DCP and NDG models. Contrary to the univariate results and multivariate analyses of individual data, the regression models for the GeoGauge show a much stronger relationship with CMV measurements when compared to the relationship with the MDP measurements. Additionally, all of the data show that there is an equal or stronger second-degree polynomial correlation with the CCC data than the linear model, although the differences vary.

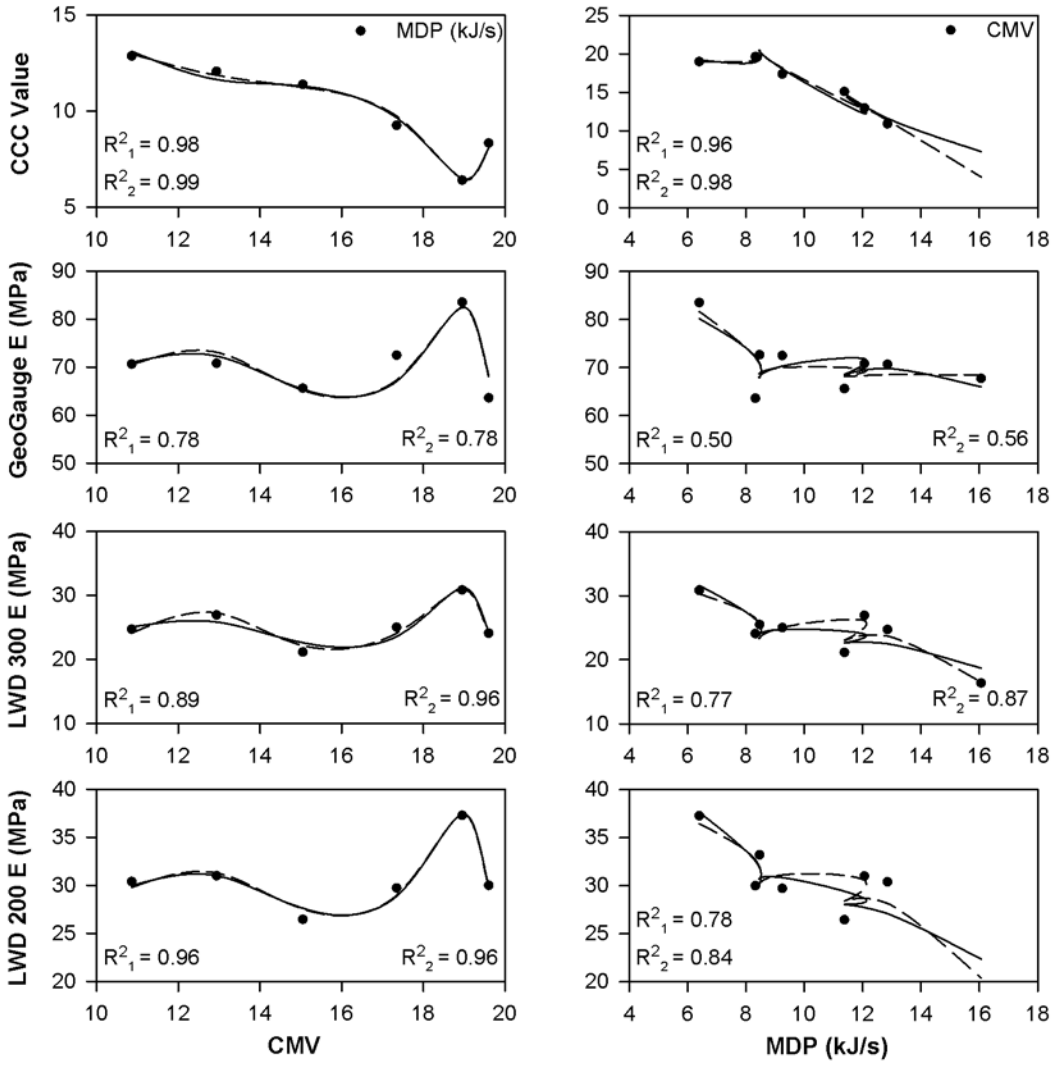

Figure 6.19 Multivariate regression analyses of average CCC, GeoGauge, and LWD measured values, vs. IDW P =4 predicted MDP and CMV measurements for all lifts and passes, excluding base layer.

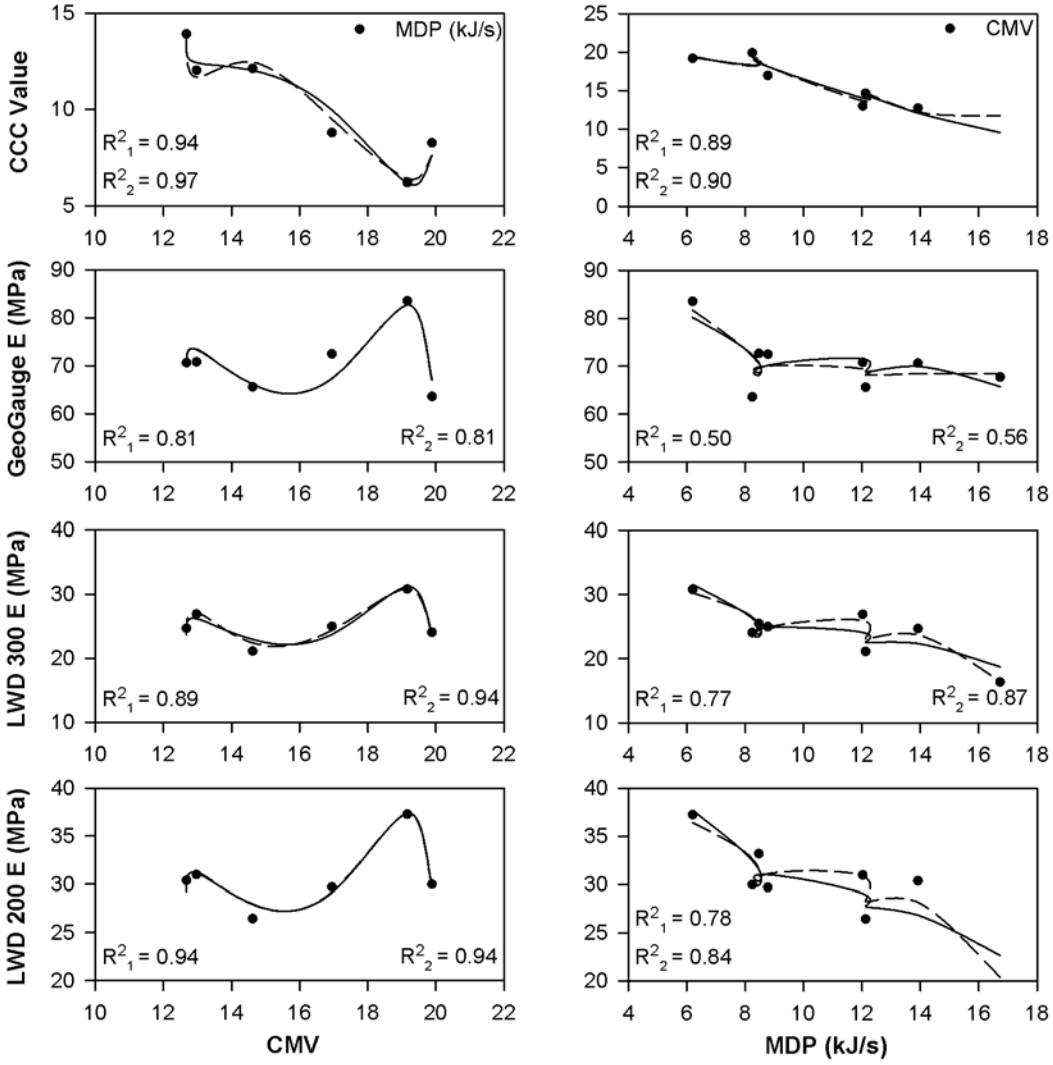

Figure 6.20 Multivariate regression analyses of average CCC, GeoGauge, and LWD measured values, vs. NN predicted MDP and CMV measurements for all lifts and passes, excluding base layer.

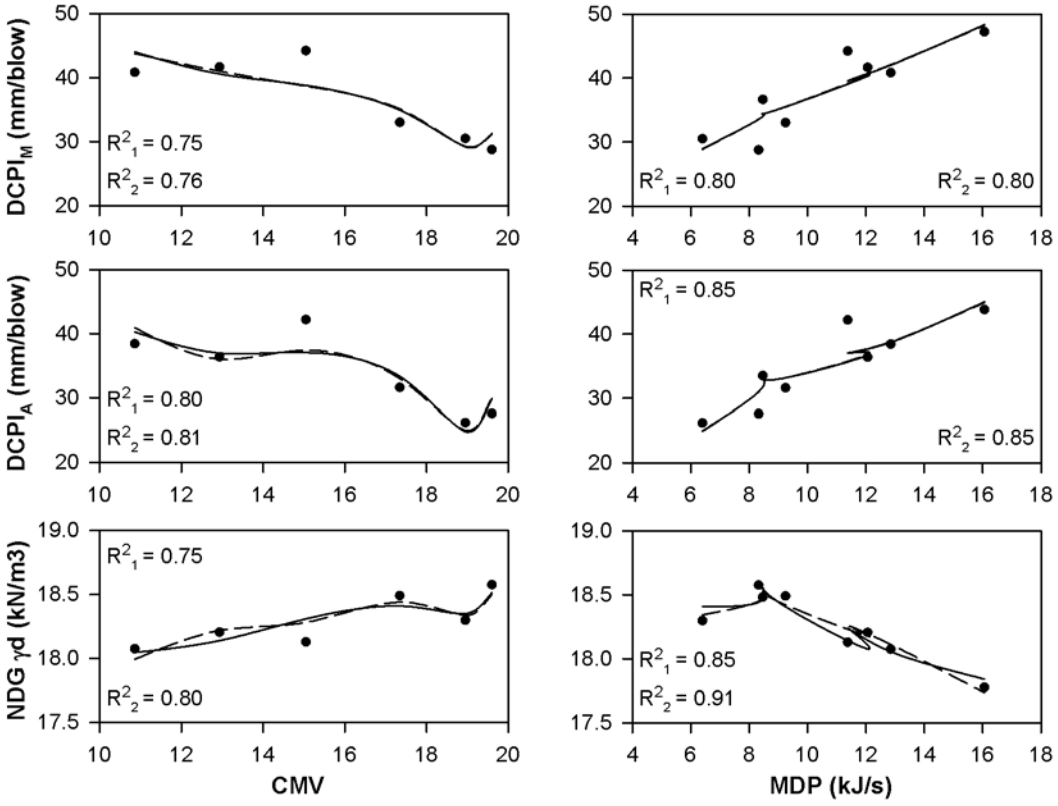

Figure 6.21 Multivariate regression analyses of average DCP and NDG measured values, vs. IDW *p* = 4 predicted MDP and CMV measurements for all lifts and passes, excluding base layer.

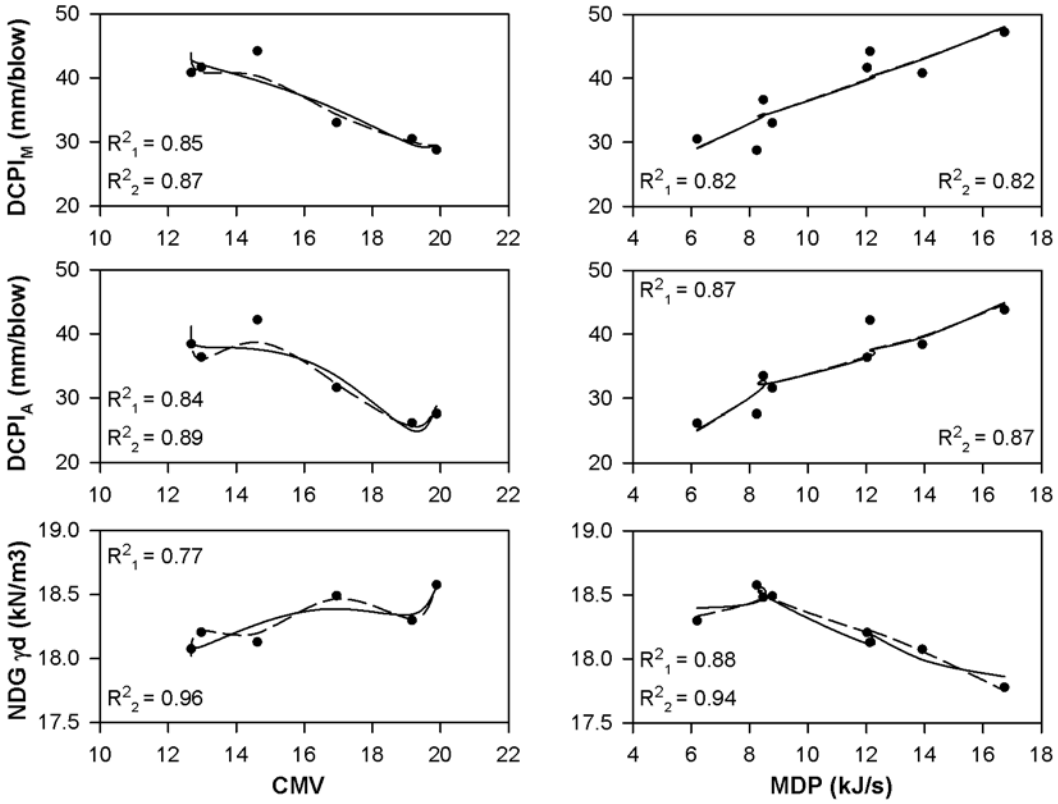

Figure 6.22 Multivariate regression analyses of average DCP and NDG measured values, vs. NN predicted MDP and CMV measurements for all lifts and passes, excluding base layer.

To allow for easy comparison of the results of the three different average data sets (Kriging, IDW, NN) used in the multivariate regression analyses, all of the coefficient of determination values are summarized in Table 6.6. As previously mentioned, the regression models that have a p-value greater than 0.05 will be denoted with an asterisk (*). The coefficient of determination values for the linear models are presented in the R^2_1 columns (shaded in grey), and the coefficient of determination values for the second-degree polynomial models are presented in the R^2_2 columns.

Table 6.6 R-Squared Values from the Multivariate Regression Analyses that were Performed on Average Data (In Situ Data as Dependent Variable)

Dependent Variable	Kriging		IDW P=4		NN	
	R^2_1	R^2_2	R^2_1	R^2_2	R^2_1	R^2_2
MDP (kJ/s) vs. CMV	0.98	1.00	0.98	0.99†	0.94†	0.97†
Geogauge *E* (MPa) vs. CMV	0.62*	0.64*	0.78*	0.78*	0.81*	0.81*
LWD 300 *E* (MPa) vs. CMV	0.70*	0.83*	0.89†	0.96*	0.89†	0.94*
LWD 200 *E* (MPa) vs. CMV	0.80*	0.89*	0.96*	0.96*	0.94†	0.94*
$DCPI_M$ (mm/blow) vs. CMV	0.76*	0.77*	0.75*	0.76*	0.85*	0.87*
$DCPI_A$ (mm/blow) vs. CMV	0.68*	0.72*	0.80*	0.81*	0.84*	0.89*
NDG γ_d (kN/m^3) vs. CMV	0.87†	0.87*	0.75*	0.80*	0.77*	0.96*
CMV vs. MDP (kJ/s)	0.99	1.00	0.96	0.98†	0.89†	0.90*
Geogauge *E* (MPa) vs. MDP (kJ/s)	0.70†	0.77*	0.50*	0.56*	0.50*	0.56*
LWD 300 *E* (MPa) vs. MDP (kJ/s)	0.70*	0.78*	0.77†	0.87†	0.77†	0.87†
LWD 200 *E* (MPa) vs. MDP (kJ/s)	0.74†	0.78*	0.78†	0.84†	0.77†	0.84†
$DCPI_M$ (mm/blow) vs. MDP (kJ/s)	0.84	0.86†	0.80†	0.80*	0.82†	0.82*
$DCPI_A$ (mm/blow) vs. MDP (kJ/s)	0.82†	0.84†	0.85	0.85†	0.87	0.87†
NDG γ_d (kN/m^3) vs. MDP (kJ/s)	0.92	0.92†	0.85	0.91†	0.88	0.94

*: Models that have a p-value greater than 0.05
†: Models that have a p-value between 0.01 and 0.05

Observation of summary Table 6.6 shows that the differences in the coefficient of determination values for the three different interpolation technique results do not follow any pattern. For several of the analyses the kriging results have higher coefficient of determination values and for other the NN interpolation method has higher values. Still, in general, the differences in coefficient of determination values appear to be fairly insignificant (i.e., a matter of a few hundredths). However, there are a few exceptions where the kriging analysis offers much stronger correlations (e.g., Geogauge vs. MDP), and others were NN and IDW offer much stronger correlations (e.g., Geogauge vs. CMV, LWD 300 vs. CMV, LWD 200 vs. CMV, and $DCPI_A$ vs.

CMV). In general, this results from this analysis seem to support the conclusion that both IDW $p = 4$ and NN interpolation could be used as an alternative for the kriging method.

6.4 Summary and Conclusions

In Chapter 5, it was shown that, in order to build relationships between CCC measurements and in situ test method measurements, it was necessary to predict the CCC measurements at the locations of the measured in situ testing data. As noted in Chapter 5, isotropic ordinary kriging interpolation was the most appropriate (and best) method for interpolating the CCC data. However, while it is the most appropriate approach to use from a mathematical standpoint, kriging is not recommended by the author for performing interpolation in a QA/QC specification framework, due to the complexity and sensitivity of user judgment on the resulting prediction values.

In this chapter two alternative methods were examined for prediction of CCC values at the spatial locations of the recorded in situ test measurements. The intent of this chapter is to find an alternative interpolation method that does not result in significant changes to the accuracy of the correlations (i.e., coefficient of determination values) that exist between the kriging predicted CCC values and the in situ test methods. This alternative interpolation method could then be recommended for use in specifications for the use of CCC technology for compaction verification.

Similar to Chapter 5, for the univariate regression analysis, two regression models were used: a linear model and a second-degree polynomial model. The univariate regression analyses were performed first on the data set of individual CCC values (predicted using IDW and NN) and the various in situ test method results. Then, just as in Chapter 5, univariate regression analyses were performed on the

average values for each lift and pass. Additionally, the resulting coefficient of determinations from the models using IDW and NN predictions were compared to the coefficient of determination values from the kriging models. The results of the univariate regression analyses resulted in the many of the same general conclusions presented in Section 5.5, which are restated below:

- Comparison of the individual values of CCC measurements and in situ test measurements at point-to-point locations showed weak correlations.
- Comparison of the average values of CCC measurements and in situ test measurements at point-to-point locations yielded relatively strong correlations. However, a number of the average data sets did not have a sufficient number of data points; therefore, several of the models and corresponding coefficient of determination values were unreliable and needed to be ignored.
- For a number of cases, the second-degree polynomial model showed significantly stronger correlations than the linear model (e.g. DCP_I values, NDG dry unit weight values, and moisture contents).
- Generally, MDP measurements showed better correlations with the in situ test methods, in comparison to the CMV measurements. This is likely related to the different influence depths of the CCC measurements. The influence depth of MDP is much closer to that of the in situ test methods, which range from approximately 20 cm to 60 cm. In contrast, the influence depth of CMV measurements is roughly 80 cm to 150 cm, as noted by White and Thompson (2008).

- In general, the DCP indices show much stronger correlations with the CCC measurements, in comparison to the other in situ testing methods used in the study.
- In general, the GeoGauge moduli values showed the weakest correlations with the CCC measurements, in comparison to the other in situ testing methods used in the study.
- In general, both sets of moisture content values showed much stronger correlations with the CCC measurements, in comparison to the density and modulus based in situ testing methods used in the study.

As concluded in Chapter 5, the moisture condition of the soil is a significant factor when measuring the modulus and dry unit weight of compacted soils. Following this conclusion, multivariate regression analyses were also performed using CCC values from IDW and NN predictions, for comparison with the kriging model regression analyses from Chapter 5.

Similar to the univariate regression analysis, for the univariate regression analysis two regression models were used: a linear model without an interaction term and a linear model with an interaction term. The same procedure used for the univariate analyses was followed for the multivariate analyses. The multivariate regression analyses were performed first on the data set of individual CCC measurements and the various in situ test method results. Then, multivariate regression analyses were performed on average values for each lift and pass. The results of the multivariate regression analyses resulted in many of the same general conclusions presented in Section 5.5, which are restated below:

- Comparison of the individual values of CCC measurements and in situ test measurements at point-to-point locations showed improved correlations compared to those seen in the univariate analyses, however, correlations were still relatively weak.
- Comparison of the average values of CCC measurements and in situ test measurements at point-to-point locations yielded very strong correlations. However, a majority of the average data sets did not have a sufficient number of data points; therefore, most of the models and corresponding coefficient of determination values were unreliable and needed to be ignored. To improve this, future studies should consider recording CCC and in situ test measurements for a significant number of passes and lifts of compacted soil, in order to create robust data set that does not have limitations due to a small amount of data.
- In general, the regression model with the interaction term resulted in slightly stronger coefficient of determination values. This observation is expected considering the additional term results in an additional regression model coefficient, which allows for a better model fit.

The general conclusions mentioned thus far reconfirm the general conclusions from Chapter 5; however, the true purpose of this chapter was to evaluate the effect of using IDW and NN interpolation methods for prediction of CCC values, by examining the effect that these interpolation methods had on the relationships between the CCC measurements and in situ test method measurements. Side by side comparisons of the coefficient of determination values from the regression analyses were provided in

summary tables throughout this chapter. Observation of the results led to the following conclusions:

- In general, for univariate regression analysis of the individual values of CCC measurements and in situ test measurements at point-to-point locations, the coefficient of determination values for IDW $p = 4$ are slightly lower than for kriging. Similarly, the NN coefficient of determination values are slightly lower than that of the IDW $p = 4$. However, the overall differences in coefficient of determination values between kriging, IDW, and NN appear to be fairly insignificant (i.e., a matter of a few hundredths).
- For univariate regression analysis of the average values of CCC measurements and in situ test measurements, the differences in coefficient of determination values for the three different interpolation technique results do not follow any pattern. For some analyses the kriging results have higher coefficient of determination value and for others the NN interpolation method has higher values. However, again, the differences in the coefficient of determination values appear to be fairly insignificant (a matter of hundredths).
- For multivariate regression analysis of the individual values of CCC measurements and in situ test measurements at point-to-point locations, none of the interpolation methods provides consistently stronger correlations. In general, the differences in coefficient of determination values appear to be insignificant (a matter of hundredths). However, there are a few exceptions where kriging analysis offer much stronger

correlations (e.g., NDG vs. MDP and Geogauge vs. MDP), and others where NN and IDW offer much stronger correlations (e.g., Geogauge vs. CMV, LWD 300 vs. CMV, and LWD 200 vs. CMV).

- For multivariate regression analysis of the average values of CCC measurements and in situ test measurements, none of the interpolation methods provides consistently stronger correlations. In general, the differences in the coefficient of determination values appear to be insignificant (a matter of hundredths). However, there are a few exceptions where kriging analysis offer much stronger correlations (e.g., Geogauge vs. MDP), and others were NN and IDW offer much stronger correlations (e.g., Geogauge vs. CMV, LWD 300 vs. CMV, LWD 200 vs. CMV, and DCPIA vs. CMV).

As mentioned previously, it is the belief of the author that the use of the ordinary kriging method for interpolation with CCC QA/QC applications is not practical, due to its complexity, for practicing Geotechnical Engineers and Field Technicians. Therefore, a simple, repeatable interpolation technique that does not significantly affect the relationships between predicted CCC measurements and the corresponding in situ testing method measurements is needed to use these relationships in a specification framework.

Assessment of the conclusions from this chapter is encouraging for the possibility of using IDW or NN interpolation in place of the more rigorous isotropic ordinary kriging method for use in a QA/QC specification framework. Based on the results, in the case of univariate regression analysis between CCC measurements and in situ method measurements, IDW $p = 4$ and NN interpolation can be used in

confidence as a replacement for isotropic ordinary kriging predictions of CCC values. However, if multivariate regression analyses methods are specified, then careful examination of the correlations between the three interpolation methods should be examined, due to inconsistent correlations for several of the in situ testing methods with the three predicted CCC data sets.

For both univariate and multivariate regression analyses, caution should be taken when speculating the use of the NN interpolation method for prediction of the CCC values at the precise locations of the in situ test method measurements. The NN method fails to smooth the data and is highly susceptible to outliers, in the event the closest measurement to the prediction location is an anomaly, the NN will not be able to adjust and consider other more representative measurements. It is for this reason that the author does not recommend the use of NN interpolation for this application. However, the author does see potential for use of the IDW interpolation method for use in a specification framework. Nonetheless, it is necessary to evaluate the IDW interpolation method on additional data sets from similar projects before making a blanket conclusion for prediction of CCC measurements.

Chapter 7 will provide a discussion on techniques for implementation of several different proposed CCC compaction verification methodologies using the data collected from this study.

Chapter 7

AN EVALUATION OF SPECIFICATION METHODOLOGIES FOR USE WITH CONTINUOUS COMPACTION CONTROL EQUIPMENT

7.1 Introduction

Continuous compaction control (CCC) and intelligent compaction (IC) technology offers an improvement over conventional in-situ spot-testing methods for earthwork compaction verification in that real-time compaction results are determined with 100% test coverage (e.g., Vennapusa et al. 2010). As noted in previous chapters, CCC systems are data acquisition systems installed on compaction equipment that read real-time feedback about the operation and performance of soil compaction (Thurner and Sandström 1980; Adam 1997; Adam and Brandl 2003). The compaction monitoring system consists of an instrumented roller with sensors to monitor machine power output in response to changes in soil-machine interaction, in the form of roller measured values (MV). It is also fitted with a global positioning system (GPS) to monitor roller location in real time (Vennapusa et. al. 2010; White et. al. 2011). Therefore, it produces spatially referenced compaction verification in real time.

In Chapter 2, the current approach to end-product assessment of compacted soils is presented and discussed, along with a discussion of the in situ test methods that are most commonly employed for QA/QC of compacted soils (e.g., compacted soil acceptance requires 95% relative compaction as measured by a nuclear density gauge). Additionally, the limitations and problems associated with these in situ test methods are discussed. One of the largest problems with the current in situ test methods is the

fact that they are spot-tests. These spot-tests offer compaction verification at discrete locations, which represent a small percentage of the actual compaction area. In comparison, the introduction of CCC and IC technology and the ability to record roller MV continuously and instantaneously allows for compaction verification of a much larger percentage of the compaction area.

For this reason and others, CCC technology has been adopted in Europe (e.g., Austria 1999; Germany 2009; Sweden 2005; Switzerland 2006; ISSMGE 2009) as a quality assurance (QA) method for compaction verification. More recently, several United States Departments of Transportation (DOT) and the Federal Highway Administration (FHWA) have developed similar CCC and IC specifications for compaction verification (Minnesota DOT 2007; Texas DOT 2008; FHWA 2011; Indiana DOT 2013). The acceptance criterion used in these specifications can be classified into four specification methodologies, as proposed by Mooney et al. 2010.

In this chapter, these four acceptance methods (QA Options 1, 2a, 2b, and 3 from Chapter 2) will be implemented for the data that was collected from the construction of the embankment described in the field study from Chapter 3. Only a brief description of the compaction process will be discussed within this chapter. An in-depth account of the field study performed can be found in Tehrani (2009) and Chapter 3. This chapter will attempt to retrospectively use the roller MV and NDG density and moisture content measurements recorded by the modified roller during compaction to evaluate the four QA CCC specification methodologies for compaction of Lift 5. It should be noted that since the four CCC QA Options were not considered at the time of the field study, the current set of data is not adequate to accurately and completely implement each of the proposed methods. Instead, the purpose of this

chapter is to provide the general framework for analyzing real CCC data in a specifications format for compaction verification.

7.2 Implementation of CCC Specification Methods

The project was performed at the Burrice Borrow Pit in Odessa, Delaware in the United States. A 61 m long by 6 m wide (200 ft by 20 ft) embankment was constructed using conventional earth moving equipment and compacted in five soil lifts. The soil that was used to construct the embankment was generally uniform (Meehan and Tehrani 2011), falling at the classification boundary between two soil types: a poorly graded sand with silt (SP-SM) and a silty sand (SM).

Using a modified Caterpillar CS56 compactor, each lift was compacted in a series of passes using three side-by-side lanes. For each lift, between six and nine compactor passes were performed to achieve the desired level of compaction. To verify the level of compaction, conventional in situ QA/QC spot tests (e.g., NDG, LWD) were performed, while CCC measurements were taken during select lifts and passes. For the final lift of the embankment (Lift 5), CCC roller MV and in situ test measurements were taken for all seven lifts. The data from Lift 5 will allow for the implementation of the four CCC specification QA/QC Options on a real set of data.

As discussed in Section 2.7.2.3 in Chapter 2, measurement passes require that roller operational parameters including roller speed and vibration amplitude be consistent. Shown in Table 7.1 are the roller operational parameters for all passes of Lift 5 and the corresponding measurement pass notation. Roller pass 1 is not considered a measurement pass due to the high vibration amplitude used during compaction, which is inconsistent with the other passes and, therefore, the roller MV

cannot be compared. Complete roller MV for roller Pass 6 was not recorded and, thus, roller pass 6 is not considered a measurement pass either.

Table 7.1 Roller Parameters During Compaction

Roller Pass	Compaction Amplitude (mm)	Mean Roller Speed (km/h)	Measurement Pass (*i*)
1	1.87	3.13	-
2	0.85	3.06	1
3	0.85	3.07	2
4	0.85	3.13	3
5	0.85	3.17	4
6	0.85	3.02	-
7	0.85	3.00	5

For purposes of the current study, the contract specified QA-TV will be assumed to be 95% of the maximum dry density, with a $\pm$2% optimum moisture content range, which is similar to the specifications that are used in Delaware (DelDOT 2001). The maximum dry density is 18.83 kN/m^3 and the optimum moisture content is 11.70%, therefore, QA-TV = 17.89 kN/m^3 and the allowable range of moisture content during compaction is 9.70% to 13.70%. Since a proper calibration area (Section 2.7.2.5) was not constructed, all correlations that are developed here are determined from the data that was collected during compaction of Lift 5. Consequently, the coefficient of determination requirement (e.g., $R^2 \geq 0.5$) will be ignored. The purpose of this section is to simply show the process by which data should be analyzed when utilizing CCC measurements to verify compaction.

7.2.1 Acceptance Testing Using Option 1

A detailed explanation of Option 1 can be found in Section 2.7.4. However, in essence, Option 1 relies on spot checking of NDG measurements at areas of lower compaction identified by the roller MV during the measurement pass. It is required that a correlation be shown between the roller MV and NDG measurements to ensure that the "weak areas" identified by the roller MV indicate areas of low compaction. Univariate regression equations are shown in Figure 7.1 for MDP and CMV. The data used for the CMV regression analysis includes data collected only during measurement passes of Lift 5. Simple linear regression was performed for the roller MV and NDG dry unit weights (γ_d) to determine if there is a positive or negative relationships. The correlation equations developed are in the form of Equations 2.6 presented in Chapter 2. The results indicate that high MDP values correlate to "weak areas" and low CMV values correlate to "weak" areas.

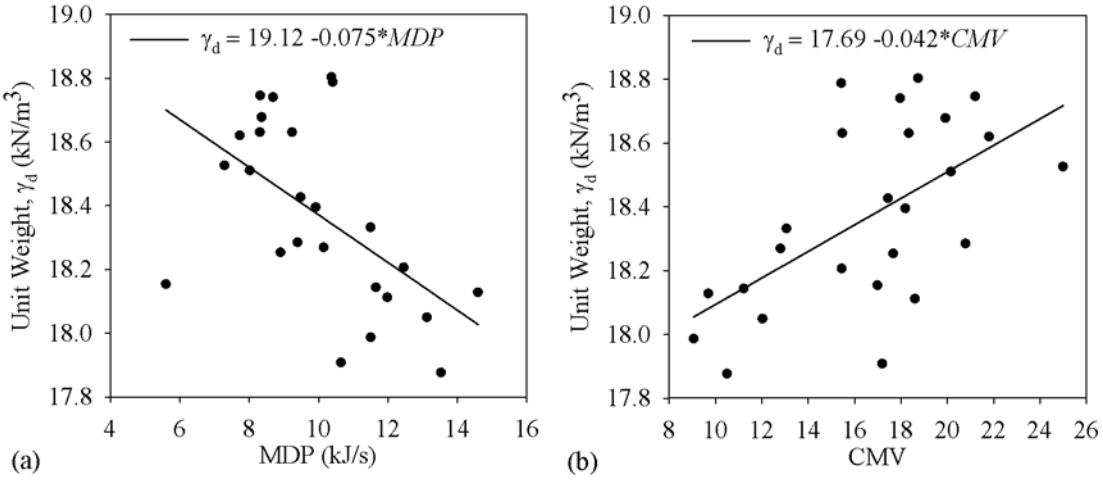

Figure 7.1 Univariate linear regression (a) MDP vs. γ_d; (b) CMV vs. γ_d.

Since Option 1 was not actually used during construction of the embankment, the ideal amount of NDG data is not available within the roller MV identified “weak areas”. The contour plots of MDP and CMV values for measurement passes 1 through 5 (Figures 7.2 and 7.3) identify the “weak areas”, designated by red boxes, that would hypothetically have been spot tested with the NDG. As can be seen from the contour plots NDG testing done in the “weak areas” is limited and, therefore, adequate compaction cannot be verified in many of the desired locations. More importantly, for purposes of this study, it can be seen that contour plots for MDP and CMV show, in general, good agreement in identifying the “weak areas” that should be spot-tested.

Assessment of the NDG data that was collected reveals that only six of the NDG measurement locations fall within these “weak areas”. Three locations for measurement pass 1; they are locations 1.2, 1.3, and 1.4 (Figures 7.2 and 7.3). Additionally, three locations for measurement pass 5; they are locations 5.4, 5.5, and 5.10 (Figures 7.2 and 7.3). Proper compaction verification would require more NDG measurements in the “weak areas” but for this exercise, Option 1 will be continued using these six test measurements. In order to easily verify compaction in the “weak areas” a summary of the dry unit weights, moisture contents, and relative compaction percentage values corresponding to all the NDG test measurement locations are presented in Table 7.2.

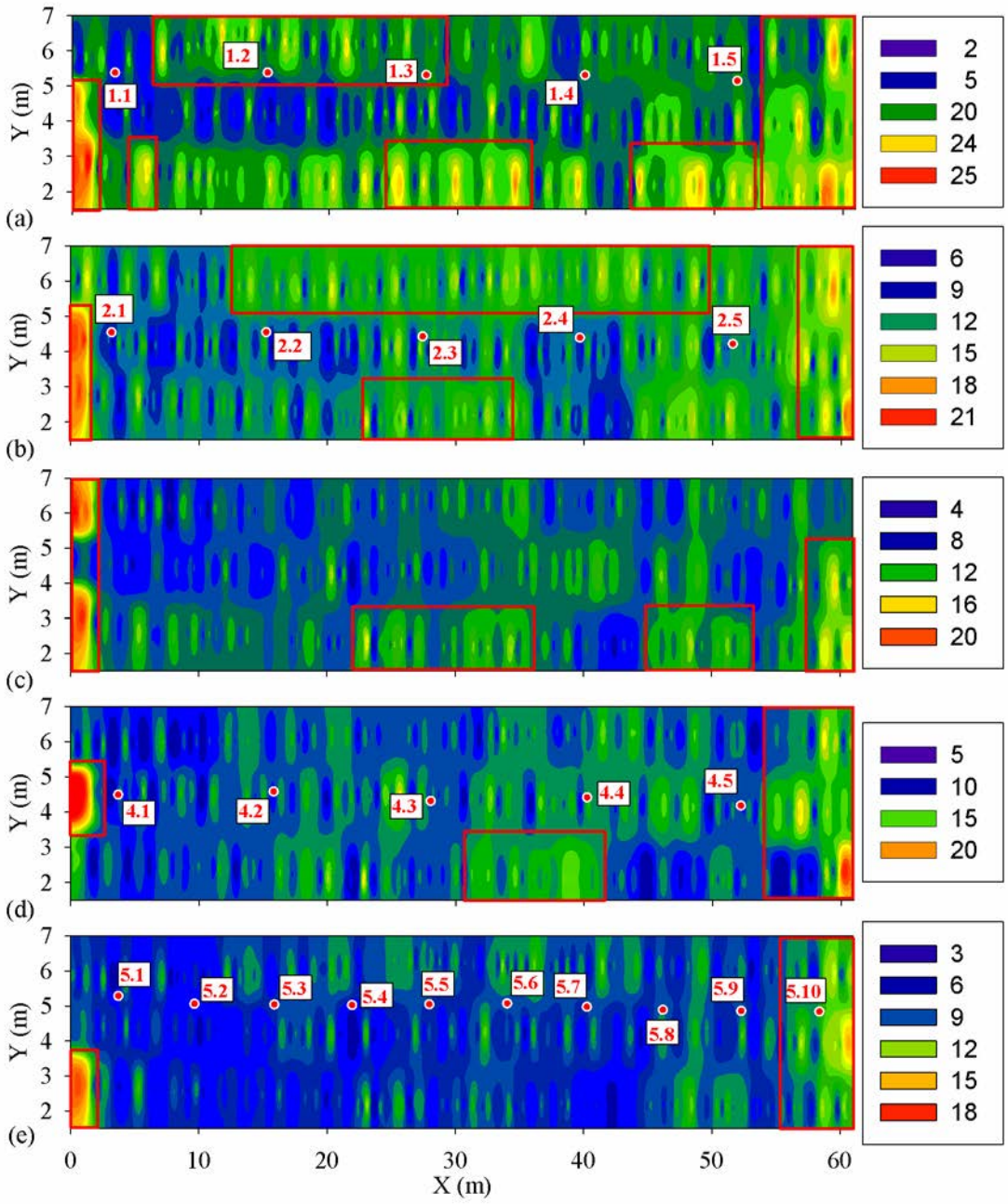

Figure 7.2 MDP contour plots: (a) Measurement Pass 1; (b) Measurement Pass 2; (c) Measurement Pass 3; (d) Measurement Pass 4; and (e) Measurement Pass 5.

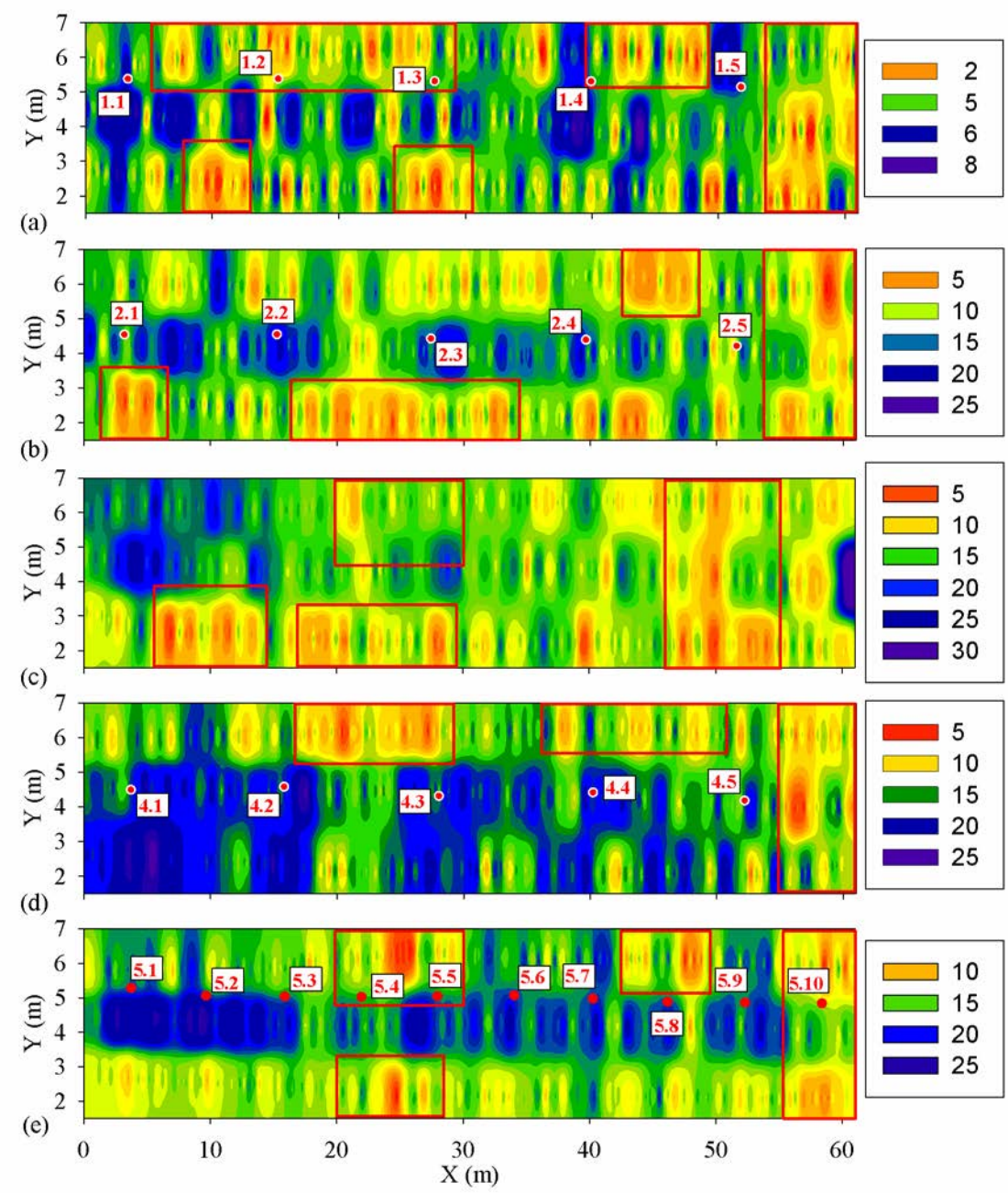

Figure 7.3 CMV contour plots: (a) Measurement Pass 1; (b) Measurement Pass 2; (c) Measurement Pass 3; (d) Measurement Pass 4; and (e) Measurement Pass 5.

Table 7.2 "Weak Area" NDG Results

Test Location	Dry Unit Weight, γ_d (kN/m3)	Moisture Content, ω (%)	Relative Compaction, RC (%)
1.1	18.33	10.28	97.4
1.2	**17.99**	**10.92**	**95.5**
1.3	**17.88**	**10.02**	***94.9***
1.4	**18.05**	**10.62**	**95.9**
1.5	18.13	12.31	96.3
2.1	18.27	10.49	97.0
2.2	18.11	10.49	96.2
2.3	18.21	10.61	96.7
2.4	17.91	11.40	95.1
2.5	18.14	11.60	96.4
4.1	18.74	*8.97*	99.5
4.2	18.25	10.24	96.9
4.3	18.43	10.40	97.9
4.4	18.39	10.93	97.7
4.5	18.63	10.96	98.9
5.1	18.62	*8.66*	98.9
5.2	18.53	*9.64*	98.4
5.3	18.51	10.55	98.3
5.4	**18.15**	**9.92**	**96.4**
5.5	**18.63**	***9.30***	**98.9**
5.6	18.68	9.98	99.2
5.7	18.75	*9.56*	99.6
5.8	18.28	*9.51*	97.1
5.9	18.80	10.39	99.9
5.10	**18.79**	**10.03**	**99.8**

In Table 7.2, the measurements that are located in the roller MV identified "weak areas" are denoted in bold-faced text. Additionally, points that fail either the moisture content criterion or the relative compaction criterion are denoted in italic text. NDG measurement at location 1.3 shows a failing point based on the relative compaction criterion, therefore, it can be concluded that additional compaction is

needed. The state of densification for measurement passes 2, 3, and 4 cannot be properly assessed because there is no NDG data in the “weak areas”. For measurement pass 5 all the NDG measurements taken signify that compaction has been completed. However, a few of the locations for measurement pass 5 do not meet the moisture content criteria. Each of these points is slightly below the 9.7 % minimum moisture content required, however, since the values are only slightly lower, on a full-scale projects these points would likely be accepted. Based on the data collected it may be possible to conclude that compaction is complete proceeding measurement pass 5, however, the author cautions against confirming compaction on real projects without performing NDG spot-test in all of the roller MV determined “weak areas”.

7.2.2 Acceptance Testing Using Option 2a

A detailed explanation of Option 2a can be found in Section 2.7.5.1. However, in essence, Option 2a defines compaction complete if the percentage change in the mean of roller MV from successive passes is less than or equal to a specified percentage change target value ($\%\Delta\mu_{MV_i} \leq$ %Δ-TV). For this study the %Δ-TV was chosen to be 5%. This compaction verification method requires that the $\%\Delta\mu_{MV_i}$being calculated be based on data from successive passes with identical roller patterns, speeds, and vibration amplitudes. This is why certain roller passes have been ignored and measurement passes have been established in Table 7.1. To preface the implementation of this Option, it is assumed that the compaction equipment utilized is completely capable of achieving the required densification levels.

The $\%\Delta\mu_{MV_i}$ has been calculated according to Equation 2.5 for the MDP and CMV data from measurement passes 1 through 5. The results are shown side by side in Table 7.3, and offer easy comparison of the two different roller MV type

evaluations. Using Option 2a there is agreement between the MDP and CMV mean percentage change in RMV that the compaction criteria ($\%\Delta\mu_{MV_i} \leq 5$ %) is reached at measurement pass 5 (Table 7.3). This indicates that compaction is complete after measurement pass 5.

Table 7.3 Percentage Change in Mean of the CCC Data

Measurement Pass	MDP $\%\Delta\mu_{MV_i}$ (%)	CMV $\%\Delta\mu_{MV_i}$ (%)
1 to 2	17.0	34.4
2 to 3	11.5	20.7
3 to 4	9.7	9.1
4 to 5	3.1	2.9

It is important to note that the %Δ-TV was chosen arbitrarily by the author for purposes of this implementation study. However, if the criteria was changed to %Δ-TV = 10 %, revaluation of Table 7.3 would determine compaction complete after measurement pass 4. The selection of the %Δ-TV is extremely critical and will drastically alter the results of compaction verification process. Therefore, the %Δ-TV should be selected by the engineer on a site-to-site basis.

7.2.3 Acceptance Testing Using Option 2b

A detailed explanation of Option 2b can be found in Section 2.7.5.2. However, in essence, Option 2b relies on a specified minimum percentage of the roller MV increasing by less than the %Δ-TV. Since more variation is observed when comparing spatial data from pass to pass versus comparing mean values (e.g., Option 2a), it is expected that the %Δ-TV be higher here than it is for Option 2a. The criteria chosen for this paper is that at least 90% of the spatial percentage change in roller MV from

successive passes be less than or equal to 10 percent ($\%\Delta MV_i \leq 10$ %). Similar to Option 2a, it is again assumed that the compaction equipment is capable of providing adequate compaction. An additional requirement for Option 2b is that the roller MV recorded at each measurement pass be interpolated onto a consistent grid, thus, enabling the calculation of the percent change in roller MV on a point-to-point basis. Based on the conclusions and reasoning provided in Chapter 6, an inverse distance weighting (IDW) interpolation technique with an exponent value equal to four (p = 4) has been utilized.

Table 7.4 shows the percentage of the $\%\Delta MV_i \leq 10\%$ for successive measurement pass data for all measurement passes. As expected, the percentage of data meeting the criteria increases with the number of passes (Table 7.4). A simple way to visualize the process is to view a cumulative distribution frequency (CDF) plot for the $\%\Delta MV_i$ data. Figure 7.4 shows the CDF data for the spatial percentage change of roller MV in the MDP and CMV measurements. By shading the area of data passing the percentage change target value criteria (%Δ-TV ≤ 10%), it is easy to identify the percentage of the data meeting the criteria.

Table 7.4 Spatial Percentage Change of the CCC Data ≤ 10 %

Measurement Pass	MDP-Percent Passing (%)	CMV-Percent Passing (%)
1 to 2	24.6	23.9
2 to 3	43.4	37.8
3 to 4	55.6	52.2
4 to 5	92.2	58.3

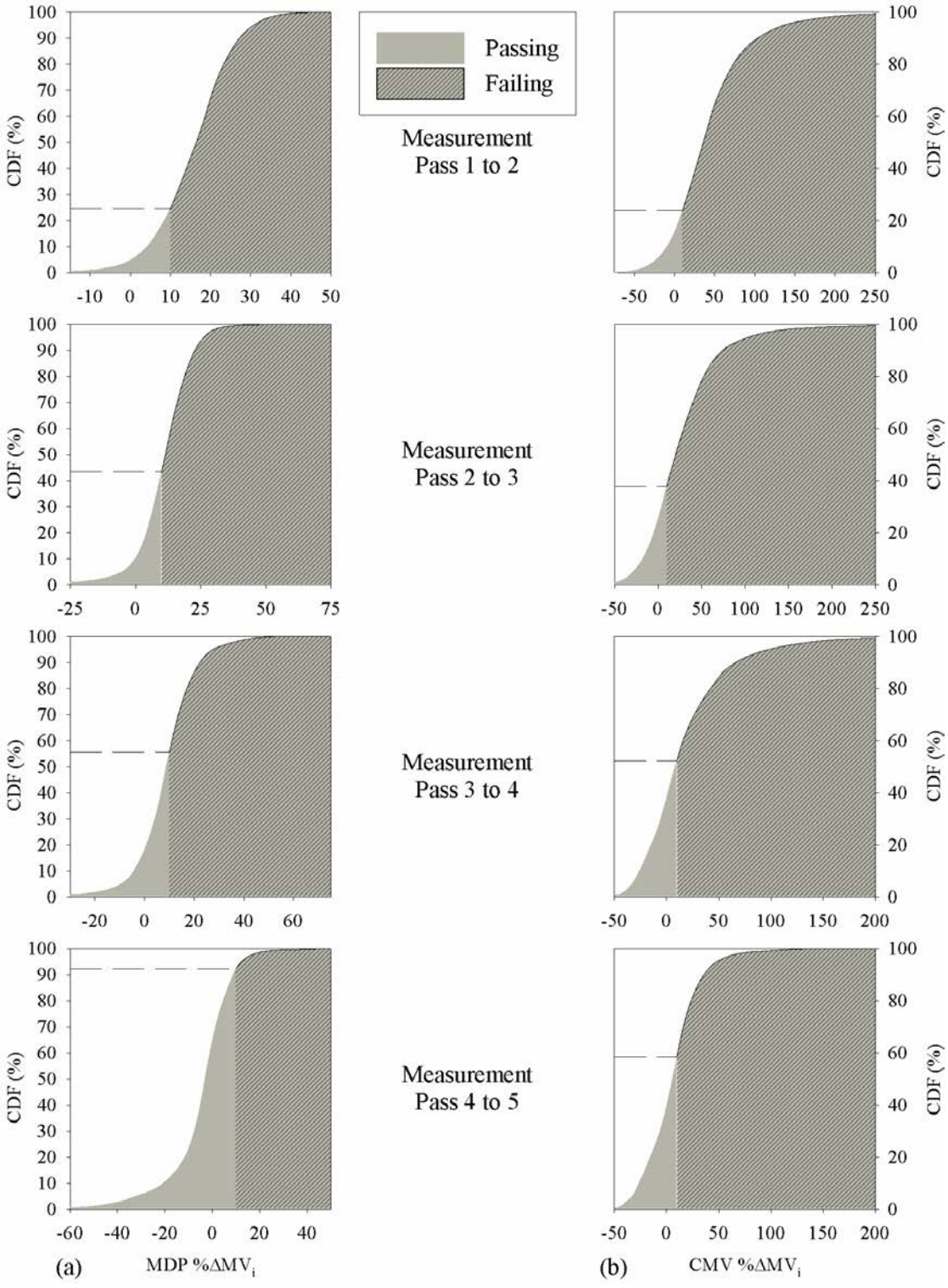

Figure 7.4 CDF of spatial percentage change in roller MV: (a) MDP; (b) CMV.

Analysis of the data in Figure 7.4 shows that, according to the MDP measurements, the compaction criterion is reached upon completion of measurement pass 5. In contrast, the CMV data never reaches the required 90 %; in fact, it falls extremely short of the value at 58.3 % after measurement pass 5. There are several reasons why this could occur. For one, as mentioned in Section 2.5.3 of Chapter 2, if the roller is compacting in an undesirable operating mode, the resulting CMV data may be detrimentally affected (Adam 1997; Adam and Kopf 2004). Previous studies have used resonant meter values RMV collected during compaction to determine the operation mode of the roller during the CMV data acquisition, and then corrected the CMV values (e.g., Vennapusa et al. 2010). As discussed in Section 5.2 of Chapter 5, the RMV and CMV data was examined for the data collected in this field study. After assessment of the data, it was concluded that the roller operation mode did not significantly affect the CMV results. Therefore, the root cause of why the CMV data never reaches the acceptance criteria for QA Option 2B must be attributed to another phenomenon.

Another possible phenomenon that may have led to the discrepancies between the MDP and CMV compaction completion results for QA Option 2A could be that CMV measurements have a much greater depth of influence beneath the surface; variations in the sub-lift material may greatly affect the readings. This depth of influence factor leads to much more variation in the CMV measurements, in comparison to the MDP measurements, as indicated by the higher standard deviation and coefficient of variation values that are presented in Table 7.5.

The general observations that are made here are also supported by the statistically-based analysis approach that is utilized in Meehan and Tehrani (2011). As they noted:

> "*The practical implications of these deviations from normality need to be understood when imposing percentage-based passing criteria when writing CCC or IC specifications that are to be used to control the construction process (e.g., a desirable specification approach might be to say that 80 % of the recorded data points must be smaller than (MDP) or larger than (CMV) a pre-specified target value from test pad construction). These data indicate that it may not be reasonable to use the same percentage passing criteria for different types of CCC indicator values (e.g., MDP, CMV, etc.), as these data are sampled from distributions that are different from normal, and more importantly, different from each other*." (Meehan and Tehrani 2011).

Since there is a higher variation in the CMV data, and because the distributions that the data are sampled from are different from normal (and different from each other), it appears the acceptance criteria needs to be changed for different CCC roller measurements. Otherwise, a given lift will not "pass" after the same number of compactor passes using a MDP versus a CMV mode of monitoring. Adjusting the acceptance criteria for roller measured values can be done in two ways: (1) Increase the %Δ-TV; and/or (2) Reduce the percentage value of $\%\Delta MV_i \leq \%\ \Delta$ –TV that is required for acceptance.

Table 7.5 Summary Statistics of CCC Measurement Data

Measurement Pass	MDP			CMV		
	Mean (kJ/s)	Standard Deviation (kJ/s)	Coefficient of Variation (%)	Mean	Standard Deviation	Coefficient of Variation (%)
1	14.49	2.49	17.22	8.69	3.07	35.34
2	12.02	1.80	14.98	11.68	3.73	31.94
3	10.65	1.71	16.05	14.10	4.26	30.24
4	9.62	1.50	15.57	15.38	3.85	25.03
5	8.48	1.41	16.61	15.82	3.65	23.07

A simple sensitivity analysis was performed to determine the necessary acceptance criteria for CMV data that would closely match the results of acceptance of compaction after measurement pass 5 for the MDP data. The resulting acceptance criteria for the CMV measurements is 80 % of the $\%\Delta MV_i \leq 25\%$. Table 7.6 shows the percentage of data meeting the new %Δ–TV = 25 %.

Table 7.6 Spatial Percentage Change of the CMV Data ≤ 25 %

Measurement Pass	CMV-Percent Passing (%)
1 to 2	38.5
2 to 3	55.2
3 to 4	68.6
4 to 5	81.3

This implementation of Option 2b is a perfect example showing the importance in the selection of the acceptance criteria (e.g. %Δ–TV). Even with consistent soils, site conditions, compaction equipment, and roller operation parameters, the acceptance criteria are still drastically affected by the type of CCC measurement used.

In Chapter 2, there is a discussion about all the various types of proprietary CCC measurements. The author believes that even with additional field studies, until consistent universally accepted CCC measurement types are determined, it will be difficult to implement Option 2b into a compaction verification specification framework.

7.2.4 Acceptance Testing Using Option 3

A detailed explanation of Option 3 can be found in Section 2.7.6. However, in essence, Option 3 relies on the determination of a CCC target value (MV-TV) based on correlation with the contract-specified required relative compaction (QA-TV), and then requiring that a specified percentage of the roller MV exceed the MV-TV. Option 3 allows the engineer to develop correlations using either univariate regression analysis or multivariate regression analysis. If univariate regression analysis is utilized, it must be shown that the moisture content variability does not significantly affect the correlation equations. Multivariate regression analysis will account for the moisture content; however, the selection of a MV-TV will be difficult due to the introduction of moisture content as a variable in the regression equations. Currently, to the author's knowledge, a solution for determination of the MV-TV using multivariate regression has not been developed.

For the sake of simplicity, Option 3 will be implemented using simple linear univariate correlations between the NDG relative compaction percentage (*RC*) measurements and the corresponding predicted IDW $p = 4$ CCC values. The CCC measurement locations do not precisely match the locations of the NDG measurements; however, the abundance of CCC data collected allows for prediction of the CCC value at the NDG measurement locations, enabling point-to-point

comparisons. The reasoning for selection of IDW $p = 4$ as the interpolation technique is thoroughly discussed in Chapter 6. The required assumption for performing univariate regression analysis with density-based data is that the variability of moisture content during compaction did not significantly affect the results.

The univariate simple linear regression analyses are shown in Figure 7.5. Provided on the plots are the correlation equations, correlation curves, and the Lift 5 data points used in the analysis. The NDG target *RC* percentage value (QA-TV) of 95 % relative compaction was used to determine the roller MV target value (MV-TV). The graphical construction can be seen in Figure 7.5.

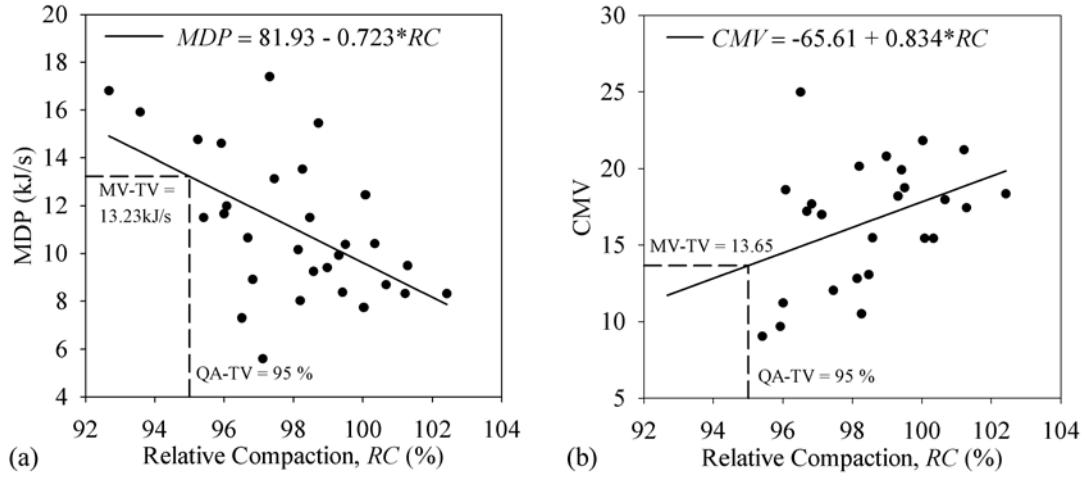

Figure 7.5 Determination of QA-TV using Option 3: (a) MDP; (b) CMV.

The resulting MV-TV values for MDP and CMV are 13.23 kJ/s and 13.65, respectively. It should be noted that the MV-TV, for both CCC measurements, falls on the correlation equation line outside of the range of data or almost all of the range. In

reality, this is not an acceptable data set for determining the MV-TV; however, since this method is being performed on data previously collected it will be used to show the process for acceptance for Option 3.

The hypothetical acceptance criteria utilized for this study will be that 95 % of the roller MV meet the MV-TV requirement. As can be seen in Figure 7.5, as the dry unit weight of soil increases, MDP values decrease and CMV values increase. Therefore, MDP roller measurements less than or equal to the $MV\text{-}TV_{MDP}$ and CMV values greater than or equal to the $MV\text{-}TV_{CMV}$ are considered passing measurements. The percentages of roller MV passing the MV-TV criteria for each successive measurement pass are presented in Table 7.7. According to the specified acceptance criteria, the MDP data defines compaction complete after measurement pass 3, while the CMV data suggest that the acceptance criteria was not met.

Table 7.7 Percentage of CCC Measurements Meeting the MV-TV (Option 3)

Measurement Pass	MDP-Percent Passing (%)	CMV-Percent Passing (%)
1	31.1	6.7
2	79.9	32.4
3	96.1	53.3
4	98.7	65.9
5	99.1	71.6

Similar to the results seen in the implementation of Option 2b, the MDP and CMV data sets do not show agreement for when the acceptance criteria is met. One reason for this anomaly in the CMV results may be a function of the regression equation and data set used for CMV to determine the MV-TV. Observation of Figure 7.5b shows that all the data points used for calibration meet the QA-TV criteria.

Proper calibration data would have data points both below and exceeding the QA-TV. In addition, there is significant scatter around the regression line. These issues likely contributed to the selection of a MV-TV that was too low for the given soil conditions. However, without more data there is no way to quantify the error in selection of the MV-TV.

As mentioned in Section 7.2.3 and shown in Table 7.5, the spatial variability of CMV data is much higher than MDP data, which may require that different acceptance criteria values be used for CMV and MDP. As previously determined, the effect of roller operation mode on the CMV data set may be ruled out because it was determined that undesirable operation modes did not significantly affect the measured CCC results.

Consequently, even with consistent soils, site conditions, compaction equipment, and roller operation parameters, the acceptance criteria are still drastically affected by the type of CCC measurement used. Results seen here further confirm the author's belief that additional field studies are necessary to determine adequate acceptance criteria requirement values for different types of roller measured values.

7.3 SUMMARY AND CONCLUSIONS

Four QA earthwork compaction verification methodologies that utilize CCC technology were examined in this chapter. QA Option 1 uses CCC roller MV to identify "weak areas" of low compaction to be tested using conventional in-situ QA compaction verification devices. QA Option 2 implements a limiting percentage change in roller MV from successive measurement passes to verify relative compaction of the earthwork material. There are two alternate approaches for QA

Option 2: (1) a limit on the percentage change of the mean roller MV for successive measurement passes; and (2) a limit on the spatial percentage change of roller MV for successive measurement passes. QA Option 3 relies on the determination of a MV-TV based on correlation to the contract specified QA-TV from a calibration area. Each of the options listed above have been retrospectively implemented on the MDP and CMV data recorded during compaction of Lift 5 for construction of the embankment described in Chapter 3.

Of the three methods examined, QA Option 3 is the most complex because correlations must be made between the roller MV and conventional compaction verification measurements. If a density-based device is used for acquisition of data for correlations, special consideration must be taken to quantify the influence of moisture content on the roller MV.

QA Option 2 offers a much higher verification percentage of the evaluation area compared to conventional in-situ spot-testing compaction verification methods. The downside to both the mean percentage change and spatial percentage change of roller MV methods for Option 2 is they are relative compaction methods. These methods do not guarantee that the contract specified relative maximum dry density has been reached but only that the earthwork material has been compacted to the maximum capability of the compaction equipment. Therefore, conventional compaction verification is necessary to ensure that the compaction equipment is capable of compacting the earthwork material to the required density. In addition, the moisture content of the material must be carefully monitored and remain within the contract specified range. Since QA Option 2 does not account for moisture content

variability, failure to compact the soil within the required range could result in false-passing lifts.

QA Option 1 still utilizes conventional in situ spot-testing (e.g., NDG and Sand Cone), however the spatial map of roller MV allows for the spot-testing to be performed in the areas of lowest compaction on a given lift. This method increases the confidence that compaction has been completed, in comparison to spot-testing random locations that could be representative of higher areas of compaction.

Based on the implementation of the four specification QA Options implemented within this chapter, the following limitations were realized:

- Option 1 still relies on the use of conventional in situ compaction verification spot testing (e.g., NDG, Sand Cone, etc.).
- Option 2a and 2b only verifies that the material has reached the compaction limit of the compaction equipment being utilized. The ability of the roller to achieve the required compaction level must be shown.
- Option 2a and 2b do not account for moisture content (in situ moisture content testing is still necessary to confirm that the material moisture content is within the contract specified range during compaction).
- Option 2b requires the roller MV to be interpolated onto a consistent grid in order to determine the percentage change in roller MV at point-to-point locations from successive passes.
- Option 2b and 3 require the use of interpolation methods. The complex nature of kriging interpolation methods, currently used in research applications, makes it difficult to produce consistent interpolation from

user to user. Consequently, future research should be performed to access the reasonability of utilizing simpler interpolation methods (e.g., NN or IDW).

- Option 3, when utilizing univariate regression correlations, requires that variability in material moisture content does not significantly influence the correlations.
- Option 3, when utilizing multivariate regression correlations, makes determination of the MV-TV difficult due to the presence of multiple varying variables (e.g., dry unit weight and moisture content).
- Options 2a, 2b, and 3 cannot be utilized unless strong correlations (e.g., $R^2 \geq 0.5$) exist between the roller MV and compaction material density.
- Options 2a, 2b, and 3 currently rely on arbitrary acceptance criteria: a specified percentage of the roller MV from a given measurement pass must meet the target value (e.g. %Δ-TV, MV-TV). Additional field studies implementing the CCC QA Options are necessary to calibrate these acceptance criteria target values.

It is the recommendation of the author that QA Option 1 be implemented into practice by State Department of Transportations during a “transition period” in order for contractors and inspectors to become more familiar with CCC equipment and procedures. Only after an adequate “transition period” has been employed is it recommended that QA Options 2 and 3 be considered on active earthwork compaction projects.

Chapter 8

CONCLUSIONS AND RECOMMENDATIONS

8.1 Conclusions

The effectiveness of using continuous compaction control (CCC) systems within an earthwork specification framework was evaluated during this research project. A small-scale embankment, constructed using poorly-graded sand with silt material, was compacted in five lifts with a compaction roller that was retrofitted to record machine drive power (MDP), compaction meter values (CMV), and real time kinematic-global positioning system (RTK-GPS) position measurements; amongst other roller operating parameters.

As a first attempt to utilize data collected during CCC compaction for an earthwork specification, a framework is presented for using field RTK-GPS position measurements made by CCC or IC equipment to monitor and control the thickness of compacted soil lifts during construction of a roadway embankment.

The lift thickness control and monitoring procedure and corresponding conclusions are as follows:

- During the compaction process, continuously record compactor position information (*X*, *Y*, and elevation data) for at least two successive compacted soil lifts.
- Select a “projection grid” that is consistent from lift to lift to enable comparison of elevation measurements for two consecutive lifts, for determination of lift thickness. According to the current study, the “projection

grid" should be isotropic, with a grid point spacing that is near the lower bound of the measured point spacing distances in the roller travel direction (the *X*-direction).

- Predict elevation values at each of the grid point locations of the "projection grid", using the measured elevation (*Z*) data from the final pass of compaction for each lift. Based upon the results from the current chapter, either an ordinary isotropic kriging approach or an inverse distance weighting (IDW) approach with an exponent value of $p = 4$ may be utilized for this purpose. The author strongly recommends the IDW method, as it is simpler and less user sensitive, and the results from this study did not differ substantially from the more sophisticated ordinary kriging approach.
- Determine the spatial lift thickness of each compacted soil lift by taking the difference in elevation values from lift to lift at each of the "projection grid" point locations. Calculate the mean lift thickness and a statistical measure of its variability (i.e., standard deviation and/or coefficient of variation). Additionally, generate spatial maps of the lift thickness to identify "thinner" and "thicker" areas; this can be done with contour plots. In the event that the mean is larger than specified or the variability is higher than desired, the spatial maps can be used to identify problem areas for the contractor to address, in an attempt to meet the specification requirements, prior to moving on to the next lift.

The next portion of this research project focused on the comparison of in situ test method measurements with the CCC measurements recorded during the field study. In

order for adequate regression analyses to be performed, the CCC measurements needed to be predicted at the precise locations that the in situ test methods were performed. Three different geospatial interpolation techniques were examined for this purpose and are listed here in order from highest complexity to lowest: ordinary kriging method, inverse distance weighting method, and nearest neighbor (NN) interpolation. The following conclusions can be made when evaluating the three previously mentioned interpolation techniques:

- In general, for univariate regression analysis of the individual values of CCC measurements and in situ test measurements at point-to-point locations, the coefficient of determination values for IDW $p = 4$ are slightly lower than those from kriging. Similarly, the NN coefficient of determination values are slightly lower than the IDW $p = 4$ values. However, the overall differences in coefficient of determination values between the kriging, IDW, and NN interpolation methods appear to be fairly insignificant (i.e., a matter of a few hundredths).
- For univariate regression analysis of the average values of CCC measurements and in situ test measurements, the differences in coefficient of determination values for the three different interpolation technique results do not follow any pattern. For some analyses the kriging results have higher coefficient of determination value and for others the NN interpolation method has higher values. However, again, the differences in the coefficient of determination values appear to be fairly insignificant (a matter of hundredths).
- For multivariate regression analysis of the individual values of CCC measurements and in situ test measurements at point-to-point locations, none

of the interpolation methods provides consistently stronger correlations. In general, the differences in coefficient of determination values appear to be insignificant (a matter of hundredths). However, there are a few exceptions where kriging analysis offer much stronger correlations (e.g., NDG vs. MDP and Geogauge vs. MDP), and others where NN and IDW offer much stronger correlations (e.g., Geogauge vs. CMV, LWD 300 vs. CMV, and LWD 200 vs. CMV).

- For multivariate regression analysis of the average values of CCC measurements and in situ test measurements, none of the interpolation methods provides consistently stronger correlations. In general, the differences in the coefficient of determination values appear to be insignificant (a matter of hundredths). However, there are a few exceptions where kriging analysis offer much stronger correlations (e.g., Geogauge vs. MDP), and others were NN and IDW offer much stronger correlations (e.g., Geogauge vs. CMV, LWD 300 vs. CMV, LWD 200 vs. CMV, and DCPIA vs. CMV).

CCC measurement predictions were made using each of the three interpolation techniques mentioned above. Regression analyses were then performed for each of the respective data sets. Univariate regression analyses were performed, first, on a point-by-point data set and, then, on a data set consisting of averaged CCC measurements and in situ test measurements of each lift and pass. The influence of moisture content was then examined by performing multivariate regression analyses on the same data sets.

The general conclusions that can be made from observation of the univariate regression analyses results are as follows:

- Comparisons of the individual values of CCC measurements and in situ test measurements at point-to-point locations showed weak correlations.
- Comparisons of the average values of CCC measurements and in situ test measurements at point-to-point locations yielded relatively strong correlations. However, a number of the average data sets did not have a sufficient number of data points; therefore, several of the models and corresponding coefficient of determination values were unreliable and should be ignored.
- For a number of the cases, the second-degree polynomial model showed significantly stronger correlations than the linear model (e.g., DCPI values, NDG dry unit weight values, and moisture contents).
- The removal of the base layer measurements from the respective data sets resulted in increased coefficients of determination. This phenomenon is likely due to the relatively low moisture content of the base layer in comparison to the "engineered" lifts, which indicates that the moisture content had a significant influence on the density and modulus of the compacted soils.
- Examination of only the measurements collected on the final pass of each respective lift did not improve correlations; however examination of the Lift 5 data on its own did slightly improve correlations. This observation is likely due to the fact that the soil within a given lift is likely more uniform in soil gradation and moisture content in comparison to the soils from all five lifts and the base layer of the embankment.
- Generally, MDP measurements showed better correlations with the in situ test methods, in comparison to the CMV measurements. This is likely related to the different influence depths of the CCC measurements. The influence depth of

MDP measurements is much closer to that of the in situ test methods, which range from approximately 20 cm to 60 cm. In contrast, the influence depth of CMV measurements is roughly 80 cm to 150 cm.

- In general, the DCP indices show much stronger correlations with the CCC measurements, in comparison to the other in situ testing methods that were used in the study.
- In general, the GeoGauge moduli values showed the weakest correlations with the CCC measurements, in comparison to the other in situ testing methods that were used in the study.
- In general, both sets of moisture content values showed much stronger correlations with the CCC measurements, in comparison to the density-based and modulus-based in situ testing methods used in the study. This indicates that moisture content has a significant contribution to the density of compacted soils, which agrees with classic soil mechanics theory.

The general conclusions that can be made from observation of the multivariate regression analyses results are as follows:

- Comparison of the individual values of CCC measurements and in situ test measurements at point-to-point locations showed improved correlations compared to those seen in the univariate analyses; however, correlations were still relatively weak.
- Comparison of the average values of CCC measurements and in situ test measurements at point-to-point locations yielded very strong correlations.

However, a majority of the average data sets did not have a sufficient number of data points; therefore, most of the models and corresponding coefficient of determination values were unreliable and needed to be ignored. To improve this, future studies should consider recording CCC and in situ test measurements for a significant number of passes and lifts of compacted soil, in order to create robust data set that does not have limitations due to a small amount of data.

- In general, the regression model with the interaction term resulted in slightly stronger coefficient of determination values. This observation is expected considering the additional term results in an additional regression model coefficient, which allows for a better model fit.

The final portion of this study was the implementation of the four earthwork compaction verification methodologies utilizing CCC technology. QA Option 1 uses CCC roller MV to identify “weak areas” of low compaction to be tested using conventional in-situ QA compaction verification devices. QA Option 2 implements a limiting percentage change in roller MV from successive measurement passes to verify relative compaction of the earthwork material. There are two alternate approaches for QA Option 2: (1) a limit on the percentage change of the mean roller MV for successive measurement passes; and (2) a limit on the spatial percentage change of roller MV for successive measurement passes. QA Option 3 relies on the determination of a MV-TV based on correlation to the contract specified QA-TV from a calibration area. Based on the implementation of the four specification QA Options implemented within this chapter, the following limitations were realized:

- Option 1 still relies on the use of conventional in situ compaction verification spot testing (e.g., NDG, Sand Cone, etc.).
- Option 2a and 2b only verifies that the material has reached the compaction limit of the compaction equipment being utilized. The ability of the roller to achieve the required compaction level must be shown.
- Option 2a and 2b do not account for moisture content (in situ moisture content testing is still necessary to confirm that the material moisture content is within the contract specified range during compaction).
- Option 2b requires the roller MV to be interpolated onto a consistent grid in order to determine the percentage change in roller MV at point-to-point locations from successive passes.
- Option 2b and 3 require the use of interpolation methods. The complex nature of kriging interpolation methods, currently used in research applications, makes it difficult to produce consistent interpolation from user to user. Consequently, future research should be performed to access the reasonability of utilizing simpler interpolation methods (e.g., NN or IDW).
- Option 3, when utilizing univariate regression correlations, requires that variability in material moisture content does not significantly influence the correlations.
- Option 3, when utilizing multivariate regression correlations, makes determination of the MV-TV difficult due to the presence of multiple varying variables (e.g., dry unit weight and moisture content).
- Options 2a, 2b, and 3 cannot be utilized unless strong correlations (e.g., $R^2 \geq 0.5$) exist between the roller MV and compaction material density.

- Options 2a, 2b, and 3 currently rely on arbitrary acceptance criteria: a specified percentage of the roller MV from a given measurement pass must meet the target value (e.g. %Δ-TV, MV-TV). Additional field studies implementing the CCC QA Options are necessary to calibrate these methods.

8.2 Recommendations

For future utilization of CCC systems to monitor and control soil lift thickness, the following recommendations are made:

- Additional research using CCC rollers is needed to determine acceptable target levels for “good construction practices” and “bad construction practices”, prior to development of specifications that utilize this approach.
- Further research is also needed to develop a better understanding of the effect that RTK-GPS measurement accuracy has on lift thickness measurements
- Once target levels of acceptability for “good construction practices” and “bad construction practices” have been defined and the effect of measurement error on the device results is better understood, incentives and penalties can be built in to the specification framework to ensure good construction practices.

For future utilization of CCC systems to monitor and verify compaction in an earthwork specification, the following recommendations are made:

- QA Option 1 should be implemented in practice by State Department of Transportations during a “transition period” in order for contractors and inspectors to become more familiar with CCC equipment and procedures.
- During this transition period, CCC data will be collected on live construction projects. The data acquired can be used to calibrate the target levels of

acceptability (e.g. %Δ-TV, MV-TV, percentage passing) required for implementation of QA Options 2a, 2b, and 3.

- Only after target levels of acceptability for QA Options 2a, 2b, and 3 have been determined, and local contractors and engineers have become adequately familiar with CCC systems, is it recommended that QA Options 2a, 2b, and/or 3 be implemented on active earthwork compaction projects.

REFERENCES

Adam, D. (1997). "Continuous Compaction Control (CCC) with Vibratory Rollers." *Proceedings of GeoEnvironment 97*, Melbourne, Australia, Balkema, Rotterdam, 245–250.

Adam, D. (2007). "Roller-Integrated Continuous Compaction Control (CCC) Technical Contractual Provisions & Recommendations." *Design and construction of pavements and rail tracks: Geotechnical aspects and processed materials*, A. G. Correia, Y. Momoya, and F. Tatsuoka, eds., CRC, Boca Raton, Fla., 111-138.

Adam, D., and Brandl, H. (2003). "Sophisticated Roller Integrated Continuous Compaction Control." *12th Asian Regional Conference on Soil Mechanics and Geotechnical Engineering* - Geotechnical Infrastructure for the New Millennium, Singapore, 427-430.

Adam, D., and Kopf, F. (1998). "Application of Continuous Compaction Control (CCC) to Waste Disposal Liners." *Proceedings of 3rd International Congress on Environmental Geotechnics*, Lisbon, Portugal, 365-370.

Adam, D., and Kopf, F. (2004). "Operational Devices for Compaction Optimization and Quality Control (Continuous Compaction Control & Light Falling Weight Device)." *Proceedings of the International Seminar on Geotechnics in Pavement and Railway Design and Construction*, Athens, Greece, 97-106.

Anderegg R., and Kaufmann, K. (2004). "Intelligent Compaction with Vibratory Rollers - Feedback Control Systems in Automatic Compaction and Compaction Control." *Transportation Research Record 1868, Journal of the Transportation Research Board*, National Academy Press, 124-134.

Anderegg, R. (1998). "Nichtlineare Schwingungen bei dynamischen Bodenverdichtern (Vibrations with Dynamic Soil Compactors)." Dissertation. Diss. ETH Nr. 12419, Eidgenössische Technische Hochschule, Zürich.

Anderegg, R., von Felten, D., and Kaufmann, K. (2006). "Compaction Monitoring Using Intelligent Soil Compactors." *Proceedings of GeoCongress 2006: Geotechnical Engineering in the Information Technology Age*, Atlanta, CDROM.

ASTM D698. (2007). "Standard Test Methods for Laboratory Compaction Characteristics of Soil Using Standard Effort (12,400 ft-lbf/ft3(600 kN-m/m3))." *Annual Book of ASTM Standards*, Vol. 04.03, ASTM International, West Conshohocken, PA.

ASTM D1196-93. (2007). "Standard Test Method for Nonrepetitive Static Plate Load Tests of Soils and Flexible Pavement Components, for Use in Evaluation and Design of Airport and Highway Pavements," *Annual Book of ASTM Standards*, Vol. 04.03, ASTM International, West Conshohocken, PA.

ASTM D1556-00. (2007) "Standard Test Method for Density and Unit Weight of Soil in Place by the Sand-Cone Method," *Annual Book of ASTM Standards*, Vol. 04.08, ASTM International, West Conshohocken, PA.

ASTM D1557. (2007). "Standard Test Methods for Laboratory Compaction Characteristics of Soil Using Modified Effort (56,000 ft-lbf/ft3 (2,700 kN-m/m3))." *Annual Book of ASTM Standards*, Vol. 04.03, ASTM International, West Conshohocken, PA.

ASTM D2216-10. (2007). "Standard Test Methods for Laboratory Determination of Water (Moisture) Content of Soil and Rock by Mass," *Annual Book of ASTM Standards*, Vol. 04.08, ASTM International, West Conshohocken, PA.

ASTM D2487-06. (2007). "Standard Practice for Classification of Soils for Engineering Purposes (Unified Soil Classification System)," *Annual Book of ASTM Standards*, Vol. 04.08, ASTM International, West Conshohocken, PA.

ASTM D4694-96. (2007). "Standard Test Method for Deflections with a Falling-Weight-Type Impulse Load Device," *Annual Book of ASTM Standards*, Vol. 04.03, ASTM International, West Conshohocken, PA.

ASTM D6758-02. (2007). "Standard Test Method for Measuring Stiffness and Apparent Modulus of Soil and Soil-Aggregate In-Pl. by an Electro-Mechanical Method," *Annual Book of ASTM Standards*, Vol. 04.09, ASTM International, West Conshohocken, PA.

ASTM D6938-10. (2012). "Standard Test Method for In-Place Density and Water Content of Soil and Soil-Aggregate by Nuclear Methods (Shallow Depth)," *Annual Book of ASTM Standards*, Vol. 04.09, ASTM International, West Conshohocken, PA.

ASTM D6951-03. (2007). "Standard Test Method for Use of 781 the Dynamic Cone Penetrometer in Shallow Pavement Applications," *Annual Book of ASTM Standards*, Vol. 04.03, ASTM International, West Conshohocken, PA.

ASTM E2583-07. (2007). "Standard Test Method for Measuring Deflections with a Light Weight Deflectometer (LWD)," *Annual Book of ASTM Standards*, Vol. 04.03, ASTM International, West Conshohocken, PA.

Brandl, H., and Adam, D. (1997). "Sophisticated Continuous Compaction Control of Soils and Granular Materials." *Proceedings of 14th International Conference on Soil Mechanics and Foundation Engineering*, Hamburg, Germany, 1-6.

Brandl, H., and Adam, D. (2004). "Continuous Compaction Control (CCC) for Fill Dams and Roller Compacted Concrete Dams." *New Developments in Dam Engineering-Proceedings of 4th International Conference on Dam Engineering*, Nanjing, China, 17-44.

Broms, B. B. and Forssblad, L. (1969). "Vibratory Compaction of Cohesionless soils." *Proceedings, Specialty Session No. 2, 7th International Conference of Soil Mechanics and Foundation Engineering*, Mexico City, 101-118.

Budrikaite, L., (2005). "Modeling of Zonel Anisotropic Variograms." *Liet. matem. rink*, Vol. 45: 339-342.

Budrikaite, L., and Dučinskas, K. (2005). "Modeling of Geometric Anisotropic patial Variation." *Proceedings of the 10th International Conference MMA2005&CMAM2*, Trakai, Lithuania, 361-366.

Cacciola, D. V., Meehan, C. L., and Khosravi, M. (2013). "An Evaluation of Specification Methodologies for Use with Continuous Compaction Control Equipment." *Proc., Geo-Congress 2013: Stability and Performance of Slopes and Embankments III*, San Diego, CA, March 3-7, 2013, ASCE, Reston, VA, 413-416.

Christakos, G. (1992). *Random Field Models in Earth Sciences*, Academic Press.

Clark, I., and W. Harper. (2002). *Practical Geostatistics 2000*. Ecosse North America LLC, Columbus, Ohio.

Cressie, N. A. C. (1993). *Statistics for Spatial Data*, Revised Ed., John Wiley & Sons, Inc., New York.

Das, B. M. (2008). *Fundamentals of Geotechnical Engineering*, 3rd Edition, Cengage Learning.

DelDOT (2001). “Specifications for Road and Bridge Construction.” August 2001, Prepared by The Delaware Department of Transportation, Nathan Hayward III, Secretary & Raymond M. Harbeson, Jr., Chief Engineer.

Deutsch, C.V. and Journel, A.G. (1992). *GSLIB: Geostatistical Software Library and User's Guide*. Oxford University Press, Oxford, New York, 340 pp.

Dore, O., Teyssier, R., Bouchet, F. R., Vibert, D., and Prunet, S. (2001). “MAPCUMBA: A Fast Iterative Multi-Grid Map-Making Algorithm for CMB Experiments.” *Astron. Astrophys.*, Vol. 374: 358-370.

Draper, N. R., and Smith, H., (1998). *Applied Regression Analysis*, 3rd Ed., John Wiley & Sons, Inc., New York.

Dučinskas, K., and Šaltytė–Benth, J., (2003). *Erdvinė Statistika*, Klaipėda: KU leidykla, 116 pp.

Facas, N., Mooney, M., and Furrer, R. (2010.), “Anisotropy in the Spatial Distribution of Roller-Measured Soil Stiffness.” *International Journal of Geomechanics*, Vol. 10 (4): 129-135.

Facas, N. W., Rinehart, R. V., and Mooney, M. A. (2011). “Development and Evaluation of Relative Compaction Specifications Using Roller-based Measurements.” *Geotechnical Testing Journal*, Vol. 34 (6): 129-135.

FHWA, (2011a). “Intelligent Compaction Technology for Aggregate Base Applications,” *Federal Highway Administration*, 10 pp.

FHWA, (2011b). “Intelligent Compaction Technology for Soils Applications,” *Federal Highway Administration*, 11 pp.

Floss, R., Gruber, N., and Obermayer, J. (1983). “A Dynamical Test Method for Continuous Compaction Control.” *Proc., 8th European Conf. on Soil Mech. and Found. Engg.*, H. G. Rathmayer and K. Saari, eds., Balkema, The Netherlands, 25-30.

Forssblad, L. (1980). “Compaction Meter on Vibrating Rollers for Improved Compaction Control.” *Proceedings of International Conference on Compaction*, Vol. II, Assoc. Amicale de Ingénieus, Paris, France, 541-546.

Goovaerts, P., (1997). *Geostatistics for Natural Resources Evaluation*. Oxford University Press, New York, 483 pp.

Hansbo, S., and Pramborg, B. (1980). “Compaction Control,” *Proceedings of the International Conference on Compaction*, Paris, France, Vol. 2: 559-564.

Holtz, R. D., and Kovacs, W. D. (1981). *An Introduction to Geotechnical Engineering*, Prentice-Hall, Inc., Englewoods Cliffs, New Jersey.

Holtz, R. D., Kovacs, W. D., and Sheahan T. C. (2011). *An Introduction to Geotechnical Engineering*, 2nd edition, Prentice-Hall, Inc., Englewoods Cliffs, New Jersey.

InDOT (2012). “Quality Control/Quality Assurance, QC/QA, Soil Embankment,” *Indiana Department of Transportation*, 11 pp.

Isaaks, E.H., and R. M. Srivastava. (1989). *An Introduction to Applied Geostatistics*, Oxford University Press, New York, 561 pp.

ISSMGE. (2005). *Roller-Integrated Continuous Compaction Control (CCC), Technical Contractual Provisions—Recommendations*. International Society for Soil Mechanics and Geotechnical Engineering: Geotechnics for Pavements in Transportation Infrastructure.

Jian X., Olea, R.A. and Yu, Y.S., (1996). ‘Semivariogram Modeling by Weighted Least Squares’, *Comput. Geosci.*, Vol. 22: 387-397.

Journel, A.G., and Huijbregts, C.J., (1978). *Mining Geostatistics*. Academic Press, New York.

Kitanidis, P. K., (1997). *Introduction to Geostatistics: Applications in Hydrogeology*, Cambridge University Press, 249 pp.

Krige, D. G., (1951). "A Statistical Approach to Some Basic Mine Valuation Problems on the Witwatersrand." *J. of the Chem., Metal. and Mining Soc. of South Africa*, Vol. 52 (6): 119-139.

Kröber, W., Floss, E., and Wallrath, W. (2001). “Dynamic Soil Stiffness as Quality Criterion for Soil Compaction.” *Geotechnics for Roads, Rail Tracks and Earth Structures*, A.A.Balkema Publishers, Lisse /Abingdon/ Exton (Pa) /Tokyo, 189-199.

Meehan, C. L. and Tehrani, F. S. (2011). “A Comparison of Simutaneously Recorded Machine Drive Power and Compactometer Measurements.” *Geotechnical Testing Journal*, Vol. 34 (3): 208-218.

Meehan, C. L., Khosravi, M., and Cacciola, D. V., "Monitoring Field Lift Thickness Using Compaction Equipment Instrumented With Global Positioning System (GPS) Technology," *Geotechnical Testing Journal*, Vol. 36, No. 5, 2013, pp. 755-767, doi:10.1520/GTJ20120124.

Mn/DOT Specification 2105, (2007). "Pilot Continuous Compaction Control (CCC) Method." *Minnesota Department of Transportation* , 4 pp.

Mn/DOT Specification 2105, (2010). "Pilot Continuous Compaction Control (CCC) Method." *Minnesota Department of Transportation* , 4 pp.

Mooney, M. A., and Adam, D. (2007). "Vibratory Roller Integrated Measurement of Earthwork Compaction: An overview." *Proceedings of 7th International Symposium on Field Measurements in Geomechanics - FMGM 2007*, ASCE, Boston, Massachusetts, CD-ROM.

Mooney, M., Rinehart, R., Facas, N., Musimbi, O., White, D., and Vennapusa, P. (2010). "Intelligent Soil Compaction Systems." *NCHRP Report 676*, Transportation Research Board, Washington, D.C.

Nohse, Y., Uchiyama, K., Kanamori, Y., Kase, J., Kawai, Y., Masumura, K., and Tateyama, K. (1999). "An Attempt Applying a New Control System for the Vibratory Compaction Using GPS and CMV in the Embankment Construction (Part 1)." *Proceedings of the 13th International Conference of the ISTVS*, Okinowa, Japan, 295-300.

Olea, R. A., (1999). *Geostatistics for Engineers and Earth Scientists*, Kluwer Academic Publishers, 303 pp.

Olea, R. A., (2006). "A Six-Step Practical Approach to Semivariogram Modeling." *Stochastic Environmental Research and Risk Assessment*, Vol. 20 (5): 307-318.

Pebesma, E.J., (2004). "Multivariable Geostatistics in S: The Gstat Package." *Computers & Geosciences*, Vol. 30: 683-691.

Petersen, L., and Peterson, R., (2006). "Intelligent Compaction and In-Situ testing at Mn/DOT TH53," *Final Report MN/RC-2006-13*, Minnesota Department of Transportation, St. Paul, Minnesota, USA.

Petersen, D., M. Erickson, R. Roberson, and J. Siekmeier. (2007). "Intelligent Soil Compaction: Geostatistical Data Analysis and Construction Specifications." *Transportation Research Board 86th Annual Meeting*, Washington, D.C., Paper #07-2858, CD-ROM.

Ping, W.V., M. Leonard, Z. Yang, and S. Putcha. (2002). “Laboratory Simulation of Field Compaction Characteristics on Sandy Soils.” *Transportation Research Record*, Vol. 1808: 84-95.

Rawlings, J. O., Pantula, S. G., Dickey, D. A. (1998). *Applied Regression Analysis (A Research Tool)*, 2nd Ed., Springer, New York.

RVS 8S.02.6. (1999). "Continuous Compactor Integrated Compaction - Proof (Proof of Compaction)," Technical Contract Stipulations RVS 8S.02.6 - Earthworks, *Federal Ministry for Economic Affairs*, Vienna.

R Development Core Team (2011). “R: A Language and Environment for Statistical Computing.” *R Foundation for Statistical Computing*, Vienna, Austria. ISBN 3-900051-07-0, URL http://www.R-project.org/.

Samaras, A. A., Lamm, R., and Treiterer, J. (1991). “Application of Continuous Dynamic Compaction Control for Earthworks in Railroad Construction.” *Transp. Res. Rec.*, Vol. 1309: 42-46.

Sandström, Å. (1994). “Numerical Simulation of a Vibratory Roller on Cohesionless Soil.” *Internal Report*, Geodynamik, Stockholm, Sweden, 1994.

Sandström, Å., and Pettersson, C. (2004). “Intelligent Systems for QA/QC in Soil Compaction.” *Proceedings of Annual Transportation Research Board Meeting, Transportation Research Board*, Washington, D.C., CD- ROM.

Scherocman, J., S. Rakowski, and K. Uchiyama. (2007). “Intelligent Compaction, Does It Exist?” *Proceedings of the Annual Conference—Canadian Technical Asphalt Association*, No. 52:. 373-398.

Schervish, M. J. (1996). “P Values: What They Are and What They Are Not.” *The American Statistician*, American Statistical Association, Vol 50 (3): 203-206.

Shepard, D. (1968). "A Two-Dimensional Interpolation Function for Irregularly-Spaced Data". *Proceedings of the 1968 ACM National Conference*. 517–524.

Tehrani, F. S. (2009). “An Investigation of Continuous Compaction Control Systems.” A thesis submitted to the Faculty of the University of Delaware in partial fulfillment of the requirements for the degree of Master of Civil Engineering.

Thompson, M., and White, D. J. (2007). “Field Calibration and Spatial Analysis of Compaction Monitoring Technology Measurements.” *Transportation Research Record 2004*, Transportation Research Board, Washington, D.C., 69-79.

Thompson, M., and White, D. J. (2008). "Estimating Compaction of Cohesive Soils from Machine Drive Power." *Journal of Geotechnical Geoenvironmental Engineering*, ASCE, Vol. 134 (12): 1771-1777.

Thurner, H. (1993). "Continuous Compaction Control - Specifications and Experience." *Proceedings of 11th IRF World Congress*, Madrid, Spain, 951-956.

Thurner, H., and Sandström, A. (1980). "A New Device for Instant Compaction Control." *Proceedings of International Conference on Compaction*, Vol. II, Assoc. Amicale de Ingénieus, Paris, 611–614.

Thurner, H., and Sandström, Å. (2000). "Continuous Compaction Control, CCC." *Workshop on Compaction of Soils and Granular Materials*, *Modeling of Compacted Materials, Compaction Management and Continuous Control*, International Society of Soil Mechanics and Geotechnical Engineering (European Technical Committee), Paris, France, 237-246.

TxDOT (2008). "Special Specification – 2008: Quality Compaction Using Intelligent Compaction Rollers," *Texas Department of Transportation Specification*, CSJ: 0172-09-031, 4 pp.

Vennapusa, P., and D.J. White. (2009). "Comparison of Light Weight Deflectometer Measurements for Pavement Foundation Materials." *Geotechnical Testing Journal*, Vol. 32 (3): 239–251.

Vennapusa, P., D. J. White, and M. Morris. (2009). "Geostatistical Analysis of Spatially Referenced Roller-Integrated Compaction Measurements." *Journal of Geotechnical and Geoenvironmental Engineering*, ASCE, Vol. 136 (6): 813-822.

Vennapusa, P., White, D. J., and Morris, M. (2010). "Geostatistical Analysis for Spatially Referenced Roller-Integrated Compaction Measurements." *Journal of Geotechnical & Geoenvironmental Engineering*, Vol. 136 (6): 813-822.

VVR Väg. (2009). *Vägverket Publication*: 2009:121, ISSN: 1401-9612, http://publikationswebbutik.vv.se/upload/5098/2009_121_vvr_vag.pdf (in Swedish).

Wackernagel, H., (1998). *Multivariate Geostatistics*. 2nd edition, Springer, Berlin.

White, D. J., and Thompson, M. (2008). "Relationships Between In-situ and Roller-Integrated Compaction Measurements for Granular Soils." *Journal of Geotechnical Geoenvironmental Engineering*, ASCE, Vol. 134 (12): 1763–1770.

White, D.J., T. Rupnow, and H. Ceylan. (2004). "Influence of Subgrade/ Subbase Nonuniformity on Pavement Performance." *Proceedings, Geo-Trans 2004—Geotechnical Engineering for Transportation Projects*, Geotechnical Special Publication No. 126, ASCE, 1058-1065.

White, D. J., Jaselskis, E., Schaefer, V., and Cackler, E. (2005). "Real-time Compaction Monitoring in Cohesive Soils from Machine Response." *Transportation Research Record 1936*, Transportation Research Board, Washington, D.C., 173-180.

White, D.J., M.D. Morris, and M.J. Thompson. (2006a). "Power-Based Compaction Monitoring Using Vibratory Pad Foot Roller." *Proceedings of GeoCongress 2006: Geotechnical Engineering in the Information Technology Age*, Atlanta, CD-ROM.

White, D.J, Thompson, M., Jovaag, K., Morris, M., Jaselskis, E., Schaefer, V. and Cackler, E. (2006b). "Field Evaluation of Compaction Monitoring Technology: Phase II." *Final Report*, Iowa DOT Project TR-495, Iowa State University, Ames, Ia.

White, D. J., Thompson, M., and Vennapusa, P. (2007). "Field Validation of Intelligent Compaction Monitoring Technology for Unbound Materials." *Final Report*, Minnesota Department of Transportation, Maplewood, Minnesota.

White, D. J., Thopmson, M., Vennapusa, P., and Siekmeier, J. (2008). "Implementing Intelligent Compaction Specifications on Minnesota TH 64: Synopsis of Measurement Values, Data management, and Geostatistical Analysis." *Transportation Research Record 2045*, Transportation Research Board, 1-9.

White, D. J., Vennapusa, P., and Gieselman,H. H., (2011). "Field Assessment and Specification Review for Roller-Integrated Compaction Monitoring Technologies," *Advances in Civil Engineering*, vol. 2011, Article ID 783836, 15 pp.

ZTVA-StB. (1997). "Additional Technical Requirements and Instructions for Excavations in Road Constructions (Zusätzliche technische vertragsbedingungen und richtlinien für erdarbeiten im straßenbau)." *Road and Transportation Research Association*, Köln (in German).

Appendix A

DETERMINATION OF WEIGHTING FUNCTIONS FOR ISOTROPIC ORDINARY KRIGING OF MDP AND CMV DATA

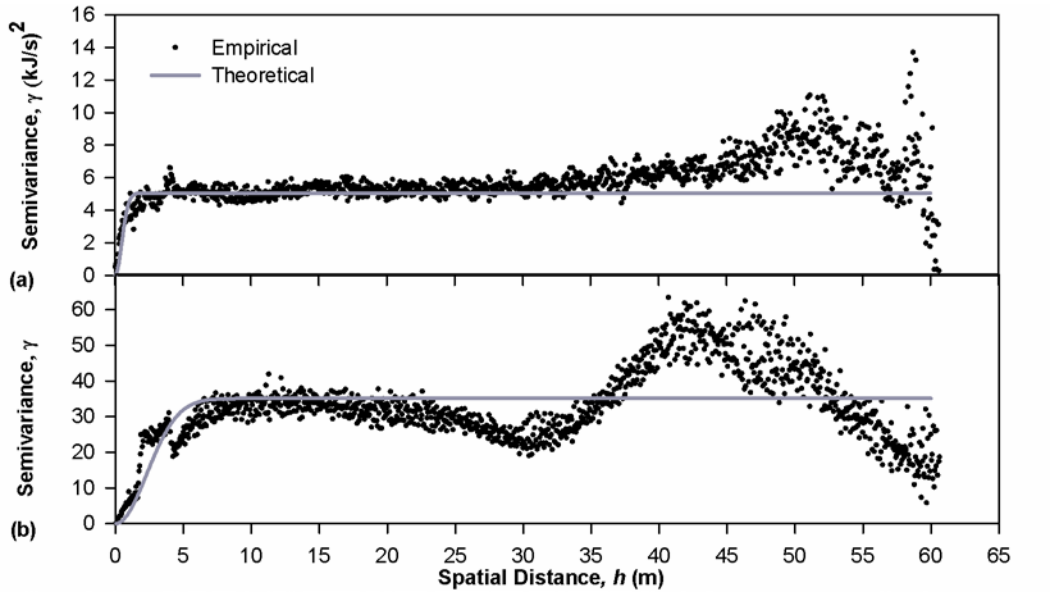

Figure A.1 Lift 0 CCC isotropic semivariograms: a) MDP; b) CMV.

Lift 0 isotropic ordinary kriging weighting function for MDP:

$$\gamma'(h,\theta) = 5.05\left(1 - \exp\left(-\frac{h}{0.70}\right)\right) \tag{A.1}$$

Lift 0 isotropic ordinary kriging weighting function for CMV:

$$\gamma'(h,\theta) = 35.08\left(1 - \exp\left(-\frac{h}{3.22}\right)\right) \tag{A.2}$$

Table A.1 Lift 0 CCC Theoretical Isotropic Semivariogram Model Parameters

CCC Measurement	Sill	Range
MDP	5.05065 $(kJ/s)^2$	0.69870 m
CMV	35.0775	3.22487 m

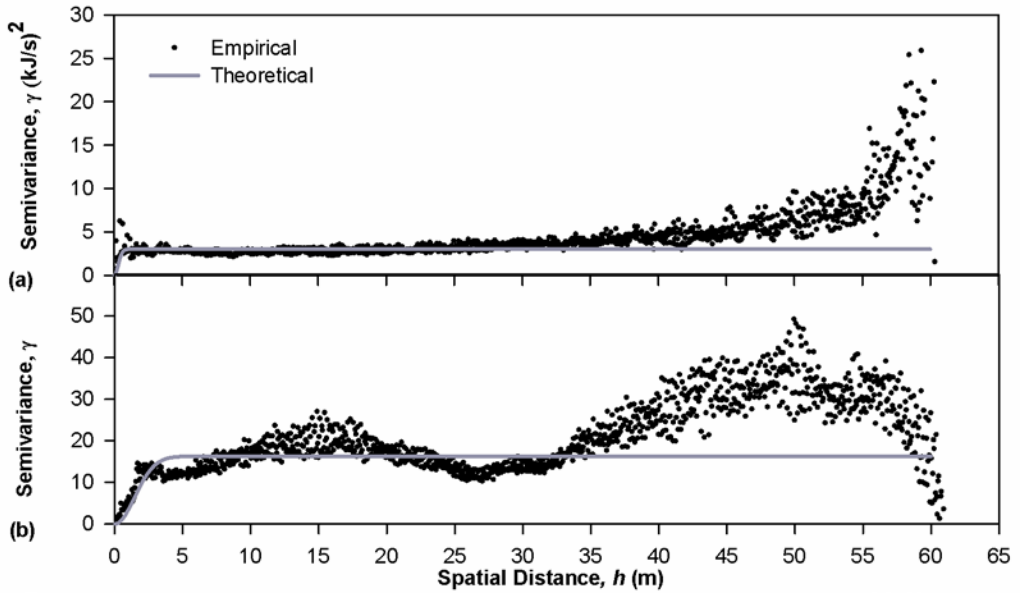

Figure A.2 Lift 2 CCC isotropic semivariograms: a) MDP; b) CMV.

Lift 2 isotropic ordinary kriging weighting function for MDP:

$$\gamma'(h,\theta) = 3.01\left(1-\exp\left(-\frac{h}{0.42}\right)\right) \tag{A.3}$$

Lift 2 isotropic ordinary kriging weighting function for CMV:

$$\gamma'(h,\theta) = 16.26\left(1-\exp\left(-\frac{h}{2.07}\right)\right) \tag{A.4}$$

Table A.2 Lift 2 CCC Theoretical Isotropic Semivariogram Model Parameters

CCC Measurement	Sill	Range
MDP	3.01366 $(kJ/s)^2$	0.42015 m
CMV	16.2647	2.07007 m

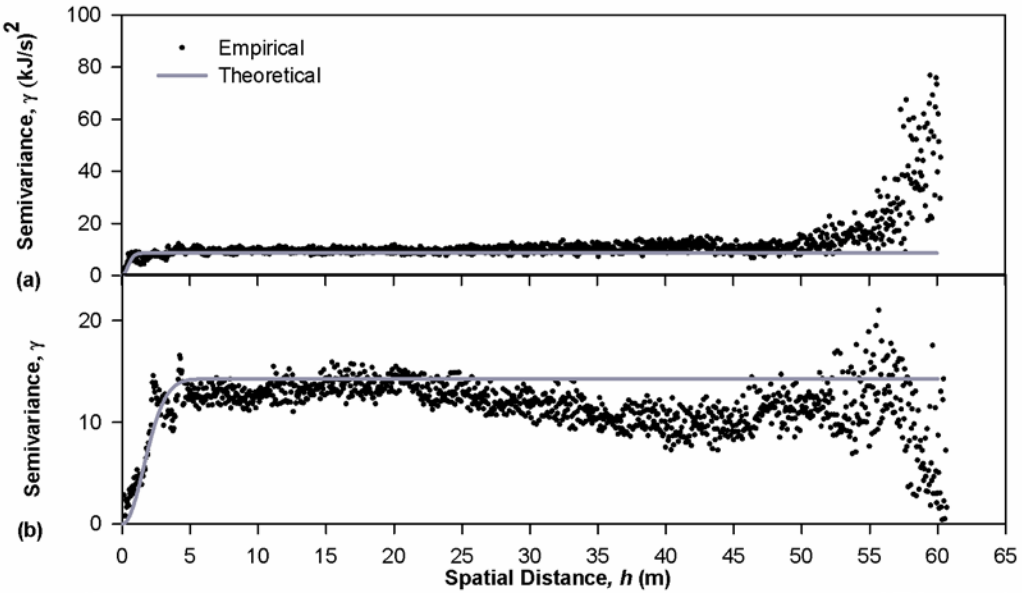

Figure A.3 Lift 4 CCC isotropic semivariograms: a) MDP; b) CMV.

Lift 4 isotropic ordinary kriging weighting function for MDP:

$$\gamma'(h,\theta) = 8.58\left(1-\exp\left(-\frac{h}{0.63}\right)\right) \tag{A.5}$$

Lift 4 isotropic ordinary kriging weighting function for CMV:

$$\gamma'(h,\theta) = 14.28\left(1-\exp\left(-\frac{h}{2.23}\right)\right) \tag{A.6}$$

Table A.3 Lift 4 CCC Theoretical Isotropic Semivariogram Model Parameters

CCC Measurement	Sill	Range
MDP	8.57653 $(kJ/s)^2$	0.62732 m
CMV	14.2811	2.22519 m

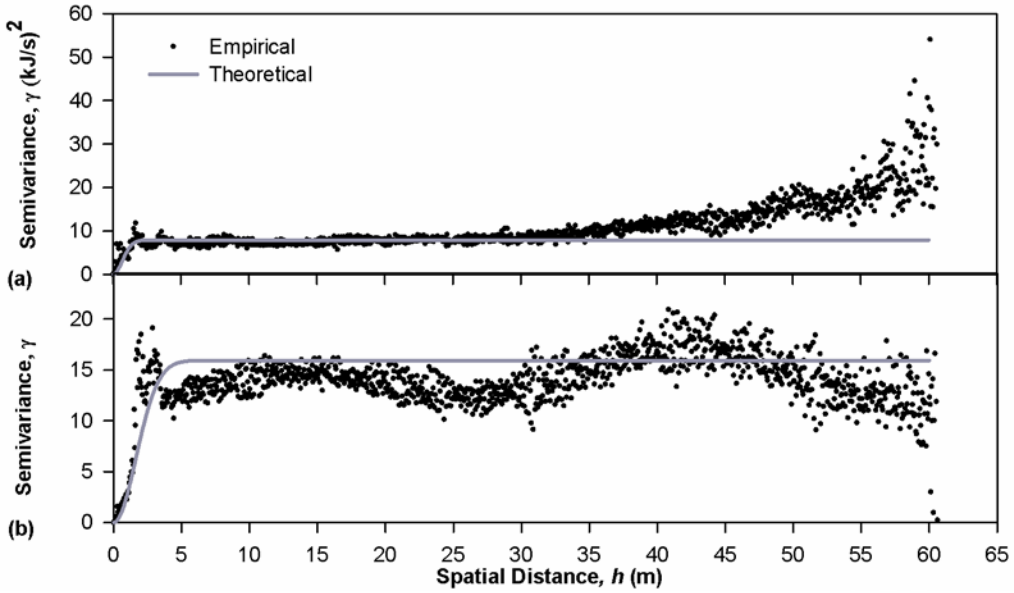

Figure A.4 Lift 5 Pass 1 CCC isotropic semivariograms: a) MDP; b) CMV.

Lift 5 Pass 1 isotropic ordinary kriging weighting function for MDP:

$$\gamma'(h,\theta) = 7.87\left(1-\exp\left(-\frac{h}{0.98}\right)\right) \tag{A.7}$$

Lift 5 Pass 1 isotropic ordinary kriging weighting function for CMV:

$$\gamma'(h,\theta) = 15.92\left(1-\exp\left(-\frac{h}{2.31}\right)\right) \tag{A.8}$$

Table A.4 Lift 5 Pass 1 CCC Theoretical Isotropic Semivariogram Model Parameters

CCC Measurement	Sill	Range
MDP	7.87483 $(kJ/s)^2$	0.97623 m
CMV	15.9249	2.30816 m

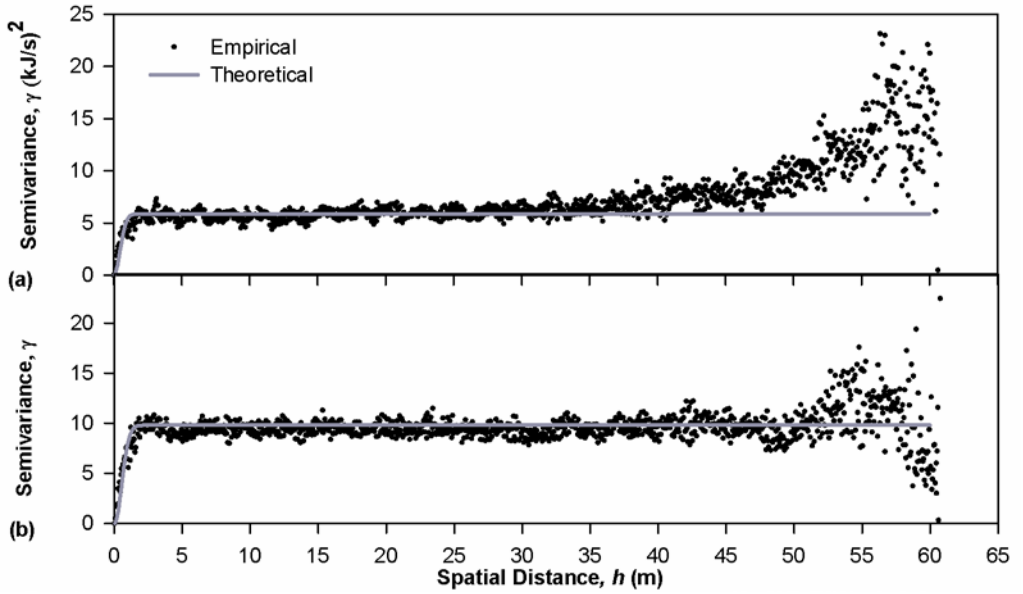

Figure A.5 Lift 5 Pass 2 CCC isotropic semivariograms: a) MDP; b) CMV.

Lift 5 Pass 2 isotropic ordinary kriging weighting function for MDP:

$$\gamma'(h,\theta) = 5.87\left(1-\exp\left(-\frac{h}{0.65}\right)\right) \tag{A.9}$$

Lift 5 Pass 2 isotropic ordinary kriging weighting function for CMV:

$$\gamma'(h,\theta) = 9.81\left(1-\exp\left(-\frac{h}{0.77}\right)\right) \tag{A.10}$$

Table A.5 Lift 5 Pass 2 CCC Theoretical Isotropic Semivariogram Model Parameters

CCC Measurement	Sill	Range
MDP	5.86992 $(kJ/s)^2$	0.65154 m
CMV	9.81336	0.76514 m

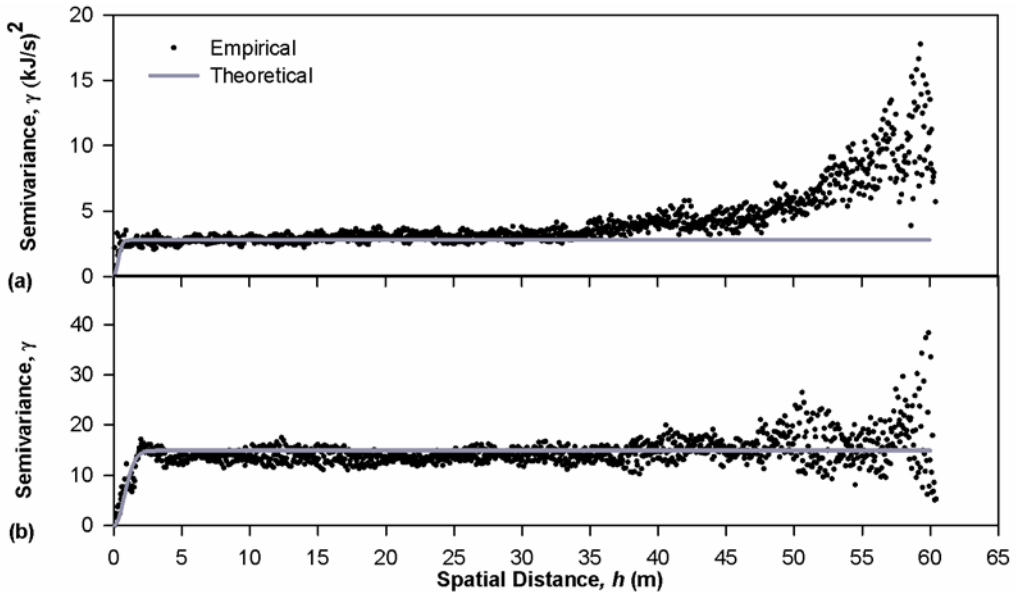

Figure A.6 Lift 5 Pass 3 CCC isotropic semivariograms: a) MDP; b) CMV.

Lift 5 Pass 3 isotropic ordinary kriging weighting function for MDP:

$$\gamma'(h,\theta) = 2.80\left(1-\exp\left(-\frac{h}{0.46}\right)\right) \tag{A.11}$$

Lift 5 Pass 3 isotropic ordinary kriging weighting function for CMV:

$$\gamma'(h,\theta) = 14.90\left(1-\exp\left(-\frac{h}{1.08}\right)\right) \tag{A.12}$$

Table A.6 Lift 5 Pass 3 CCC Theoretical Isotropic Semivariogram Model Parameters

CCC Measurement	Sill	Range
MDP	2.79728 $(kJ/s)^2$	0.45731 m
CMV	14.8977	1.08072 m

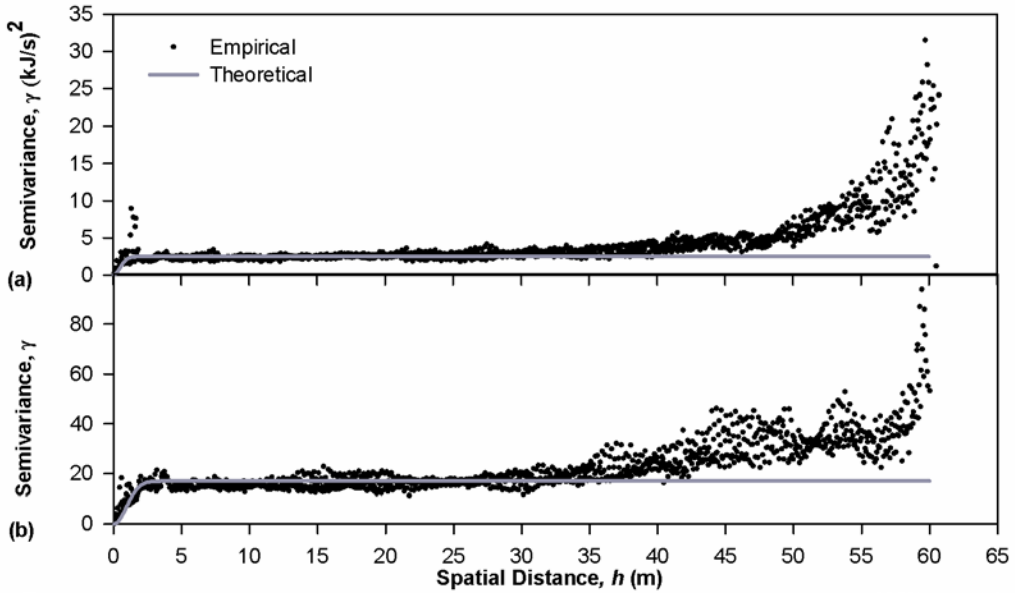

Figure A.7 Lift 5 Pass 4 CCC isotropic semivariograms: a) MDP; b) CMV.

Lift 5 Pass 4 isotropic ordinary kriging weighting function for MDP:

$$\gamma'(h,\theta) = 2.49\left(1-\exp\left(-\frac{h}{0.72}\right)\right) \tag{A.13}$$

Lift 5 Pass 4 isotropic ordinary kriging weighting function for CMV:

$$\gamma'(h,\theta) = 17.00\left(1-\exp\left(-\frac{h}{1.31}\right)\right) \tag{A.14}$$

Table A.7 Lift 5 Pass 4 CCC Theoretical Isotropic Semivariogram Model Parameters

CCC Measurement	Sill	Range
MDP	2.48635 $(kJ/s)^2$	0.71695 m
CMV	17.0005	1.31186 m

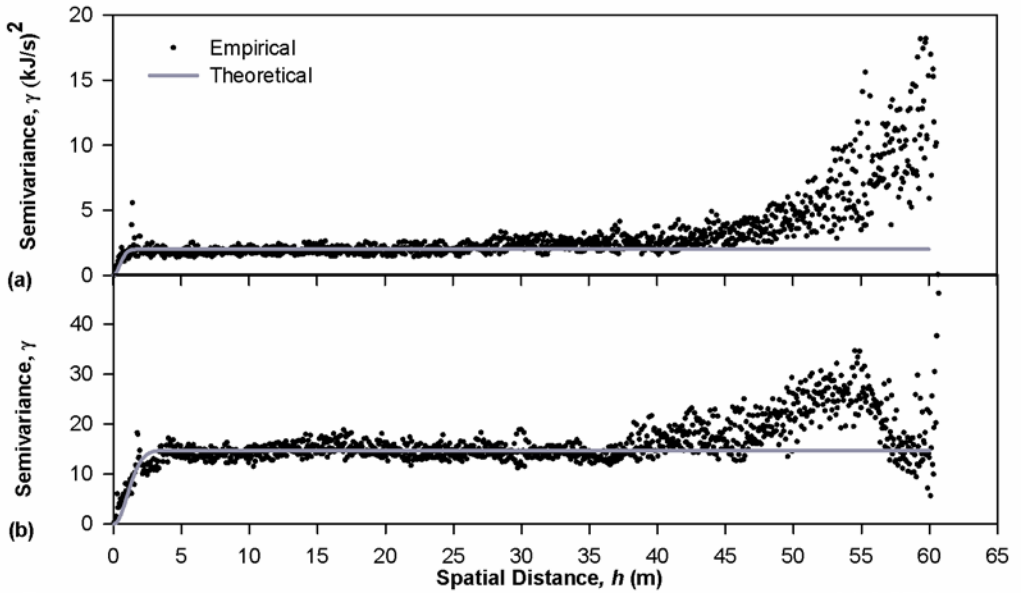

Figure A.8 Lift 5 Pass 5 CCC isotropic semivariograms: a) MDP; b) CMV.

Lift 5 Pass 5 isotropic ordinary kriging weighting function for MDP:

$$\gamma'(h,\theta) = 2.01\left(1-\exp\left(-\frac{h}{0.70}\right)\right) \tag{A.15}$$

Lift 5 Pass 5 isotropic ordinary kriging weighting function for CMV:

$$\gamma'(h,\theta) = 14.74\left(1-\exp\left(-\frac{h}{1.44}\right)\right) \tag{A.16}$$

Table A.8 Lift 5 Pass 5 CCC Theoretical Isotropic Semivariogram Model Parameters

CCC Measurement	Sill	Range
MDP	2.00821 $(kJ/s)^2$	0.70273 m
CMV	14.7449	1.44228 m

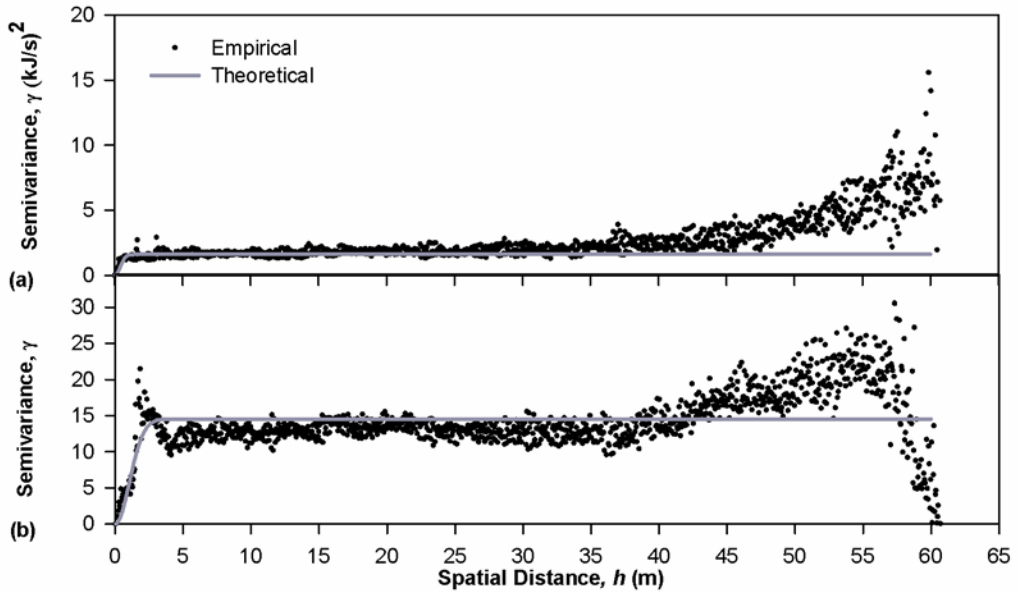

Figure A.9 Lift 5 Pass 7 CCC isotropic semivariograms: a) MDP; b) CMV.

Lift 5 Pass 7 isotropic ordinary kriging weighting function for MDP:

$$\gamma'(h,\theta) = 1.62\left(1-\exp\left(-\frac{h}{0.58}\right)\right) \tag{A.17}$$

Lift 5 Pass 7 isotropic ordinary kriging weighting function for CMV:

$$\gamma'(h,\theta) = 14.54\left(1-\exp\left(-\frac{h}{1.47}\right)\right) \tag{A.18}$$

Table A.9 Lift 5 Pass 7 CCC Theoretical Isotropic Semivariogram Model Parameters

CCC Measurement	Sill	Range
MDP	1.62237 $(kJ/s)^2$	0.57548 m
CMV	14.5383	1.47182 m

Appendix B

DETERMINATION OF WEIGHTING FUNCTIONS FOR ISOTROPIC ORDINARY KRIGING OF MDP AND CMV DATA

Table B.1 Regression Coefficients from the Univariate Regression Analyses that were Performed on Individual Data Points (Linear Model)

Dependent Variable vs. Independent Variable	All		All Excluding Base Layer		Finals		Finals Excluding Base Layer		Lift 5	
	C_0	C_1	C_0	C_1	C_0	C_1	C_0	C_1	C_0	C_1
MDP (kJ/s) vs. CMV	17.24	-0.4591	17.31	-0.4714	16.07	-0.4065	16.82	-0.4557	18.00	-0.4772
Geogauge *E* (MPa) vs. CMV	67.78	0.2565	65.36	0.4041	70.76	0.1039	67.89	0.2799	68.49	-0.1353
LWD 300 *E* (MPa) vs. CMV	24.83	0.1560	22.91	0.2190	28.03	0.0147	25.57	0.0998	20.09	0.2230
LWD 200 *E* (MPa) vs. CMV	24.00	0.4868	24.05	0.4806	25.01	0.4561	25.01	0.4561	24.56	0.2908
$DCPI_M$ (mm/blow) vs. CMV	51.93	-1.113	54.91	-1.228	50.31	-1.0548	54.23	-1.218	56.38	-1.360
$DCPI_A$ (mm/blow) vs. CMV	45.40	-0.9283	49.62	-1.102	41.69	-0.7753	47.13	-1.010	53.26	-1.264
NDG γ_d (kN/m^3) vs. CMV	17.86	0.0225	17.84	0.0297	17.81	0.0237	17.99	0.0222	17.72	0.0403
CMV vs. MDP (kJ/s)	26.39	-1.039	27.16	-1.125	26.55	-1.055	26.59	-1.061	31.34	-1.453
Geogauge *E* (MPa) vs. MDP (kJ/s)	82.93	-1.116	84.10	-1.254	86.79	-1.567	86.50	-1.542	61.30	0.4939
LWD 300 *E* (MPa) vs. MDP (kJ/s)	32.50	-0.6083	33.08	-0.7517	28.68	-0.1178	29.88	-0.3422	25.42	-0.1570
LWD 200 *E* (MPa) vs. MDP (kJ/s)	41.36	-0.9924	42.46	-1.120	39.81	-0.7737	39.81	-0.7737	32.41	-0.2947
$DCPI_M$ (mm/blow) vs. MDP (kJ/s)	19.47	1.572	18.13	1.815	19.89	1.499	18.44	1.771	10.01	2.354
$DCPI_A$ (mm/blow) vs. MDP (kJ/s)	17.37	1.435	16.03	1.699	19.63	1.117	17.52	1.487	10.38	2.166
NDG γ_d (kN/m^3) vs. MDP (kJ/s)	18.85	-0.0614	18.93	-0.0626	18.96	-0.0765	18.47	-0.0070	19.17	-0.0766

Table B.2 Regression Coefficients from the Univariate Regression Analyses that were Performed on Individual Data Points for Moisture Content (Linear Model)

Dependent Variable vs. Independent Variable	All		All Excluding Base Layer		Finals		Finals Excluding Base Layer		Lift 5	
	C_0	C_1	C_0	C_1	C_0	C_1	C_0	C_1	C_0	C_1
Lab ω vs. CMV	21.43	-0.5351	37.77	-2.207	18.04	-0.0291	35.86	-1.9713	50.67	-3.451
NDG ω vs. CMV	21.31	-0.5464	31.55	-1.552	16.08	0.1597	26.42	-0.9439	49.57	-3.241
Lab ω vs. MDP (kJ/s)	3.609	0.6449	-5.402	1.535	7.703	0.0484	-0.7098	0.9174	-8.240	1.869
NDG ω vs. MDP (kJ/s)	1.980	0.8357	-4.865	1.467	7.893	0.0887	1.389	0.7365	-7.168	1.713

Table B.3 Regression Coefficients from the Univariate Regression Analyses that were Performed on Individual Data Points (Polynomial Model)

Dependent Variable vs. Independent Variable	All			All Excluding Base Layer		
	C_0	C_1	C_2	C_0	C_1	C_2
MDP (kJ/s) vs. CMV	22.05	-1.088	0.0192	21.59	-1.019	0.0165
Geogauge *E* (MPa) vs. CMV	73.11	-0.4414	0.0213	75.38	-0.8779	0.0385
LWD 300 *E* (MPa) vs. CMV	33.52	-0.9798	0.0347	26.56	-0.2484	0.0140
LWD 200 *E* (MPa) vs. CMV	31.28	-0.4546	0.0285	31.69	-0.4978	0.0294
$DCPI_M$ (mm/blow) vs. CMV	52.77	-1.223	0.0034	65.10	-2.532	0.0392
$DCPI_A$ (mm/blow) vs. CMV	35.41	0.3786	-0.0399	52.66	-1.491	0.0117
NDG γ_d (kN/m^3) vs. CMV	16.78	0.1632	-0.0042	17.02	0.1335	-0.0031
CMV vs. MDP (kJ/s)	22.75	-0.2534	-0.0391	20.92	0.2582	-0.0709
Geogauge *E* (MPa) vs. MDP (kJ/s)	115.21	-7.6204	0.3012	118.19	-8.268	0.3329
LWD 300 *E* (MPa) vs. MDP (kJ/s)	29.25	0.0459	-0.0303	35.02	-1.151	0.0190
LWD 200 *E* (MPa) vs. MDP (kJ/s)	44.92	-1.713	0.0333	44.04	-1.445	0.0154
$DCPI_M$ (mm/blow) vs. MDP (kJ/s)	27.70	-0.0879	0.0769	22.24	0.9696	0.0401
$DCPI_A$ (mm/blow) vs. MDP (kJ/s)	24.83	-0.0686	0.0696	17.05	1.490	0.0100
NDG γ_d (kN/m^3) vs. MDP (kJ/s)	18.54	-0.0007	-0.0027	17.80	0.1620	-0.0103

Table B.3 cont.

Dependent Variable vs. Independent Variable	Finals			Finals Excluding Base Layer			Lift 5		
	C_0	C_1	C_2	C_0	C_1	C_2	C_0	C_1	C_2
MDP (kJ/s) vs. CMV	20.88	-1.013	0.0179	23.00	-1.217	0.0222	24.53	-1.366	0.0283
Geogauge *E* (MPa) vs. CMV	81.67	-1.2720	0.0407	85.78	-1.927	0.0643	72.29	-0.6532	0.0165
LWD 300 *E* (MPa) vs. CMV	39.76	-1.4647	0.0438	31.40	-0.6199	0.0210	23.89	-0.2939	0.0164
LWD 200 *E* (MPa) vs. CMV	32.36	-0.4503	0.0264	32.36	-0.4503	0.0264	33.86	-0.9746	0.0402
$DCPI_M$ (mm/blow) vs. CMV	58.08	-2.035	0.0290	72.34	-3.453	0.0651	55.30	-1.213	-0.0047
$DCPI_A$ (mm/blow) vs. CMV	33.24	0.2906	-0.0315	53.47	-1.792	0.0228	53.86	-1.346	0.0026
NDG γ_d (kN/m^3) vs. CMV	16.44	0.1933	-0.0049	16.83	0.1571	-0.0037	17.16	0.1162	-0.0024
CMV vs. MDP (kJ/s)	21.92	-0.0102	-0.0545	21.56	0.0754	-0.0591	23.20	0.1073	-0.0711
Geogauge *E* (MPa) vs. MDP (kJ/s)	142.62	-13.96	0.6441	146.18	-14.79	0.6870	100.89	-7.102	0.3463
LWD 300 *E* (MPa) vs. MDP (kJ/s)	46.98	-4.177	0.2110	56.04	-6.148	0.3011	47.46	-4.385	0.1927
LWD 200 *E* (MPa) vs. MDP (kJ/s)	63.97	-6.137	0.2782	63.97	-6.137	0.2782	67.74	-7.074	0.3090
$DCPI_M$ (mm/blow) vs. MDP (kJ/s)	42.65	-3.552	0.2626	32.61	-1.376	0.1632	-18.73	7.868	-0.2514
$DCPI_A$ (mm/blow) vs. MDP (kJ/s)	32.38	-1.714	0.1472	20.23	0.8849	0.0312	-21.34	8.251	-0.2774
NDG γ_d (kN/m^3) vs. MDP (kJ/s)	17.44	0.2750	-0.0194	17.17	0.2980	-0.0169	17.84	0.1769	-0.0115

Table B.4 Regression Coefficients from the Univariate Regression Analyses that were Performed on Individual Data Points for Moisture Content (Polynomial Model)

Dependent Variable vs. Independent Variable	All			All Excluding Base Layer		
	C_0	C_1	C_2	C_0	C_1	C_2
Lab ω vs. CMV	-19.82	10.11	-0.6515	-36.71	13.81	-0.8490
NDG ω vs. CMV	-27.94	11.34	-0.6860	-21.80	9.988	-0.6121
Lab ω vs. MDP (kJ/s)	22.75	-4.123	0.2827	-26.10	5.899	-0.2267
NDG ω vs. MDP (kJ/s)	27.17	-4.920	0.3151	10.25	-1.648	0.1573

Table B.4 cont.

Dependent Variable vs. Independent Variable	Finals			Finals Excluding Base Layer			Lift 5		
	C_0	C_1	C_2	C_0	C_1	C_2	C_0	C_1	C_2
Lab ω vs. CMV	-19.37	10.04	-0.6446	-51.84	17.03	-1.016	-22.35	11.35	-0.7462
NDG ω vs. CMV	-33.05	12.71	-0.7687	-91.83	25.82	-1.489	44.96	-2.350	-0.0428
Lab ω vs. MDP (kJ/s)	23.14	-3.889	0.2389	-0.7595	0.9279	-0.0006	46.08	-9.139	0.5551
NDG ω vs. MDP (kJ/s)	20.09	-2.889	0.1739	-34.99	8.690	-0.4262	4.892	-0.6202	0.1122

Table B.5 Regression Coefficients from the Univariate Regression Analyses that were Performed on Average Data (Linear Model)

Dependent Variable vs. Independent Variable	All		All Excluding Base Layer		Finals		Finals Excluding Base Layer		Lift 5	
	C_0	C_1	C_0	C_1	C_0	C_1	C_0	C_1	C_0	C_1
MDP (kJ/s) vs. CMV	22.36	-0.7697	22.37	-0.7699	22.84	-0.8068	22.37	-0.7699	20.95	-0.6533
Geogauge *E* (MPa) vs. CMV	65.15	0.3878	65.11	0.3886	67.18	0.3086	65.11	0.3886	74.60	-0.4299
LWD 300 *E* (MPa) vs. CMV	24.36	0.2039	21.44	0.2592	39.44	-0.5489	21.44	0.2592	23.22	0.0325
LWD 200 *E* (MPa) vs. CMV	25.25	0.3597	25.25	0.3597	26.79	0.3514	25.25	0.3597	28.82	0.0199
$DCPI_M$ (mm/blow) vs. CMV	57.25	-1.499	60.50	-1.560	49.42	-1.155	60.50	-1.560	58.89	-1.458
$DCPI_A$ (mm/blow) vs. CMV	51.73	-1.366	55.98	-1.446	35.26	-0.5765	55.98	-1.446	54.98	-1.316
NDG γ_d (kN/m^3) vs. CMV	17.41	0.0494	17.58	0.0461	16.84	0.0781	17.58	0.0461	17.40	0.0601
CMV vs. MDP (kJ/s)	27.98	-1.197	27.99	-1.197	26.80	-1.082	27.99	-1.197	32.02	-1.527
Geogauge *E* (MPa) vs. MDP (kJ/s)	80.36	-0.8606	80.36	-0.8605	85.36	-1.387	80.36	-0.8605	65.25	0.2261
LWD 300 *E* (MPa) vs. MDP (kJ/s)	36.90	-0.9884	34.53	-0.9273	25.72	0.3940	34.53	-0.9273	31.58	-0.7722
LWD 200 *E* (MPa) vs. MDP (kJ/s)	43.02	-1.204	43.02	-1.204	40.18	-0.8089	43.02	-1.204	38.70	-0.9439
$DCPI_M$ (mm/blow) vs. MDP (kJ/s)	15.81	1.830	18.36	1.764	22.64	0.9597	18.36	1.764	13.68	2.076
$DCPI_A$ (mm/blow) vs. MDP (kJ/s)	12.73	1.799	16.04	1.713	23.04	0.4550	16.04	1.713	14.81	1.811
NDG γ_d (kN/m^3) vs. MDP (kJ/s)	18.86	-0.0634	18.99	-0.0668	18.95	-0.0809	18.99	-0.0668	19.37	-0.0961

Table B.6 Regression Coefficients from the Univariate Regression Analyses that were Performed on Average Data for Moisture Content (Linear Model)

Dependent Variable vs. Independent Variable	All		All Excluding Base Layer		Finals		Finals Excluding Base Layer		Lift 5	
	C_0	C_1	C_0	C_1	C_0	C_1	C_0	C_1	C_0	C_1
Lab ω vs. CMV	20.02	-0.4989	42.54	-2.715	17.94	-0.1732	42.54	-2.715	71.22	-5.495
NDG ω vs. CMV	21.60	-0.6624	36.60	-2.124	17.72	-0.1490	36.60	-2.124	80.65	-6.260
Lab ω vs. MDP (kJ/s)	6.200	0.4987	-10.02	2.077	8.512	0.0972	-10.02	2.077	-26.04	3.739
NDG ω vs. MDP (kJ/s)	1.768	0.9361	-12.25	2.254	8.152	0.1386	-12.25	2.254	-27.07	3.636

Table B.7 Regression Coefficients from the Univariate Regression Analyses that were Performed on Average Data (Polynomial Model)

Dependent Variable vs. Independent Variable	All			All Excluding Base Layer		
	C_0	C_1	C_2	C_0	C_1	C_2
MDP (kJ/s) vs. CMV	18.76	-0.2676	-0.0168	17.51	-0.0853	-0.0229
Geogauge *E* (MPa) vs. CMV	80.65	-1.775	0.0722	85.75	-2.516	0.0971
LWD 300 *E* (MPa) vs. CMV	-18.27	6.148	-0.1984	44.70	-3.013	0.1094
LWD 200 *E* (MPa) vs. CMV	61.67	-4.765	0.1713	61.67	-4.765	0.1713
$DCPI_M$ (mm/blow) vs. CMV	71.13	-3.434	0.0646	-7.549	8.014	-0.3201
$DCPI_A$ (mm/blow) vs. CMV	90.36	-6.753	0.1798	-7.386	7.470	-0.2981
NDG γ_d (kN/m^3) vs. CMV	21.35	-0.4997	0.0183	17.98	-0.0091	0.0018
CMV vs. MDP (kJ/s)	16.97	1.062	-0.1093	14.69	1.56	-0.1330
Geogauge *E* (MPa) vs. MDP (kJ/s)	111.03	-6.590	0.2493	114.14	-7.237	0.2780
LWD 300 *E* (MPa) vs. MDP (kJ/s)	13.41	3.401	-0.1910	31.18	-0.2946	-0.0276
LWD 200 *E* (MPa) vs. MDP (kJ/s)	39.34	-0.5086	-0.0303	39.34	-0.5086	-0.0303
$DCPI_M$ (mm/blow) vs. MDP (kJ/s)	32.53	-1.292	0.1359	12.54	2.862	-0.0479
$DCPI_A$ (mm/blow) vs. MDP (kJ/s)	31.31	-1.674	0.1511	5.001	3.796	-0.0908
NDG γ_d (kN/m^3) vs. MDP (kJ/s)	18.92	-0.0760	0.0006	17.80	0.1585	-0.0098

Table B.7 cont.

Dependent Variable vs. Independent Variable	Finals			Finals Excluding Base Layer			Lift 5		
	C_0	C_1	C_2	C_0	C_1	C_2	C_0	C_1	C_2
MDP (kJ/s) vs. CMV	34.33	-2.280	0.0458	220.71	-26.82	0.8201	20.74	-0.6234	-0.0010
Geogauge *E* (MPa) vs. CMV	-16.72	11.060	-0.3344	-1613.69	221.30	-6.9688	63.54	1.170	-0.0546
LWD 300 *E* (MPa) vs. CMV	-307.73	43.938	-1.3835	-539.12	74.40	-2.3448	45.46	-3.182	0.1097
LWD 200 *E* (MPa) vs. CMV	-595.06	82.077	-2.5767	-595.06	82.08	-2.5767	58.57	-4.279	0.1467
$DCPI_M$ (mm/blow) vs. CMV	442.56	-51.533	1.5667	-7.856	7.764	-0.3045	-12.74	8.894	-0.3533
$DCPI_A$ (mm/blow) vs. CMV	529.28	-63.881	1.9688	229.99	-24.48	0.7254	-15.64	8.890	-0.3483
NDG γ_d (kN/m^3) vs. CMV	39.61	-2.840	0.0907	39.45	-2.819	0.0901	18.58	-0.1100	0.0058
CMV vs. MDP (kJ/s)	12.23	2.160	-0.1695	1.911	4.454	-0.2843	31.11	-1.360	-0.0073
Geogauge *E* (MPa) vs. MDP (kJ/s)	169.72	-19.808	0.9557	195.09	-25.24	1.2175	44.21	3.819	-0.1446
LWD 300 *E* (MPa) vs. MDP (kJ/s)	16.77	2.349	-0.1014	77.87	-10.73	0.5290	5.388	3.702	-0.1800
LWD 200 *E* (MPa) vs. MDP (kJ/s)	74.83	-8.345	0.3855	74.83	-8.345	0.3855	5.126	4.791	-0.2308
$DCPI_M$ (mm/blow) vs. MDP (kJ/s)	90.30	-13.814	0.7665	30.39	-0.9892	0.1483	-27.76	9.153	-0.2848
$DCPI_A$ (mm/blow) vs. MDP (kJ/s)	84.32	-12.925	0.6942	4.908	4.073	-0.1252	-28.60	9.225	-0.2984
NDG γ_d (kN/m^3) vs. MDP (kJ/s)	20.01	-0.312	0.0120	16.00	0.5467	-0.0294	19.74	-0.1595	0.0026

Table B.8 Regression Coefficients from the Univariate Regression Analyses that were Performed on Average Data for Moisture Content (Polynomial Model)

Dependent Variable vs. Independent Variable	All			All Excluding Base Layer		
	C_0	C_1	C_2	C_0	C_1	C_2
Lab ω vs. CMV	-31.57	13.02	-0.8259	-80.87	23.35	-1.362
NDG ω vs. CMV	-52.44	17.55	-1.065	-96.06	26.91	-1.560
Lab ω vs. MDP (kJ/s)	33.99	-6.718	0.4371	-182.52	38.27	-1.880
NDG ω vs. MDP (kJ/s)	51.25	-10.71	0.6526	30.10	-6.531	0.4480

Table B.8 cont.

Dependent Variable vs. Independent Variable	Finals			Finals Excluding Base Layer			Lift 5		
	C_0	C_1	C_2	C_0	C_1	C_2	C_0	C_1	C_2
Lab ω vs. CMV	-30.66	12.67	-0.7940	-139.62	35.38	-1.964	11747.92	-2356.94	118.12
NDG ω vs. CMV	-62.00	20.17	-1.239	-364.77	88.33	-5.019	-35.07	16.16	-1.084
Lab ω vs. MDP (kJ/s)	41.66	-8.509	0.5210	-12.48	2.739	-0.0562	-3858.17	775.51	-38.78
NDG ω vs. MDP (kJ/s)	49.38	-10.15	0.6118	-56.28	12.97	-0.6340	-66.41	10.87	-0.3308

Table B.9 Regression Coefficients from the Multivariate Regression Analyses that were Performed on Individual Data Points (Without Interaction Term)

Dependent Variable vs. Independent Variable	All			All Excluding Base Layer		
	C_0	C_1	C_2	C_0	C_1	C_2
MDP (kJ/s) vs. CMV	10.30	-0.3050	0.4736	2.902	-0.2458	1.109
Geogauge *E* (MPa) vs. CMV	97.50	0.0263	-2.817	131.13	-0.2634	-5.673
LWD 300 *E* (MPa) vs. CMV	56.05	-0.0461	-3.013	46.64	0.0116	-2.175
LWD 200 *E* (MPa) vs. CMV	49.76	0.1841	-2.182	49.76	0.1841	-2.182
$DCPI_M$ (mm/blow) vs. CMV	20.11	-0.8371	2.861	33.75	-0.9913	1.764
$DCPI_A$ (mm/blow) vs. CMV	2.469	-0.5866	3.968	21.37	-0.8348	2.497
NDG γ_d (kN/m^3) vs. CMV	16.76	0.0320	0.1017	17.92	0.0288	-0.0067
CMV vs. MDP (kJ/s)	26.41	-1.303	0.2827	24.28	-1.498	0.6804
Geogauge *E* (MPa) vs. MDP (kJ/s)	96.71	-0.7555	-1.815	112.09	0.1003	-4.123
LWD 300 *E* (MPa) vs. MDP (kJ/s)	54.85	0.0507	-3.017	47.61	-0.3092	-1.970
LWD 200 *E* (MPa) vs. MDP (kJ/s)	53.17	-0.9396	-1.285	53.17	-0.9396	-1.285
$DCPI_M$ (mm/blow) vs. MDP (kJ/s)	-0.8140	0.9607	2.668	8.930	1.443	1.270
$DCPI_A$ (mm/blow) vs. MDP (kJ/s)	-10.30	0.5725	3.699	1.681	1.214	1.928
NDG γ_d (kN/m^3) vs. MDP (kJ/s)	18.08	-0.1078	0.1266	18.72	-0.0729	0.0311

Table B.9 cont.

Dependent Variable vs. Independent Variable	Finals			Finals Excluding Base Layer			Lift 5		
	C_0	C_1	C_2	C_0	C_1	C_2	C_0	C_1	C_2
MDP (kJ/s) vs. CMV	10.72	-0.2603	0.3099	1.524	-0.2053	1.170	10.92	-0.3615	0.5046
Geogauge *E* (MPa) vs. CMV	100.79	0.0434	-3.339	148.04	-0.2720	-7.703	114.18	-0.4099	-3.854
LWD 300 *E* (MPa) vs. CMV	58.16	-0.0359	-3.303	49.21	-0.0396	-2.361	37.47	0.0659	-1.412
LWD 200 *E* (MPa) vs. CMV	48.45	0.2437	-2.139	48.45	0.2437	-2.139	42.83	0.1058	-1.455
$DCPI_M$ (mm/blow) vs. CMV	20.56	-0.8558	2.811	37.57	-1.030	1.358	35.28	-1.144	1.775
$DCPI_A$ (mm/blow) vs. CMV	2.583	-0.5443	3.814	25.68	-0.8201	1.907	29.85	-1.026	1.964
NDG γ_d (kN/m^3) vs. CMV	16.56	0.0207	0.1518	17.73	0.0240	0.025	18.60	0.0340	-0.0766
CMV vs. MDP (kJ/s)	23.47	-1.130	0.4631	20.63	-1.483	1.079	39.53	-1.394	-0.8671
Geogauge *E* (MPa) vs. MDP (kJ/s)	112.11	-2.144	-2.282	121.05	-1.027	-4.140	99.70	0.8246	-3.916
LWD 300 *E* (MPa) vs. MDP (kJ/s)	51.11	0.5454	-3.054	47.11	0.2271	-2.377	40.92	0.0322	-1.674
LWD 200 *E* (MPa) vs. MDP (kJ/s)	50.38	-0.5466	-1.305	50.38	-0.5466	-1.305	46.15	-0.2746	-1.337
$DCPI_M$ (mm/blow) vs. MDP (kJ/s)	2.689	0.5823	2.610	9.815	1.313	1.278	-4.696	2.365	1.497
$DCPI_A$ (mm/blow) vs. MDP (kJ/s)	-4.134	-0.0221	3.518	3.989	0.9252	1.892	-6.410	2.062	1.811
NDG γ_d (kN/m^3) vs. MDP (kJ/s)	17.63	-0.0869	0.1554	18.07	-0.0276	0.0604	19.79	-0.0699	-0.0689

Table B.10 Regression Coefficients from the Multivariate Regression Analyses that were Performed on Individual Data Points (With Interaction Term)

Dependent Variable vs. Independent Variable	All				All Excluding Base Layer			
	C_0	C_1	C_2	C_3	C_0	C_1	C_2	C_3
MDP (kJ/s) vs. CMV	7.5915	-0.1175	0.7777	-0.0212	-3.109	0.1239	1.729	-0.0388
Geogauge *E* (MPa) vs. CMV	86.07	0.8171	-1.535	-0.0892	111.92	0.9181	-3.691	-0.1239
LWD 300 *E* (MPa) vs. CMV	48.83	0.4533	-2.203	-0.0564	37.57	0.5692	-1.240	-0.0585
LWD 200 *E* (MPa) vs. CMV	28.90	1.467	-0.0304	-0.1345	28.90	1.467	-0.0304	-0.1345
$DCPI_M$ (mm/blow) vs. CMV	4.4468	0.2467	4.619	-0.1223	-1.111	1.153	5.360	-0.2248
$DCPI_A$ (mm/blow) vs. CMV	-17.46	0.7918	6.203	-0.1555	1.804	0.3683	4.515	-0.1261
NDG γ_d (kN/m^3) vs. CMV	18.58	-0.0937	-0.1022	0.0142	20.68	-0.1413	-0.2920	0.0178
CMV vs. MDP (kJ/s)	8.0495	0.4975	2.345	-0.1986	4.063	0.9417	2.769	-0.2455
Geogauge *E* (MPa) vs. MDP (kJ/s)	152.13	-6.321	-7.274	0.5350	145.03	-3.847	-7.150	0.3570
LWD 300 *E* (MPa) vs. MDP (kJ/s)	46.81	0.8585	-2.225	-0.0777	48.29	-0.3902	-2.032	0.0073
LWD 200 *E* (MPa) vs. MDP (kJ/s)	48.48	-0.3783	-0.8547	-0.0508	48.48	-0.3783	-0.8547	-0.0508
$DCPI_M$ (mm/blow) vs. MDP (kJ/s)	8.8363	-0.0084	1.717	0.0932	6.848	1.692	1.461	-0.0226
$DCPI_A$ (mm/blow) vs. MDP (kJ/s)	5.4274	-1.006	2.150	0.1518	-2.171	1.675	2.282	-0.0417
NDG γ_d (kN/m^3) vs. MDP (kJ/s)	17.43	-0.0428	0.1904	-0.0063	16.80	0.1573	0.2076	-0.0208

Table B.10 cont.

Dep. Variable vs. Ind. Variable	Finals				Finals Excluding Base Layer				Lift 5			
	C_0	C_1	C_2	C_3	C_0	C_1	C_2	C_3	C_0	C_1	C_2	C_3
MDP (kJ/s) vs. CMV	9.676	-0.1903	0.4381	-0.0085	-8.547	0.3857	2.278	-0.0656	6.035	-0.0581	0.9717	-0.0294
Geogauge *E* (MPa) vs. CMV	72.95	1.903	0.0645	-0.2253	113.52	1.754	-3.904	-0.2248	132.35	-1.539	-5.591	0.1093
LWD 300 *E* (MPa) vs. CMV	48.61	0.6026	-2.135	-0.0773	33.03	0.9098	-0.5805	-0.1053	23.73	0.9196	-0.0983	-0.0826
LWD 200 *E* (MPa) vs. CMV	15.72	2.165	1.463	-0.2131	15.72	2.165	1.463	-0.2131	57.49	-0.81	-2.857	0.0882
$DCPI_M$ (mm/blow) vs. CMV	-20.20	1.867	7.794	-0.3298	-77.26	5.709	14.00	-0.7476	121.70	-6.513	-6.488	0.5197
$DCPI_A$ (mm/blow) vs. CMV	-37.79	2.153	8.751	-0.3267	-43.73	3.254	9.546	-0.4519	99.49	-5.352	-4.694	0.4188
NDG γ_d (kN/m^3) vs. CMV	18.70	-0.1220	-0.1093	0.0173	22.73	-0.2695	-0.5253	0.0326	17.72	0.0889	0.0079	-0.0053
CMV vs. MDP (kJ/s)	8.171	0.4032	2.288	-0.1819	-1.578	1.463	3.441	-0.3072	48.60	-2.26	-1.749	0.0834
Geogauge *E* (MPa) vs. MDP (kJ/s)	175.51	-9.003	-9.581	0.7893	162.25	-6.692	-8.430	0.5816	116.19	-0.7504	-5.521	0.1517
LWD 300 *E* (MPa) vs. MDP (kJ/s)	39.77	1.772	-1.749	-0.1411	50.87	-0.2902	-2.769	0.0531	72.41	-2.975	-4.737	0.2897
LWD 200 *E* (MPa) vs. MDP (kJ/s)	74.32	-3.839	-3.799	0.3380	74.32	-3.839	-3.799	0.3380	44.05	-0.0747	-1.133	-0.0193
$DCPI_M$ (mm/blow) vs. MDP (kJ/s)	40.21	-3.476	-1.709	0.4671	47.46	-3.863	-2.642	0.5313	-122.62	13.63	12.97	-1.085
$DCPI_A$ (mm/blow) vs. MDP (kJ/s)	42.23	-5.037	-1.819	0.5772	16.43	-0.7856	0.5966	0.1756	-106.92	11.66	11.59	-0.9246
NDG γ_d (kN/m^3) vs. MDP (kJ/s)	20.24	-0.3693	-0.1451	0.0325	18.11	-0.0329	0.0564	0.0005	20.86	-0.1715	-0.1724	0.0098

Table B.11 Regression Coefficients from the Multivariate Regression Analyses that were Performed on Average Data (Without Interaction Term)

Dependent Variable vs. Independent Variable	All			All Excluding Base Layer		
	C_0	C_1	C_2	C_0	C_1	C_2
MDP (kJ/s) vs. CMV	19.13	-0.6506	0.1409	8.72	-0.4866	0.9152
Geogauge *E* (MPa) vs. CMV	82.55	0.1513	-1.466	151.63	-0.9370	-6.603
LWD 300 *E* (MPa) vs. CMV	69.02	-0.4937	-3.590	64.96	-0.4299	-3.288
LWD 200 *E* (MPa) vs. CMV	74.30	-0.4213	-3.700	74.30	-0.4213	-3.700
$DCPI_M$ (mm/blow) vs. CMV	14.83	-0.8291	3.431	43.96	-1.288	1.264
$DCPI_A$ (mm/blow) vs. CMV	-7.281	-0.4293	4.747	19.81	-0.86	2.732
NDG γ_d (kN/m^3) vs. CMV	15.06	0.0858	0.1880	16.63	0.0610	0.0711
CMV vs. MDP (kJ/s)	28.54	-1.36	0.1132	18.58	-1.981	1.738
Geogauge *E* (MPa) vs. MDP (kJ/s)	86.23	-0.6755	-0.8176	112.30	0.5444	-4.578
LWD 300 *E* (MPa) vs. MDP (kJ/s)	59.23	0.1083	-3.486	53.41	-0.1641	-2.646
LWD 200 *E* (MPa) vs. MDP (kJ/s)	58.29	-0.6557	-2.080	58.29	-0.6557	-2.080
$DCPI_M$ (mm/blow) vs. MDP (kJ/s)	-6.463	0.8119	3.414	12.45	1.697	0.6851
$DCPI_A$ (mm/blow) vs. MDP (kJ/s)	-16.64	0.3688	4.581	2.216	1.251	1.862
NDG γ_d (kN/m^3) vs. MDP (kJ/s)	17.75	-0.1330	0.1871	18.18	-0.1126	0.1241

Table B.11 cont.

Dependent Variable vs. Independent Variable	Finals			Finals Excluding Base Layer			Lift 5		
	C_0	C_1	C_2	C_0	C_1	C_2	C_0	C_1	C_2
MDP (kJ/s) vs. CMV	21.75	-0.7834	0.0850	9.054	-0.5440	0.998	8.999	-0.4581	0.8375
Geogauge *E* (MPa) vs. CMV	81.40	0.2733	-1.612	199.69	-1.957	-10.12	48.30	-0.0937	2.029
LWD 300 *E* (MPa) vs. CMV	73.09	-0.7576	-3.554	71.19	-0.7218	-3.417	70.89	-0.4015	-3.919
LWD 200 *E* (MPa) vs. CMV	74.81	-0.4608	-3.694	74.81	-0.4608	-3.694	92.35	-0.5754	-5.196
$DCPI_M$ (mm/blow) vs. CMV	16.81	-0.9450	3.450	75.98	-2.061	-0.8067	-103.91	0.0816	13.33
$DCPI_A$ (mm/blow) vs. CMV	-8.053	-0.2991	4.574	44.73	-1.294	0.7771	-104.66	0.1945	13.07
NDG γ_d (kN/m^3) vs. CMV	14.64	0.0926	0.2299	15.91	0.0687	0.1389	20.33	0.0330	-0.2416
CMV vs. MDP (kJ/s)	26.84	-1.146	0.0710	16.64	-1.838	1.835	19.70	-2.181	1.820
Geogauge *E* (MPa) vs. MDP (kJ/s)	94.28	-1.360	-1.037	115.47	0.0267	-4.467	73.60	0.4819	-1.046
LWD 300 *E* (MPa) vs. MDP (kJ/s)	50.65	0.7184	-3.128	45.55	0.3843	-2.302	89.12	1.077	-7.382
LWD 200 *E* (MPa) vs. MDP (kJ/s)	49.35	-0.3838	-1.353	49.35	-0.3838	-1.353	114.02	1.490	-9.676
$DCPI_M$ (mm/blow) vs. MDP (kJ/s)	-4.589	0.6590	3.370	14.40	1.902	0.2960	-49.09	0.1179	8.030
$DCPI_A$ (mm/blow) vs. MDP (kJ/s)	-11.61	0.0415	4.316	6.824	1.248	1.332	-46.32	-0.1199	7.840
NDG γ_d (kN/m^3) vs. MDP (kJ/s)	17.34	-0.1045	0.2050	17.82	-0.0734	0.1280	20.27	-0.0752	-0.1091

Table B.12 Regression Coefficients from the Multivariate Regression Analyses that were Performed on Average Data (With Interaction Term)

Dependent Variable vs. Independent Variable	All				All Excluding Base Layer			
	C_0	C_1	C_2	C_3	C_0	C_1	C_2	C_3
MDP (kJ/s) vs. CMV	57.84	-3.085	-3.687	0.244	46.71	-2.509	-2.651	0.1900
Geogauge *E* (MPa) vs. CMV	-140.30	14.16	20.57	-1.402	154.58	-1.094	-6.880	0.0148
LWD 300 *E* (MPa) vs. CMV	99.64	-2.419	-6.617	0.193	196.22	-7.416	-15.61	0.6565
LWD 200 *E* (MPa) vs. CMV	107.71	-2.199	-6.836	0.167	107.71	-2.199	-6.836	0.1671
$DCPI_M$ (mm/blow) vs. CMV	-76.54	4.916	12.46	-0.575	64.75	-2.395	-0.6871	0.1040
$DCPI_A$ (mm/blow) vs. CMV	-109.61	6.005	14.86	-0.644	-91.09	5.046	13.14	-0.5546
NDG γ_d (kN/m^3) vs. CMV	10.92	0.346	0.597	-0.026	23.67	-0.3136	-0.5895	0.0352
CMV vs. MDP (kJ/s)	-7.949	2.147	4.136	-0.380	-5.482	1.704	3.932	-0.3410
Geogauge *E* (MPa) vs. MDP (kJ/s)	154.66	-7.322	-7.502	0.635	145.86	-4.284	-7.348	0.4127
LWD 300 *E* (MPa) vs. MDP (kJ/s)	23.88	3.542	-0.032	-0.328	21.18	4.474	0.0148	-0.3965
LWD 200 *E* (MPa) vs. MDP (kJ/s)	27.43	3.785	0.468	-0.380	27.43	3.785	0.4676	-0.3795
$DCPI_M$ (mm/blow) vs. MDP (kJ/s)	25.64	-2.306	0.278	0.298	15.17	1.307	0.4610	0.0334
$DCPI_A$ (mm/blow) vs. MDP (kJ/s)	14.90	-2.694	1.501	0.293	4.362	0.9422	1.685	0.0264
NDG γ_d (kN/m^3) vs. MDP (kJ/s)	16.96	-0.056	0.264	-0.007	16.36	0.1498	0.2745	-0.0224

Table B.12 cont.

Dependent Variable vs. Independent Variable	Finals				Finals Excluding Base Layer			
	C_0	C_1	C_2	C_3	C_0	C_1	C_2	C_3
MDP (kJ/s) vs. CMV	60.56	-3.253	-4.009	0.2634	9.054	-0.5440	0.9981	0.0000
Geogauge *E* (MPa) vs. CMV	-280.30	23.29	36.54	-2.455	199.69	-1.957	-10.12	0.0000
LWD 300 *E* (MPa) vs. CMV	78.89	-1.127	-4.167	0.0394	71.19	-0.7218	-3.417	0.0000
LWD 200 *E* (MPa) vs. CMV	74.81	-0.4608	-3.694	0.0000	74.81	-0.4608	-3.694	0.0000
$DCPI_M$ (mm/blow) vs. CMV	-164.11	10.57	22.53	-1.228	75.98	-2.061	-0.8067	0.0000
$DCPI_A$ (mm/blow) vs. CMV	-169.45	9.970	21.60	-1.095	44.73	-1.294	0.7771	0.0000
NDG γ_d (kN/m^3) vs. CMV	10.77	0.3388	0.6381	-0.0263	15.91	0.0687	0.1389	0.0000
CMV vs. MDP (kJ/s)	-5.216	1.908	3.801	-0.35	16.64	-1.838	1.835	0.0000
Geogauge *E* (MPa) vs. MDP (kJ/s)	216.50	-13.63	-14.81	1.378	652.97	-79.66	-57.42	7.808
LWD 300 *E* (MPa) vs. MDP (kJ/s)	37.34	2.055	-1.628	-0.15	187.40	-20.65	-16.28	2.061
LWD 200 *E* (MPa) vs. MDP (kJ/s)	234.58	-27.85	-19.60	2.691	234.58	-27.85	-19.60	2.691
$DCPI_M$ (mm/blow) vs. MDP (kJ/s)	93.18	-9.156	-7.648	1.102	298.30	-40.19	-27.67	4.124
$DCPI_A$ (mm/blow) vs. MDP (kJ/s)	77.03	-8.858	-5.674	0.999	177.12	-24.00	-15.44	2.474
NDG γ_d (kN/m^3) vs. MDP (kJ/s)	18.89	-0.2605	0.0299	0.0175	9.85	1.107	0.9122	-0.1157

Table B.12 cont.

Dependent Variable vs. Independent Variable	Lift 5			
	C_0	C_1	C_2	C_3
MDP (kJ/s) vs. CMV	25.83	-1.351	-0.7147	0.0824
Geogauge *E* (MPa) vs. CMV	2221.53	-115.41	-198.43	10.64
LWD 300 *E* (MPa) vs. CMV	811.21	-39.69	-72.21	3.624
LWD 200 *E* (MPa) vs. CMV	639.31	-29.60	-55.65	2.678
$DCPI_M$ (mm/blow) vs. CMV	-930.07	43.92	89.54	-4.044
$DCPI_A$ (mm/blow) vs. CMV	-924.44	43.70	88.69	-4.013
NDG γ_d (kN/m^3) vs. CMV	43.62	-1.203	-2.390	0.1140
CMV vs. MDP (kJ/s)	0.0812	0.1325	3.622	-0.2127
Geogauge *E* (MPa) vs. MDP (kJ/s)	-20.25	7.512	7.939	-0.6653
LWD 300 *E* (MPa) vs. MDP (kJ/s)	9.213	7.063	0.2686	-0.5665
LWD 200 *E* (MPa) vs. MDP (kJ/s)	16.11	8.825	-0.3019	-0.6941
$DCPI_M$ (mm/blow) vs. MDP (kJ/s)	-194.30	11.00	21.93	-1.029
$DCPI_A$ (mm/blow) vs. MDP (kJ/s)	-195.32	11.04	22.10	-1.056
NDG γ_d (kN/m^3) vs. MDP (kJ/s)	22.10	-0.2129	-0.2851	0.0130

Appendix C

REGRESSION ANALYSIS COEFFICIENTS FOR CCC MEASUREMENTS PREDICTED USING ISOTROPIC ORDINARY KRIGING, IDW P = 4, AND NEAREST NEIGHBOR INTERPOLATION

Table C.1 Regression Coefficients from the Univariate Regression Analyses that were Performed on Individual Data Points (Linear Model)

Dependent Variable vs. Independent Variable	Kriging		IDW $P = 4$		NN	
	C_0	C_1	C_0	C_1	C_0	C_1
MDP (kJ/s) vs. CMV	17.31	-0.4714	16.39	-0.4218	16.63	-0.4301
Geogauge *E* (MPa) vs. CMV	65.36	0.4041	67.23	0.2866	66.75	0.3113
LWD 300 *E* (MPa) vs. CMV	22.91	0.2190	23.65	0.1711	23.34	0.1877
LWD 200 *E* (MPa) vs. CMV	24.05	0.4806	24.54	0.4446	24.35	0.4509
$DCPI_M$ (mm/blow) vs. CMV	54.91	-1.228	54.25	-1.172	53.79	-1.130
$DCPI_A$ (mm/blow) vs. CMV	49.62	-1.102	48.81	-1.039	48.46	-1.005
NDG γ_d (kN/m^3) vs. CMV	17.84	0.0297	17.85	0.0289	17.90	0.0254
CMV vs. MDP (kJ/s)	27.16	-1.125	26.37	-1.041	24.23	-0.7903
Geogauge *E* (MPa) vs. MDP (kJ/s)	84.10	-1.254	84.02	-1.270	81.80	-1.032
LWD 300 *E* (MPa) vs. MDP (kJ/s)	33.08	-0.7517	33.05	-0.7625	31.56	-0.6042
LWD 200 *E* (MPa) vs. MDP (kJ/s)	42.46	-1.120	42.11	-1.106	39.62	-0.8409
$DCPI_M$ (mm/blow) vs. MDP (kJ/s)	18.13	1.815	19.06	1.753	21.97	1.442
$DCPI_A$ (mm/blow) vs. MDP (kJ/s)	16.03	1.699	16.81	1.651	19.50	1.363
NDG γ_d (kN/m^3) vs. MDP (kJ/s)	18.93	-0.0626	18.88	-0.0587	18.77	-0.0475

Table C.2 Regression Coefficients from the Univariate Regression Analyses that were Performed on Individual Data Points for Moisture Content (Linear Model)

Dependent Variable vs. Independent Variable	Kriging		IDW $P = 4$		NN	
	C_0	C_1	C_0	C_1	C_0	C_1
Lab ω vs. CMV	37.77	-2.207	37.05	-2.117	38.01	-2.193
NDG ω vs. CMV	31.55	-1.552	30.59	-1.433	31.18	-1.469
Lab ω vs. MDP (kJ/s)	-5.402	1.535	-4.819	1.459	-5.941	1.578
NDG ω vs. MDP (kJ/s)	-4.865	1.467	-4.915	1.455	-7.708	1.736

Table C.3 Regression Coefficients from the Univariate Regression Analyses that were Performed on Individual Data Points (Polynomial Model)

Dependent Variable vs. Independent Variable	Kriging			IDW $P = 4$			NN		
	C_0	C_1	C_2	C_0	C_1	C_2	C_0	C_1	C_2
MDP (kJ/s) vs. CMV	21.59	-1.019	0.0165	20.29	-0.9124	0.0145	21.99	-1.092	0.0192
Geogauge E (MPa) vs. CMV	75.38	-0.8779	0.0385	71.82	-0.2904	0.0170	62.54	0.8308	-0.0151
LWD 300 E (MPa) vs. CMV	26.56	-0.2484	0.0140	25.87	-0.1080	0.0082	22.18	0.3302	-0.0041
LWD 200 E (MPa) vs. CMV	31.69	-0.4978	0.0294	30.69	-0.3281	0.0228	27.11	0.1100	0.0099
$DCPI_M$ (mm/blow) vs. CMV	65.10	-2.532	0.0392	62.97	-2.268	0.0324	62.26	-2.175	0.0303
$DCPI_A$ (mm/blow) vs. CMV	52.66	-1.491	0.0117	50.56	-1.259	0.0065	49.91	-1.184	0.0052
NDG γ_d (kN/m^3) vs. CMV	17.02	0.1335	-0.0031	16.98	0.1349	-0.0031	17.26	0.1026	-0.0022
CMV vs. MDP (kJ/s)	20.92	0.2582	-0.0709	23.46	-0.3874	-0.0339	23.69	-0.6720	-0.0058
Geogauge E (MPa) vs. MDP (kJ/s)	118.19	-8.268	0.3329	113.74	-7.456	0.2960	101.23	-5.020	0.1829
LWD 300 E (MPa) vs. MDP (kJ/s)	35.02	-1.151	0.0190	34.39	-1.042	0.0133	33.41	-0.9838	0.0174
LWD 200 E (MPa) vs. MDP (kJ/s)	44.04	-1.445	0.0154	43.97	-1.492	0.0185	41.22	-1.169	0.0150
$DCPI_M$ (mm/blow) vs. MDP (kJ/s)	22.24	0.9696	0.0401	23.09	0.9144	0.0401	22.15	1.406	0.0016
$DCPI_A$ (mm/blow) vs. MDP (kJ/s)	17.05	1.490	0.0100	18.22	1.357	0.0141	18.58	1.551	-0.0086
NDG γ_d (kN/m^3) vs. MDP (kJ/s)	17.80	0.1620	-0.0103	17.83	0.1538	-0.0098	18.21	0.0669	-0.0052

Table C.4 Regression Coefficients from the Univariate Regression Analyses that were Performed on Individual Data Points for Moisture Content (Polynomial Model)

Dependent Variable vs. Independent Variable	Kriging			IDW $P = 4$			NN		
	C_0	C_1	C_2	C_0	C_1	C_2	C_0	C_1	C_2
Lab ω vs. CMV	-36.71	13.81	-0.8490	-46.93	15.94	-0.9572	-68.62	20.73	-1.215
NDG ω vs. CMV	-21.80	9.988	-0.6121	-26.31	10.87	-0.6527	-35.65	12.99	-0.7668
Lab ω vs. MDP (kJ/s)	-26.10	5.899	-0.2267	-29.38	6.637	-0.2690	-29.19	6.479	-0.2546
NDG ω vs. MDP (kJ/s)	10.25	-1.648	0.1573	11.63	-1.957	0.1723	15.90	-3.130	0.2457

Table C.5 Regression Coefficients from the Univariate Regression Analyses that were Performed on Average Data (Linear Model)

Dependent Variable vs. Independent Variable	Kriging		IDW $P = 4$		NN	
	C_0	C_1	C_0	C_1	C_0	C_1
MDP (kJ/s) vs. CMV	22.37	-0.7699	20.56	-0.6659	24.28	-0.8763
Geogauge *E* (MPa) vs. CMV	65.11	0.3886	65.80	0.3347	63.91	0.4475
LWD 300 *E* (MPa) vs. CMV	21.44	0.2592	21.82	0.2285	20.35	0.3163
LWD 200 *E* (MPa) vs. CMV	25.25	0.3597	25.43	0.3392	23.10	0.4792
$DCPI_M$ (mm/blow) vs. CMV	60.50	-1.560	61.68	-1.596	67.51	-1.934
$DCPI_A$ (mm/blow) vs. CMV	55.98	-1.446	56.79	-1.461	62.10	-1.769
NDG γ_d (kN/m^3) vs. CMV	17.58	0.0461	17.55	0.0474	17.46	0.0523
CMV vs. MDP (kJ/s)	27.99	-1.197	28.89	-1.304	26.13	-0.9869
Geogauge *E* (MPa) vs. MDP (kJ/s)	80.36	-0.8605	81.10	-0.9663	80.17	-0.8614
LWD 300 *E* (MPa) vs. MDP (kJ/s)	34.53	-0.9273	35.61	-1.067	34.46	-0.9401
LWD 200 *E* (MPa) vs. MDP (kJ/s)	43.02	-1.204	44.35	-1.380	42.66	-1.195
$DCPI_M$ (mm/blow) vs. MDP (kJ/s)	18.36	1.764	17.37	1.931	19.14	1.729
$DCPI_A$ (mm/blow) vs. MDP (kJ/s)	16.04	1.713	15.09	1.874	16.70	1.688
NDG γ_d (kN/m^3) vs. MDP (kJ/s)	18.99	-0.0668	19.03	-0.0733	18.97	-0.0661

Table C.6 Regression Coefficients from the Univariate Regression Analyses that were Performed on Average Data for Moisture Content (Linear Model)

Dependent Variable vs. Independent Variable	Kriging		IDW $P = 4$		NN	
	C_0	C_1	C_0	C_1	C_0	C_1
Lab ω vs. CMV	42.54	-2.715	41.81	-2.602	42.20	-2.616
NDG ω vs. CMV	36.60	-2.124	35.44	-1.968	34.95	-1.894
Lab ω vs. MDP (kJ/s)	-10.02	2.077	-8.202	1.854	-9.552	2.008
NDG ω vs. MDP (kJ/s)	-12.25	2.254	-11.17	2.106	-13.60	2.362

Table C.7 Regression Coefficients from the Univariate Regression Analyses that were Performed on Average Data (Polynomial Model)

Dependent Variable vs. Independent Variable	Kriging			IDW $P = 4$			NN		
	C_0	C_1	C_2	C_0	C_1	C_2	C_0	C_1	C_2
MDP (kJ/s) vs. CMV	17.51	-0.0853	-0.0229	11.61	0.5520	-0.0397	40.60	-2.952	0.0639
Geogauge E (MPa) vs. CMV	85.75	-2.516	0.0971	78.85	-1.442	0.0578	34.76	4.153	-0.1142
LWD 300 E (MPa) vs. CMV	44.70	-3.013	0.1094	47.13	-3.218	0.1122	61.82	-4.955	0.1624
LWD 200 E (MPa) vs. CMV	61.67	-4.765	0.1713	64.83	-5.026	0.1747	76.75	-6.341	0.2101
$DCPI_M$ (mm/blow) vs. CMV	-7.549	8.014	-0.3201	-16.31	9.022	-0.3458	17.74	4.392	-0.1949
$DCPI_A$ (mm/blow) vs. CMV	-7.386	7.470	-0.2981	-16.62	8.533	-0.3255	-8.292	7.180	-0.2757
NDG γ_d (kN/m^3) vs. CMV	17.98	-0.0091	0.0018	18.15	-0.0355	0.0027	16.92	0.1205	-0.0021
CMV vs. MDP (kJ/s)	14.69	1.555	-0.1330	5.628	3.776	-0.2620	23.15	-0.35	-0.0315
Geogauge E (MPa) vs. MDP (kJ/s)	114.14	-7.237	0.2780	113.59	-7.203	0.2785	109.90	-6.544	0.2485
LWD 300 E (MPa) vs. MDP (kJ/s)	31.18	-0.2946	-0.0276	30.84	-0.1522	-0.0409	29.98	-0.0834	-0.0375
LWD 200 E (MPa) vs. MDP (kJ/s)	39.34	-0.5086	-0.0303	39.09	-0.3701	-0.0451	37.65	-0.2391	-0.0418
$DCPI_M$ (mm/blow) vs. MDP (kJ/s)	12.54	2.862	-0.0479	10.06	3.333	-0.0626	11.65	3.161	-0.0627
$DCPI_A$ (mm/blow) vs. MDP (kJ/s)	5.001	3.796	-0.0908	2.679	4.256	-0.1064	5.560	3.817	-0.0931
NDG γ_d (kN/m^3) vs. MDP (kJ/s)	17.80	0.1585	-0.0098	18.00	0.1244	-0.0088	18.03	0.1126	-0.0078

Table C.8 Regression Coefficients from the Univariate Regression Analyses that were Performed on Average Data for Moisture Content (Polynomial Model)

Dependent Variable vs. Independent Variable	Kriging			IDW $P = 4$			NN		
	C_0	C_1	C_2	C_0	C_1	C_2	C_0	C_1	C_2
Lab ω vs. CMV	-80.87	23.35	-1.362	-95.03	26.30	-1.510	-108.59	29.23	-1.664
NDG ω vs. CMV	-96.06	26.91	-1.560	-84.42	24.26	-1.409	-68.73	20.80	-1.219
Lab ω vs. MDP (kJ/s)	-182.52	38.27	-1.880	-172.98	36.42	-1.796	-202.11	42.41	-2.098
NDG ω vs. MDP (kJ/s)	30.10	-6.531	0.4480	34.69	-7.404	0.4850	39.12	-8.572	0.5576

Table C.9 Regression Coefficients from the Multivariate Regression Analyses that were Performed on Individual Data Points (Without Interaction Term)

Dependent Variable vs. Independent Variable	Kriging			IDW $P = 4$			NN		
	C_0	C_1	C_2	C_0	C_1	C_2	C_0	C_1	C_2
MDP (kJ/s) vs. CMV	2.902	-0.2458	1.109	1.829	-0.2107	1.146	-1.712	-0.1881	1.475
Geogauge *E* (MPa) vs. CMV	131.13	-0.2634	-5.673	130.19	-0.2411	-5.609	127.67	-0.1555	-5.492
LWD 300 *E* (MPa) vs. CMV	46.64	0.0116	-2.175	47.07	-0.0021	-2.196	45.66	0.0431	-2.130
LWD 200 *E* (MPa) vs. CMV	49.76	0.1841	-2.182	49.74	0.1904	-2.195	48.64	0.2221	-2.142
$DCPI_M$ (mm/blow) vs. CMV	33.75	-0.9913	1.764	31.34	-0.9438	1.950	30.22	-0.8898	1.995
$DCPI_A$ (mm/blow) vs. CMV	21.37	-0.8348	2.497	19.35	-0.7951	2.654	18.57	-0.7550	2.683
NDG γ_d (kN/m^3) vs. CMV	17.92	0.0288	-0.0067	17.99	0.0273	-0.0123	18.10	0.0233	-0.0172
CMV vs. MDP (kJ/s)	24.28	-1.498	0.6804	24.62	-1.292	0.4380	25.70	-0.7235	-0.2021
Geogauge *E* (MPa) vs. MDP (kJ/s)	112.09	0.1003	-4.123	111.81	0.0421	-4.038	112.44	0.1092	-4.166
LWD 300 *E* (MPa) vs. MDP (kJ/s)	47.61	-0.3092	-1.970	47.52	-0.3263	-1.949	47.92	-0.1553	-2.154
LWD 200 *E* (MPa) vs. MDP (kJ/s)	53.17	-0.9396	-1.285	53.01	-0.9631	-1.262	52.30	-0.7055	-1.439
$DCPI_M$ (mm/blow) vs. MDP (kJ/s)	8.930	1.443	1.270	8.318	1.304	1.490	9.736	1.015	1.624
$DCPI_A$ (mm/blow) vs. MDP (kJ/s)	1.681	1.214	1.928	1.262	1.116	2.084	2.625	0.8886	2.165
NDG γ_d (kN/m^3) vs. MDP (kJ/s)	18.72	-0.0729	0.0311	18.76	-0.0644	0.0179	18.68	-0.0510	0.0127

Table C.10 Regression Coefficients from the Multivariate Regression Analyses that were Performed on Individual Data Points (With Interaction Term)

Dependent Variable vs. Independent Variable	Kriging				IDW $P = 4$				NN			
	C_0	C_1	C_2	C_3	C_0	C_1	C_2	C_3	C_0	C_1	C_2	C_3
MDP (kJ/s) vs. CMV	-3.109	0.1239	1.729	-0.0388	-3.146	0.0951	1.662	-0.0322	-11.12	0.3868	2.448	-0.0603
Geogauge *E* (MPa) vs. CMV	111.92	0.9181	-3.691	-0.1239	112.81	0.8275	-3.807	-0.1124	123.56	0.0954	-5.068	-0.0263
LWD 300 *E* (MPa) vs. CMV	37.57	0.5692	-1.240	-0.0585	37.35	0.5951	-1.189	-0.0628	43.58	0.1701	-1.915	-0.0133
LWD 200 *E* (MPa) vs. CMV	28.90	1.467	-0.0304	-0.1345	28.39	1.503	0.0192	-0.1381	33.84	1.126	-0.6122	-0.0948
$DCPI_M$ (mm/blow) vs. CMV	-1.111	1.153	5.360	-0.22	0.8276	0.9320	5.114	-0.1973	7.356	0.5073	4.358	-0.1466
$DCPI_A$ (mm/blow) vs. CMV	1.804	0.3683	4.515	-0.1261	2.874	0.2177	4.362	-0.1065	7.666	-0.0886	3.811	-0.0699
NDG γ_d (kN/m^3) vs. CMV	20.68	-0.1413	-0.2920	0.0178	20.53	-0.1290	-0.2759	0.0164	20.01	-0.0934	-0.2145	0.0122
CMV vs. MDP (kJ/s)	4.063	0.9417	2.769	-0.2455	4.356	1.183	2.538	-0.2499	13.38	0.9042	1.025	-0.1581
Geogauge *E* (MPa) vs. MDP (kJ/s)	145.03	-3.847	-7.150	0.3570	144.87	-3.980	-7.072	0.3633	139.28	-3.292	-6.597	0.3034
LWD 300 *E* (MPa) vs. MDP (kJ/s)	48.29	-0.3902	-2.032	0.0073	48.61	-0.4597	-2.050	0.0121	47.80	-0.1399	-2.143	-0.0014
LWD 200 *E* (MPa) vs. MDP (kJ/s)	48.48	-0.3783	-0.85	-0.0508	49.26	-0.5076	-0.92	-0.0412	48.47	-0.2201	-1.092	-0.0433
$DCPI_M$ (mm/blow) vs. MDP (kJ/s)	6.848	1.692	1.461	-0.0226	7.996	1.343	1.519	-0.0035	6.080	1.479	1.955	-0.0413
$DCPI_A$ (mm/blow) vs. MDP (kJ/s)	-2.171	1.675	2.282	-0.0417	-1.252	1.422	2.315	-0.0276	-2.334	1.517	2.615	-0.0561
NDG γ_d (kN/m^3) vs. MDP (kJ/s)	16.80	0.1573	0.2076	-0.0208	16.81	0.1722	0.1964	-0.0214	17.34	0.1181	0.1336	-0.0151

Table C.11 Regression Coefficients from the Multivariate Regression Analyses that were Performed on Average Data (Without Interaction Term)

Dependent Variable vs. Independent Variable	Kriging			IDW $P = 4$			NN		
	C_0	C_1	C_2	C_0	C_1	C_2	C_0	C_1	C_2
MDP (kJ/s) vs. CMV	8.717	-0.4866	0.9152	7.528	-0.4547	0.9713	10.50	-0.6228	0.9723
Geogauge *E* (MPa) vs. CMV	151.63	-0.9370	-6.603	159.04	-1.176	-6.950	169.90	-1.503	-7.482
LWD 300 *E* (MPa) vs. CMV	64.96	-0.4299	-3.288	67.20	-0.5070	-3.383	70.33	-0.6036	-3.528
LWD 200 *E* (MPa) vs. CMV	74.30	-0.4213	-3.700	75.79	-0.4769	-3.754	76.49	-0.5034	-3.769
$DCPI_M$ (mm/blow) vs. CMV	43.96	-1.288	1.264	42.24	-1.281	1.449	58.91	-1.776	0.6065
$DCPI_A$ (mm/blow) vs. CMV	19.81	-0.8560	2.732	17.95	-0.83	2.895	29.09	-1.162	2.331
NDG γ_d (kN/m^3) vs. CMV	16.63	0.0610	0.0711	16.69	0.0612	0.0634	16.28	0.0738	0.0828
CMV vs. MDP (kJ/s)	18.58	-1.981	1.738	17.72	-2.064	1.883	20.77	-1.259	0.81
Geogauge *E* (MPa) vs. MDP (kJ/s)	112.30	0.5444	-4.578	112.29	0.5394	-4.562	111.91	0.4148	-4.406
LWD 300 *E* (MPa) vs. MDP (kJ/s)	53.41	-0.1641	-2.646	52.32	-0.2608	-2.444	52.08	-0.2318	-2.446
LWD 200 *E* (MPa) vs. MDP (kJ/s)	58.29	-0.6557	-2.080	56.92	-0.7728	-1.839	57.31	-0.6059	-2.035
$DCPI_M$ (mm/blow) vs. MDP (kJ/s)	12.45	1.697	0.6851	12.74	1.708	0.6773	14.79	1.553	0.6046
$DCPI_A$ (mm/blow) vs. MDP (kJ/s)	2.216	1.251	1.862	2.503	1.266	1.841	4.818	1.210	1.649
NDG γ_d (kN/m^3) vs. MDP (kJ/s)	18.18	-0.1126	0.1241	18.12	-0.1169	0.1323	18.01	-0.1048	0.1336

Table C.12 Regression Coefficients from the Multivariate Regression Analyses that were Performed on Average Data (With Interaction Term)

Dependent Variable vs. Independent Variable	Kriging				IDW $P = 4$				NN			
	C_0	C_1	C_2	C_3	C_0	C_1	C_2	C_3	C_0	C_1	C_2	C_3
MDP (kJ/s) vs. CMV	46.71	-2.509	-2.651	0.1900	27.45	-1.520	-0.9054	0.1006	-73.47	3.866	8.973	-0.4297
Geogauge E (MPa) vs. CMV	154.58	-1.094	-6.880	0.0148	229.86	-4.965	-13.62	0.3578	177.36	-1.902	-8.194	0.0382
LWD 300 E (MPa) vs. CMV	196.22	-7.416	-15.61	0.6565	197.32	-7.468	-15.64	0.6573	184.38	-6.700	-14.40	0.5836
LWD 200 E (MPa) vs. CMV	107.71	-2.199	-6.836	0.1671	100.22	-1.784	-6.055	0.1234	88.44	-1.143	-4.908	0.0612
DCPIM (mm/blow) vs. CMV	64.75	-2.395	-0.69	0.1040	80.18	-3.311	-2.126	0.1917	-78.67	5.579	13.72	-0.7041
DCPIA (mm/blow) vs. CMV	-91.09	5.046	13.14	-0.5546	-72.88	4.029	11.45	-0.4589	-192.25	10.67	23.42	-1.133
NDG γd (kN/m3) vs. CMV	23.67	-0.3136	-0.5895	0.0352	24.01	-0.3301	-0.6256	0.0369	30.01	-0.6599	-1.225	0.0702
CMV vs. MDP (kJ/s)	-5.482	1.704	3.932	-0.3410	-0.13	0.7330	3.499	-0.2576	31.29	-3.036	-0.1036	0.1611
Geogauge E (MPa) vs. MDP (kJ/s)	145.86	-4.284	-7.348	0.4127	146.11	-4.591	-7.262	0.4316	143.79	-4.478	-6.985	0.4151
LWD 300 E (MPa) vs. MDP (kJ/s)	21.18	4.474	0.0148	-0.3965	21.44	4.424	0.0216	-0.3941	24.33	4.026	-0.2018	-0.3612
LWD 200 E (MPa) vs. MDP (kJ/s)	27.43	3.785	0.4676	-0.3795	29.03	3.458	0.3881	-0.3559	30.09	3.572	0.1666	-0.3545
DCPIM (mm/blow) vs. MDP (kJ/s)	15.17	1.307	0.4610	0.0334	10.95	1.979	0.8200	-0.0228	12.52	1.902	0.79	-0.0296
DCPIA (mm/blow) vs. MDP (kJ/s)	4.362	0.9422	1.685	0.0264	0.93	1.504	1.966	-0.0200	1.672	1.693	1.904	-0.0410
NDG γd (kN/m3) vs. MDP (kJ/s)	16.36	0.1498	0.2745	-0.0224	16.63	0.1103	0.2519	-0.0191	16.67	0.0999	0.2415	-0.0174

Appendix D

COPYRIGHT PERMISSION

Permissions for Table 3.1 and Figures 3.1 through 3.6:

Daniel Cacciola <dcacc@udel.edu>

Permission to reproduce Figures and Table from your Thesis

Faraz S. Tehrani <faraz.stehrani@gmail.com> Thu, Jun 27, 2013 at 12:42 PM
To: Daniel Cacciola <dcacc@udel.edu>

Hello Daniel,

You have my permission to use **Figures 3.1, 3.2, 3.6, 3.7, 3.9,** and **3.10** and **Table 3.2** of my Master's thesis in your Master's thesis.

Regards,

Faraz

[Quoted text hidden]

--

****

Faraz S.Tehrani
PhD Candidate in Geotechnical Engineering
School of Civil Engineering
Purdue University
550 Stadium Mall Drive
West Lafayette, IN 47907
E-mail: ftehrani@purdue.edu
faraz.stehrani@gmail.com